Clusterin in the Brain

By

Sarah K. Woody

Submitted to the graduate degree program in Pharmacology and Toxicology and the Graduate Faculty of the University of Kansas in partial fulfillment of the requirements for the degree of Doctor of Philosophy.

_____

Committee Chairperson: Dr. Liqin Zhao

_____

Dr. Eduardo Rosa-Molinar

_____

Dr. Elias Michaelis

_____

Dr. Shirley ShiDu Yan

_____

Dr. Russell Swerdlow

Date Defended

12/11/2017

The Thesis Committee for Sarah K. Woody certifies that this is the approved version of the following thesis:

Clusterin in the Brain

_____

Committee Chairperson: Dr. Liqin Zhao

Date Accepted

Abstract

Late-onset Alzheimer's disease (LOAD) is an age-related chronic neurodegenerative disorder traditionally characterized by the presence of neurotoxic amyloid beta (Aβ) plaques, neurofibrillary tangles, and progressive, irreversible cognitive decline. Though extensively studied, the molecular mechanisms underlying the onset of AD-related neuropathologies are not understood. Moreover, over 200 clinical trials have failed to produce a viable therapeutic treatment strategy in the last 15 years. The inability to generate a treatment for clinical AD has led to a shift in focus from disease treatment to disease prevention and early intervention in the preclinical stage of AD development (pAD). As sex, genetics, and epigenetic influence have been identified as key contributors to early neurophysiological changes, it is imperative that research be conducted to elucidate intersecting risk mechanisms that would allow for the development of novel therapeutic entities that could be targeted in pAD. Clusterin (CLU), initially identified in 1983, is a multifaceted, nearly ubiquitously expressed homeostatic regulator that is postulated to exist as multiple protein isoforms including a glycosylated mature/secreted form (mCLU) and smaller non-modified nuclear and/or intracellular forms. CLU, also known as apolipoprotein J (APOJ) which belongs to the same protein family as APOE, is currently listed as the third most potent genetic risk factor for the development of LOAD. However, despite many clinical observations of CLU SNPs-conferred increased AD risk, an extensive gap exists pertaining to the basic molecular properties of CLU in the healthy brain. Therefore, this dissertation focuses on the neurophysiological characterization of brain CLU with specific emphasis on understanding the expression, distribution, and potential physiological function(s) of individual CLU protein isoforms. The data indicate that at least two CLU mRNAs are generated from the CLU gene which are translated to 3 different CLU pre-proteins. These pre-proteins, which are differentially modified by N-linked glycosylation, are targeted to distinct cellular compartments in both adult rodent brain and embryonic brain cell types. Moreover, we observe a distinct difference in the CLU protein expression profile between astrocytes and neurons with astrocytes generating and secreting extracellular mCLU and neurons primarily generating intracellular CLU protein isoforms. Of particular significance, we demonstrate for the first time

that CLU protein isoforms are integrally associated with brain mitochondrial function. Specifically, we identify a previously unknown mitochondria-targeted CLU protein isoform that is localized to the mitochondrial matrix where it directly interacts with a key component of the MICOS complex. In addition, the data indicate that non-mitochondrial CLU regulates some aspect of brain mitochondrial respiration in young adult female mice. Furthermore, we show for the first time that the mCLU pre-protein is significantly and positively regulated by estrogen in the brain. Specifically, the data indicate direct ligand-mediated regulation via estrogen receptor beta (ERβ) signaling through one or more previously unidentified estrogen receptor response elements on the CLU promoter. Collectively, these data suggest a possible hypothesis whereby CLU SNPs, which are associated with reduced circulating CLU, may contribute increased AD risk via interaction with brain mitochondrial bioenergetics and female sex hormones.

Acknowledgements

I would like to formally thank all those who have been integrally involved in the generation of my dissertation studies. The academic, personal, and professional mentoring and experience that I have gained during this time have molded me into a confident, independent scientist and I am eager to continue contributing to the biomedical research industry. First and foremost, I would like to thank my mentor, Dr. Liqin Zhao for her unceasing support in the past 3 years. Dr. Zhao, you brought me into your laboratory and have given much more than your time to help develop those skills that are invaluable for my future career. However, you are more than a mentor to me; you have become a personal and professional role model. Through your example and leadership, you have unknowingly demonstrated your honesty, integrity, dedication, professionalism, and passion for helping the world around you through scientific research. I do now, and will always, cherish you as a friend and a mentor. In addition, I would like to thank Dr. Elias Michaelis, Dr. Shirley ShiDu Yan, Dr. Eduardo Rosa-Molinar, and Dr. Russell Swerdlow for serving on my dissertation committee. Your advice and critiques have been instrumental in the completion of the studies presented herein. I would also like to formally thank our collaborators, Heather Shinogle, Dr. Yakov Mikhailovich, Dr. Robert Hanzlik, Dr. Antonio Artigues, Dr. Karim Rumi, and Dr. Yafeng Dong, for their experimental assistance during the course of my studies.

I feel my acknowledgements would not be complete without a description of my gratitude for the Pharmacology and Toxicology professors, both past and present, who have guided me through the last 6 years of my life. Each and every one of you has contributed to my development in your own way and I appreciate the time you have given me. Specifically, I would like to thank Dr. Jeff Staudinger, Dr. Rick Dobrowsky, and Dr. Eduardo Rosa-Molinar for their personal and academic contributions. Dr. Staudinger, the molecular biology training that I received during my time in your lab has been crucial during the course of my studies in the Zhao Lab. Dr. Dobrowsky, for the past 6 years you have continually challenged me to do better. Your honesty and critiques, have taught me how to critically analyze myself in a constructive

manner; a skill that has helped my personal development immeasurably. Dr. Rosa-Molinar, you have not only introduced me to novel and exciting fields of research, you have challenged me to expand my scientific knowledge and fostered my critical thinking skills. Moreover, your continual sense of humor and the personal support I have received from both you and the members of your lab has provided relief on even the most frustrating days.

I would also like to thank the members of the Zhao Lab, both past and present, for providing a work environment that was, and still is, extremely uplifting. Specifically, I would like to thank Anindit Chhibber, who is now and will always be a true friend and colleague. Anindit, you have challenged my personal belief system more than it has ever been challenged and I am extremely thankful for that. Through our academic, political, personal, and religious debates you have opened my eyes to opinions that I would not have previously considered and challenged me to keep an open mind. Moreover, I have never in my life had more fun in a science lab than I did with you. Your constant sense of humor made even the most mundane tasks enjoyable and there is no one that I would rather share a lab bench with.

And finally, I would like to thank my family for their unwavering support for the past 6 years. Specifically, I would like to thank my husband, Laramie Herring, for spending many late nights in the Zhao Lab washing dishes, for bringing me dinner when I had to work late, and for making late night lab runs with me. I could not ask for a more supportive partner. I would also like to thank my sisters, Elizabeth Foster, Danielle Souza, and Kristina Wlasow for their continual support. Each and every one of you has allowed me to miss births, birthdays, and family celebrations in the name of lab work and have never once held it against me. And last, but certainly not least, I would like to thank my parents, Robert and Cynthia Woody. You have never stopped supporting me and I know that you never will. However, what I appreciate most is that you have taught me to make my own decisions and to be responsible for my actions and the outcome of those actions. There are not enough words to explain my gratitude, however, I know that this journey would have ended long ago without your support.

List of Schematics and Figures

Schematics:

Figures:

List of Tables

List of Abbreviations

AA	Antimycin A
Ab	Antibody
AD	Alzheimer's Disease
ADP	Adenosine Diphosphate
ANOVA	Analysis of Variance
AP-1	Activator protein 1
AP-2	Activator protein 2
APOE	Apolipoprotein E
ApoJ	Apolipoprotein J
ARE	Androgen Response Element
Arg	Arginine
ATP	Adenosine Triphosphate
Aβ	Amyloid beta
BBB	Blood-brain Barrier
cDNA	complementary DNA
ChIP	Chromatin Immunoprecipitation
CLI	Complement Lysis Inhibitor
CLU	Clusterin
CLU-KO	Clusterin knockout
CLUα	Clusterin alpha
CLUβ	Clusterin beta
CNS	Central nervous system
Co-IP	Co-immunoprecipitation
COMMD1	Copper Metabolism Domain Containing 1
CRPC	Castration Resistance Prostate Cancer
DAG	Dimeric acidic glycoprotein
DHT	Dihydrotestosterone
DNA	deoxyribonucleic Acid
E2	17β-estradiol
EEC-1	human endometrial adenocarcinoma cells
ER	Estrogen receptor
ERE	Estrogen receptor response element
ERK	extracellular-signal-regulated kinase
Erα	Estrogen Receptor alpha
Erβ-KO	Estrogen Receptor beta knockout
fAD	familial Alzheimer's Disease
FDR	False Discovery Rate
Gapdh	Glyceraldehyde-3-Phosphate Dehydrogenase
GDH	Glutamate Dehydrogenase
GFAP	Glial fibrillary acidic protein
GlcNAC	N-Acetylglucosamine

GRE	Glucocorticoid response element
Grp75	Glucose regulated protein 75
H3K4me3	Trimethlated Histone H3 Lysine 4
hCLU-OE	Human Clusterin Overexpression
Hetero	Heterozygous
HPRT	hypoxanthine guanine phosphoribosyl transferase
HRP	Horseradish Peroxidase
HSE	Heat Shock Response Element
Hsp60	Heat Shock Protein 60
Hspa9	Stress-70 protein, mitochondrial precursor
icCLU	intracellular clusterin
IgG	Immunoglobulin
IMM	Inner Mitochondrial Membrane
Immt	Inner Membrane Mitochondrial Protein
IMS	Intermembrane Space
IP	Immunoprecipitation
IR	Infrared
IκB	Inhibitor of kappa B kinase
KA	Kanic Acid
KLE	Human uterus endometrium adenocarcinoma Cells
KUB1	KU-70 Binding Protein
LDH	lactate Dehydrogenase
LnCAP	androgen-sensitive human prostate adenocarcinoma cells
LOAD	Late-onset Alzheimer's Disease
LRP2	low density lipoprotein-related protein 2
LS	Leader Sequence
MAC	Membrane Attack Complex
Mal	Malate
Man	Mannose
MAP2	Microtubule associated protein 2
MCAO	Middle Cerebral Artery Occlusion
MCI	Mild Cognitive Impairment
mCLU	mature Clusterin
mCLU-KO	mature Clusterin knockout
MG132	Magnesium 132
MHCII	Major Histocompatibility Complex II
MIB	Mitochondrial Isolation Buffer
MICOS	mitochondrial contact site and cristae organizing system
miRNA	micro RNA
MMP-9	Matrix Metallopeptidase 9
MUD-Pit	Multidimenstional Protein Identification Technology
MW	Molecular Weight
MYB	Myb proto-oncogene

NF-κB	nuclear factor kappa-light-chain-enhancer of activated B cells
NIA	National Institutes of Aging
NMDA	N-methyl-D-aspartate receptor
NT	Non-transfected
OE	Overexpressed
Oligo	Oligomycin A
OMM	Outer Mitochondrial Membrane
ON	Overnight
OVX	Ovariectomized
OXPHOS	Oxidative Phosphorylation
P4	Progesterone
PAM	presequence translocase-associated motor
PCR	Polymerase chain reaction
PGK	Phosphoglycerate kinase
PN	Post-natal
PTM	Post-translational Modification
pVHL	von Hippel–Lindau tumor suppressor
Pyr	Pyruvate
Rb	Rabbit
RNA	Ribonucleic Acid
Rot	Rotenone
RT	Room Temperature
RUCA-1	rat endometrial adenocarcinoma cells
SAM	sorting and assembly machinery
sCLU	secreted Clusterin
Ser	Serine
SGP2	Sulfated glycoprotein 2
siRNA	silencing RNA
SNP	Single nucleotide polymorphism
SP-1	specificity protein 1
SP-40,40	serum protein 40 kDa,40 kDa
Succ	Succinate
SUMO	Small ubiquitin-like modifier
TCA	tricarboxylic acid
TGF-β	Transforming growth factor beta
Thr	Threonine
TIM	Translocase of the Inner Mitochondrial Membrane
TOM	Translocase ouf the Outer Mitochondrial Membrane
TRPM-2	Testosterone Repressed
UV	ultraviolet
VDAC	Voltage-dependent anion channel
Wt	Wild-type

Table of Contents

Introduction

Late-onset Alzheimer's disease (LOAD): current status and challenges.

Alzheimer's disease (AD) currently affects 35 million people worldwide, including 5.4 million Americans; a number that is estimated to triple by the year 2050 (Alzheimer's, 2015). As the prevalence of AD increases the AD-associated economic burden will also increase. In 2015 the direct costs associated with the care of AD patients in the United States reached $226 billion. This number is predicted to reach $1.1 trillion by the year 2050 making AD one of the most costly chronic illnesses in the world (Alzheimer's, 2015). At present, AD is the 6th leading cause of death in the United States and is the only leading cause of death that cannot be prevented or cured. There are currently 5 FDA approved drugs available to treat AD-related symptoms, however, these drugs do not address the underlying cause of AD. Moreover, these drugs provide only temporary therapeutic relief in a fraction of the patients to whom they are administered making them relatively inefficient. Driven by the lack of an effective treatment, an extensive amount of clinical trials aimed at treating AD have been performed in the last 15 years; all of which have failed (McBride, 2012; Schnabel, 2013). These unanticipated challenges combined with the estimated rapid increases in AD prevalence stress the importance of identifying novel therapeutic entities and/or treatment strategies.

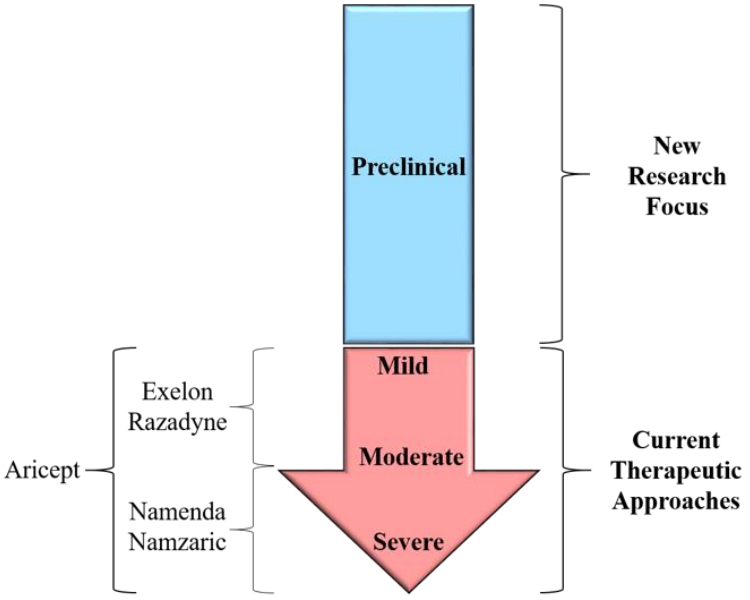

Schematic 1. Preclinical LOAD: A Therapeutic Window of Opportunity. Current therapeutic approaches aim to treat LOAD following the clinical diagnosis of mild cognitive impairment (MCI) in the very early stages of disease progression. There are currently 5 FDA approved drugs available for the treatment of memory issues associated with mild to severe LOAD, all of which regulate the levels of acetylcholine (Ach) or glutamate in the brain. However, as these drugs provide only temporary relief in a subset of patients to whom they are administered, new therapeutic targets and/or approaches are being extensively researched. The preclinincal stage of AD is of particular interest as a delay in the clinical onset of LOAD would dramatically reduce the prevalence of LOAD thus, several lines of research are now focused on elucidating the mechanisms by which neurocognitive decline occurs in the at-risk population.

One such strategy that has emerged in the last decade is to prevent or delay the onset of clinically diagnosable LOAD by identifying the molecular mechanisms that trigger neurocognitive decline in the 20-30 year period prior to the onset of AD; a period of time now classified as preclinical AD. While the molecular mechanism(s) that trigger the initial onset of neurocognitive decline are still not known, studies have indicated irregularities in both amyloid and glucose metabolism several years prior to diagnosis. These findings, and many more, point to the preclinical phase of AD as a novel therapeutic window of opportunity in the treatment and/or prevention of LOAD (Schematic 1).

An overview of LOAD-associated risk factors

There are two types of AD: early-onset familial AD (fAD) and late-onset sporadic AD (LOAD). fAD is rare and mostly caused by inherited genetic mutations that result in abnormal overproduction of neurotoxic β-amyloid (Aβ) peptides. Alternatively, LOAD, the most common form of AD representing 95% of human cases, develops after age 60 and involves a heterogeneous and multifactorial etiology. It is now widely accepted that a person's risk for developing LOAD is primarily influenced by a combination of complex interactions between multiple genetic and environmental risk factors including age, sex, genetic predisposition, and epigenetic influence (Schematic 2). Each LOAD risk factor will be discussed briefly in the following section.

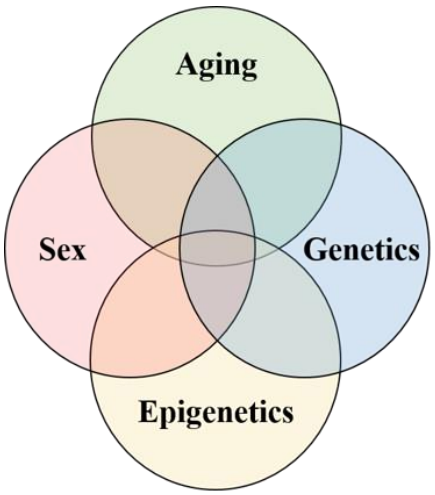

Schematic 2. Overview of LOAD Risk Factors. Age, sex, genetic predisposition, and epigenetic influence have all been identified as LOAD-contributing risk factors. It is thought that the interaction between 2 or more risk factors may trigger the onset or neurophysiological decline in preclinical AD.

Age. At present, age remains the most predominant risk factor for LOAD. It is estimated that 1 in 9 (11.1%) senior citizens age 65 or older have been diagnosed with LOAD; a number that increases to 1 in 3 (33.3%) by age 85 (Alzheimer's, 2015). The National Institute on Aging (NIA) indicates that the risk of developing

LOAD doubles every 5 years past the age of 65 (Aging, 2015). Additionally, epidemiologic studies from the NIA estimate that the total percentage of senior citizens in the U.S. will increase 7% by 2030 making senior citizens the fastest growing age group in the U.S. and consequently the most at-risk population (Aging, 2015).

Sex. Of the 5.4 million Americans currently living with AD, approximately 65% are women (Alzheimer's, 2015). It was originally postulated that the higher percentage of women living with AD was due to an increased life span of the female population, however, as the average world-wide life expectancy of men and women differs by only 4 years, this presumption is incorrect. A meta-analysis of 7 sex-specific clinical studies revealed that women are 1.5 times more likely to develop AD than age-matched men, indicating that the female sex confers AD risk independent of age (Gao, Hendrie, Hall, & Hui, 1998). In addition to a higher incidence of AD, it is now well-established that sex influences both the development and progression of LOAD. For example, female AD patients have been shown to exhibit more severe cognitive decline than men during the progression of AD pathology (Chapman et al., 2011; Irvine, Laws, Gale, & Kondel, 2012; Schmidt et al., 2008). While the exact mechanisms underlying this sex bias are currently unknown, mounting evidence suggests that female vulnerability to AD is largely associated with the irreversible decline of female sex hormones during the onset of menopause (Zhao & Brinton, 2005; Zhao, Mao, & Brinton, 2009; Zhao, Wu, & Brinton, 2004). However, despite these findings, the precise molecular mechanisms underlying female vulnerability remain uncharacterized.

Epigenetic Influence. Epigenetics is loosely defined as a heritable or acquired change in gene expression and/or function that does not result from a change in the DNA sequence. It is suggested that these heritable changes in gene expression are passed through generations and are strongly influenced by environmental factors [Reviewed in (Amy S. Yokoyama, 2017)]. Epigenetics, a broad term that encompasses aspects of DNA methylation, histone modification, and non-coding RNA, is also now hypothesized to significantly contribute to the development of LOAD pathology. Several studies have examined DNA methylation and

hydroxyl-methylation in un-related individuals discordant for LOAD and have consistently observed alterations in global DNA methylation and hydroxy-methylation in a brain region-specific (Bradley-Whitman & Lovell, 2013; Chouliaras et al., 2013; Coppieters et al., 2014; Mastroeni et al., 2010; Rao, Keleshian, Klein, & Rapoport, 2012) and cell type-specific (Hof & Morrison, 1990; Phipps, Vickers, Taberlay, & Woodhouse, 2016) manner. However, perhaps the best evidentiary support for the impact of environmental factors on LOAD development arises from the examination of DNA methylation in monozygotic twins with opposing neuropathological outcomes (i.e. one with AD and one neurologically normal). One such study from Mastroeni and colleagues, which examined 5–methylcytosine levels in a set of monozygotic twins, revealed a significant decrease in global DNA methylation in two brain regions of the twin with AD. As one of the only key differences between the twins pertained to the twin with AD being exposed to pesticides on a regular basis, it was postulated that the alterations in brain DNA methylation were the result of environmental influence (Mastroeni, McKee, Grover, Rogers, & Coleman, 2009). In addition to DNA methylation and hydroxyl-methylation, non-coding RNAs, which comprise nearly 98% of the genome, are also being recognized for the contribution to neurological function or dysfunction [Reviewed in (Esteller, 2011)]. Micro RNAs (miRNAs) are short non-coding RNAs the function to regulate RNA silencing and post-transcriptional gene regulation. Within the brain, it has been demonstrated that miRNA dysregulation significantly impacts dendritic spine formation and neurite outgrowth (Cao, Yeo, Muotri, Kuwabara, & Gage, 2006) and thus significantly contributes to multiple CNS disorders including ataxia, multiple sclerosis, Parkinson's and Alzheimer's Disease [Reviewed in (Esteller, 2011).

Genetic risk factors. A long-standing observation in the field of LOAD research is the significantly increased AD risk associated with possession of the human apolipoprotein E ε4 allele (APOE ε4) (Saunders et al., 1993); a mutation that now represents the most predominant genetic risk factor for LOAD. Possession of the ε4 allele is clinically associated with an increased rate and severity of cognitive decline, a younger age of onset, and altered response to AD treatments (Blacker et al., 1997; Corder et al., 1994; Corder et al.,

1993; C. C. Liu, Kanekiyo, Xu, & Bu, 2013). Moreover, the ε4 allele has been shown to reduce brain glucose utilization (Langbaum et al., 2009), increase neuronal inflammation (Lynch et al., 2003), and is associated with increased Aβ dyshomeostasis (Drzezga et al., 2009; Drzezga et al., 2005). In addition to these data, studies have demonstrated that the APOE ε4-associated AD risk is significantly more pronounced in the female population. For example, a recent clinical study conducted in a cohort of 8,084 elderly individuals (healthy controls: n=5,496; MCI cases: n=2,588) demonstrated that the risk of clinical conversion from healthy aging to MCI or from MCI to AD conferred by the ε4 allele was significantly greater in women than in men; a finding that corresponds with several earlier reports (Altmann, Tian, Henderson, Greicius, & Alzheimer's Disease Neuroimaging Initiative, 2014; Farrer et al., 1997; Fleisher et al., 2005; Payami et al., 1994; Payami et al., 1996).

In addition to APOE ε4, two of the largest genome-wide association studies ever conducted have recently identified several other genetic risk factors that confer significant LOAD risk (Harold et al., 2009; Lambert et al., 2009). Of the genetic risk factors identified in these studies and the data collected from 1395 studies that collectively discuss 695 genes and over 2000 polymorphisms, clusterin (CLU), also known as apolipoprotein J (APOJ), has been established as the third most predominant genetic risk factor for LOAD. CLU, which belongs to the same protein family as APOE, has been demonstrated to regulate inflammation, oxidative stress, and amyloid homeostasis in the brain. Moreover, a pilot study conducted in our laboratory indicated a significant and irreversible decline in CLU mRNA in the early aging female, but not male, brain (Zhao, Mao, Woody, & Brinton, 2016). These data suggest that, similar to APOE ε4, CLU is also influenced by sex in the brain aging process and the pathogenesis of LOAD. Therefore, while numerous alternative genetic risk factors do exist, the remainder of this dissertation will focus on CLU. The following sections will summarize the current understanding of CLU and the known biological functions of CLU in the brain.

Clusterin: from form to function

Clusterin: discovery and nomenclature

In 1983, Blaschuk et al. identified a high molecular weight protein in ram rete testis fluid (Fritz, Burdzy, Setchell, & Blaschuk, 1983). Further analyses indicated that this unknown protein was capable of eliciting the "clustering" of Sertoli cells, TM-4 cells, and erythrocytes resulting in the name clusterin. In 1984, Griswold and colleagues purified a dimeric acidic glycoprotein (DAG) from the Sertoli cells of rat testes (Sylvester, Skinner, & Griswold, 1984). This abundantly expressed but uncharacterized protein was detected at several molecular weights via reducing chromatography (41 kDa and 29 kDa), Western blot (27 kDa, 21 kDa), and immunoprecipitation (70 kDa) (Sylvester et al., 1984). In 1988, another study identified a "novel" protein in human serum. This heterodimeric protein had a molecular mass of 80 kDa, was composed of two 40 kDa chains, and was sequentially unique to all other proteins. Furthermore, it was concluded that this protein, which was deposited in the renal glomeruli of patients with glomerulonephritis, was integrally involved in kidney health (Murphy, Kirszbaum, Walker, & d'Apice, 1988). As a result of these observations, Murphy and colleagues named this protein serum protein 40 kDa,40 kDa (SP-40,40) (Murphy et al., 1988). In 1990 and the years following, Harmony and colleagues identified and extensively characterized a component of high density lipoproteins in human plasma which was referred to as apolipoprotein J (ApoJ) (de Silva, Stuart, et al., 1990). However, upon the advent of DNA sequencing technology, it was determined that clusterin, DAG, SP-40,40, and ApoJ were in fact the same protein. In addition, clusterin was also "re-discovered" and subsequently re-labeled with alternative names including testosterone-repressed prostrate message-2 (TRPM-2) (Wong et al., 1993), KU70-binding protein 1 (KUB1) (Yang et al., 1999), complement lysis inhibitor (CLI) (Jenne & Tschopp, 1989) and sulfated glycoprotein-2 (SGP2) (Purrello et al., 1991). In 1992, a forum conducted at Cambridge University officially deemed this diverse protein clusterin (CLU).

Clusterin: from gene to protein

Generation of CLU mRNA and Protein Isoforms. CLU is a single copy gene located on the short arm of chromosome 8 in humans (8p21-12) (Dietzsch, Murphy, Kirszbaum, Walker, & Garson, 1992; Tobe et al., 1991) where it spans approximately 18,115 base pairs. Upon the splicing of 8 introns this 9-exon product spans approximately 2,877 base pairs, and is transcribed into at least 2 distinct mRNA isoforms with 1-3 canonical translational start sites (Exon 1, Exon 2, and Exon 3). CLU mRNA Isoform 2 (NM_001831.3), the most extensively characterized CLU mRNA isoform, is translated into the mature/secreted isoform of CLU (mCLU) that has been predominantly identified and studied in the field of CLU research. This mRNA isoform is translated into a 449 amino acid pre-protein beginning at a canonical translational start site located at base pair 187 in exon 2 (Schematic 3, lower panel). This pre-protein contains an N-terminal 22 amino acid endoplasmic reticulum (ER) signaling peptide (Exon 2, amino acids 1-22 or bp 187-252) and two nuclear localization sequences in exon 3 (amino acids 78-81 or bp 418-429) and exons 8-9 (amino acids 443-447 or bp 1513-1528). Following translation, the pre-protein is targeted to the ER where the 22 amino acid leader sequence (LS) is cleaved. Following LS cleavage, the peptide is heavily modified by N-linked glycosylation and proteolytically processed between R227 and S228 to form the two individual CLU subunits: the alpha subunit (CLUα, 34-37 kDa) and the beta subunit (CLUβ, 36-39 kDa). These two subunits are subsequently linked by 5 disulfide bonds to form an anti-parallel heterodimer (Burkey, deSilva, & Harmony, 1991) which, in non-reducing SDS-PAGE, is indicated to resolve at a molecular weight of 75-80 kDa (Stewart et al., 2007).

While the generation of mCLU is relatively well characterized in the literature, significant controversy still exists pertaining to the generation of alternative CLU mRNA isoforms. For instance, it is postulated that at least 1 alternative CLU mRNAs isoform is generated that lacks Exon 2. The most prominent of the hypothesized transcripts is an mRNA isoform that contains Exons 3-9. Translation of this secondary

transcript would therefore begin at the translational start site in exon 3 and would result in the production of a CLU protein isoform that lacks the ER signaling peptide but retains the nuclear localization sequences. This alternative CLU isoform, which would be non-ER targeted and therefore unglycosylated, is speculated to shuttle between the cytoplasm and the nucleus and is generally referred to in the literature as "nuclear" CLU (Schematic 3, middle panel). In contrast, some studies postulate that this secondary transcript lacks Exon 2 but contains both Exon 1 and Exon 3 with translation beginning in either Exon. To complicate matters, some studies indicate the generation of multiple minor CLU mRNA isoforms which lack portions of exon 2 and/or exon 5. The proteins translated from these relatively uncharacterized mRNA isoforms are generally referred to in the literature as "intracellular" CLU (Leskov, Klokov, Li, Kinsella, & Boothman, 2003; Prochnow et al., 2013; Reddy, Jin, Karode, Harmony, & Howe, 1996).

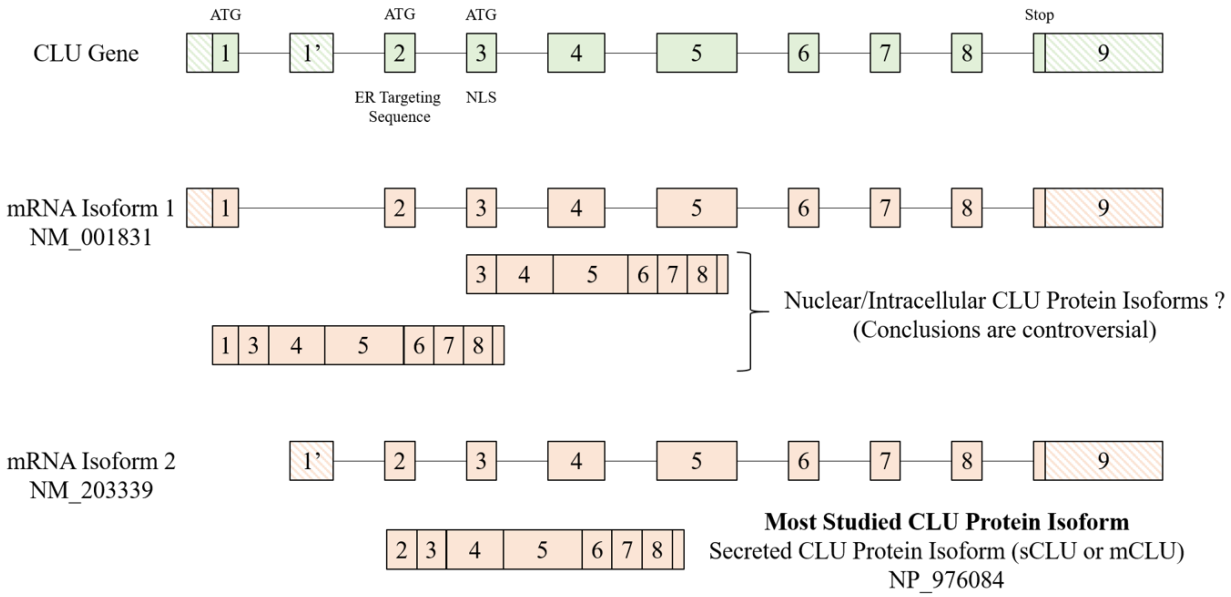

Schematic 3. Overview of Identified and Postulated CLU mRNA Isoforms. The CLU gene contains 9 exons that are transcribed into at least 2 CLU mRNAs. The generation of mRNA isoform 1 is still somewhat controversial, though it is generally agreed upon that this mRNA isoform lacks Exon 2 and therefore protein products translated from the mRNA would remain unglycosylated. In contrast, mRNA Isoform 2 has been extensively characterized in prior literature. This mRNA isoform is translated starting in Exon 2 to generate the secreted/mature CLU protein isoform that is predominantly studied in currently available literature.

mRNA and Protein Distribution. Initial characterization by Harmony et al. indicated the expression of CLU mRNA in liver, lung, spleen, heart, reproductive tissues, and brain with predominant expression in brain and reproductive tissues (de Silva, Harmony, Stuart, Gil, & Robbins, 1990). Since this initial characterization, several other research groups, including our own, have detected CLU mRNA and protein

expression in nearly all cell lines and tissue types tested. Moreover, CLU appears to be ubiquitously expressed on the subcellular level with multiple studies demonstrate CLU protein expression in the cytosol (Nizard et al., 2007), nucleus (Leskov et al., 2003), ER, Golgi apparatus, and mitochondria (Trougakos et al., 2009; H. Zhang et al., 2005). Within the brain, CLU expression has been detected within neurons (Pasinetti, Johnson, Oda, Rozovsky, & Finch, 1994), astrocytes (Cordero-Llana et al., 2011; Pasinetti et al., 1994; Zwain, Grima, & Cheng, 1994), microglia (Xie et al., 2005), and within the extracellular space (Kumita et al., 2007). Though the exact physiological functions of CLU in the brain remain a mystery, the nearly ubiquitous nature of CLU indicates the significance of this protein in cellular homeostasis.

Protein Structure. Despite being studied for over 35 years, very little information is available regarding the structure of CLU: a challenge that is likely due to the promiscuous nature of CLU as a binding/interacting partner (A. R. Wyatt, Yerbury, & Wilson, 2009) and tendency for CLU to self-aggregate (Fritz et al., 1983). For example, it has been previously demonstrated that CLU forms high molecular weight dimers and tetramers depending upon the pH of the cellular environment (Poon et al., 2002). This self-aggregating nature combined with the high levels of N-linked glycosylation have rendered the acquisition of replicable X-ray structures relatively difficult. Moreover, as the protein turnover time for mCLU is estimated to be approximately 30 minutes, the acquisition of sufficient quantities of pure recombinant heterodimerized mCLU have only been recently achieved (Dabbs & Wilson, 2014). However, despite these challenges some information is available pertaining to the primary, secondary and tertiary structure of CLU. For example, it is established that the primary structure of CLU, or the amino acid sequence of CLU, is highly homologous across species, with the highest degree of homology occurring within the disulfide bonding region (Londou, Mikrou, & Zarkadis, 2008; Purrello et al., 1991). Moreover, several studies using IR spectroscopy have indicated that nearly 60% of the secondary structure of CLU is comprised of α-helices (Rohne, Prochnow, Wolf, Renner, & Koch-Brandt, 2014; Stewart et al., 2007) with follow-up in silico analyses confirming the presence of 5 predominant amphipathic α-helices (Bailey, Dunker, Brown, Garner,

& Griswold, 2001). Regarding the tertiary structure of CLU, a study from Dunker et al. indicates that mCLU, which contains at least 2 flexible hydrophobic molten globule domains, is classified as a member of the intrinsically disordered protein family (Dunker et al., 2001). This family of proteins is defined by a general lack of tertiary structure. In reference to mCLU, this disorganized tertiary arrangement results in the exposure of molten globule domains to the cellular environment allowing for diverse hydrophobic interactions (Bailey et al., 2001). Despite these findings, CLU protein isoforms are yet to be crystallized in their entirety meaning that there is still an extensive amount of information that could be gleaned from this field of research.

Transcriptional regulation of CLU. Though the gene promoter of CLU is highly conserved across species, the transcriptional regulation of CLU is complex and controversial as the predominant CLU transcriptional regulators appear to differ between tissue and cell type. However, despite the controversy in the literature, it is generally agreed that CLU is primarily upregulated by cellular injury, cytotoxic insult, and various stress stimuli (Loison et al., 2006; Michel, Chatelain, North, & Brun, 1997; Trougakos & Gonos, 2006). For instance, Loisen and colleagues demonstrated that the CLU gene promoter contains an MG132 responsive region and a heat-shock element (HSE) indicating that proteasomal stress directly influences CLU transcription (Loison et al., 2006). Another study demonstrated that the CLU gene promoter contains both HSEs and an activator protein-1 (AP-1) response element indicating direct transcriptional regulation by stimuli derived from cellular proliferation and differentiation (Trougakos & Gonos, 2006). In addition to these data, alternative stress-related transcription factor response elements have been identified in the CLU gene promoter including a cAMP response element (CRE), an AP-2 response element, a specificity protein-1 (SP1) response element, and a glucocorticoid response element (GRE) (Michel et al., 1997; Wong et al., 1993). It has also been demonstrated that apoptotic stimuli, modulates CLU transcription, specifically in cancer. An early study from Cervellera et al. identified a MYB binding site in the 5' flanking region of CLU and that B-MYB, a MYB family member that regulates cellular proliferation and apoptosis, directly bound to and transactivated the CLU gene (Cervellera et al., 2000). CLU

transcription is also regulated by several different growth factors including nerve growth factor (NGF) and transforming growth factor beta (TGFβ) (Gutacker, Klock, Diel, & Koch-Brandt, 1999; Jin & Howe, 1997, 1999). For instance, it has been demonstrated that TGFβ induces the upregulation of CLU gene expression by stimulating the interaction between the CLU gene promoter and AP-1 (Jin & Howe, 1997). An extension of these studies demonstrated that TGFβ deficiency resulted in the repression of CLU gene expression via interaction between c-Fos and the CLU gene promoter; an interaction that was abrogated upon cellular stimulation with TGFβ (Jin & Howe, 1999).

Post-translational modification. In addition to transcriptional regulation, CLU is also regulated by several types of post-translational modification (PTM); the most predominant type being N-linked glycosylation. N-linked glycosylation, the addition of oligosaccharides to the N in the side chain of an asparagine residue, occurs in the ER/golgi body (Schematic 4) and is known to influence a myriad of cellular processes by mediating the response to extra- and intracellular signaling cues. mCLU is N-glycosylated at 6-7 asparagine residues (N86, N103, N145, N291, N354, and N374) during ER-Golgi processing: a modification that comprises approximately 20-25% of the total mass of mCLU (Kapron et al., 1997). While glycosylation status was originally thought to have little to no impact on CLU function (Dunker et al., 2001; Stewart et al., 2007) a recent study demonstrated that the chaperone activity of mCLU is dependent upon mCLU glycosylation (Rohne et al., 2014). This study also demonstrated that the glycosylation of a non-secreted CLU protein isoform did not result in chaperone activity indicating that glycosylation-mediated effects are specific to the mCLU isoform. It has also been established that complete deglycosylation of mCLU results in a 70-90% decrease in mCLU chaperone activity and a significant decrease in the number of α-helices in the secondary structure of CLU. These data suggest that the lack of chaperone activity in deglycosylated mCLU could be, in part, due to the significant changes in secondary structure. Additionally, this study indicates that partially glycosylated mCLU retains chaperone activity suggesting that the core glycan is crucial for mCLU function while the side chains of added N-linked glycans may be dispensable (Schematic

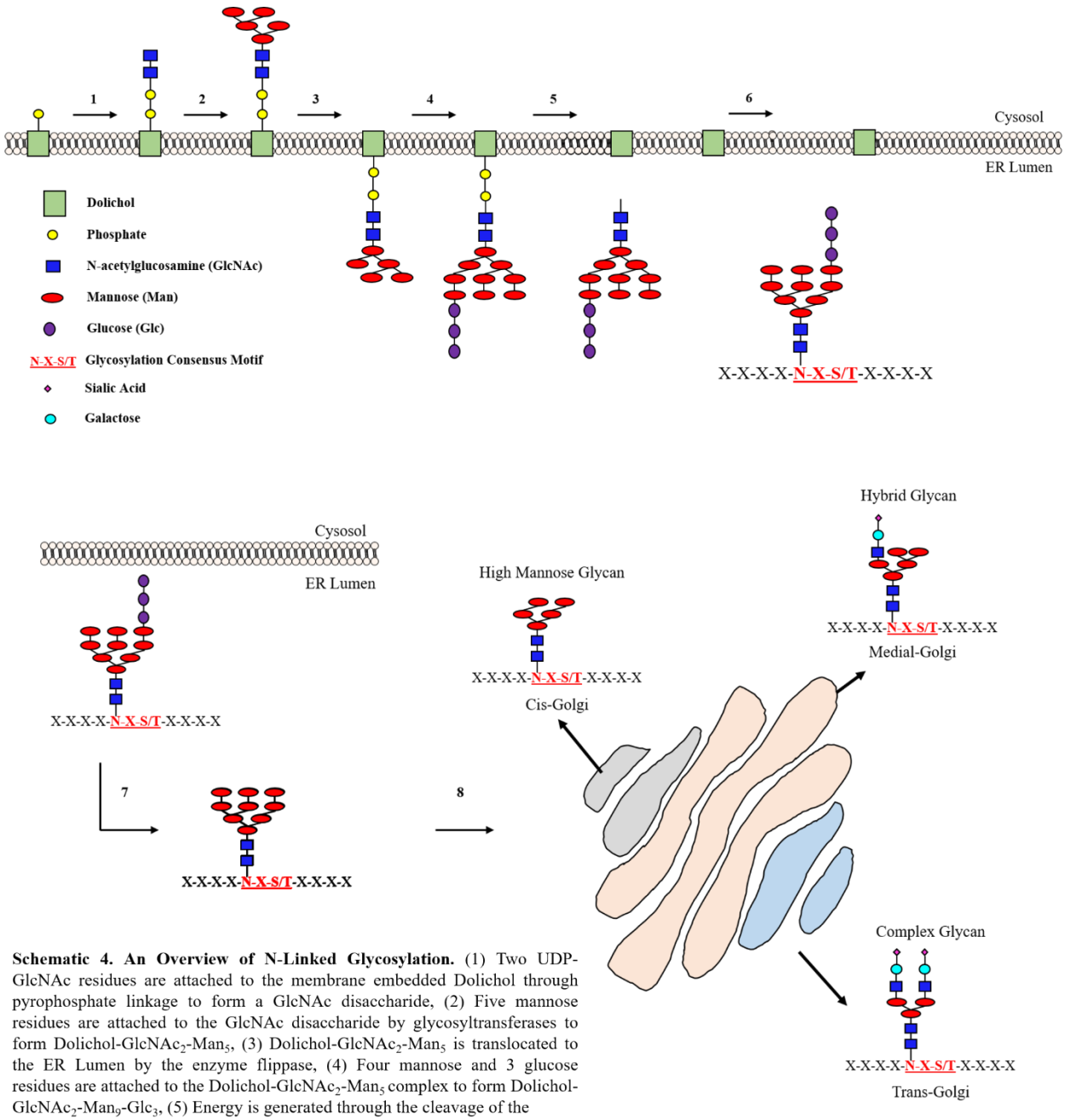

Schematic 4. An Overview of N-Linked Glycosylation. (1) Two UDP-GlcNAc residues are attached to the membrane embedded Dolichol through pyrophosphate linkage to form a GlcNAc disaccharide, (2) Five mannose residues are attached to the GlcNAc disaccharide by glycosyltransferases to form Dolichol-$GlcNAc_2$-Man_5, (3) Dolichol-$GlcNAc_2$-Man_5 is translocated to the ER Lumen by the enzyme flippase, (4) Four mannose and 3 glucose residues are attached to the Dolichol-$GlcNAc_2$-Man_5 complex to form Dolichol-$GlcNAc_2$-Man_9-Glc_3, (5) Energy is generated through the cleavage of the pyrophosphate bond between the dolichol and $GlcNAc_2$-Man_9-Glc_3 complex, (6) The glycosyltransferase oligosaccharyltransferase utilizes the energy generated in step 1 to transfer the $GlcNAc_2$-Man_9-Glc_3 complex to an asparagine residue in a select polypeptide, (7) following the transfer of the glycan to an appropriate Asn residue, glucosidases cleave the three Glc residues from the $GlcNAc_2$-Man_9-Glc_3 glycan, and (8) The $GlcNAc_2$-Man_9 modified protein is then transferred to the Golgi apparatus where it is modified into 1 of three types of glycans: High Mannose Glycans, Hybrid Glycans, or Complex Glycans.

5) (Rohne et al., 2014). Parallel to these findings, a study from Kang et al. indicated that ER stress, which inhibits protein glycosylation, resulted in rapid retro-translocation of mCLU from the ER yielding several hypo-glycosylated CLU isoforms. These hypo-glycosylated isoforms, which are misfolded and generally non-functional, are rapidly poly-ubiquitinated under normal conditions and cleared through proteasomal

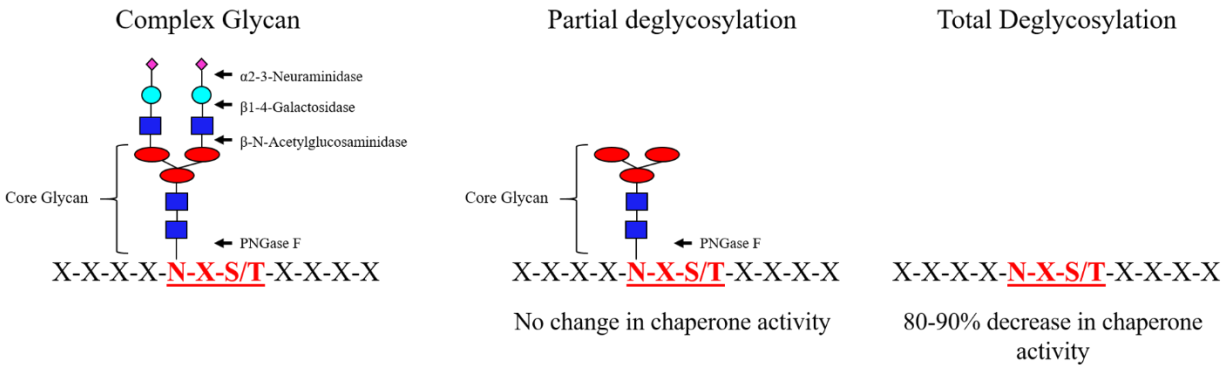

Schematic 5. Core N-linked Glycosylation is Essential for mCLU Chaperone Activity. Previous data from Harmony and colleagues indicate that mCLU is modified by sialic acid-containing complex glycans (left panel). Partial de-glycosylation via enzymatic digestion with indicated endoglycosidases results in the cleaveage of complex glycan side chains without impacting the core glycan structure or CLU chaperone activity (Middle Panel). Full deglycosylation via enzymatic digestion with PNGase F results in a 80-90% decrease in the chaperone activity of mCLU (Right panel).

degradation. However, if the proteasome is chemically inhibited following ER stress, hypo-glycosylated CLU accumulates in the cytosolic compartment resulting in cytotoxicity. Collectively, these studies indicate that glycosylation is crucial for specifically mCLU chaperone activity. CLU is also a primary target for ubiquitination and phosphorylation. It has been demonstrated that "nCLU" is a target for K63 ubiquitination through the ubiquitin E3 ligase, product of von Hippel-Lindau (pVHL). However, contrary to the canonical function of protein ubiquitination, K63-linked ubiquitination of CLU does not target CLU for destruction, rather it promotes CLU translocation to the nuclear compartment for reasons that are currently unknown (Xue et al., 2012). Pertaining to CLU phosphorylation, a recent proteomics study which focused on the identification of the serum phospho-proteome has identified three different phosphorylation sites at residues Thr393, Ser394, and Ser39 within the CLU protein. Additionally, a more recent study indicated that treatment of hepatocytes with 10 mM glucose and fructose significantly increased the levels of mCLU serine phosphorylation. This same study demonstrated increased mCLU serine phosphorylation in both the skeletal muscle and the liver of rats that were orally administered high doses of glucose and/or fructose indicating that phosphorylated CLU may interact with or respond to the activation of glucose-sensitive cellular bioenergetic pathways. In addition to phosphorylation and ubiquitination, an early report indicated that CLU is iodinated at 1 of the 12 tyrosine residues within the CLU protein. This iodination occurs within the apical plasma membrane of thyrocytes and is suggested to serve as a mechanism by which the thyroid

gland can conserve iodine, which is relatively rare in the body (Lemansky, Brix, & Herzog, 1999). It is also suggested that CLU activity is regulated by both sialylation (Ghosh, Hale, & Lakshman, 2001), most likely through N-linked glycosylation, and acetylation (Nuutinen, Suuronen, Kyrylenko, Huuskonen, & Salminen, 2005), however, definitive acetylation sites have not been identified.

Clusterin in Cancer: Current understanding

Perhaps one of the most thoroughly understood areas of CLU research is the role of mature secreted CLU in cancer development. Findings from multiple cancer cell and tumor types consistently indicate a role for CLU specifically in regards to cancer cell survival, tumor metastasis, and chemoresistance. The following sections will briefly discuss the current understanding of CLU in cancer and the potential of CLU inhibition as a therapeutic option.

Clusterin in cancer development. Increased sCLU expression is often associated with aggressive chemo-resistant cancers [Reviewed in (Koltai, 2014)]. Clinical studies indicate that higher levels of CLU are often found in aggressive or highly metastatic tumors derived breast cancer carcinoma (Redondo et al., 2000) and triple negative breast cancer (D. Zhang et al., 2012), ovarian cancer (Yang, Li, & Xie, 2009), prostate cancer [Reviewed in (Higano, 2013)] as well as several other cancer/tumor types (He et al., 2009; Hoeller et al., 2005; Lau et al., 2006; Miyake, Gleave, Kamidono, & Hara, 2002; Miyake, Gleave, Arakawa, Kamidono, & Hara, 2002). In contrast cancer cell and/or tumor types with low endogenous CLU expression exhibit increased chemosensitivity. For example, human testicular seminoma, which exhibits relatively low CLU expression, is highly sensitive to both radio- and chemotherapy (B. Liu et al., 2013; Tang et al., 2013). sCLU expression levels are also associated with tumor aggressiveness and metastatic potential. For instance, increased sCLU expression in clear cell renal carcinoma results in aggressive tumor behavior mediated via induction of extracellular signal-regulated kinase (ERK)1/2 signaling and matrix metallopeptidase (MMP)-9 expression while knockdown of sCLU resulted in reduced cancer cell migration

and invasion, and decreased tumor metastasis (X. Wang, Luo, Dong, Yu, & Zhao, 2014). In prostate cancer cells, sCLU has been shown to regulate the ubiquitination and degradation of COMM domain-containing protein 1 (COMMD1) and inhibitor of kappa B (IκB) which results in the increased translocation of NF-κB to the nucleus and subsequent up-regulation of NF-κB target genes. Parallel to these findings, knockdown of sCLU results in the sequesterization of NF-κB to the cytosol via stabilization of COMMD1 and IκB (Essabbani, Margottin-Goguet, & Chiocchia, 2010; Zoubeidi et al., 2010). In epithelial ovarian cancer cells, sCLU is correlated with increased angiogenesis (Fu et al., 2013) and increased chemoresistance (Wei et al., 2009) while depletion of sCLU is associated with reduced proliferation, invasion, and migration in human breast adenocarcinoma (Li et al., 2012; Niu et al., 2012) and renal carcinoma (Shi et al., 2013) cells and increased tumor sensitivity to Paclitaxel (Hassan et al., 2011) and Cisplatin treatment (C. H. Lee et al., 2002).

Two primary models exist to explain the sCLU-mediated cancer survival and chemoresistance. First, studies pertaining to Paclitaxel-resistant ovarian cancer have demonstrated that sCLU mediates chemoresistance by physically binding the drug paclitaxel thereby decreasing drug bioavailability (Park et al., 2008). However, as tumors with high CLU levels are known to exhibit chemoresistance to multiple chemotherapeutic agents, most of which do not physically interact with CLU, this interaction does not fully explain the pro-survival properties of increased sCLU. It is now widely accepted that the primary mechanism of sCLU-mediated cancer cell survival revolves around the interaction between sCLU, Ku-70, and the pro-apoptotic protein Bax. It has been repeatedly demonstrated that elevated sCLU levels increase cancer cell and/or tumor survival by interfering with Bax-mediated apoptosis. Specifically, sCLU sequesters Bax to the cytosol via interaction with Ku-70 thus inhibiting Bax translocation to the outer mitochondrial membrane (Hsu, Wolter, & Youle, 1997; Trougakos et al., 2009; H. Zhang et al., 2005). While there are several other minor pathways suggested to play a role in sCLU-mediated cancer cell survival and a myriad of studies indicating the cytoprotective role of CLU in cancer, these studies discussed

here clearly indicate that overexpression of sCLU results in enhanced tumor aggressiveness and survival by inhibiting intrinsic apoptosis while knockdown of sCLU results in increased chemosensitivity.

Clusterin as a therapeutic target for cancer treatment. As sCLU expression clearly plays a prominent role in cancer cell and tumor survival, therapeutic strategies designed to inhibit or repress sCLU expression in combination with multi-drug treatment are now being investigated. *In vitro* administration of CLU-targeting siRNA or shRNA have indicated a reduction in the metastatic potential of cancer cells and thus provide promising preliminary data for the development of CLU inhibitors. These data along with others resulted in the generation of Custirsen (OGX-011); a second generation 2'-methoxyethyl modified phosphorothioate antisense oligonucleotide inhibitor of CLU. Custirsen, which blocks the generation of 90% of serum CLU protein at a dose of 640 mg, was found to be relatively well tolerated by patients and distributed evenly throughout intended tissues in phase I clinical trials (Chi et al., 2005; Chi et al., 2008) Furthermore, 6 phase II clinical trials performed on patients with non-small cell lung cancer (Laskin et al., 2012), metastatic breast cancer (Chia et al., 2009), and metastatic castration-resistant prostate cancer (CRPC) (Chi et al., 2010; Saad et al., 2011) successfully confirmed the safety and efficacy of Custirsen in combination with various chemotherapy regimens. Moreover, 33% of patients in the breast cancer trial and 31% of patients in the lung cancer trial responded to therapies involving co-treatment with Custirsen and exhibiting consistently reduced serum CLU levels. These findings were consistent with those from the prostate cancer studies which concluded that that clusterin is a useful therapeutic target in the treatment of CRPC [Reviewed in (Xiu, Dong, Li, & Li, 2015)]. With successful Phase I/II trials completed Custirsen has recently been the focus of three randomized, global, phase III trials: the SYNERGY trial (NCT01188187), the AFFINITY trial (NCT01578655) and the ENSPIRIT trial (NCT01630733). The SYNERGY trial, which was completed in 2014, investigated the impact of adding Custirsen to standard first-line docetaxel/prednisone for men with CRPC (Chi et al., 2015). The AFFINITY trial, which was completed in 2015, investigated the effect of Custirsen in combination with Cabazitaxel and Prednisone as

a second-line chemotherapy in prostate cancer (Beer et al., 2017). Unfortunately, results from both studies indicate that, while the treatments were well-tolerated, overall survival was not significantly impacts in patients treated with Custirsen and chemotherapeutic regimens, when compared with patients treated with chemotherapeutic agents alone (Beer et al., 2017; Chi et al., 2015). While the ENSPIRIT trial is still ongoing, it is crucial that investigators attempt to understand possible reasons why these clinical trials, which had reasonably large study populations (600-1100 patients), were not successful. One key contributing factor could be the stage of cancer in the study populations. As the studies in question investigated the impact of Custirsen in only those patients with advanced metastatic cancers, it is highly possible that disease progression in the study population was beyond the stage where inhibition of CLU protein expression would yield beneficial effects; however this hypothesis requires further testing.

Clusterin in Late-onset Alzheimer's disease: clinical findings

The clinical association of CLU with AD pathology has recently been a matter of significant interest with numerous clinical trials and meta-analyses examining the association of CLU SNPs with AD risk in various ethnic populations. In addition, it has been suggested that circulating CLU levels may be used as a predicative biomarker for rate and/or severity of neurocognitive decline, though results on this topic are inconsistent. The following sections will review the literature pertaining to CLU SNPs and AD risk as well as literature pertaining to CLU as an AD biomarker.

Clusterin gene polymorphisms in LOAD. Since the initial determination of CLU SNP-associated AD risk by Harold et al. and Lambert et al. (Harold et al., 2009; Lambert et al., 2009), there have been approximately 40 independent follow-up meta-analyses and case-control studies that have examined the association between CLU SNPs and AD risk. These reports were located using the following search and filter parameters: a PubMed search focused on articles pertaining to CLU SNPs in AD was performed. Resulting articles were reviewed and those studies which provided a listing of the CLU SNP(s) studied,

population demographics, and a thorough description of statistical analysis in which ApoE status was included as a variable are included in this comparison. Though conflicting evidence exists, the majority of the studies indicate that genetic variation in CLU increases the risk of developing AD independent of APOE ε4 status. There are approximately 355 identified SNPs in the CLU gene (Masoodi, Al Shammari, Al-Muammar, Alhamdan, & Talluri, 2013), however, it appears that the primary risk-conferring CLU SNP is the C allele of the rs11136000 SNP. Of the 33 studies examined, 25 studies either include or exclusively focus on the impact of the rs11136000 SNP on AD risk; however, the results are inconsistent. 13 studies conclude that possession of rs11136000 does confer increased AD risk (Braskie et al., 2011; Chen et al., 2012; Corneveaux et al., 2010; Ferrari et al., 2012; Harold et al., 2009; G. Jun et al., 2010; Lambert et al., 2009; Lancaster et al., 2011; Ma et al., 2011; Schurmann et al., 2011; Seshadri et al., 2010; Thambisetty et al., 2013) while 10 studies conclude no significant association between rs11136000 and AD (Golenkina et al., 2010; Kamboh et al., 2012; Klimkowicz-Mrowiec et al., 2013; Komatsu et al., 2011; J. H. Lee et al., 2011; Lu et al., 2014; Yu et al., 2010; Yu et al., 2013). Moreover, 2 studies conclude that possession of the rs11136000 SNP reduces risk of AD development (Lin et al., 2012; Pedraza et al., 2014). A possible explanation for these discrepancies may be found by examining the population ethnicities. Of the 13 studies that conclude rs11136000 confers AD risk, 11 studies are performed in a predominantly or exclusively western European or American Caucasian population. Alternatively, 9 of the 10 studies that conclude no significant association (NSA) between rs11136000 and AD were performed in Asian, eastern European and Russian, Middle Eastern, or Hispanic populations indicating that the risk associated with the rs11136000 SNP may vary based on ethnicity. Contrary to these data, 2 separate studies performed in exclusively German and American Caucasian populations found NSA between rs11136000 and AD risk. Moreover, the notion that rs11136000 does not confer AD risk in Asian populations is contradicted by 2 independent studies that indicate rs11136000-mediated AD risk in exclusively Chinese populations. As all the presented studies performed in Asian populations are adjusted for age, gender, and APOE status, and are comprised of numerically similar sample sizes, it is difficult to identify the exact reason underlying these discrepancies. One observation is that some studies have divided study populations into smaller groups based upon the

specific nucleotide substitution located at the rs11136000 SNP site (i.e. C,T substitution) while others have examined only rs11136000 carriers vs. non-carriers. The failure to stratify study populations based on the rs11136000 allele/genotype would have a significant impact on study outcome as the C allele of rs11136000 is considered the risk-conferring allele while the T allele is considered normal and neuroprotective, respectively (i.e. C = risk allele, T = protective). Specifically, studies have indicated that one copy of the C allele confers a 1.16-fold increased chance of developing LOAD and is present in 88% of Caucasians (Harold et al., 2009; Lambert et al., 2009) while 2 copies of the C-allele are present in 36% of the Caucasian population (Bertram, McQueen, Mullin, Blacker, & Tanzi, 2007; Braskie et al., 2011). From a clinical standpoint, possession of the C allele is associated with faster cognitive decline in pre-clinical AD (Thambisetty et al., 2013) and lower memory scores in healthy elderly controls and elderly AD patients (Masoodi et al., 2013). In addition, young healthy carriers of the C allele exhibit neural hyper-activation in memory-associated brain regions during working memory tasks (Lancaster et al., 2011), neural inefficiency in memory-related pre-frontal and limbic areas during working memory (Lancaster et al., 2015), and reduced coupling between hippocampus and pre-frontal cortex during memory processing (Erk et al., 2011). Structurally speaking, possession of the C allele is associated with diminished white matter integrity in several brain regions (Thambisetty et al., 2012) and increased longitudinal ventricular expansion in elderly patients independent of APOE ε4 and dementia status (Roussotte et al., 2014). Taken together, these data indicate that the rs11136000 SNP is significantly associated with the development of AD in predominantly Caucasian populations and that the rs11136000 AD-associated risk may be initiated several decades prior to the onset of AD.

In addition to rs11136000, another CLU SNP, rs9331888, which was also identified by Lambert and colleagues in the original GWAS, has also been repeatedly investigated as an AD risk SNP. Of the 33 studies examined, 7 clinical studies and 2 meta-analyses focus on the association of rs9331888 with AD risk (Chen et al., 2012; Komatsu et al., 2011; Lambert et al., 2009; Lu et al., 2014; Shuai et al., 2015; Toral-

Rios et al., 2015; Xing et al., 2012; Yu et al., 2010; S. Zhang et al., 2015). However, similar to that of rs11136000, the results vary and appear to be dependent upon population ethnicity. For instance, two separate meta-analyses conclude that rs9331888 confers AD risk in Caucasian but not Asian populations (Shuai et al., 2015; S. Zhang et al., 2015). However, 2 separate case-control studies performed in exclusively Chinese populations both indicate that rs9331888 is significantly associated with AD risk (Xing et al., 2012; Yu et al., 2010). In addition to differing and/or small sample sizes, one possible confounding factor could be sex of the study population. As sex modulates an individual's risk for LOAD, it is likely that stratification of study populations by sex will have a significant impact on the study results. In conclusion, future studies should strongly consider variables such as ethnicity and gender stratification to accurately gauge AD risk conferred by CLU SNPs.

Clusterin as an AD biomarker. In 1992, it was suggested that peripheral CLU (then referred to as SGP-2) expression may serve as a potential genetic biomarker for predicting the onset and/or severity of neurodegenerative disorders such as LOAD (Michel, Chabot, Moyse, Danik, & Quirion, 1992). Though this concept was proposed over 20 years ago, the possibility of CLU as an AD biomarker is only recently being examined. Since 2010, 10 different studies have been performed with the aim of determining the validity of CLU as an AD biomarker. However, the conclusions of these studies are contradictory at best. Of the 10 studies examined, 6 studies conclude that increased plasma CLU levels are associated with increased rate of cognitive decline (Sattlecker et al., 2014), increased white matter atrophy (Song et al., 2012), increased risk for AD (Jongbloed et al., 2015), and were indicative of greater fibrillar Aβ burden (Schrijvers, Koudstaal, Hofman, & Breteler, 2011). However, contrary to these findings, 4 studies conclude that CLU levels are not significantly different between control subjects and subjects with AD, dementia, depression or MCI suggesting that peripheral CLU is unreliable as an AD biomarker (Dukic et al., 2016; L et al., 2011; Mukaetova-Ladinska et al., 2015; Mukaetova-Ladinska et al., 2012; Silajdzic, Minthon, Bjorkqvist, & Hansson, 2012). One primary difference between these studies is the fluid that was analyzed

for CLU concentration. The 6 studies concluding that CLU would be a reliable biomarker utilize plasma samples for analysis whereas the 3 of the 4 studies indicating no difference between control and AD subjects measure serum or platelets. Another key difference between these conflicting reports is the sample size. In 3 of the 4 studies concluding that CLU would not be a reliable AD biomarker, the sample size per group is less than 70 subjects whereas most of the studies indicating the possibility of CLU as a peripheral biomarker contain several hundred subjects per group. Therefore, it is also possible that these differences are the result of inadequate sample size. Despite these discrepancies, these studies collectively suggest that at least plasma CLU could provide a predictive biomarker for determining the risk for AD.

Clusterin in the brain: proposed mechanisms of action

Of the identified and postulated CLU protein isoforms, mCLU is by far the most studied and has been described as a chaperone-like protein that clears misfolded proteins, cellular debris, and protein aggregates from the cytosol and extracellular space (Bailey et al., 2001; Bartl, Luckenbach, Bergner, Ullrich, & Koch-Brandt, 2001; Kounnas et al., 1995; Lakins et al., 2002; Law & Griswold, 1994; Leeb, Eresheim, & Nimpf, 2014; Poon et al., 2002; A. Wyatt, Yerbury, Poon, Dabbs, & Wilson, 2009). In contrast, the alternative CLU protein isoforms (nCLU and icCLU in the literature) are suggested to exhibit solely pro-apoptotic characteristics, though these results are inconsistent at best (Debure et al., 2003; Dia & Mejia, 2010; Kimura, Asami, & Yamamoto, 1997; Leskov et al., 2003; Prochnow et al., 2013). This section will review the available literature pertaining to CLU isoforms in the brain with particular emphasis on the molecular mechanisms by which CLU protein isoforms regulate amyloid homeostasis, inflammation, and apoptosis.

Clusterin and the regulation of Aβ. In the early 1990s, CLU mRNA and protein levels were found to be significantly elevated in AD brain, specifically in the frontal cortex and hippocampus of post-mortem AD brain tissue (Lidstrom et al., 1998; May et al., 1990). Shortly after these discoveries, McGeer et al.

demonstrated robust CLU immunoreactivity within senile plaques (McGeer, Klegeris, Walker, Yasuhara, & McGeer, 1994). It was further demonstrated that mCLU bound soluble Aβ proteins in the cerebral spinal fluid (CSF) (Ghiso et al., 1993) and that CLU expression increased the solubility of Aβ and prevented Aβ aggregation (Matsubara, Soto, Governale, Frangione, & Ghiso, 1996). These data strongly suggested that CLU may play an important role in the pathogenesis of AD via regulation of brain amyloid burden. However, contrary to these findings, it has also been demonstrated that increased CLU expression exacerbated $A\beta_{1-42}$-induced neurotoxicity (Oda et al., 1995). Moreover, DeMattos et al. demonstrated that Aβ plaque formation was facilitated by CLU in an animal model of AD suggesting that brain CLU is pro-amyloidogenic in nature (DeMattos et al., 2002). These literary contradictions continued to persist until 2007 when a study from Yerbery and colleagues provided a possible explanation for the simultaneously pro- and anti-amyloidogenic effects associated with mCLU (Yerbury et al., 2007). This study indicated that the pro-amyloidogenic effects of mCLU were restricted to conditions in which $A\beta_{1-42}$ was present in molar excess. Under these conditions, mCLU, which functions as a chaperone-like protein to temporarily stabilize misfolded proteins (Poon, Easterbrook-Smith, Rybchyn, Carver, & Wilson, 2000), bound to and stabilized $A\beta_{1-42}$ thereby facilitating Aβ aggregation. Alternatively, when mCLU was present at much higher but still substoichiometric levels, mCLU provided substantial anti-amyloidogenic effects by inhibiting plaque formation (Yerbury et al., 2007). These data suggest that CLU may exhibit neuroprotective characteristics in preclinical or early stages of AD when brain amyloid burden is significantly lower. Alternatively, CLU may exert a negative impact during later stages of AD when brain amyloid burden is extensive, though this hypothesis is yet to be tested. Parallel to this notion, a more recent study performed in rat brains indicated that mCLU prevented Aβ42-induced learning and memory impairments, reduced Aβ42-induced glia inflammation, and reduced Aβ42-mediated neuronal degeneration when Aβ42 oligomers were incubated with mCLU prior to brain injection. However, these effects were not observed in rats injected with pre-formed Aβ42 oligomers and mCLU without pre-incubation indicating that mCLU does prevent Aβ42-induced neurotoxicity prior to extensive Aβ42 oligomerization (Cascella et al., 2013). In addition to these studies, mCLU has been shown to impact the rate of Aβ42 clearance. A study from Bell and colleagues

demonstrated that the rate of Aβ clearance was increased by as much as 83% when bound to CLU. This same study further demonstrated that CLU-bound Aβ is transported across the blood-brain barrier specifically through LRP2-mediated transport while APOE-bound Aβ was transported through LRP-1

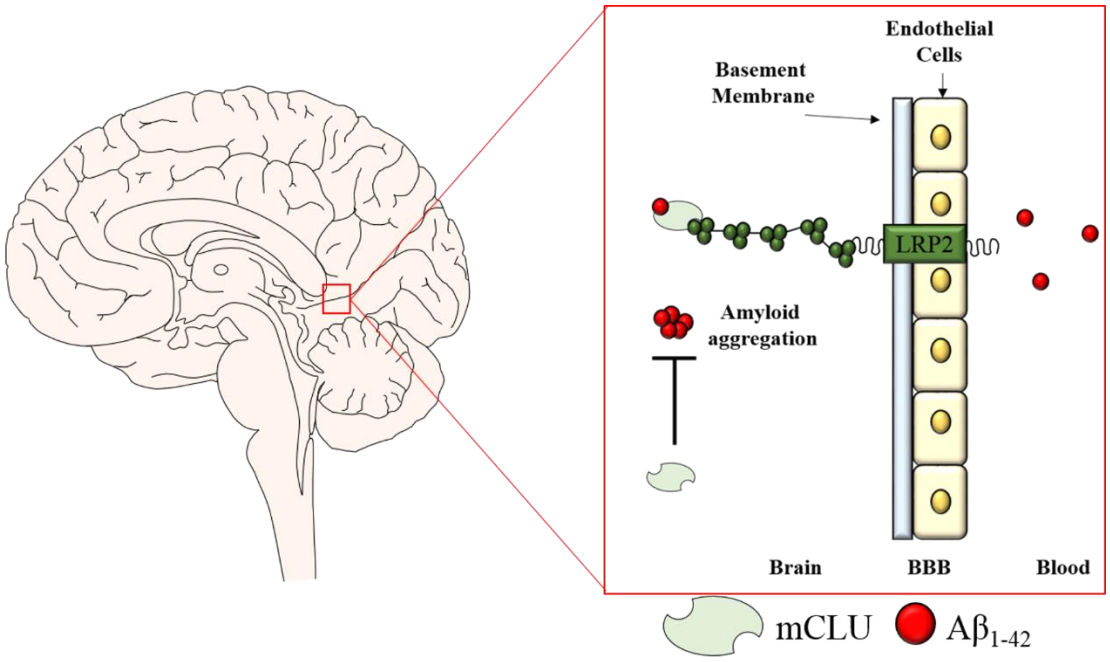

Schematic 6. The Relationship Between Secreted Mature CLU and Neurotoxic Aβ1-42. Previous studies have determined that extracellular mCLU binds to and clears neurotoxic $A\beta_{1-42}$ from the brain via LRP-2 mediated transport. Moreover, mCLU inhibits $A\beta_{1-42}$ aggregation by inhibiting oligomerization.

(Bell et al., 2007) (Schematic 6). While, the regulation of Aβ by mCLU is relatively well characterized, one question that remains unanswered is whether alternative CLU isoforms exert some impact on amyloid homeostasis. It has been demonstrated that Aβ toxicity induces the expression of intracellular CLU protein isoforms in neurons, however, the physiological impact of increased icCLU expression was not determined in this study (Killick et al., 2014). At present, no literature specifically implicates a role for alternative CLU protein isoforms in the regulation of Aβ, however, as these isoforms are reportedly induced by cellular stress in multiple peripheral cell lines and upon treatment with exogenous Aβ, it is likely that these CLU protein isoforms mediate some unknown effect on amyloid homeostasis in the brain, however more research is needed before a conclusion can be made.

Clusterin and Brain Inflammation. It has been postulated that persistent inflammation, likely caused by the deposition of neurotoxic protein aggregates in the brain, is a key component of LOAD (Akiyama et al., 2000). Early studies suggest that CLU inhibits the activation of the complement system in the brain (Choi, Mazda, & Tomita, 1989; Choi, Nakano, Tobe, Mazda, & Tomita, 1990; Kirszbaum, Bozas, & Walker, 1992; Murphy et al., 1988). For instance, CLU (then referred to as SP-40,40) was demonstrated to prevent the formation of the membrane attack complex (MAC), suggesting that increased CLU would suppress initiation of acute inflammation. However, these data were contradicted by a more recent study that demonstrated CLU-mediated activation of the major histocompatibility complex class II (MHC II) antigen in primary cultures of rat microglia. This same study showed that administration of exogenous CLU resulted in the direct activation of microglia in the brain and the subsequent secretion of pro-inflammatory cytokines such as tumor necrosis factor alpha (TNF-α) indicating that increased CLU expression induces the acute inflammatory response (Xie et al., 2005). These findings were corroborated by another study that demonstrated increased CLU staining within reactive microglia in the cortices of rats following cerebral ischemia (Van Beek et al., 2000). Collectively, these studies suggest that increased CLU expression results in the activation of glial cells and the subsequent secretion of pro-inflammatory mediators. Therefore, it is possible that the increased secretion of cytokines such as TNF-α could contribute to chronic inflammation in AD brain, however this hypothesis requires further testing.

Clusterin in Neurotoxicity, Oxidative Stress, and Apoptosis. Several studies performed in human cancer cell lines have demonstrated that mCLU and the intracellular "nCLU" protein isoforms exhibit opposing effects on cell death pathways. mCLU has been shown to protect cells from oxidative stress and inhibit intrinsic apoptosis by interacting with and stabilizing the KU-70-Bax protein complex (H. O. Jun et al., 2011; N. Kim, Han, et al., 2012; Miyake, Chi, & Gleave, 2000; Trougakos et al., 2009; H. Zhang et al., 2005). In contrast, the proposed nCLU isoform is suggested to initiate intrinsic apoptotic pathways resulting in rapid cell death (Dia & Mejia, 2010; Miyake et al., 2000). The contrasting functions of these two protein

isoforms appear to also exist in the brain, however, unlike cancer-focused studies, relatively few brain-based investigations have included an examination of the apoptotic characteristics of alternative CLU protein isoforms. An early study from Schreiber et al. demonstrated that CLU (then referred to as SGP-2) mRNA expression was rapidly and transiently increased in astrocytes, but not CA3 and CA1 neurons, following administration of kanic acid (KA), a neurotoxic seizure-inducing compound (Schreiber, Tocco, Najm, & Baudry, 1993). Another study performed in WT, human CLU overexpressing (hCLU-OE) mice, and Clu-knockout (CLU-KO) mice subjected to middle cerebral artery occlusion (MCAO) indicated that CLU overexpression resulted in reduced brain injury. Specifically, this study demonstrated a 30-50% increase in CLU mRNA expression 7 days post-ischemia in the ischemic brain hemisphere specifically in the penumbral area (the area that separates necrotic from normal brain tissue). Morphometric analysis of the ischemic hemisphere revealed that the penumbra was significantly thinner in hCLU-OE mice and significantly thicker in CLU-KO mice when compared with WT mice indicating an inverse relationship between CLU mRNA expression and brain injury (Wehrli et al., 2001). Collectively, these two studies strongly support a neuroprotective role for CLU in the brain following significant brain injury. In contrast, ethanol-mediated toxicity has been shown to significantly increase CLU expression in the cortex and amygdala. This up-regulated CLU, which was shown to interact with Bcl-XL, was translocated to the nucleus upon exposure to ethanol, and was associated with increased cell death suggesting that these effects were mediated by an intracellular CLU protein isoform (N. Kim, Han, et al., 2012). Another study performed in neonatal mice subjected to hypoxic-ischemic brain injury indicated that CLU accumulated in dying neurons following brain injury. Moreover, this study indicated that CLU deficient mice exhibited 50% less brain injury when compared to wild-type controls indicating that CLU expression exacerbates neuronal cell death following brain injury (Han et al., 2001). Collectively, these studies indicate that intracellular CLU protein isoforms may be associated with increased cell death following traumatic brain injury or in response to cytotoxic stimuli.

Significance of this Dissertation

Clinical studies have clearly indicated the association of the rs11136000 SNP (CC) with the development of LOAD. Moreover, studies in cancer cell lines have demonstrated that at least 1 CLU protein isoform (mCLU) plays a significant role in cellular survival and resistance to drug-induced apoptosis. In addition, mCLU is known to significantly regulate the levels and aggregation of extracellular Aβ in a mechanism that is thought to confer some type of neuroprotection. However, despite these findings, significant gaps exist in the field of brain based CLU research. For instance, it is known that alternative "intracellular" CLU protein isoforms are generated, however, the number of CLU mRNAs that are transcribed from the CLU gene and the corresponding translated protein isoforms are yet to be identified. Moreover, while studies demonstrate the expression of CLU mRNA and protein in rodent brain, neurons, and astrocytes from an early age, a full characterization of the CLU protein isoform expression profile in the brain and brain cell types is not currently available. Furthermore, as CLU protein has been detected in multiple subcellular compartments in immortalized cells, it is feasible to assume that brain CLU protein is localized to individual cellular organelles; though this characterization is also missing from the currently available literature. In addition to the presence of several research gaps, the currently available literature contains several controversies pertaining to the basic molecular properties of CLU protein. One such controversy is the presence of a "nuclear" CLU protein isoform (usually deemed nCLU in the literature), and the mRNA isoform from which this protein is translated. Numerous studies suggest that the nCLU isoform is generated from Exon 3-9 CLU mRNA and remains unglycosylated. In contrast, other studies suggest that the nCLU isoform is derived from Exon 1, 3-9 CLU mRNA while some have concluded that no such nCLU protein isoform exists. Another key controversy is the notion that brain CLU is solely generated and secreted by astrocytes and that the presence of CLU in neurons is the result of neuronal uptake of astrocytic CLU. However, several publications indicate the expression of CLU in primary cultures of neurons where no astrocytes are present and thus conclude that neurons are capable of generating *de novo* CLU protein.

In reviewing the literature and the deficiencies therein it is clear that many of the unanswered molecular questions and controversies may be resolved through a thorough characterization of CLU in the brain. Moreover it is clear that several research methodologies need to be changed in order to gain a thorough and translational understanding of this complex protein. **(1)** One such method that is used consistently in the field of CLU research is the preferential examination of CLU mRNA rather than protein. As CLU protein isoforms are speculated to exhibit opposing effects on cellular function and are thought to be derived from multiple CLU mRNAs this research application does not provide an accurate representation of fluctuations and/or cellular responses by individual CLU protein isoforms. **(2)** Those studies that do examine CLU protein expression in response to a cellular stimuli or pathological condition, are often conducted in immortalized cancer cell lines. As the environment in a tumor-derived cell line is remarkably different from physiological conditions, the use of only immortalized cells lines in the study of CLU protein function may contribute to the controversies that currently exist in this field. Moreover, as mCLU is a key contributor to cancer cell survival and is known to be highly upregulated in multiple cancer cell lines, it is highly unlikely that the expression profile of healthy non-stressed neurons and/or astrocytes can be accurately represented in this manner. **(3)** In addition to using immortalized cell lines, my review of the literature indicates that the predominant amount of CLU studies rely on the use of a single polyclonal CLU antibody. As different CLU antibodies are shown to recognize distinct CLU protein isoforms by both the commercial vendor and previously published studies, the use of a single antibody may provide only a partial picture of the response of CLU to a certain pathology or stress signal. Therefore the purpose of this dissertation is to provide an in-depth characterization of brain CLU mRNA and protein isoforms under physiological conditions. This analysis will include a characterization of brain, neuronal, and astrocytic CLU protein expression and is expected to provide insight into the function and distribution of individual CLU protein isoforms and their in healthy cells. In order to obtain the full CLU protein expression profile, multiple antibodies will be used in to evaluate CLU protein expression in each experiment. The data generated from these studies will provide key foundational information that is required for researchers to understand how CLU mRNA and protein expression is altered during neurodegenerative decline.

Materials and Reagents

All materials and reagents used in this dissertation are listed in the following tables. Chemicals are listed in **Table 1**, buffers and solutions are listed in **Table 2**, and antibodies, sera, and immunoglobulins are listed in **Table 3**, and cell culture media and supplements can be found in **Table 4**.

Chemicals

Commercially Available Chemicals		
Chemical Name	**Vendor**	**Catalog #**
4-(2-hydroxyethyl)-1-piperazineethanesulfonic acid (HEPES)	Sigma	H4034
Adenosine Diphosphate (ADP)	Sigma	A2754
Agarose, PCR Grade	Biorad	161-3103
Albumin from Bovine Serum (BSA)	Sigma	A7906
Ammonium Acetate (NH_4OAc)	MP Biomedicals	194000
Ammonium Bicarbonate (NH_4HCO_3)	Sigma	A-6141
Ammonium Persulfate	Biorad	161-0700
Ampicillin Sodium Salt	Sigma	A9518
Antimycin A	Sigma	A8674-25MG
Blotting-Grade Blocker	Biorad	170-6404
Boric Acid	Sigma	B6768
Calcium Chloride ($CaCl_2$)	Sigma	C4901-100G
Calcium Chloride x $2H_2O$	Sigma	C-3881
Carbonyl cyanide 4-(trifluoromethoxy)phenylhydrazone (FCCP)	Sigma	C2920-10MG
Deoxycholic Acid	Alfa Aesar	B20061
Digitonin	Sigma	D141
Dithiothreitol (DTT)	GE HealthCare	17-1318-01
Ethylene glycol-bis(β-aminoethyl ether)-N,N,N',N'-tetraacetic acid (EGTA)	Sigma	E3889
Ethylenediaminetetraacetic acid (EDTA)	Fisher Scientific	S311
Gelatin	Biorad	170-6537
Glucose	Sigma	G8270
Glycine	Sigma	G8898
Iodoacetamide (IAA)	Sigma	I1149-5G
LB Agar, Miller (Granulated)	Fisher Scientific	BP9724
LB Broth, Miller (powder)	Fisher Scientific	BP1426
L-Glutamic acid monosodium salt hydrate	Sigma	G5889
Lithium Chloride (LiCl)	VWR	6416

Magnesium Chloride ($MgCl_2$)	Sigma	M8266-100G
Malic acid	Sigma	112577
Mannitol	Sigma	M1425
Monopotassium phosphate (KH_2PO_4)	Fisher Scientific	P285-500
Oligomycin	Sigma	O4876-5MG
Poly-D-Lysine	Sigma	P7280
Potassium Chloride (KCl)	Sigma	P3911
Protease and Phosphatase Inhibitor (PPI)	Thermo Scientific	88669
Rotenone	Sigma	R8875-1G
Sodium Bicarbonate	Sigma	S6014
Sodium Chloride (NaCl)	Sigma	S9888
Sodium Deoxycholate	Sigma	D5670-5G
Sodium Dodecyl Sulfate (SDS)	JT Baker	4095-02
Sodium phosphate monobasic	Fisher Scientific	S397-500
Sodium Pyruvate	Sigma	P2256-5G
Sodium Tetraborate Decahydrate (Borax)	Fisher Scientific	BP175
Styptic powder	Arc Laboratories	463501
Disodium Succinate	Sigma	W327700
Sucrose	Fisher Scientific	S5-500
Thiourea	Acros	A0326078
Tris Base	Fisher Scientific	BP152
Tris Hcl	Fisher Scientific	BP153
Trypsin, sequencing grade	Roche	1418475

Table 1. Chemicals. A list of all commercially available powdered chemicals used in this dissertation

Buffers and Solutions

Commercially Available Solutions and Buffers		
Solution/Buffer Name	**Vendor**	**Catalog #**
6X DNA Loading Buffer	Promega	G1881
Acetone	Sigma-Aldrich	650501
Isopropanol 70%	RICCA Chem. Co.	4210-1
Hydrochloric Acid	Fisher Scientific	A144-212
50X TAE Buffer	BioRad	161-0743
50% Polyethyleneimine	Sigma	P3143
Dimethyl Sulfoxide	ATCC	4-X
20X PBS	Amresco	E703
16% Paraformaldehyde	Electron Microscopy Sciences	15710-S
Ethidium Bromide	Biorad	1610433
Triton X-100	Acros	A0341006
NP-40 (Igepal)	Boston BioProducts	P877

100 % Glycerol	Biorad	170-6537
100% Percoll Solution	Sigma	P1644
5N Sodium Hydroxide Solution (NaOH)	Fisher Scientific	55256
1N Potassium Hydroxide (KOH)	Fisher Scientific	SP208-500
Tween-20 Solution	Biorad	161-0781
Tissue Protein Extraction Reagent	Thermo Scientific	78510
Neuronal Protein Extraction Reagent	Thermo Scientific	87792
Mammalian Protein Extraction Reagent	Thermo Scientific	78503
Lower Tris (Resolving Gel Buffer)	Biorad	161-0798
Upper Tris (Stacking Gel Buffer)	Biorad	161-0799
TEMED	Biorad	161-0801
30% Acrylamide/Bis Solution 29:1	Biorad	161-0156
Precision Plus Protein Standards	Biorad	1610374
Western Blot Stripping Buffer	Thermo Scientific	21063
2X Laemmli sample	Biorad	161-0737
β-mercaptoethanol	BioRad	161-0710
SYPRO Ruby Stain	Invitrogen	S12000
Methanol	Fisher Scientific	A412
Glacial Acetic Acid	Fisher Scientific	BP2401
100% MeCN	Fisher Scientific	A998-4
Trifluoroacetic Acid	Fisher Scientific	O4902-100
TRIzol Reagent	Life Technologies	15596026
Chloroform	MP Biomedicals	2194002
37% Formaldehyde	Fisher Scientific	BP531
Phenol:Chloroform:Isoamyl Alcohol 25:24:1	Sigma	P2069
PowerUP SYBR Green MasterMix	Thermo Scientific	A25741
UltraPure Distilled Water	Invitrogen	10977-015
Ethanol 200 Proof	Decon Labs 2301	2701
Lab-generated Solutions and Buffers		
Solution/Buffer Name	**Solution/Buffer Recipe**	
Genotyping Solution A	25 mM NaOH, 0.2 mM EDTA	
Genotyping Solution B	40 mM Tris-HCl	
1X TAE Buffer	980 mL ddH_2O + 20 mL 50X TAE Buffer + 8 µL Ethidium Bromide	
Borate Buffer	3.1 g Boric Acid and 4.74 g Borax to 950 mL ddH_2O - adjust pH to 8.3	
0.1% Polyethylenimine	2 g of 50% PEI + 100 mL Borate Buffer - dissolve and bring to 1L with ddH_2O	
Poly-D-Lysine Stock (100 µg/mL)	5mg poly-D-lysine + 50 mL ddH2O	
Poly-D-Lysine Working Solution (50 µg/mL)	25 mL Poly-D-Lysine Stock Solution + 25 mL ddH_2O	
4% Paraformaldehyde	4 mL 16% Stock PFA + 12 mL ddH_2O	

1X PBST	1X PBS supplemented with 0.1 % Triton X-100
ICC Blocking Solution	1X PBST supplemented with 5% Normal Goat Serum (NGS)
Antigen Preservation Solution	50% PBS, 50% ethylene glycol and 1% polyvinyl pyrrolidone, pH 7.0
IHC Blocking Buffer	1X PBS supplemented with 5% NGS and 0.3% Triton X-100
1 M Acetic Acid	15 ml Glacial Acetic Acid + 235 mL ddH_2O
1 M Ammonium Acetate	19.27 g Ammonium Acetate + 250 mL ddH_2O
Acetate Buffer - pH 4.9	15 mL 1 M Acetic Acid + 35 mL 1 M Ammonium Acetate
Acetate Buffer - pH 6.0	1.875 mL 1 M Acetic Acid + 48.125 mL 1 M Ammonium Acetate
Subbing Solution	0.5 g Gelatin in 100 mL ddH_2O - stir at 60 °C until dissolved
95% Ethanol (EtOH)	95 mL 100% EtOH + 5 mL ddH_2O
IHC Mounting Medium	2 mL Subbing Solution + 50 mL 95% EtOH + 12 mL Acetate Buffer (6 mL of each pH) + 188 mL ddH_2O
Cytosolic Extraction Buffer	10 mM HEPES, 60 mM KCl, 1 mM EDTA, and 0.075% (v/v) Igepal
Nuclear Extraction Buffer	20 mM TrisHCl , 420 mM NaCl, 1.5 mM MgCl2, 0.2 mM EDTA, 25% (v/v) glycerol , 0.5% Igepal
Lysis Buffer A	150 mM NaCl, 50 mM HEPES, pH 7.4, 25 µg/mL Digitonin (freshly added)
Lysis Buffer B	150 mM NaCl, 50 mM HEPES pH 7.4, 1% v/v Igepal
Lysis Buffer C	150 mM NaCl, 50 mM HEPES pH 7.4, 0.5% w/v Sodium Deoxycholate, 0.1% w/v SDS
Mitochondria Isolation Buffer	320mM Sucrose, 1 mM EDTA, 10 mM Tris-HCl, pH – adjusted to 7.4
Stock Isotonic Percoll	90 mL Percoll Solution + 10 mL 1.5 M NaCl
15% Percoll	1.5 mL Stock Isotonic Percoll + 8.5 mL MIB without PPI
23% Percoll	2.3 mL Stock Isotonic Percoll + 7.7 mL MIB without PPI
40 % Percoll	4 mL Stock Isotonic Percoll + 6 mL MIB without PPI
Mitochondria Subfractionation Buffer	220 mM Mannitol, 70 mM Sucrose, 2 mM HEPES, pH adjusted to 7.4 with KOH,
1.6 % Digitonin	16 mg Digitonin + 1 mL ddH_2O
1X HEPES Buffer	100 mM NaCl, 2.0 mM KCl, 2.5 mM CaCl2, 1.0 mM MgCl2, 1.0 mM NaH2PO4, 4.2 mM NaHCO3, 12.5 mM HEPES, 10.0 mM glucose, pH 7.4
IP Buffer	50 mM Tris, pH 7.4, 100 mM NaCl, 0.5% Triton X-100 and 10 mM EGTA
Co-IP Buffer	50 mM Tris-HCl, 10 mM EGTA, 10 mM NaCl, 0.5% (v/v) Triton X-100
20% APS	100 mg ammonium persulfate + 500 µL ddH_2O
10X Western Blot Running Buffer	250 mM Tris Base, 1.92 M Glycine

1X Western Blot Running Buffer	100 mL 10X Western Blot Running Buffer + 890 mL ddH2O + 10 mL 10% SDS
Western Blot Transfer Buffer	100 mL 10X Western Blot Running Buffer + 200 mL 100% Methanol + 700 mL ddH_2O
2% Blocking Buffer	2 grams non-fat dry milk + 100 mL 1X TBST
10X TBS	200 mM Tris, 1.5 mM NaCl, pH 7.6
10% SDS	10 g SDS powder + 90 mL ddH_2O
1X TBST	100 mL 10X TBS + 890 mL ddH_2O + 10 mL 10% Tween-20 Solution
1X PBS (non-cell culture grade)	50 mL 20X PBS + 950 mL ddH_2O
70% Ethanol	700 mL 100% Ethanol + 300 mL ddH_2O
LB Broth	25 g LB Broth Powder in 1L of ddH_2O - Autoclaved
Fixing Solution	7% acetic acid v/v, 10% methanol v/v in water
1 M NH_4HCO_3 Stock Solution	1.186g/15 mL H2O, no pH adjustment (actual pH 8.5-8.8)
50 mM $CaCl_2$ Stock Solution	100 mg $CaCl_2$ x $2H_2O$ + 13.6 mL ddH_2O
100 mM NH_4HCO_3	1.5 mL of 1 M stock + 13.5 mL ddH_2O
TD Washing Solution	200 mM NH_4HCO_3/50% (v/v) MeCN
TD Reducing Solution	3.1 mg DTT + 2 mL of 100 mM NH_4HCO_3
TD Alkylating Solution	38 mg IAA + 2 mL of 100 mM NH_4HCO_3
TD Digestion Buffer	50 mM NH_4HCO_3, 5 mM $CaCl_2$, 6 ng trypsin/ul
1 M Pyruvate	88.06 mg Pyruvic Acid + 1 mL ddH_2O, pH-7.2
0.4 M Malate	53.6 mg L-malic acid + 1 mL ddH_2O, pH 7.3
1 M Succinate	162.05 mg disodium succinate in 1 mL, pH-7.2
200 mM ADP	85.44 mg ADP + 1 mL ddH_2O
10 mg/mL Oligomycin Stock	5 mg Oligomycin + 500 µL DMSO
1 mg/mL Oligomycin	10 µL 10 mg/mL Oligomycin Stock + 90 µL Mitochondrial Respiration Buffer
10 mM FCCP Stock	10 mg FCCP + 3.93 mL DMSO
100 µM FCCP	1 µL 10 mM FCCP Stock + 999 µL Mitochondrial Respiration Buffer
100 mM Rotenone Stock	1 g + 25 mL DMSO
1 mM Rotenone	10 µL 100 mM Rotenone Stock + 990 µL Mitochondrial Respiration Buffer
10 mM Antimycin A Stock	25 mg Antimycin A + 4.68 mL DMSO
1 mM Antimycin A	100 µL 10 mM Antimycin A Stock + 900 µL Calibration Buffer
Mitochondrial Respiration Buffer	210 mM Mannitol, 70 mM Sucrose, 1 mM EDTA, 5 mM HEPES, 0.5 mg/mL BSA – pH a 7.2
Calibration Buffer	80 mM KCl, 10 mM Tris-HCl, 3 mM $MgCl_2$, 1 mM EDTA, 5 mM KH_2PO_4 – pH 7.2
ChIP Fixing Solution	1.23 mL 37% Formaldehyde in 43.76 mL 1X PBS
1 M Glycine Stock Solution	75.066 g Glycine + 100 mL ddH_2O
0.125 M Glycine	12.5 mL 1 M Glycine Stock + 87.5 mL ddH_2O

ChIP Lysis Buffer	150 mM NaCl, 1% v/v NP-40, 0.5% w/v Sodium deoxycholate,0.1% w/v SDS, 50 mM Tris-Cl pH 8.0, and 5 mM EDTA
ChIP Dilution Buffer	0.01% (w/v) SDS, 1.1% (v/v) Triton X-100, 1.2 mM EDTA, 16.7 mM Tris-HCl pH 8.1, 167 mM NaCl
Low Salt Wash Buffer	0.1% SDS, 1% Triton X-100, 2 mM EDTA, 20 mM Tris-HCl, pH 8.1, 15 mM NaCl
High Salt Wash Buffer	0.1% SDS, 1% Triton X-100, 2 mM EDTA, 20 mM Tris-HCl, pH 8.1, 500 mM NaCl
Lithium Chloride Wash Buffer	0.25 M LiCl, 1% (v/v) NP-40, 1% deoxycholic acid, 1 mM EDTA, 10 mM Tris-HCl, pH 8.1
TE Wash Buffer	10 mM Tris-HCl, pH 7.5, 1 mM EDTA
ChIP Elution Buffer	1% SDS, 0.1M NaHCO3
5M NaCl	29.22 g NaCl + 100 mL ddH_2O
5X Protein Digestion Buffer	50 mM Tris-HCl, pH 7.5, 25 mM EDTA, 1.25% SDS
7.5 M NH_4OAc	57.81 g NH_4OAc into a total of 100 mL ddH_2O

Table 2. Buffers and Solutions A list of all commercially available and lab generated buffers and solutions used in this dissertation

Antibodies, Sera, and Immunoglobulins

Primary Antibodies				
Antibody	**Species**	**Vendor**	**Catalog #**	**Lot #**
Actin Beta	Rabbit	Pierce	PA5-16914	SF2405982E
APOE	Goat	Millipore	178479	2626398
Bax	Rabbit	Cell Signaling	2772T	10
Beta-Tubulin (TBN06 (Tub 2.5))	Mouse	Pierce	MA5-11732	QK2115682
Calnexin (H70)	Rabbit	Santa Cruz	sc-11397	I1914
Calreticulin (D3E6)	Rabbit	Cell Signaling	12238	2
Clusterin (H-330)	Rabbit	Santa Cruz	sc-8354	F0316, F0515
Clusterin - α (M18)	Goat	Santa Cruz	sc-6420	L3113, D0815
Clusterin - α (C-18)	Goat	Santa Cruz	sc-6419	
Clusterin - α (A-11)	Mouse	Santa Cruz	sc-166831	B1012
Clusterin - α (B-5)	Mouse	Santa Cruz	sc-5289	J2913
COX IV (3E11)	Rabbit	Cell Signaling	4850	7
Cytochrome C	Rabbit	Cell Signaling	119402	3
Estrogen Receptor α (HC-20)	Rabbit	Santa Cruz	sc-543	F0515
Estrogen Receptor β (H150)	Rabbit	Santa Cruz	sc- 8974	K0513
GAPDH	Mouse	Santa Cruz	sc3223	C1315
GFAP	Rat	Calbiochem	345860	
GPR30 (N-15)	Rabbit	BioRad	sc- 48525-R	B1115
GRP75	Mouse	BioRad	VMA00084T	140715
GRP78 (H-129)	Rabbit	Santa Cruz	sc-13968	
HSP60 (D6F1)	Rabbit	Cell Signaling	12165	

Immt	Rabbit	ProteinTech	10179-1-AP	
Lamin A/C (4C11)	Mouse	Cell Signaling	4777	4
MAP2	Mouse	Thermo Fisher	MA1-25043	RB2160802
TAU	Mouse	Thermo Fisher	MA5-12808	PL1952344
Tom70	Rabbit	ProteinTech	14528-1-AP	
Tri-methyl Histone H3 (K4) (C42D8)	Rabbit	Cell Signaling	9751T	10
V5-Tag	Rabbit	Cell Signaling	13202S	2
VDAC (D73D12)	Rabbit	Cell Signaling	4661	6
HRP-Conjugated Secondary Antibodies				
Antibody		**Vendor**	**Catalog Number**	**Lot #**
Goat anti-mouse IgG (H+L) HRP		Pierce	31430	PA196831
Goat anti-rabbit IgG (H+L) HRP		Pierce	31462	
Rabbit anti-goat IgG (H+L) HRP		Pierce	31402	RI2271393
Fluorophore-Conjugated Secondary Antibodies				
Antibody		**Vendor**	**Catalog Number**	**Lot #**
Goat anti-mouse IgG (H+L) FITC		Abcam	ab6785	GR6891-23
Goat anti-rabbit IgG (H+L) Cy3 preadsorbed		Abcam	ab6939	GR1836606-3
Goat anti-rabbit IgG - FITC		Abcam	ab97050	GR216167-1
Goat anti-rat IgG (H+L) Cy5 preadsorbed		Abcam	ab6565	GR117398-3
Goat anti-rat IgG Alexa Flour 568		Abcam	ab175710	GR146096-1
Sera and Antibody Controls				
Product Description		**Vendor**	**Catalog Number**	**Lot #**
Normal Goat Serum		Vector Laboratories	s-1000	ZB1027
Rabbit IgG		Santa Cruz	sc-2027	D1415
Goat IgG		Santa Cruz	sc-2028	J2114
Mouse IgG		Santa Cruz	sc-2025	D1416

Table 3. Antibodies, Sera, and Immunoglobulins. A list of all primary and secondary antibodies, sera, and non-specific immunoglobulins used in this dissertation. However, as dilutions were customized for individual experimental purposes, antibody dilutions and incubation conditions can be found in the corresponding figure captions.

Cell Culture Media and Supplements

Culture Medium and Supplements	Vendor	Catalog Number
Neurobasal Medium	GIBCO	12348-017
DMEM/F12 - Phenol red-free	GIBCO	21041-025
DMEM - Phenol red-free	GIBCO	21063-029
DMEM	GIBCO	11965-092
B27 Supplement	GIBCO	17504-044

GlutaMAX Supplement	GIBCO	35050-061
Penicillin-Streptomycin Solution	GIBCO	15140-122
Fetal Bovine Serum	GIBCO	10437028
1X PBS - pH 7.4	GIBCO	10010-023
1X HBSS	GIBCO	14170-112
OptiMEM	GIBCO	11058-021
0.25% Trypsin-EDTA	GIBCO	25200056
Lab Generated Maintenance Media		
Neuron Growth Medium		
NBM, B27, 1% Pen-Strep, 0.5 mM glutamine and 25 µM glutamate		
Neuron Maintenance Medium		
NBM, B27, 1% Pen-Strep, and 0.5 mM glutamine		
Astrocyte Maintenance Medium		
DMEM/F12, 10% FBS, 1% Pen-Strep		
Neuro-2a Maintenance Medium		
DMEM, 10% FBS, 1% Pen-Strep		

Table 6. Cell Culture Media and Supplements. A list of all cell culture reagents and lab-generated maintenance mediums used in this dissertation

Methods

Animal Models. The use of animals was approved by the Institutional Animal Care and Use Committee at the University of Kansas and followed NIH guidelines for the care and use of laboratory animals.

Clusterin-knockout (CLU-KO) mice. ApoJ-deficient (CLU-KO) mice were developed using standard techniques of homologous recombination as previously discussed (McLaughlin et al., 2000). Briefly, a targeting vector, deemed pApoJ-KO3, was constructed in pBluescript II to include 2 homology fragments: (1) a 7.2 kb *Bsa*HI-EcoRI long homology restriction fragment which contained the hypoxanthine phosphoribosyl-transferase (HPRT) cassette under the control of the mouse phosphoglycerol kinase (PGK) promoter and ApoJ

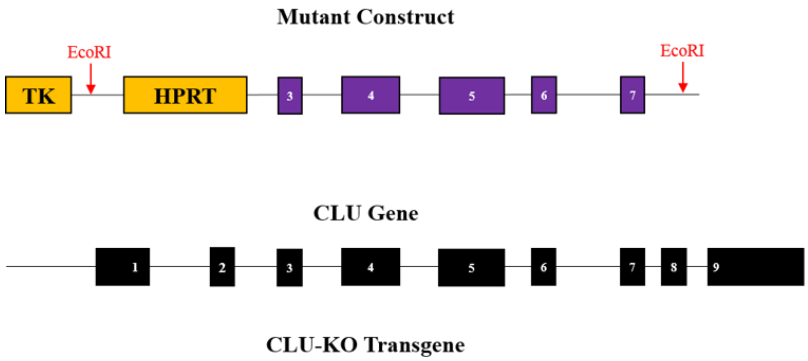

Schematic 7: Schematic of the Mutant CLU Construct used in the Generation of CLU-KO Mice.

exons 3-7 in the same orientation as the endogenous ApoJ gene, and (2) a 5' *Eco*RI-*Age*I short homology fragment. The targeting vector was then electroporated into 129S2/SvPas-derived D3 embryonic stem (ES) cells and successfully targeted ES cells were injected into C57BL/6J blastocysts followed by implantation into pseudopregnant (C3H/HeN x C57BL/6J) F1 females. Resulting chimeric males were then back-crossed to ensure germ-line transmission to F1 females followed by successive backcrossing of resultant heterozygotes with Swiss Black Mice for 1 generation and with C57BL/6J for more than 7 generations. The resultant CLU-KO animals, should exhibit no protein or mRNA expression in either serum, heart, or liver tissue and are physically and reproductively normal (McLaughlin et al., 2000). All animals used in this dissertation were derived from 3 heterozygous breeding pairs purchased from The Jackson Laboratories (JAX stock #005642). Heterozygotes were allowed to breed and at 21 days of age, the resulting pups were tagged for purposes of identification and a 2 mm tail segment was removed for genotyping. Successfully generated CLU-KO animals were bred for 2 generations prior to the initiation of any experimentation and genotyping was performed consistently to ensure the validity of animal models.

Genomic DNA Isolation. 80 µL Genotyping Solution A was added to each tail segment and samples were centrifuged briefly to bring solution and tail snips to the bottom. Samples were then incubated at 95 °C 1 hr. Following incubation, 80 µL Genotyping Solution B was added to each tube and samples were vortexed on max speed for 30 seconds. Samples were centrifuged at 2,000 rpm for 5 min at RT and 100 µL of the cleared supernatant was removed and pipetted into a new labeled centrifuge tube. 1 µL of the resulting crude genomic DNA was used for PCR amplification.

DNA Oligonucleotides. DNA oligonucleotide sequences were provided from The Jackson Laboratories for successful identification of WT, heterozygous and homozygous knockout animals. All DNA oligonucleotides were purchased from Integrated DNA Technologies. For both WT and mutant animals, a common forward primer is used with reverse primers providing the genotype differentiation. Primers used and the resulting amplimers are as follows: Common Forward: 5' - AAC GAT GTG GAA GGA TGT GG

– 3', WT Reverse (200 bp amplimer): 5' - CTT TCT GGA AGC CTA GAG GTG – 3' and Mutant Reverse (180 bp amplimer): 5' - GCC AGA GGC CAC TTG TGT AG – 3'.

Genotyping. As PCR reactions could not be combined due to the close size in resulting amplimers, two PCR reactions were assembled for each tail snip. Assembly of PCR reactions was performed as indicated in Table 5. PCR reactions were performed in thin-walled 0.2 mL PCR Strips (Molecular BioProducts,

Genotyping PCR Reaction Components			
Component	**Volume (per rxn)**	**Vendor**	**Catalog #**
Genomic DNA	1 µL	N/A	N/A
iTaq DNA Polymerase	0.0625 µL	BioRad	170-8870
10X iTaq Buffer	1.25 µL	BioRad	170-8870
50 mM $MgCl_2$	0.375 µL	BioRad	170-8872
10 mM PCR Nucleotide Mix	0.25 µL	Promega	C114G
Forward Primer	100 ng	IDT	N/A
Reverse Primer	100 ng	IDT	N/A
ddH_2O	7.56 µL	N/A	N/A

Table 5. Genotyping PCR Reaction Components. A list of items and their corresponding volumes, vendors, and catalog numbers for all components included in PCR Reactions for CLU-KO mouse line genotyping

Cat. #3418) using a T100 Thermal Cycler (BioRad) with the following conditions: 95 °C for 5 min, 1 cycle of 95 °C – 20 sec, 65 °C – 60 °C (0.5 °C decrease with each cycle (total of 10 cycles)) – 30 sec, and 72 °C – 30 sec, followed by 28 cycles of 95 °C – 15 sec, 60 °C – 30 sec, and 72 °C – 30 sec with a final polishing step of 72 °C for 10 min. Following PCR, amplimers were removed from the Thermocycler and 2 µL of 6X DNA Loading Buffer was added to each tube. Samples were run on a 2% agarose gel (1 g Agarose in 50 mL 1X TAE Buffer) for 40 min at 120 V and bands were visualized using the Gel Doc EZ Imaging System (BioRad) equipped with a UV Tray (BioRad, Cat. #1708271). Guidelines for the successful identification of animal genotypes are as follows: WT animals: 1

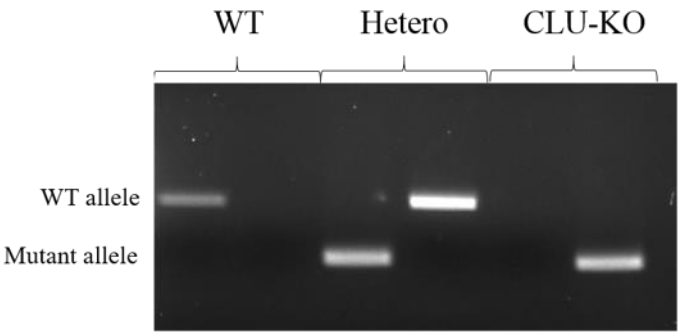

Schematic 8: Confirmation of WT, Heterozygous, and CLU-KO Mouse Genotype

amplimer at 200 bp with no amplification occurring in the mutant reaction, heterozygous animals: 200 bp amplimer in WT reaction and 180 bp amplimer in mutant reaction, and CLU-KO animals: 1 amplimer at 180 bp with no amplification occurring in the WT reaction. An example of the appropriate results for WT, Heterozygous, and CLU-KO mice is provided in Schematic 8.

Estrogen receptor beta-knockout (Erβ$^{-/-}$) rats. Two ERβ knockout rat models were generated and generously provided by Dr. Karim Rumi (Institute for Reproductive Health and Regenerative Medicine, Kansas University Medical Center). The rat models were generated using zinc finger nuclease (ZFN)-mediated genome editing to target deletion of exon 3 (Ex 3−/−) or exon 4 (Ex 4−/−) in the ERβ gene. The Ex 3−/− mutation results in a frameshift and null mutation whereas Ex 4−/− is translated into a DNA-binding domain deficient form of ERβ (Rumi et al., 2017). Confirmation of successful deletion of targeted sequences was achieved through reverse transcription-PCR (RT-PCR) using primers within exons flanking the targeted exons 3 and 4 while alterations in the open reading frames (ORFs) were determined via DNA sequencing. Animals were euthanized according to the appropriate AUS and at 6 and 10 months of age and brain tissue sections were extracted as indicated (n=5 animals/genotype). Ex 3−/− and Ex 4−/− animals can be obtained from the Rat Resources & Research Center at the University of Missouri in Columbia, MO.

Cell Culture Techniques. Primary rat neurons and astrocytes were isolated in sterile conditions under a Labconco type A2 Biological Safety Cabinet and maintained at 37 °C with 5% CO_2. All surgical instruments were sterilized by autoclaving 2 days prior to animal euthanasia. On the morning of isolation, all components of the isolation procedure, with the exception of culture media, were placed in the Biological Safety Cabinet and subjected to UV light sterilization for 30 min. All immortalized cell lines were cultured and maintained according to the guidelines set forth by ATCC or the cell line donors. Individual protocols are provided in the sections below.

Isolation of Primary Rat Cortical and Hippocampal Neurons. Primary cultures of rat hippocampal and cortical neurons were isolated from Day 18 Embryonic rat pups as previously described (Zhao et al., 2004). Briefly, cortical and hippocampal tissues were dissected from the brains of rat fetuses and treated with 0.02% trypsin in Hank's balanced salt solution (HBSS) for 5 min at 37 °C. Tissues were dissociated by repeated passage through a series of fire-polished constricted Pasteur pipettes. Cortical neurons were plated onto polyethyleneimine (PEI)-coated 100 mm dishes at a density of $5x10^5$ for biochemical analysis. For morphological analyses, hippocampal neurons were plated onto poly-D-lysine coated 22 mm glass coverslips (NeuVitro) at a density of $2x10^5$ in covered 35 mm petri dishes. Neurons were grown in Neuron Growth Medium at 37 °C in a humidified 5% CO2 atmosphere for the first 3 days and Neuron Maintenance Medium (Neuron Growth Medium without Glutamate) afterwards. Cultures grown in serum-free Neuron Maintenance Medium yield approximately 99.5% neurons and 0.5% glial cells.

Isolation of Primary Rat Cortical Astrocytes. For isolation of primary cortical astrocytes, euthanasia, dissection, and dissociation were performed as indicated in the previous paragraph. Following dissociation, tissues were centrifuged for 10 min at 170 x g and re-suspended in 50 mL Astrocyte Medium. Cells were plated at a density of $1x10^6$ in poly-d-lysine coated T75 flasks and allowed to incubate for 7 days at 37 °C in a humidified 5% CO2 atmosphere. On day 7, medium was replaced with fresh Astrocyte medium and the flasks were incubated for 16 hrs on an orbital shaker at a speed of 220 rpm at 37 °C. The next day, medium containing dead neurons, oligodendrocytes, and microglia was aspirated and isolated astrocytes were passaged using 2 mL 0.25% Trypsin and plated on poly-d-lysine coated dishes in Astrocyte Medium. Astrocytes were allowed to grow for 2 weeks prior to use during which time astrocytes were passaged 2 times. For biochemical analysis, astrocytes were plated in 100 mm dishes at a density of 2×10^5 and for immunohistology astrocytes were plated in 8 well glass-bottom chamber slides.

Mouse Neuroblastoma (Neuro-2a) Cells. Mouse neuroblastoma (Neuro-2a) cells were purchased from ATCC (ATCC® CCL-131™) and cultured according to the established guidelines. Briefly, cells were maintained in glucose containing (4.5 g/L D-Glucose), sodium pyruvate-free Neuro-2a Maintenance

Medium. Cells were allowed to grow in cell-culture treated T-75 flasks at 37 °C in 5 % CO_2 until 80% confluency. At 80% confluency cells were passaged using 3 mL 0.25% trypsin and re-plated using 10-20% of the trypsinized cells. N2a cells were used until passage number 25 after which time cells were discarded.

siRNA-mediated Knockdown of CLU. siRNA constructs targeting Exon 2 (Life Technologies, Cat. #AM16708, siRNA Construct #70870) and Exon 3 (Life Technologies, Cat. #4390771, siRNA Construct #s201172) of rodent CLU were purchased and re-suspended in supplied ddH_2O to a concentration of 100 µM. To facilitate dilution for transfection, a 4.5 nm stock solution was generated by serial dilutions and the 100 µM solution was stored at -20 °C. Gapdh siRNA targeting murine Gapdh (positive control, Life Technologies, Cat. # AM4624) and Scramble siRNA (negative control, Life Technologies, Cat. #AM4611) were both supplied as 50 µM stock solutions. 4.5 nM stock solutions were generated by serial dilutions and remaining stock tubes were stored at -20 °C. For transfection, Neuro-2a cells were plated at 1 x 10^5 cells/mL (2 mL/well) and allowed to attach overnight at 37 °C at 5% CO_2 in antibiotic-free Neuro-2a Maintenance Medium. The following day, medium was replaced with 1.7 mL OptiMEM and allowed to incubate for 30 min at 37 °C prior to transfection. siRNAs and corresponding positive and negative controls were transfected at concentrations ranging from 25 pM to 600 pM for 18 hr at 37°C. Following transfection, medium was replaced with antibiotic containing Neuro-2a Maintenance Medium and cells were incubated for another 48-72 hrs. Following incubation cells were harvested using the Whole Cell Protein Extraction protocol provided below and analyzed for CLU immunoreactivity via SDS-PAGE. Sequences for the CLU targeting siRNA constructs are as follows: Exon 2 Targeting: Sense: 5'-GGUCUCUGACAAUGAGCUCtt– 3' Antisense: 5'-GAGCUCAUUGUCAGAGACCtc– 3' Exon 3 Targeting: Sense: 5'- GCUCAACAGUUUAGAGGAAtt – 3' Antisense: 5'-UUCCUCUAAACUGUUGAGCaa – 3'

Human Bone-Marrow Neuroblastoma (SH-SY5Y) Cells. Human bone marrow derived neuroblastoma cells were a kind gift from Dr. Russell Swerdlow at The University of Kansas Medical Center. Cells were maintained in pyruvate-free DMEM containing 25 mM glucose supplemented with 10% FBS and 1%

penicillin-streptomycin at 37 °C in 5% CO_2. For trypsinization, cells were processed as previously indicated in the Neuro-2a section.

Immunocytochemistry. For purposes of immunocytochemistry primary neurons were plated on 25 mm poly-D-lysine coated coverslips (NeuVitro) individually placed in 35 mm cell culture dishes at a density of 2 x 10^5 cells/mL (300 µL). Tools required for mounting of neuron coated coverslips are as follows: 1.0 mm thick Plain Microscope Slides (Fisher Scientific, Cat. #12-550B), 4" Coverslip Forceps (VWR, Cat # 470018-968), and 22 G needles. Primary astrocytes were plated at a density of 1.5 x 10^5 (200 µL) in optical quality plastic iBiTreated 8-well chamber slides (ibidi, Cat. # 80826-G500). Control staining was performed for each staining paradigm by incubating one coverslip or well in 1X PBST supplemented with 1% NGS without primary antibody. Concentrations and incubation conditions were kept identical for secondary antibody staining across control and experimental groups resulting in a secondary antibody control. This control allows for the visualization of auto-fluorescence caused by the secondary antibody alone and is essential to ensure the specificity of chosen primary antibodies in immunostaining.

Mitotracker staining. Prior to the initiation of Mitotracker staining, 1 tube of Mitotracker Deep Red FM (Life Technologies, Cat. #M22426, Lot # 1654296) or Mitotracker Red CMXRos (Life Technologies, Cat. # M7512) was reconstituted to a concentration of 1 mM in cell culture grade dimethyl sulfoxide (DMSO). Stock concentration was then diluted in pre-warmed neuronal or astrocytic maintenance medium to a concentration of 250 nM. DIV 9 primary hippocampal neurons or DIV 16 primary cortical astrocytes were then incubated in Mitotracker Red supplemented medium for 25 min at 37°C. Medium was aspirated and neurons/astrocytes were washed with 1X PBS, pH 7.4 2 x 5 min at RT.

Fixing, Permeabilization, and Blocking. 1X PBS (if stained with Mitotracker Red) or culture medium (if no Mitotracker Red staining) was aspirated and neurons/astrocytes were fixed in freshly prepared 4% paraformaldehyde (PFA) for 15 min at RT. PFA was aspirated at cells were washed 2 x 5 min with RT 1X

PBS, pH 7.4. Following fixation and washing, samples were permeabilized in 1X PBST for 5 min at RT. Following incubation, samples were washed 3 x 5 min in 1X PBS, pH 7.4. Permeabilized cells were then blocked in ICC Blocking Solution for 30 min at RT with continual rocking followed by 1 x 5 min wash in 1X PBS.

Double Labeling of Primary Hippocampal Neurons. MAP2/CLU: Fixed, permeabilized, and blocked primary hippocampal neurons were incubated overnight with continual rocking in 1X PBST supplemented with 1% NGS and the primary antibodies mouse monoclonal anti-MAP2 (1:750) and rabbit polyclonal anti-Clusterin H-330 (1:500) The next morning, samples were washed 3 x 5 min with 1X PBS and incubated for 1 hr at RT in 1X PBST supplemented with 1% NGS and the fluorophore conjugated secondary antibodies Goat anti-rabbit Cy3 (1:1000) and Goat anti-mouse FITC (1:1000). **CLU/Mitotracker Red:** Mitotracker Deep Red stained primary neurons were incubated over night with continual rocking in 1X PBST supplemented with 1% NGS and rabbit polyclonal anti-Clusterin H-330 (1:500). The next morning, samples were washed 3 x 5 min with 1X PBS and incubated for 1 hr at RT in 1X PBST supplemented with 1% NGS and the fluorophore conjugated secondary antibodies Goat anti-rabbit Cy3 (1:1000) for 1 hr at RT with continual rocking protected from light.

Double Labeling of Primary Cortical Astrocytes. GFAP/CLU: Fixed, permeabilized, and blocked primary cortical astrocytes were incubated overnight with continual rocking in 1X PBST supplemented 1% NGS and the primary antibodies rat polyclonal anti-GFAP (1:500) and rabbit polyclonal anti-Clusterin H-330 (1:500) The next morning, samples were washed 3 x 5 min with 1X PBS and incubated for 1 hr at RT in 1X PBST supplemented with 1% NGS and the fluorophore conjugated secondary antibodies Goat anti-rat Cy5 (1:1000) and Goat anti-rabbit FITC (1:1000). Samples were incubated with continual rocking and were protected from light. **CLU/Mitotracker Red:** Mitotracker Red CMXRos stained primary astrocytes were incubated over night with continual rocking in 1X PBST supplemented with 1% NGS and rabbit polyclonal anti-Clusterin H-330 (1:500). The next morning, samples were washed 3 x 5 min with 1X PBS and incubated for 1 hr at RT in 1X PBST supplemented with 1% NGS and the fluorophore conjugated

secondary antibodies Goat anti-rabbit FITC (1:1000) for 1 hr at RT with continual rocking protected from light.

DAPI Staining and Coverslip Mounting. Neurons: Following immunolabeling of fixed cells, all samples were washed 3 x 5 min with 1X PBS and mounted on glass microscopy slides using 1 drop of Vectashield Hardset Mounting Medium containing DAPI (Vector Laboratories). Briefly, residual PBS was removed with a P1000 pipette and the coverslip was gently lifted off the dish using a 22 G needle and coverslip tweezers. Excess PBS was removed by dabbing the edge of the coverslip on a kim wipe and the coverslip was inverted and placed on the microscopy slide containing mounting medium. Mounting medium was allowed to dry overnight protected from light before imaging. **Astrocytes:** Following immunolabeling, all samples were washed 3 x 5 min with 1X PBS and 1 drop of Vectashield Hardset Mounting Medium containing DAPI (Vector Laboratories) was added to each well of the chamber slide. Mounting medium was allowed to dry overnight protected from light before imaging.

Immunohistochemistry. Tools utilized in the removal of free floating brain sections from antigen preservation solution are as follows: Hockey Sticks for section transfers (NeuroScience Associates, Histo Tools Cat. # 10015) and #1 and #3 sized paint brushes (American Painter, Cat. #4000-1T). All immunostaining was performed in 80 x 40 mm Crystallizing Dishes (ChemGlass, Cat. # CG-8276-P80) equipped with a Small Section Transfer Basket (NeuroScience Associates, Histo Tools Cat. # 10014). Brain sections were mounted on 2" x 3" Subbed Slides (NeuroScience Associates, Histo Tools Cat. # 10004) and cover slipped with 2" x 3" coverslips (NeuroScience Associates, Histo Tools Cat. # 10088).

Multi-brain sectioning. Rat brain hemispheres were sectioned using MultiBrain processing at NeuroScience Associates as previously described (Zhao et al., 2011). Briefly, hemispheres were dissected and treated with a solution of 20% glycerol and 2% DMSO to prevent freeze-artifacts. Hemispheres were then embedded in a gelatin matrix and cured. After curing, the block of embedded hemispheres was rapidly

frozen by immersion in −70 ◦C and mounted on a freezing stage of an AO 860 sliding microtome. The block of rat hemispheres was sectioned at 40 μm in the coronal plane through the hippocampus (Bregma−1.5 to−6.5 mm). Cut sections were collected sequentially into 12 containers filled with Antigen Preservation Solution.

Triple Labeling of Mouse and Rat Brain Hemispheres. Free-floating rat hemisphere sections were removed from the freezer and allowed to acclimate to RT. Hockey sticks and #1 paint brushes were used to carefully remove brain sections from antigen preservation solution after which sections were washed 2 x 5 min with PBST in a crystallizing dish equipped with a small section transfer basket. Brain sections were then incubated in IHC Blocking Buffer at RT for 1 h. Sections were incubated overnight at 4 ◦C in PBST supplemented with 1% NGS and a mixture of primary antibodies containing mouse monoclonal anti-MAP2 (1:1000), rat anti-GFAP (1:500), and rabbit polyclonal anti-Clusterin H-330 (1:500). The following day, brain sections were washed 3 x 5 min with PBST and subsequently incubated at RT for 1 hr in PBST supplemented with 1% NGS and a mixture of secondary antibodies containing goat-anti-mouse FITC (1:1000), goat-anti-rabbit Cy3 (1:1000), and goat-anti-rat Cy5 (1:750). Sections were washed 3 x 5 min with 1X PBST and mounted on 2" x 3" Subbed Slides immersed in IHC Mounting Medium. 3 drops of Vectasheild Mounting Medium containing DAPI was added to corresponding 2" x 3" coverslips and coverslips were placed over mounted tissue sections and sealed with clear nail polish.

Equipment and Image Analysis. For imaging cells: Confocal images were acquired using a customized Olympus IX81/spinning disk confocal inverted microscope equipped with an Olympus 40X 0.95 NA air objective or an Olympus 60X NA 1.42 oil objective (Olympus). Images were collected and analyzed using the Slidebook Software Version 6.0 with 15-20 image stacks with a 0.1 μm step size through the cells. **For imaging of tissue sections:** Confocal images were acquired using a customized Olympus IX81/spinning disk confocal inverted microscope (Olympus, Yokogawa) equipped with an Olympus 40X 0.95 NA air objective (Olympus). Images were collected and analyzed using the Slidebook Software Version 6.0 (Intelligent Imaging Innovations) with 60-80 image stacks with a 0.5 μm step size through the tissue.

Protein Biochemistry

Tissue Isolation. All tissues were extracted on ice using sterile surgical tools. Following dissection, selected tissues were immediately frozen on dry ice. Tools used for dissection of rodent brain and peripheral tissues are as follows: Bone Pliers (Fine Science Tools, Cat. #16025-14), Lempert Rongeurs (Fine Science Tools, Cat. #16004-16), Tungsten Carbide Straight Bone Scissors (Fine Science Tools, Cat. #16030-12), Micro Spoons (Fisher Scientific, Cat. #21-401-15), Dissecting Tissue Forceps (Fisher Scientific, Cat. #13-812-36), Curved Precision Tip Forceps (Fisher Scientific, Cat. #16-100-123), and a Metal Scalpel (Fisher Scientific, Cat. #08-920B).

Brain Region Dissection. Female Erβ$^{-/-}$ rats aged 6 months or 10 months (n=5 animals per age group), male and female CLU-KO (variable ages) mice and corresponding age-matched WT controls were euthanized via CO_2 asphyxiation. Following euthanasia, animals were decapitated and the upper portion of the skull was immediately removed using fine tipped rongeurs (rats) or fine tipped curved forceps (mice). The entire brain was carefully removed with a sterile micro spoon and immediately placed ventral side up on a sterile pre-chilled dissection board. The whole hypothalamus was removed first using sterile curved tip forceps. The edges of the forceps were placed directly around the hypothalamus and pinched together to gently lift the hypothalamic tissue from the brain. The tissue was placed in a labelled tube and immediately snap frozen on dry ice. Following removal of the hypothalamus, the brain was placed dorsal side up and the cerebellum was removed by placing the fine edge of the scalpel between the cerebellum and the cortices. The whole cerebellum was placed in a labeled tube and snap frozen on dry ice. The remaining brain tissue was divided into the left and right hemispheres by cutting down through the longitudinal fissure. Each hemisphere was placed medial side up and the remaining white matter was removed. Left and right hippocampi were gently removed using two sterile micro spoons, placed in the appropriate tubes and snap frozen on dry ice. The remaining left and right cortices were divided into 4 pieces of relatively equal weight and either placed in the appropriately labeled tubes.

Peripheral Tissue Dissection. Selected peripheral tissues were dissected from indicated animals following CO_2 euthanasia. Briefly, the abdominal cavity was opened using scissors and one lobe of the liver was extracted and snap frozen in a labeled tube. The rib cage was then severed using sterile bone scissors allowing for the extraction of lung and heart tissues. The pancreas was removed by gently severing the connection between the pancreas and intestines and lastly selected reproductive tissues were removed. All tissue samples were snap frozen on ice and stored in -80 °C until tissue processing.

Protein Extraction Techniques

Whole Tissue Protein Extraction. 30 mg tissue from indicated peripheral organs or brain regions was homogenized using the Bullet Blender 24 Homogenizer (Next Advance, Averill Park, NY) with 100 µL 0.5 mm glass beads in variable volumes of Tissue Protein Extraction Reagent (TPER) supplemented with protease and phosphatase inhibitors according to the manufacturer's instructions. Briefly, whole tissues were combined with glass beads and TPER and homogenized at speed 8 for 3 min at 4 °C. Following homogenization, lysates were cleared via centrifugation at 10,000 x g for 10 min at 4 °C. Protein concentrations were then assessed using the commercially available BCA Assay (Pierce Biotechnology)

Whole Cell Protein Extraction. Whole neuron or neuro-2a cell extracts were collected using the commercially available Neuronal Protein Extraction Reagent (NPER) according to the manufacturer's instructions. Briefly, cell-type-specific maintenance medium was removed and cells were washed 1 time with sterile 1X PBS. PBS was aspirated and 100-200 µL NPER supplemented with PPI was added to each well of neurons/neuro-2a cells and allowed to incubate on ice for 5 min. Following incubation, cells were removed by scraping and collected in labeled 1.5 mL centrifuge tubes. Tubes were sonicated for 10 seconds followed by centrifugation at 10,000 x g for 10 min at 4 °C. Remaining supernatants were transferred to new sterile centrifuge tubes and stored at -80 °C until use.

Subcellular Fractionation of Cultured Cells. Cultured neurons, astrocytes, or neuro-2a cells were washed 1 time with 1X PBS. PBS was aspirated and cells were removed from dishes by gently scraping in 1 mL 1X PBS. Cell suspensions were collected and cells were pelleted by centrifugation at 4,000 x g for 5 min at 4 °C. PBS was aspirated and cell pellets were resuspended in 200 µL Cytosolic Extraction Buffer (CEB). Samples were incubated for 10 min at 4 °C with rotation followed by 8 passes through a 22 G needle. Samples were centrifuged at 1,500 x g for 8 min at 4 °C and the supernatant was removed and placed in a separate tube. The supernatant was then centrifuged at 8,000 x g for 10 min at 4 °C after which the supernatant (cytosolic proteins) was pipetted into a new labeled tube. The remaining pellet from this spin (crude mitochondrial fraction) was resuspended in 30 µL Mammalian Protein Extraction Reagent (MPER) supplemented with PPI and stored at -80 °C. The pellet from the first spin (nuclear proteins) was resuspended in 200 µL Nuclear Extraction Buffer and sonicated 2 x 10 sec with 10 sec intervals on ice. Following sonication, the samples were cleared of cellular debris by centrifugation at 10,000 x g for 10 min at 4 °C and supernatants were placed in a new labeled centrifuge tube.

Three-Buffer Tissue Fractionation. Cytosolic, organelle, and nuclear proteins were extracted from freshly dissected brain tissue sections using a previously described three-buffer extraction system (Baghirova, Hughes, Hendzel, & Schulz, 2015) with slight modifications. Briefly, cortical tissues were dissected from indicated animals as previously described (Brain Tissue Dissection). Tissues were minced into smaller sections using a scalpel and homogenized 5 times with Pestle A in a 2 mL Dounce Homogenizer containing 1 mL Lysis Buffer A supplemented with PPI. Tissue suspension was then placed in a 1.5 mL centrifuge tube and centrifuged at 500 x g for 10 min at 4 °C. The supernatant was placed in a new centrifuge tube and incubated on an end-over-end rocker for 10 min at 4 °C. Following incubation the tissue suspension was centrifuged at 4,000 x g for 10 min at 4 °C and the supernatant (Cytosolic Fraction) was removed and placed in a sterile labeled centrifuge tube. The remaining pellet was then re-suspended in 500 µL Lysis Buffer B supplemented with PPI. Samples were incubated for 30 min at 4 °C on an end-over-end rotator followed by centrifugation at 6,000 x g for 10 min at 4 °C. The supernatant (Organelle Fraction), which

contains proteins from membrane-bound organelles (mitochondria, endoplasmic reticulum, Golgi, etc.) except those from the nucleus, was stored in a labeled tube at -80 °C until use. The remaining pellet was then re-suspended in 500 µL Lysis Buffer C supplemented with PPI and incubated for 10 min at 4 °C on an end-over-end rocker followed by centrifugation at 6,800 x g for 10 min at 4 °C. The supernatant (Nuclear Fraction) was removed and stored at -80 °C until use.

Mitochondria Isolation Techniques. All mitochondrial samples were isolated from freshly harvested cortical tissues extracted from female WT mice between 5-7 months of age. All isolation procedures were performed on ice with pre-chilled buffers or in pre-chilled refrigerated centrifuges.

Discontinuous Percoll Gradient. 5-7 month old female WT mice were euthanized (2 mice/isolation) and whole cortical tissues were dissected as previously described. Brain sections were washed for 10 seconds by gently swirling tissues in 20 mL ice cold Mitochondria Isolation Buffer (MIB) without PPI or BSA. Tissues were then transferred to a small weigh boat and minced into 8-10 small pieces. Brain tissue was then transferred to a 5 mL glass dounce homogenizer containing 5 mL ice cold MIB supplemented with PPI and 0.05% BSA (added fresh) and gently homogenized using 10 slow strokes on ice. The homogenate was then transferred to a 30 mL polycarbonate tube on ice and centrifuge at 1,330 x g for 8 min at 4°C (Spin 1). The supernatant was pipetted into a separate polycarbonate tube and placed on ice and the homogenization was repeated on the pellet followed by centrifugation 1,330 x g for 8 min at 4°C (Spin 2). Supernatants from Spin 1 and Spin 2 were combined and centrifuged once more at 1,330 x g for 8 min at 4°C (Spin 3). The supernatant from Spin 3 was pipetted into a sterile 30 mL polycarbonate tube and a 100 µL aliquot was removed and stored in a labeled tube (WCL). The remaining supernatant was centrifuged at 21,200 x g for 10 min at 4°C (Spin 4). The supernatant was discarded and the remaining pellet was resuspended by pipetting in 6 mL 15% Percoll. The resuspended pellet was centrifuged at 21,200 x g for 10 min at 4°C (Spin 5). Using a P-1000 pipette, the loose pellet of 'crude' mitochondria (~1-2 ml) on the bottom of the tube was layered onto a pre-made Percoll 23%/40% discontinuous Percoll gradient. The

gradient was centrifuged at 40,000 x g for 18 min at 4°C (Spin 6). The cloudy white interface between the two percoll layers was removed with a glass pasteur pipette and placed into a new 15 mL polycarbonate tube. In addition, the upper layer of the percoll gradient containing crude mitochondria was also removed and placed into a second 15 mL polycarbonate tube. MIB without protease inhibitors was added to a total of 10 mL and the mitochondrial samples were centrifuged at 21,700 x g for 13 min at for 4°C (Spin 7). The loose pellet at the bottom of the tube was removed and pipetted into a sterile labeled 1.5 mL centrifuge tube and centrifuged at 6,600 x g for 8 min at 4°C (Spin 8) in a table top centrifuge. The supernatant was removed and the remaining mitochondrial pellets were re-suspended in 50-100 µL MIB. Protein concentration was determined via BCA Assay and samples were analyzed as indicated.

Digitonin Mitochondrial Subfractionation. Pure mitochondria were isolated from female mouse brain tissue as previously indicated (previous paragraph) and subjected to a Digitonin-based Mitochondrial Subfractionation (Tropschug et al., 1988) in a protocol adapted from Nair et. al (Nair & McGuire, 2005). Mitochondria were resuspended in 200 uL Mitochondria Subfractionation Buffer (MSF Buffer) supplemented with 0.5 mg/mL BSA. The mitochondrial suspension was then separated into 4 50 µL aliquots and 50 µL of either MSF Buffer (Control) or 0.2%, 0.4%, or 0.6% Digitonin (diluted from a 1.6% stock solution in MSF Buffer) was added to respective tubes to yield a final concentration range of 0-0.3% Digitonin (100 µL total volume). Tubes were incubated for exactly 5 minutes on ice and quickly diluted with 100 µL cold MSF Buffer. Samples were transferred to polypropylene tubes and centrifuged at 50,000 x g for 25 min at 4°C in a Beckman SW-41 Ti Swinging Bucket Rotor. Supernatants were carefully removed and the pellet was resuspended in 30 µL MPER supplemented with PPI. Pellet suspensions were analyzed via SDS-PAGE to examine the expression profile of CLU against those of specific mitochondrial subfraction markers: VDAC (outer mitochondrial membrane), Cyt. C (intermembrane space), CoxIV (inner mitochondrial membrane), and Grp75 (Matrix).

Enzymatic Deglycosylation. Deglycosylation of CLU protein isoforms was achieved using 2 separate commercially available endoglycosidases according to the manufacturer's instructions. Briefly, 10-15 µg of selected cellular or tissue fraction lysates were incubated in Denaturing buffer for 10 min at 95 °C in a 10 µL reaction volume. Samples were then cooled to RT and deglycosylation reactions were assembled as indicated in Table 7. Reactions were incubated for 75 min at 37 °C. Following incubation, 20 µL Reducing 2X Laemmli Sample Buffer was added to each reaction and samples were analyzed for CLU immunoreactivity using SDS-PAGE. Denaturing Buffer, corresponding glycol buffers, and NP-40 were provided by NEB with the corresponding endoglycosidase.

Deglycosylation Reactions	
PNGase F (Total removal of all glycans)	Endo H (High Mannose Glycans)
10 uL denatured protein sample	
2 µL 10X Glyco Buffer 2	2 µL 10X Glyco Buffer 3
2 µL 10% NP-40	--
1 µL PNGase F (NEB, Cat. # P0704S, 500,000 units/mL)	2 µL Endo H (NEB, Cat. # P0702S, 500,000 units/mL)
5 µL ddH_2O	6 µL ddH_2O
Total Reaction Volume = 20 µL	

Table 6. Deglycosylation Reaction Composition. A list of components included in deglycosylation reactions.

Glutamate Toxicity. Primary cortical neurons were cultured as described and plated at a density of $5x10^5$ on PEI-coated 100 mm dishes (3 dishes per time point). At DIV7 neurons were exposed to 100 µM glutamate for 5 min at RT in pre-warmed 1X HEPES buffer. Following glutamate exposure, neurons were gently washed 1 time with 1X HEPES Buffer. HEPES Buffer was aspirated and 8 mL pre-warmed Neuron Maintenance Medium was added to each dish. Neurons were returned to the incubator and allowed to incubate for indicated time points. Neurotoxicity was assessed prior to cell harvest using the commercially available LDH Cytotoxicity Assay Kit (Pierce) according to the manufacturer's instructions. Following the confirmation of neurotoxicity, neurons were harvested using the previously described Subcellular Fractionation Protocol. A schematic of the neurotoxicity study performed in this dissertation is provided in

Immunoprecipitation. For neuronal lysate immunoprecipitation, primary cortical and hippocampal neurons were isolated and grown to maturity as previously described and lysed NPER supplemented with protease and phosphatase inhibitors as previously described. Protein concentration was determined and 1 mg of lysate was brought to a volume of 500 µL with IP Buffer and pre-cleared using 50 µL of Protein-A conjugated Dynabeads for 1 hr at 4°C with continuous rotation. Lysates were then divided into equal portions and incubated with either goat polyclonal anti-CLU C-18 (4 µg), rabbit polyclonal anti-CLU H-330 (4 µg), or equal concentrations of species specific IgG overnight at 4°C with continuous rotation. The immune complex was pulled out of solution using 50 µL Protein-A conjugated Dynabeads for 2 hr at 4°C with continuous rotation. Beads were washed 3 times with 500µL IP buffer and protein was eluted using 30 µL 2X SDS Sample Buffer at 37°C for 10 min. Eluted proteins were then analyzed via SDS-PAGE as indicated.

SDS-PAGE and Immunoblotting.

BCA Protein Assay. Protein concentrations were determined via the commercially available BCA Assay according to the manufacturer's instructions with minor modifications. Briefly, a standard curve was created using the guidelines provided in Table 7. 2 µL protein sample was used to measure total protein concentration. BCA Assay was incubated at 37 °C for 20 min and absorbance was measured at 562 nm.

BCA Standard Curve Layout			
Row in 96 well plate	Volume of BSA (2mg/mL) stock solution to add to well	Final protein amount in well	Volume of BCA reagent mixture to add to well
A	0 µL	0 µg	100 µL
B	1.25 µL	2.5 µg	98.75 µL
C	2.5 µL	5 µg	97.5 µL
D	5.0 µL	10 µg	95.0 µL
E	7.5 µL	15 µg	92.5 µL
F	10.0 µL	20 µg	90.0 µL
G	12.5 µL	25 µg	87.5 µL
H	15.0 uL	30 µg	85.0 µL

Table 7. BCA Standard Curve Layout. BCA Protein Standard Layout for analysis of protein concentration.

Preparation of Gels and Protein Samples. 7.5%, 10%, or 12.5 % resolving gels and stacking gels were generated using the recipes indicated in Table 8. Samples were diluted in appropriate buffers to an equal concentration and volume followed by the addition of 1 volume of 2X Reducing Laemli Sample Buffer. Prepared samples were then denatured by incubation at 95 °C for 5 min followed by centrifugation at 2,000 x g for 5 sec at RT.

Western Blot Gel Recipes				
	Resolving Gels			**Stacking Gel**
	7.5%	**10%**	**12.5%**	
ddH_2O (mL)	6.0	5.0	4.0	3.25
Lower Tris (mL)	3.0	3.0	3.0	1.25 (use Upper Tris)
30% Acyrlamide (mL)	3.0	4.0	5.0	0.55
TEMED	12µL	12µL	12µL	10µL
20% APS	28µL	28µL	28µL	20µL
Total Volume	**12mL (2 gels)**	**12mL (2 gels)**	**12mL (2 gels)**	**5.05 (2 gels)**

Table 8. Western Blot Gel Recipes. Western blot gel recipes for resolving and stacking gels used in SDS-PAGE.

Electrophoresis and Immunoblotting. 20-50 µg of total protein sample isolated from tissue or cells was resolved via reducing SDS-PAGE. Gels were run for 15 min at 125 V followed by 40 min at 180 V in 1X Western Blot Running Buffer. Resolved proteins were then transferred to 0.2 µm pore-sized PVDF membranes for 1 Hr on ice in Western Blot Transfer Buffer and blocked with 2% Blocking Buffer in 1X TBST for 1 hr at RT. Membranes were incubated with customized dilutions of the indicated primary antibodies for indicated time points (ranging from 1 hr at RT to 4°C overnight), followed by incubation with the appropriate HRP-conjugated secondary antibody for 1 hr at RT. Membranes were washed 3 x 10 min with continual rocking after each incubation with 1X TBST. Bands were visualized using chemiluminescence with an ECL detection kit (BioRad) and scanned using the C-Digit Blot Scanner (LI-COR). Where applicable membranes were stripped and re-probed using a panel of fraction-specific markers as indicated in the accompanying Relative intensities of the immunoreactive bands were quantified using

image digitizing software, Image Studio Version 4.0. Specific information regarding antibodies used for western blotting including dilutions, catalog and lot numbers, and vendors are listed in the following section.

3,3',5,5',-Tetramethylbenzidine Staining. For better visualization of protein isoform molecular weights, cellular fractionations, enzymatic deglycosylations, and tissue panels were stained using TMB Peroxidase (HRP) Substrate Kit (Vector Laboratories, Cat. # SK-4400) following antibody based detection and blot acquisition. TMB allows for the visualization of secondary antibody bound proteins on the membrane by forming a blue precipitate on HRP-bound antigens. Following acquisition of immunoblots, excess chemiluminescence was washed off with 1X TBST for 10 min at RT with constant rocking. While the immunoblot was washing, TMB solution was generated by diluting 2 drops of buffering solution, 3 drops of TMB substrate, 2 drops of stabilizing solution, and 2 drops of H_2O_2 in 5 mL ddH_2O. TBST was dumped and residual buffer was removed with a P1000 pipette. TMB Solution was added and blot was incubated for ~30 min – 1 hr at RT with continual rocking. Following incubation, TMB Solution was removed and the blot was washed 1 x 10 min at RT with continual rocking. Blots were dried for 30 min at 37 °C and scanned using a standard scanner.

Gene Expression Studies. All gene expression studies were performed using the QuantStudio 7 Flex Real-time PCR System (Applied Biosystems) equipped with a fast block. PCR reactions were loaded using Filtered Low Retention Pre-sterilized pipette tips (VWR, Cat. # 10017-060) into MicroAmp Fast Optical 96-well Reaction Plates (Applied Biosystems, Cat. #4346906 and sealed with MicroAmp Optical Adhesive Film (Applied Biosystems, Cat. #4311971), and briefly centrifuged at 1,000 x g for 1 min at 4 °C before PCR was initiated. I would like to formally thank Jennifer Hackett at the University of Kansas Sequencing Core for performing RNA quality analysis. All other experimentation in this section was performed by me.

RNA Isolation. Total RNA was isolated from 30 mg cortical tissue harvested from CLU-KO mice or ERβ-KO rats and corresponding WT controls using the commercially available Pure Link RNA Mini Kit with slight modifications. Briefly, 200 µL of TRIzol Reagent and 1 scoop of pre-chilled 400 µM Silica Beads (OPS Diagnostics, Cat. # BMBG 400-200-05) was added to 30 mg cortical tissue and homogenized using a pre-chilled Bullet Blender 24 Homogenizer for 1 min at speed 6. 400 µL TRIzol Reagent was added to each tube and samples were re-homogenized at speed 2 for 1 min. Samples were cleared of tissue debris via centrifugation at 10,000 x g for 1 min at 4 °C and 500 µL of the resulting supernatant was pipetted into a new sterile microcentrifuge tube. 100 µL Chloroform was added to each 500 µL sample and tubes were mixed by inversion for 15 seconds. Samples were centrifuged at 12,000 x g for 15 min at 4 °C and ~200 µL of the upper aqueous portion was pipetted into a new microcentrifuge tube. 1 volume of 70% ethanol was added to each sample and mixed by vortexing at max speed for 15 seconds. RNA was then purified using the PureLink RNA Mini kit according to the manufacturer's instructions. RNA quality was assessed and RNA with a RNA Integrity Number of 8 or above was used for reverse transcription.

Reverse Transcription. 2 µg total RNA was reverse transcribed using the Applied Biosystems High Capacity RNA-to-cDNA Kit (Applied BioSciences, Cat. # 4387406) according to the manufacturer's instructions. Reactions were performed in thin-walled PCR tubes (Molecular BioProducts, Cat. # 3418) on a T100 Thermo Cycler (BioRad). Reaction conditions were 37 °C for 1 hr followed by 95 °C for 5 min.

Rt-QPCR. Total CLU (tCLU), Exon 1-containing CLU, and mCLU gene expression was evaluated in 10 µL reactions containing 5 µL PowerUP SYBR Green MasterMix, 100 ng cDNA, 500 nM of forward and reverse primers (Table 9), and ultrapure ddH2O. In all gene expression studies, at least 2 control genes were also amplified and the gene that remained more consistent across groups was utilized: in this case β-Actin. Cycling conditions used are as follows: 50 °C for 2 min, 95 °C for 10 min followed by 40 cycles of 95 °C for 15 sec and 65°C for 1 min. To ensure the specificity of each primer, melt curve analysis was also performed for every primer set used.

Clusterin and Actin qPCR Primers		
Target	Forward (5'→3')	Reverse (5'→3')
Exon 1	CTTCCAGAAAGCTCCTGGTG	CTCCAGTGCGCTCCTCCT
Mature CLU (mCLU)	GCTGCTGATCTGGGACAATG	ACCTACTCCCTTGAGTGGACA
Total CLU (tCLU)	CCTTGCTCAACAGTTTAGAGGAA	CATCATGGTCTCGGTACACACTT
β-actin	GTGACGTTGACATCCGTAAAGA	GCCGGACTCATCGGACTCC

Table 9. rt-qPCR Primer Sequences. Primers used to amplify CLU mRNAs and β-actin.

Mitochondrial Co-immunoprecipitation Studies. The following 10 methods paragraphs (pLX304-hCLU-v5 Plasmid Description - Secondary Confirmation of Identified Interacting Partners) pertain to a single experimental study that is presented in Chapter 2 (Section 2.2) of the Results in this dissertation and are therefore grouped together for the convenience of the reader. I would to formally thank Dr. Yakov Mikhailovich Koen (University of Kansas) for performing the Trypsin Digestion and Dr. Antonio Artigues (University of Kansas Medical Center) for performing the LC-MS/MS Analysis (MudPIT). All other experiments and bioinformatics in this study were performed by me.

pLX304-hCLU-v5 Plasmid Description. The plasmid construct used in these studies was generated by Dr. David Root and deposited into the DNASU Plasmid Repository • PSI:Biology-Materials Repository. Briefly, full length human CLU (Accession #: NM_001831.3) cDNA was inserted into the mammalian expression vector pLX304 to create a fusion protein. The resultant plasmid expresses full-length hCLU protein fused to a c-terminal V5 epitope tag and is referred to here as pLX304-hCLU-v5 (Clone: HsCD00435174, Schematic 9). Protein expression is driven by the CMV promoter and immunoblot analysis of transfected cells indicates robust expression of multiple CLU isoforms by both anti-CLU antibodies as well as the anti-V5 antibody.

Plasmid Amplification and Isolation. LB ampicillin plates (18.5 g LB Agar, 12.5 g LB Broth, Miller, 100 µg/mL Ampicillin) were inoculated with bacteria taken from the DNASU pLX304-hCLU-v5 stab culture and incubated for 16 hrs at 37 °C. The following morning, 5 mL LB Broth supplemented with 100 µg/mL ampicillin was inoculated with a single colony and allowed to grow for 8-10 hrs at 37 °C at 200 rpm on a floor shaker. This volume was expanded to 150 mL LB Broth supplemented with 100 µg/mL ampicillin

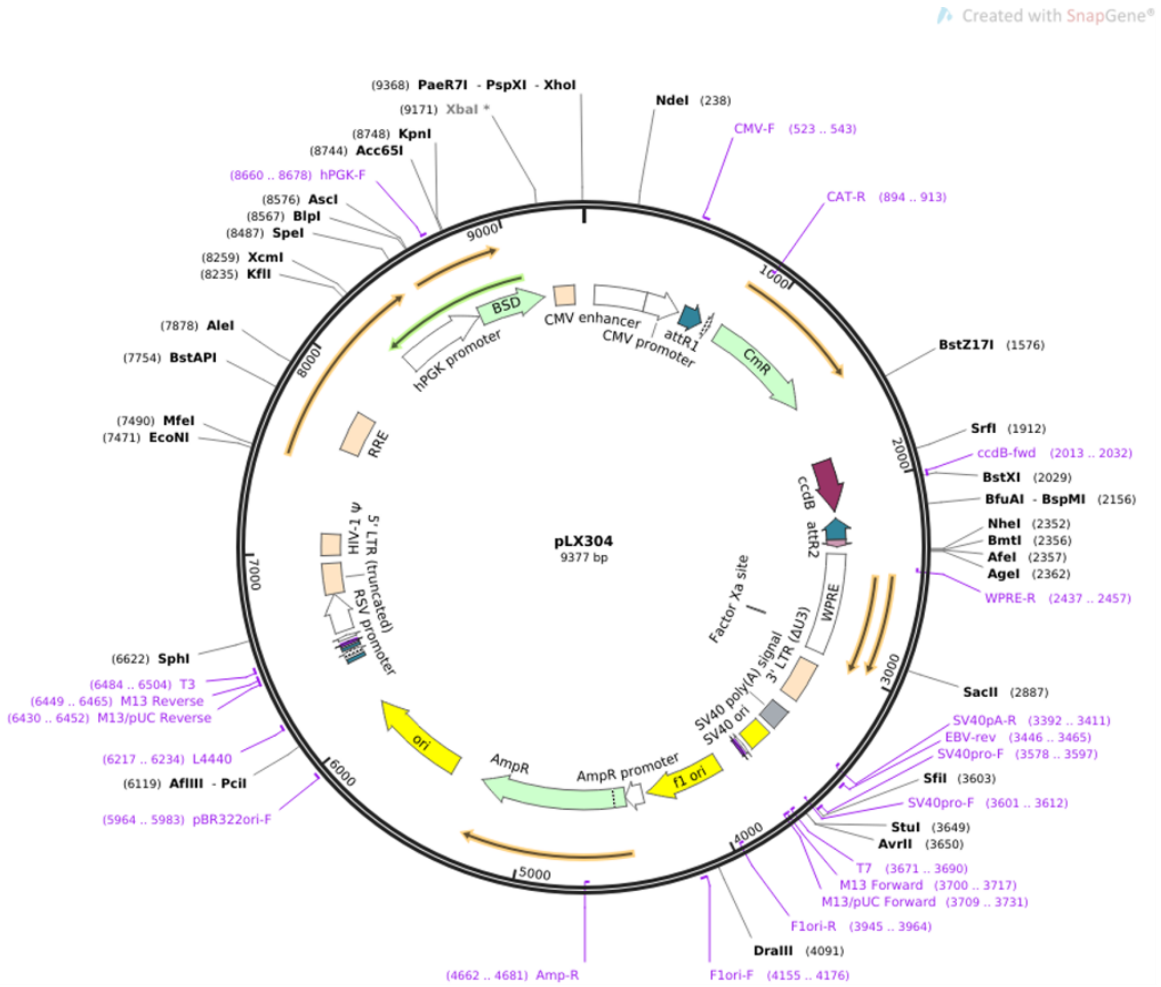

pLX304-hCLU-V5
(DNAsu Plasmid Repository)

Schematic 9. Description of the pLX304-hCLU-v5 Plasimd used in this Dissertation. Full length human CLU cDNA fused to a c-terminal v5 epitope tag was inserted into the multiple cloning site of the lentiviral expression vector pLX304 to generate pLX304-hCLU-v5. This plasmid was generated by Dr. David Root and is available for purchase from the DNAsu Plasmid Repository.

over the course of 2 days at which time 2 mL bacterial suspension was removed, centrifuged, and the pellet was resuspended in LB Broth supplemented with 50% glycerol and 100 µg/mL Ampicillin in a 2 mL Cryopreservation tube. Tubes were labeled with colony ID and stored at -80 °C as a bacterial stock. The remaining bacterial culture was pelleted at 6,000 x g for 15 min at 4°C and plasmid DNA was extracted

and purified using the commercially available QIAGEN Midi Kit according to the manufacturer's instructions.

pLX304-hCLU-v5 Overexpression. Neuro-2a cells were plated in 150 mm dishes in antibiotic-free Neuro-2a Maintenance Medium and allowed to grow at 37 °C until the confluency reached 40%. At 40% confluency 20 µg of pLX304-hCLU-v5 was transfected using Lipofectamine 3000 according to the manufacturer's instructions. Briefly, 30 minutes prior to transfection, medium was replaced with 15 mL OptiMEM. 20 µg of plasmid was diluted in 500 µL OptiMEM supplemented with 80 µL P3000 Reagent (Tube A). In an additional tube (Tube B), 40 µL Lipofectamine 3000 Reagent was diluted in 500 µL Opti-MEM. Both tubes were incubated at RT for 5 min, after which time Tube A and Tube B were combined to make 1 sample (Transfection mixture). The transfection mixture was incubated at RT for 45 min and added drop-wise to the 150 mm dish. Transfection was allowed to occur overnight at 37 °C. The following morning, the OptiMEM/Transfection Mixture was replaced with Neuro-2a Maintenance Medium and allowed to grow for 96 hrs prior to harvest.

Co-immunoprecipitation. Crude mitochondria were isolated from N2a cells overexpressing pLX304-hCLU-v5 using subcellular fractionation as previously indicated. The crude mitochondrial pellet was resuspended in 500 µL Co-IP Buffer supplemented with protease and phosphatase inhibitors and protein concentration was determined using BCA Assay. While protein concentration was being measured, 100 µL Protein G Dynabeads (Thermo Scientific) were washed 2 x 1 mL with cold Co-IP buffer and re-suspended in 100 µL cold Co-IP Buffer. Beads were kept on ice until pre-clearing step. 400 µg crude mitochondrial lysate was combined with 600 µL cold Co-IP buffer to bring the volume to 1 mL. 30 µL of pre-washed Protein G Dynabeads were added to the 1 mL sample and sample was incubated for 1 hr at 4°C with rotation. Following pre-clear, beads and cleared supernatant were separated and the supernatant was divided equally between 2 tubes. The volume in each tube was brought to 1 mL with cold Co-IP buffer and 4 µg of Rabbit IgG (Control) or Rabbit anti-V5-Tag (IP) was added. Samples were incubated overnight at 4°C with rotation to allow the antibody-antigen complex to form. Following overnight immunoprecipitations, complexes

were pulled out of solution using 30 µL pre-washed Protein G Dynabeads per immunoprecipitation. Bead-antibody-antigen complexes were allowed for form by incubating mixtures for 2 hrs at 4°C with rotation. The supernatant was then removed and the beads were washed 5 times with 1 mL ice-cold Co-IP buffer. Beads were incubated for 4 min at 4°C with rotation between each wash. Following the 5th wash, all Co-IP buffer was removed and beads were resuspended in 40 µL 2X Laemmli sample buffer containing β-mercaptoethanol and samples were incubated at 95 °C for 5 min. Following elution, beads were removed from samples and 30 µL of sample was resolved via SDS-PAGE. For purposes of LC-MS/MS analysis the resulting gel was stained with SYPRO Ruby as indicated in the following section. In addition, 5 µL of the eluted sample was analyzed for CLU expression to ensure the immunoprecipitation of CLU.

SYPRO Ruby Staining. Following Co-IP of overexpressed pLX304-hCLU-v5 and electrophoresis of eluted proteins/protein complexes, gels were placed in Fixing Solution and incubated for 60 min at RT with continuous rocking. Gels were then incubated in 50 mL SYPRO Ruby fluorescent gel stain (Bio-Rad) overnight at RT with constant rocking. Following overnight incubation, SYPRO Ruby stain was removed and the gels were washed 3 times for 10 min with 50 mL ddH_2O.

Band Excision and Proteolytic Digestion. Following SYPRO Ruby staining, gels were visualized and protein bands specific to the IP lane (i.e. not present in the Control lane) were excised using a UV transilluminator and sterilized razor blades. Gel pieces were then minced into 2 mm square pieces and transferred to sterile microcentrifuge tubes and covered in deionized water and stored at 4°C until Trypsin digestion. On the day of trypsin digestion, samples were removed from 4 °C and allowed to acclimate to RT. Samples were then washed 2 times with 150 uL of freshly prepared TD Washing Solution by incubation in a shaking water bath at 30 °C for 30 min. Following each incubation, samples were chilled at 4 °C for 3 min then briefly centrifuged (3-5 sec) to collect condensation from tube caps. Following the second wash, the supernatant was completely removed from the gel pieces and gels were dehydrated by adding 150 uL 100% MeCN. Samples were vortexed and incubated at RT for 5-7 min. MeCN was then removed and gel pieces were allowed to air dry for 5-7 min. Samples were reduced by the addition of 70-90 µL of TD

Reducing Buffer to each tube. Samples were incubated at 50°C in a shaking water bath for 60 min followed by a brief centrifugation (3-5 sec). Following centrifugation, the supernatant was completely removed. Immediately following the removal of TD Reducing Buffer, 70-90 µL TD Alkylating Buffer was added to each tube. To ensure this step was performed in haste, individual samples were processed successively in the following manner: Reducing Buffer was removed from first tube, Alkylating Buffer was immediately added, and sample was vortexed and placed in the dark. All samples were then incubated at RT in the dark for 45 min with occasional vortexing after which time the supernatant was removed. 100 µL 100 mM Ammonium Bicarbonate (Bicarb). Was added to each sample and tubes were briefly vortexed and incubated for 10 min at RT. Bicarb was removed and replaced with 100 µL 100% MeCN and incubated for 10 min. The 100% MeCN was removed and the Bicarb/MeCN cycle was repeated once again. Following the second Bicarb/MeCN cycle, dehydrated gel pieces were dried for 50-60 min in a fume hood with constant air flow. 70-100 µL Digestion Buffer was added to each tube and samples were incubated for 15-20 min at RT to facilitate the re-swelling of gel pieces. Following incubation, 20-60 µL of Digestion Buffer without trypsin was added to each tube and samples were incubated at 37 °C in a shaking water bath overnight. The next morning, samples were briefly centrifuged to collect condensation and incubation was continued for a total incubation time of 19 hrs. Hydrolysis was terminated by placing tubes on ice for 3-5 min followed by brief centrifugation. Supernatants were collected (variable volumes) and transferred to sterile 1.5 mL Eppendorf tubes. 1% TFA was added to a final concentration of 0.1% and samples were vortexed and stored at -20°C until needed for analysis. A complete outline of buffers, 1% TFA added, and final digest volumes is provided in Table 10.

Multidimensional Protein Identification Technology (MUDPit). Following enzymatic digestion, the extracted peptides were concentrated on a centrivac concentrator (Labconco) to a final volume of 20µl. The peptide extracts were analyzed using an Orbitrap Fusion Lumos mass spectrometer (Thermo Fisher Scientific) coupled to an uHPLC (nLC 1200, Thermo Fisher Scientific). In each run, the sample was injected directly into the reversed phase column (50 µm ID fused silica packed in-house with 15cm of 100

Å, 5 µ, Magic C18 particles, Michrom Bioresources), and washed with 0.1% formic acid for 15 minutes at 300 nl/min. The column was mounted on the electrospray stage of the mass spectrometer, and the peptides were eluted with a gradient of acetonitrile (solvent B: 90 % acetonitrile, 0.1% formic acid) in 0.1% formic acid in water (solvent A). The gradient profile was as follows: 0-5 min, 5-15% B; 5-60 min, 15-40% B; 60-70 min, 40% B; 70-75 min, 40-75% B; 75-83 min 75% B. At the end of each chromatographic run, the column was washed with 100% B. The flow rate was maintained at 300 nl/min. The mass spectrometer was controlled by the Xcalibur software to perform continuously mass scan analysis on the Orbitrap in the range of 400-1900 m/z at 50,000 resolution, followed by MSMS scans on the ion trap, with a dynamic exclusion of one repeat scans of the same ion, 30 s repeat duration and 90 sec exclusion duration. Normalized collision energy for MS/MS was set to 35%. The isolation window used was 1.6 amu. For data analysis all MSMS scans were searched using Proteome Discoverer (version 2.0, Thermo Fisher Scientific) running the Sequest HT algorithm. Database search was conducted against a Mus musculus protein database derived from the NIBInr repository as in January 9, 2017. The refined data were subjected to database search using Trypsin cleavage specificity, with a maximum of 2 missed cleavages. The following variable modifications were selected: pyroglutamination from Q and E (N-terminal), oxidation of M, and deamidation of N, Q. Carboxymethylation of C was selected as a fixed modification, and a maximum of 3 modifications/peptide was allowed. Estimation of false positive rate (FDR) was conducted by searching all spectra against a decoy database consisting of the inverted sequences of all proteins in the original (direct) database. For peptide identification a FDR 0.5 was defined and a minimum of two unique peptides per protein was required for protein identification. Amino acid sequence assignment of all peptides of interest were subsequently inspected manually.

STRING Pathway Analysis. Protein interaction networks were generated from the list of identified mitochondrial proteins listed in Table 14 using STRING Pathway Analysis Software. STRING is a database containing experimental and curated protein-protein interaction data from over 9 million proteins derived from 2000+ organisms (Szklarczyk et al., 2015). Experimental evidence is

collected from BIND, DIP, GRID, HPRD, IntAct, MINT, and PID while curated data is extracted from Biocarta, BioCyc, GO, KEGG, and Reactome. The probability of a given interaction, which was set to medium in our studies, is calculated by combining the probabilities from the different evidence channels and corrected for the probability of randomly observing an interaction (von Mering et al., 2005). For more information regarding specific aspects of the STRING software, please visit https://string-db.org/cgi/help.pl?UserId=MwnaiLZ0llBq&sessionId=f1dbaG6Rj9wg.

Secondary Confirmation of Identified Interacting Partners. Fresh brain tissue was extracted from 6-month-old female mice and minced in ice-cold Co-IP Buffer supplemented with PPI. Minced tissue was homogenized with 10 strokes using a glass handheld homogenizer and crude mitochondria were isolated using differential centrifugation as previously discussed. The crude mitochondrial pellet was re-suspended in 500 µL Co-IP Buffer and protein concentration was determined. 500 µg of crude mitochondrial lysate was utilized for each co-immunoprecipitation and each lysate was pre-cleared as previously described. Pre-cleared lysates were subjected to immunoprecipitation overnight at 4 °C with rotation using the following antibodies: mouse anti-Grp75 (2 µg, BioRad), rabbit anti-Mitofilin (2 µg, ProteinTech), goat anti-Clusterin M-18 (4 µg), or rabbit anti-Tom70 (4 µg). In all experiments, control immunoprecipitations were performed using identical concentrations of the appropriate species-specific immunoglobulin. Following overnight immunoprecipitations, complexes were pulled out of solution using 30 µL pre-washed Protein G Dynabeads per immunoprecipitation. Bead-antibody-antigen complexes were allowed for form by incubating mixtures for 2 hrs at 4°C with rotation. The supernatant was then removed and the beads were washed 5 times with 1 mL ice-cold Co-IP buffer. Beads were incubated for 4 min at 4°C with rotation between each wash. Following the 5th wash, all Co-IP buffer was removed and beads were resuspended in 40 µL 2X Laemmli sample buffer containing β-mercaptoethanol and samples were incubated at 95 °C for 5 min. Following elution, beads were removed from samples and 30-35 µL of sample was resolved via SDS-PAGE.

Sample Outline for Protein Identification					
Sample #	**Digestion buffer added, µL**	**Buffer (no trypsin) added, µL**	**Incubation super collected, µL**	**1% TFA added, µL**	**Final digest ("Super") vol., µL**
Co-IP 1	50	15	33.0	3.6	36.6
Co-IP 2	50	15	32.0	3.4	35.4
Co-IP 3	50	15	34.0	3.8	37.8
Co-IP 4	50	15	35.0	4.1	39.1
Co-IP 5	50	15	42.5	4.7	47.2
Co-IP 6	50	15	45.0	5.0	50
Co-IP 7	50	15	38.0	4.3	42.3
Co-IP 8	50	15	32.0	3.4	35.4
Co-IP 9	50	20	30.0	3.2	33.2
Co-IP 10	50	15	36.0	4.0	40
Co-IP 11	50	15	46.5	5.1	51.6
Co-IP 12	50	15	40.0	4.4	44.4
Co-IP 13	50	15	30.0	3.3	33.3
Co-IP 14	50	15	28.5	3.0	31.5
Co-IP 15	50	15	18.0	2.0	20
Co-IP 16	50	45	55.0	6.1	61.1
Co-IP 17	50	30	39.0	4.4	43.4
Co-IP 19	50	15	21.0	2.3	23.3

Table 10. List of Samples Submitted for Protein Identification. List of buffers, 1% TFA added, and final digest volumes is provided for protein identification

Mitochondrial Respirometry. The following 5 methods paragraphs (Equipment and Calibration – Data Analysis) pertain to a single experimental study that is presented in Chapter 2 (Section 2.4) of the Results in this dissertation and are therefore grouped together for the convenience of the reader. All experiments, calibration, troubleshooting, and analyses in this study were performed by me.

Equipment and Calibration. Brain mitochondrial respiration was evaluated using the OROBOROS Oxygraph-2K Machine at 37 °C with constant stirring. Prior to use, the chambers were cleaned for 30 min with 2 mL freshly prepared 70% ethanol with constant stirring. Ethanol was removed and residual ethanol was washed from the chamber using 2.2 mL ultrapure ddH_2O for 10 min with constant stirring. 2 mL sterile Calibration Buffer was then added to the machine and allowed to acclimate for 30 min with constant stirring

to achieve a stable readings in both temperature and oxygen concentration. All solutions and mitochondria were injected into the calibrated chambers using Hamilton Glass Microsyringes. Before and after each injection, syringes were cleaned 2 times with 70% ethanol and 2 times with ultrapure ddH_2O and tips were dried with a kim wipe.

Mitochondrial Enrichment. Crude mitochondria were isolated from freshly dissected cortical tissues isolated from 6-month-old female WT and CLU-KO mice (n=5 animals/genotype) using the commercially available Abcam Mitochondria Isolation Kit with slight modifications. Briefly, cortical tissues were extracted as previously described and minced in ice cold kit provided mitochondrial isolation buffer supplemented with PPI. Minced brain tissue was transferred to a 2 mL kit provided glass dounce homogenizer and homogenized using 5 strokes with pestle A and 5 strokes with pestle B. The homogenate was transferred into 2 2.0 mL centrifuge tubes and the volume was brought to 2 mL with kit provided mitochondrial isolation buffer. Tubes were inverted 5 times slowly to mix the homogenates and then centrifuged at 1,000 x g for 10 min at 4°C (Spin 1). The supernatant from Spin 1 was pipetted into new 2.0 mL centrifuge tubes, filled to 2 mL with mitochondrial isolation buffer and re-centrifuged (Spin 2). The supernatant from Spin 2 was removed and placed into 2 new 2.0 mL centrifuge tubes. Tubes were filled to 2 mL with mitochondrial isolation buffer and centrifuge at 5,500 x g for 15 min at 4°C (Spin 3). The supernatant from Spin 3 was removed and saved in a new 2.0 mL centrifuge tube as the Cytosolic Fraction while the remaining pellets were gently resuspended in a total volume of 200 µL Mitochondrial Respiration Buffer. Protein concentration was then determined using a BCA Assay as previously described.

Mitochondrial Substrates and Inhibitors. A complete list of mitochondrial substrates and inhibitors, solution concentrations (working and final), volumes added, as well as substrate/inhibitor targets in provided in Table 11.

Mitochondrial Respirometry Information – Substrates and Inhibitors				
Compound	**Working []**	**Volume added (µL)**	**Final []**	**Target**
Pyruvate	1 M	20	10 mM	Complex I
Malate	0.4 M	10	2 mM	Complex I
Succinate	1 M	10	5 mM	Complex II
ADP	200 mM	20	2 mM	Complex V
Oligomycin	1 mg/mL	2	2 µM	ATP Synthase
FCCP	100 µM	2.5	125 nM	Membrane
Rotenone	1 mM	2	2 µM	Complex I
Antimycin A	1 mM	2	2 µM	Complex III

Table 11. Components Used in the Analysis of Mitochondrial Respiratory Capacity. Compounds, solution concentrations, and compound targets used in Mitochondrial Respirometry studies.

Analysis of Mitochondrial Respirometry. 300 µg crude mitochondria from WT and CLU-KO mice were injected into the 2 chambers of the Oxygraph using glass syringes. Following injection mitochondria were incubated in chambers for 8-10 minutes to allow for the generation of a stable baseline respiration reading. After baseline respiration was established substrates an inhibitors were injected into each chamber simultaneously in the following order: Pyruvate, Malate, Succinate, ADP, Oligomycin, FCCP, Rotenone, Antimycin A. For a complete list of volumes and concentrations of each compound, see Table 10. Following each injection, mitochondria were incubated for 2-3 min or until a stable signal was observed in the chamber. Following the completion of Antimycin A injection, mitochondria lysate was aspirated from the chamber and the chambers were cleaned and calibrated as previously described.

Glutamate Dehydrogenase Activity Assay. Glutamate dehydrogenase-mediated production of NADH was assessed in 30 µg crude mitochondria isolated from female WT and mCLU-KO mice using the commercially available Glutamate Dehydrogenase Activity Assay (Sigma, Cat. #MAK099) as per the manufacturer's instructions. Data were analyzed using Student's T-test (n=4 animals/genotype)

Data Analysis. The respirometry protocol used in these experiments allows for the visualization of baseline respiration, oxidative phosphorylation, maximal respiratory response, and non-mitochondrial respiration. OROBOROS DatLab software was used to calculate the OCRs and to generate the graphical representation of experimental data: an example of the expected output is provided in Schematic 12. This analysis is

performed by polarographic oxygen sensors which monitor alterations in oxygen concentration over time. The negative time derivative is accordingly corrected for instrumental background and resulting data is

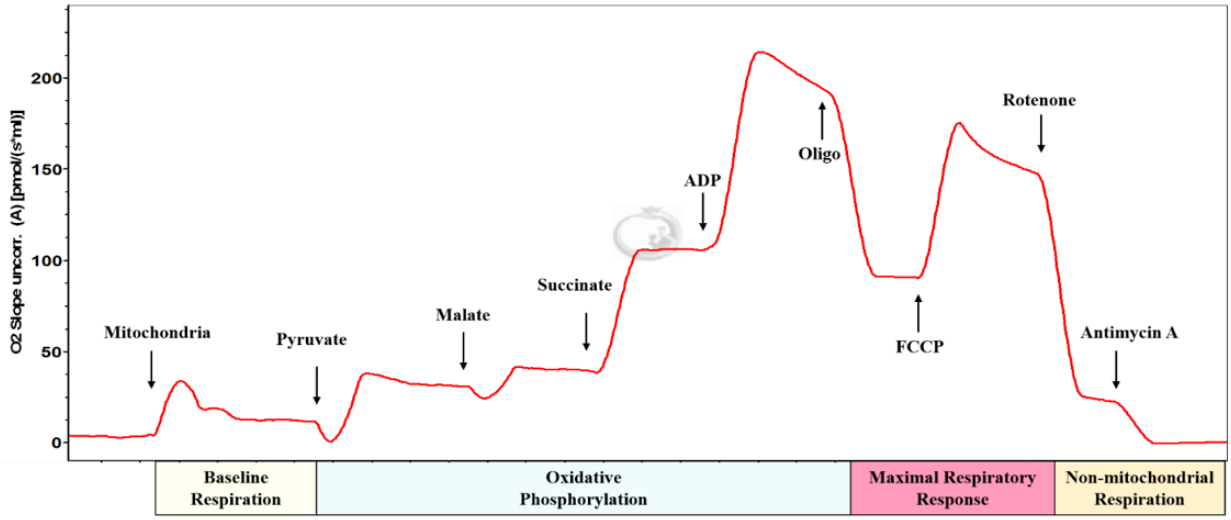

Schematic 10. Representation of Output Expected Following Analysis of Mitochondrial Respirometry.

displayed simultaneously from both chambers in real time as oxygen flux. For comparisons between WT and CLU-KO, average values are collected from 25 time points approximately 1-2 min following the addition of each compound (this is generally the time when a stable signal was generated) Averages for each compound taken from 3-4 independent comparisons are analyzed via Student's T-Test where * = $p<0.05$ when compared to WT control .

Sex Hormone Work. The following 6 methods paragraphs (Sex Hormone and Receptor-specific agonist Treatment - DNA Amplification and Calculation of Fold Enrichment) pertain to experimental studies presented in Chapter 3 (Sections 3.1-3.2) of the Results in this dissertation. All experiments, troubleshooting, and analyses in these studies were performed by me.

Sex Hormone and Receptor-specific Agonist/Inhibitor Treatment. Following 7 days in vitro (DIV), primary cortical neurons were treated with customized concentrations of progesterone (P4, 10 nM – 100 nM), 17β-estradiol (E2, 10 nM – 100), 4,4',4"-(4-Propyl-[1H]-pyrazole-1,3,5-triyl)trisphenol (PPT, 100

nM,), or 2,3-bis(4-Hydroxyphenyl) propionitrile (DPN, 100 nM,) for 48 hours. For inhibitor studies, DIV 7 neurons were pre-treated for 2 hours with 1,3-Bis(4-hydroxyphenyl)-4-methyl-5-[4-(2-piperidinylethoxy)phenol]-1H-pyrazole dihydrochloride (MPP, 1 μM) followed by 48 hours co-treatment with MPP plus E2. Following treatment, neurons were harvested via Whole Cell Protein Extraction with NPER as indicated and analyzed for CLU expression via SDS-PAGE

In silico Promoter Analysis. To determine (a) if the CLU promoter to contains one or more un-defined estrogen response elements (EREs) and (b) if the possibility of CLU EREs is consistent across species, human and murine CLU promoters were analyzed using Genomatix MatInspector Software. The Genomatix software is a tool that utilizes a large library of matrix descriptions for transcription factor binding sites to locate matches in DNA sequences. For more detailed information regarding the features of the MatInspector Software, see Cartharius et al. 2005 (Cartharius et al., 2005)

Genomatix MatInspector Promoter Analysis of Human CLU			
Gene	**Start**	**Stop**	**Strand**
ESR1 (ER-alpha)	861 73	879 91	- -
ESR2 (ER-beta)	470	488	+

Table 12. Genomatix Software Promoter Analysis. Predicted estrogen receptor response elements in the human CLU promoter.

Generation of ER-specific primers. Genomatix promoter analysis indicated the presence of three possible EREs within the human and murine CLU promoters (Figure 6): two ER-alpha binding sites (1 proximal and 1 distal) and 1 ER-beta binding site. Information regarding the specific location and strand of predicted EREs is provided in Table 13. Using this information, we performed a search of all known CLU promoter analyses and were able to identify a previously published primer set that amplifies the region adjacent to the predicted ER-alpha binding site. The individual primers were developed by IDT and are deemed ER-alpha Forward (5' – CGGTGCTGCACCGGCCC - 3') and ER-alpha Reverse (5' –

CTGGGAGGCGCCGTATTTATAGC - 3'). Following a search of the literature, we were unable to identify a primer set that would amplify the region with a predicted ER-beta binding site, therefore we purchased a primer set from Qiagen that amplifies a region approximately 100 bp downstream from the predicted ER-beta binding site (EpiTect ChIP qPCR Primer Assay For Human CLU, NM_203339.1 (-)01Kb (GPH1026114(-)01A))

Crosslinking and Analysis of Sheared Chromatin. Human bone-marrow-derived neuroblastoma cells (SH-SY5Y) were treated with either Vehicle, DPN (100 nM), or PPT (100 nM) for 48 hours. Following treatment, DNA and protein were crosslinked for 15 min in 10 mL ChIP Fixing Solution at RT. Crosslinking was neutralized by the addition of 0.125 M Glycine followed by one wash in 1X PBS. Cells were scraped in 10 mL 1X PBS and pelleted at 1,000 x g for 5 min at RT. Cell pellets were re-suspended in 1 mL ChIP Lysis Buffer supplemented with protease and phosphatase inhibitors and sonicated 5 x 30 sec with 10 sec breaks between each sonication. Following sonication, insoluble particles were cleared from the lysate by centrifuging at 17,000 x g for 45 min at 4°C. To ensure the proper size of sheared chromatin fragments, 10 µL sheared chromatin was purified by reversal of crosslinking (see below) and run on a 2% agarose gel. In addition, purified DNA from treated and un-treated SH-SY5Y cells was utilized to validate the previously described ER-specific primers to ensure (a) primers amplified CLU DNA in SH-SY5Y cells and (b) sex hormone treatment did not significantly alter CLU amplification (Figure 7)

Chromatin Immunoprecipitation. Following the analysis of sheared chromatin and validation of ER-specific primers *t*he remaining supernatants from the chromatin clearing step were pipetted into sterile microcentrifuge tubes and 10% of each supernatant (100 µL of each sample) was removed and combined into 1 tube to represent the total chromatin (Input). 100 µL of each sample was then placed into 3 separate tubes (300 µL total sample/tube) to represent the Positive ChIP Control, Antibody Control, and Total Negative Control. For experimental IP's the remaining 600 µL of Vehicle-treated sample was divided into two tubes and 300 µL of either PPT- or DPN-treated DNA was added to 2 new tubes to represent 7 individual immunoprecipitations containing 300 µL crosslinked chromatin/tube: Positive ChIP Control,

Antibody Control, Total Negative Control, ERα-untreated, ERα-treated, ERβ-untreated, ERβ-treated. 700 µL of ChIP Dilution Buffer supplemented with protease and phosphatase inhibitors was added to each tube to make the final volume 1 mL. 2 µg of antibody was added to the appropriate tubes as indicated here: rabbit monoclonal anti-Tri-Methyl-Histone H3 (Lys4) (Positive ChIP Control), non-specific Rabbit IgG (Antibody Control), no antibody (Total Negative Control), rabbit polyclonal anti-Estrogen Receptor alpha (ERα-untreated, ERα-treated) or rabbit polyclonal anti-Estrogen Receptor beta (ERβ-untreated, ERβ-treated). Antibody-protein-DNA complexes were allowed to form via rotation overnight at 4 °C. Antibody complexes were pulled out of solution using 30 µL pre-washed Protein G Dynabeads for 4 hours with rotation at 4 °C. Following immunoprecipitation, beads were washed 2 x 1 mL with Low Salt Wash Buffer, 2 x 1 mL High Salt Wash Buffer, 1 x 1 mL Lithium Chloride Wash Buffer, and 5 x 1 mL TE Wash Buffer. Protein-DNA complexes were eluted from beads by vortexing beads for 15 min in 200 µL ChIP Elution Buffer. The first eluate was removed and the elution process was repeated a second time with the eluates being combined into 1 sample (400 µL/tube) at the end of the elution process.

Reverse Crosslinking and DNA Purification. To reverse protein-DNA crosslinks, 5M NaCl was added to a final concentration of 0.3M to each of the immunoprecipitated eluates and total chromatin (Input) sample and incubated at 65 °C for 16 hours. Following incubation, samples were removed and briefly centrifuged to bring the liquid to the bottom of the tube. 100 µL 5X Protein Digestion Buffer (50 mM Tris-HCl, pH 7.5, 25 mM EDTA, 1.25% SDS) and 40 µg/mL proteinase K (1.25 µL/tube from 20 mg/mL stock solution) was added to each tube and samples were incubated for 1 hr at 45 °C to digest residual proteins. 1 volume of Phenol:Chloroform:Isoamyl Alcohol 25:24:1 was added to each tube and tubes were vortexed on max speed for 15 seconds followed by centrifugation at 17,000 x g for 10 min at 4 °C. 450 µL of the upper aqueous phase was pipetted into a new tube and mixed with 2 volumes 100% Ethanol and ½ volume 7.5 M NH4OAc. Samples were mixed by tapping and incubated at -80°C for 1 hour. Following incubation, precipitated DNA was pelleted via centrifugation at 17,000 x g for 30 min. The supernatant was carefully decanted and the DNA pellet was washed with 1 mL 70% ethanol followed by centrifugation at 17,000 x g

for 10 min. Tubes were carefully inverted to remove ethanol and a P200 pipette tip was used to remove large drops of residual liquid. Samples were incubated at 37 °C for 10 min and pellets were re-suspended in 12 µL (immunoprecipitated samples) or 120 µL (input sample) ultrapure ddH2O.

DNA Amplification and Calculation of Fold Enrichment. rt-QPCR was used to amplify any immunoprecipitated CLU using the previously described ER-alpha and ER-beta primer sets with 2 µL purified DNA/reaction. To quantify the results, Fold Enrichment was calculated using a two-step process. In step 1, Data was adjusted for non-specific Fold Enrichment by subtracting the Mock (IgG) Ct value from the Experimental (ER-alpha or ER-beta) Ct value (ΔCt): $((Ct_{Experimental})-(Ct_{IgG}))$. The Fold enrichment was then calculated using the following equation $2^{-(\Delta Ct)}$. An example of the full procedure is provided in Table 14.

ChIP Fold Enrichment Calculations			
		Step 1	Step 2
Group	Ct Value	ΔCt Value	$2^{-(\Delta Ct)}$
Mock (IgG)	33.6	0	1
+ control	29.5	-4.1	17.14838
ER-beta - Vehicle	33.3	-0.3	1.231144
ER-beta - DPN	31.2	-2.4	5.278032

Table 13. Calculation of Fold Enrichment. Example of calculation of Fold Enrichment used in Chromatin Immunoprecipitation studies

Results and Conclusions

Chapter 1: Clusterin Protein Isoforms in the Brain

1.1. Multiple CLU Protein Isoforms with Distinct Subcellular Localizations are Expressed in Rodent Brain Tissue.

Previous studies indicate that CLU mRNA is expressed in multiple tissue types with predominant CLU mRNA expression in the brain or CNS (Connor et al., 2001; de Silva, Harmony, et al., 1990). However, as robust mRNA levels do not necessarily translate to robust protein levels, CLU protein levels were first examined in a panel of rodent tissues known to contain CLU mRNA. Brain, liver, heart, lung, and reproductive tissues harvested from 6-month-old male and female C57Bl/6 mice were probed for CLU immunoreactivity. The data indicate the expression of multiple CLU

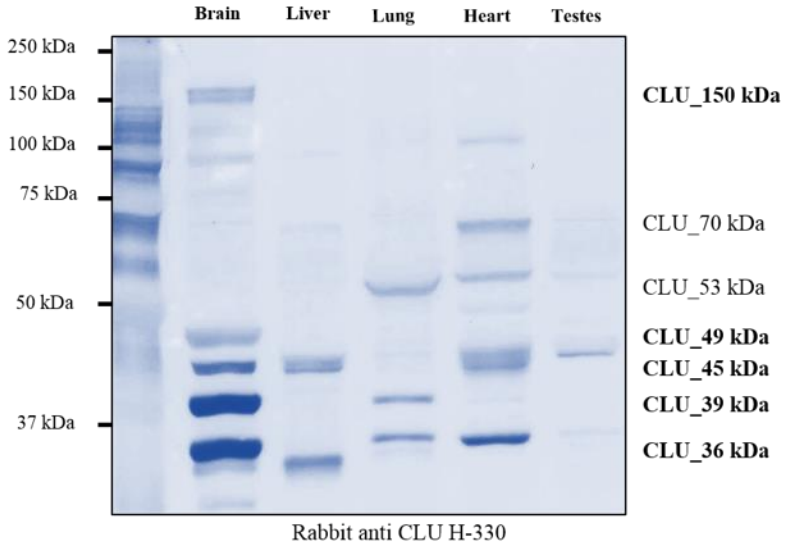

Figure 1.1.1. Characterization of Brain and Peripheral CLU Protein Isoforms. Whole brain, liver, lung, heart, and testicular tissue was homogenized as indicated and analyzed via immunoblotting for CLU immunoreactivity. Blot was incubated overnight with rabbit anti-CLU H-330 (1:1000) at 4° C with continual rocking followed by 1 hr in goat-anti-rabbit (1:5000) at RT. Following acquisition, the blot was stained with TMB to confirm molecular weights. Isoforms localized in whole brain tissue are indicated in bold font.

immunoreactive bands throughout each tissue tested. Specifically, a whole brain lysate reveals 5 individual CLU immunoreactive bands: CLU_150 kDa, CLU_49 kDa, CLU_45 kDa, CLU_39 kDa, and CLU_36 kDa (Figure 1.1.1).

Parallel to findings in previously published mRNA studies, CLU immunoreactive bands are also detected in peripheral tissues, however, the CLU protein expression profile of the peripheral tissues tested appears to differ from that of brain tissue. Moreover, while fold change in protein expression levels cannot be calculated from this study, it is noteworthy to mention that the tissue-specific CLU protein expression profiles do not differ between male and female animals (data not shown). These data validate early northern blot analyses and confirm the robust expression of CLU protein isoforms in brain tissue. To determine if CLU protein isoforms are expressed in a brain region-specific manner, CLU protein expression was examined within in the hippocampus, hypothalamus, cortex, and cerebellum of 6-month-old WT mice. Consistent with the CLU protein expression profile observed in a whole brain tissue lysate, 5 CLU immunoreactive bands of similar molecular weight were observed in each brain region analyzed indicating that CLU protein isoforms are expressed throughout most of the brain (data not shown). As the brain-specific protein expression profiles do not differ between sexes and LOAD more frequently impacts the female population, female animals were utilized throughout the remainder of this dissertation. Moreover, as the CLU protein expression profile previously detected in a whole brain lysate appears to be consistent across all brain regions tested and LOAD predominantly impacts the hippocampus and cortex, the remaining studies in this dissertation were performed primarily in cortical and hippocampal tissues and/or primary cortical neurons or astrocytes.

Several controversies currently exist concerning basic molecular properties of brain CLU protein isoforms. Two of the more controversial, and currently unanswered, questions pertain to the

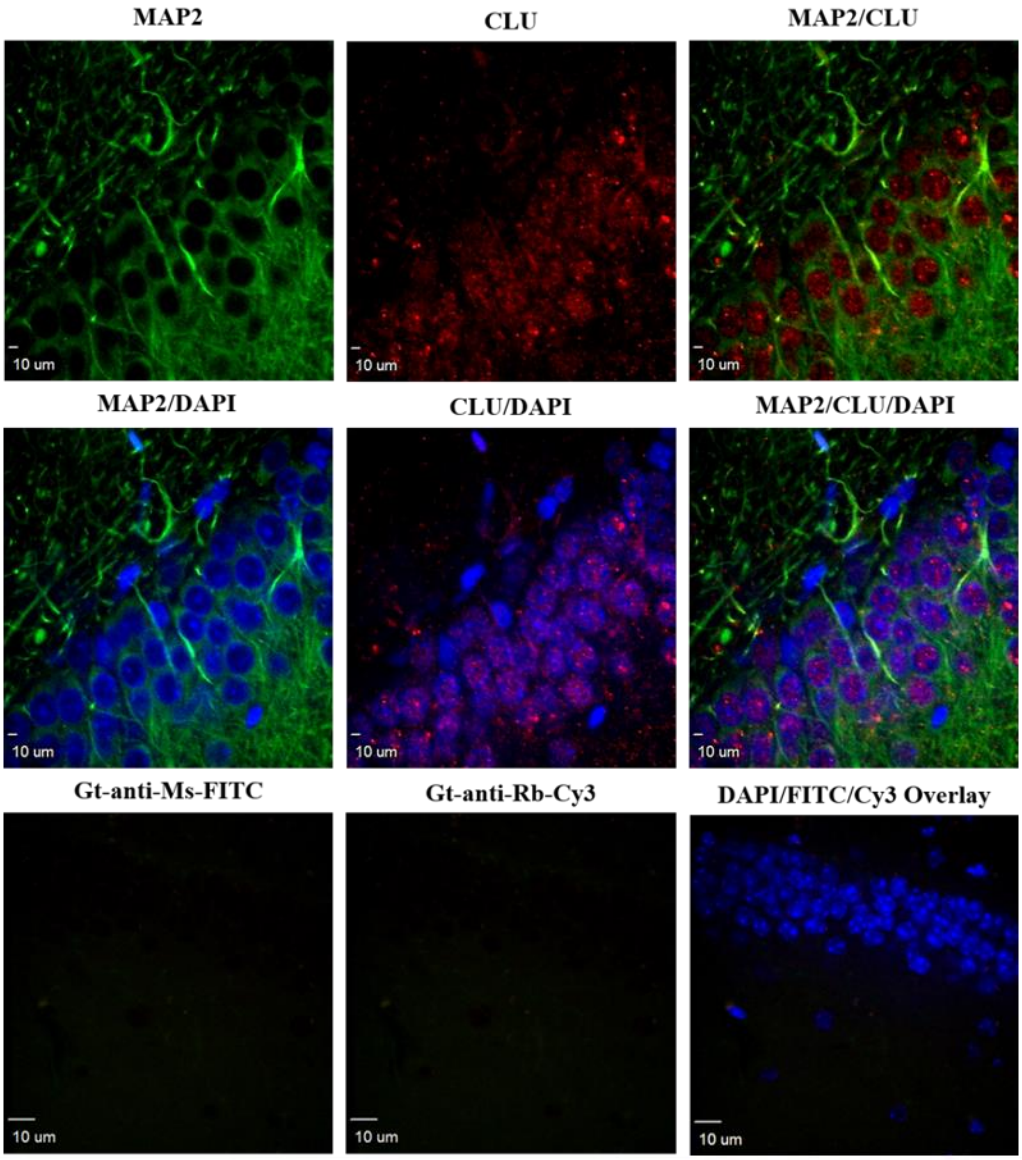

Figure 1.1.2. Examination of CLU Immunoreactivity in Adult Rodent Hippocampus. 40 µM thick rodent brain sections were generated using Multi-brain processing as indicated. Free-floating brain sections were permeabilized and blocked as indicated and double labeled using mouse monoclonal anti-MAP2 (1:750, green) and rabbit polyclonal anti-CLU H-330 (1:500, red) overnight at 4 °C with continual rocking. Brain sections were washed and probed with goat-anti-mouse FITC (1:1000) and preadsorbed goat-anti-rabbit Cy3 (1:1000) for 1 hr at RT protected from light. To generate a secondary antibody control, 1 group of free floating brain sections was incubated overnight in the same conditions without the addition of any primary antibody. Control sections were then incubated with the same concentrations of secondary antibody for the same amount of time, thus generating a secondary antibody control group. Experimental and control brain sections were imaged using a customized Olympus IX81/spinning disk confocal inverted microscope equipped with an Olympus 40X 0.95 NA air objective. Images were collected and analyzed using the Slidebook Software Version 6.0 (Intelligent Imaging Innovations) with 60-80 image stacks with a 0.5 µm step size through the tissue.

presence of a nuclear CLU protein isoform and the cell type from which brain CLU is derived or produced (neurons, glia, etc….). In order to determine if CLU immunoreactivity is localized to a specific brain cell-type, 40 μM thick rodent brain sections were co-stained for CLU immunoreactivity (red) and the neuronal marker MAP2 (green) or the astrocytic marker, GFAP and visualized using confocal microscopy. The data indicate robust CLU immunoreactivity localized to both the nuclear and cytosolic compartment of neurons (Figure 1.1.2.) with low CLU immunoreactivity present in GFAP-positive astrocytes (data not shown). These data indicate that CLU immunoreactivity is expressed in neurons in at least 2 subcellular compartments (nucleus and cytosol). Collectively, these data and findings from the currently available literature suggest that CLU protein isoforms are localized to both astrocytes and neurons and thus provide rationale for investigating the expression and localization of CLU protein isoforms within both cell types. Moreover, the presence of CLU in both the nucleus and cytosol suggests that CLU protein isoforms may have distinct subcellular localizations.

In order to determine if the previously observed CLU protein isoforms are localized to specific subcellular compartments, freshly harvested cortical tissues were subjected to a Three Buffer Tissue Fractionation. This technique allows for the release of cytosolic proteins, organelle-encased proteins, and nuclear proteins in a successive manner. Harvested samples were analyzed via immunoblotting and probed with 3 different CLU antibodies (H-330, M-18, and B-5) to obtain a full CLU protein expression profile. To confirm isolation of indicated fractions, western blots were stripped and re-probed for fraction-specific markers: Grp75 (mitochondria), Calnexin and Calreticulin (Endoplasmic reticulum), Lamin C (Nucleus), and Gapdh (cytosol). Following acquisition, immunoblots were stained with TMB to confirm molecular weights of identified CLU immunoreactive bands. The data indicate the expression of 7 CLU immunoreactive bands in the

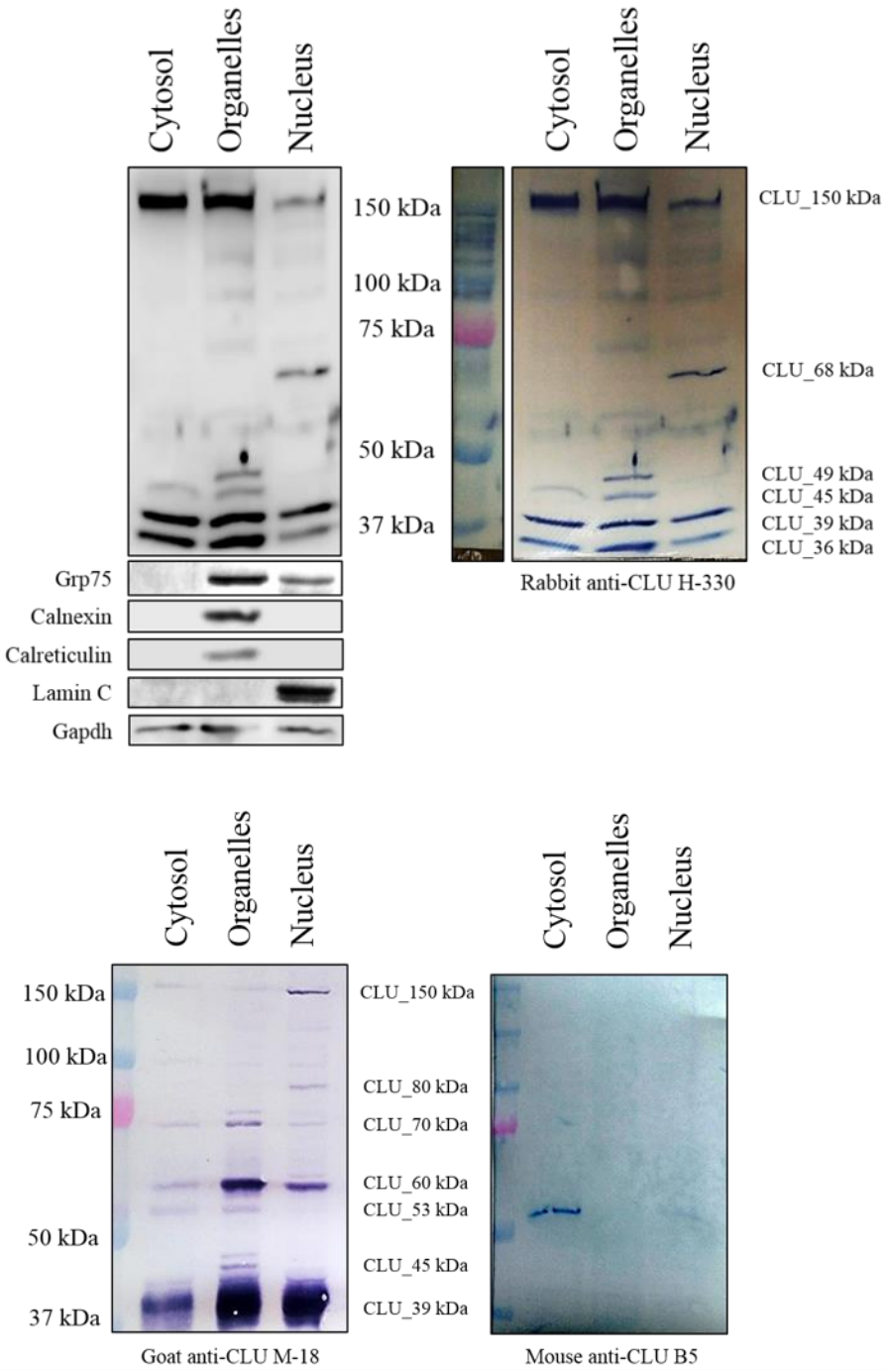

Figure 1.1.3. Characterization of CLU Protein Isoforms in Adult Cortex. 30 mg cortical tissue was subjected to a Three Buffer Tissue Fractionation as indicated. Cytosolic, Organelle, and Nuclear Fractions were probed with **(A)** rabbit anti-CLU H330 (1:1000), **(B, left panel)** goat anti-CLU M-18 (1:1000), or **(B, right panel)** mouse anti-CLU B-5 (1:1000) overnight at 4°C. Blots were washed and probed with species specific HRP-conjugates secondary antibodies (1:5000) for 1 hr at RT with continual rocking. To ensure fraction purity, blots were stripped and re-probed with fraction/organelle-specific biochemical markers: Grp75 (mitochondria, 1:8000, 1 hr RT), Calnexin and Calreticulin (ER, 1:8000, 1 hr RT), Lamin C (Nucleus, 1:4000, 3 Hr RT), and Gapdh (cytosol, 1:8000, 2 Hr RT).

cytosolic fraction (CLU_150 kDa, CLU_70 kDa, CLU_60 kDa, CLU_53 kDa, CLU_45 kDa, CLU_39 kDa, and CLU_36 kDa), 8 CLU immunoreactive bands in the organelle fraction (CLU_150 kDa, CLU_70 kDa, CLU_60 kDa, CLU_53 kDa, CLU_49 kDa, CLU_45 kDa, CLU_39 kDa, and CLU_36 kDa), and 2 CLU immunoreactive bands specific to the nuclear fraction (CLU_80 kDa and CLU_68 kDa) of cortical tissue (Figure 1.1.3.). It is important to note that several other CLU immunoreactive bands are detected in the nuclear fraction (CLU_150 kDa, CLU_70 kDa, CLU_60 kDa, CLU_39 kDa, and CLU_36 kDa), however, analysis with fraction-specific markers suggests that these CLU-immunoreactive bands are likely due to the minor amounts of cytosolic and/or organelle contamination in the nuclear fraction. These data suggest that CLU protein isoforms have different subcellular targets.

To further investigate the expression and distribution of CLU protein isoforms in the brain and to examine brain cell type-specific CLU protein expression profiles, primary cortical and hippocampal neurons or astrocytes were isolated from embryonic rat pups, grown to maturity, harvested via subcellular fractionation and analyzed for CLU protein isoform expression using two different CLU antibodies (H-330 and M-18). Similar to that of tissue samples, the purity of isolated fractions was analyzed using fraction-specific biochemical markers (Gapdh (cytosol), Grp75 (mitochondria), and Lamin A (nucleus)) and the isolation of indicated cell types was confirmed via immunocytochemistry using cell-type specific antibodies (MAP2 (neurons), GFAP (astrocytes)). Analysis of primary neurons indicates the expression of 4 CLU immunoreactive bands in the cytosolic fraction (CLU_150 kDa, CLU_80 kDa, CLU_49 kDa, and CLU_60 kDa), 2 CLU immunoreactive bands in the crude mitochondrial fraction (containing ER and mitochondria; CLU_80 kDa, and CLU_68 kDa), and 4 CLU immunoreactive bands in the nuclear fraction (CLU_150 kDa, CLU_68 kDa, CLU_60 kDa, and CLU_49 kDa) of primary neurons

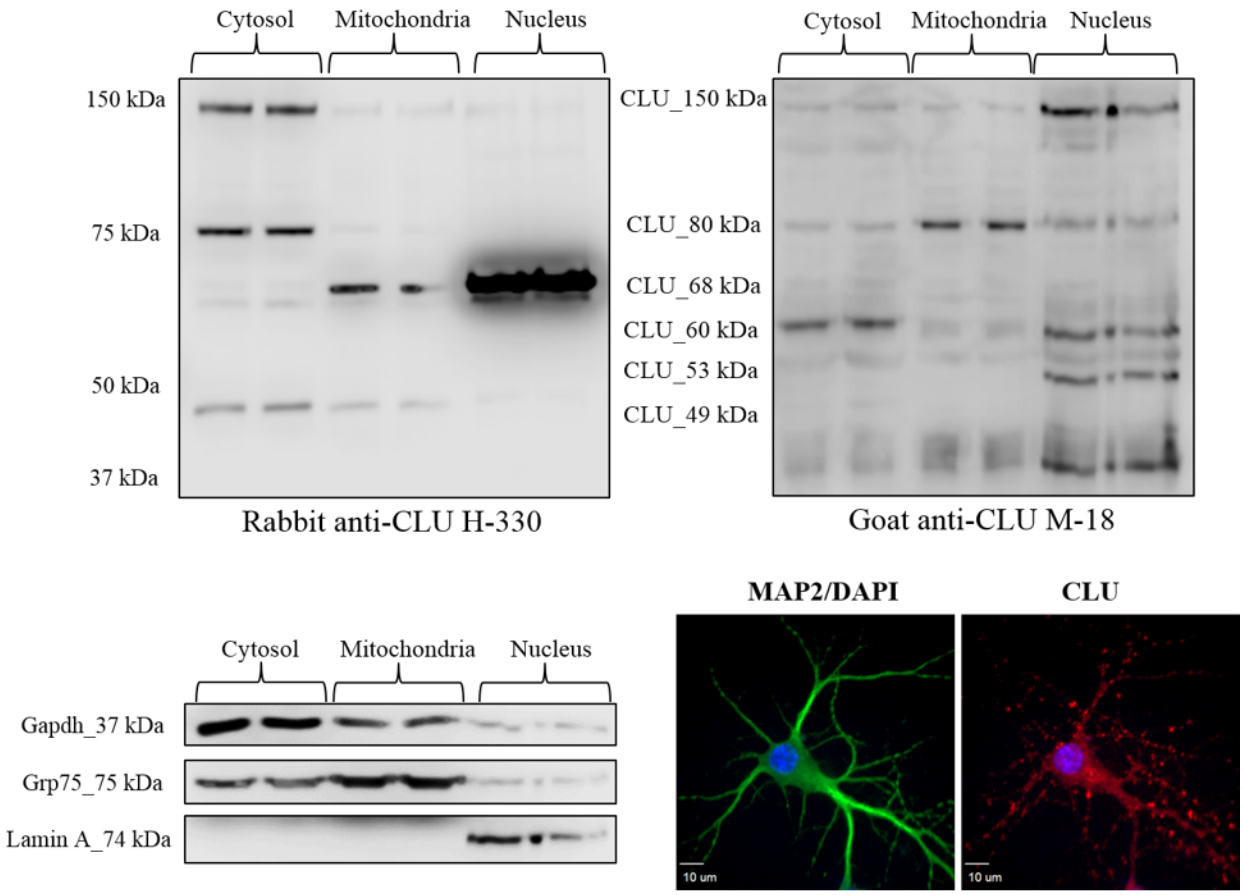

Figure 1.1.4. Characterization of Neuronal CLU Protein Isoforms. Primary neurons were isolated from E18 embryonic rat pups as indicated. **(A)** At DIV 7 neurons were subjected to a subcellular fractionation to isolate the cytosolic, crude mitochondrial, and nuclear fractions. 30 µg of each fraction was analyzed for CLU protein expression using 2 CLU antibodies: rabbit anti-CLU H-330 (1:1000, right panel) and goat anti-CLU M-18 (1:1000, left panel) **(B)** Fraction purity was analyzed using three fraction-specific markers (Gapdh (1:8000, 1 hr RT, cytosol), Grp75 (1:8000, 1 hr RT, mitochondria), and Lamin A (1:4000, 1 hr RT, nucleus). (C) Isolation of primary neurons was confirmed by double labeling DIV 9 primary neurons with the neuronal marker MAP2 (1:750, green) and CLU H-330 (1:500, red) overnight at 4 °C followed by goat-anti-mouse FITC (1:1000) and goat-anti-rabbit Cy3 (1:1000) for 1 hr at RT protected from light. Confocal images were acquired using a customized Olympus IX81/spinning disk confocal inverted microscope equipped with an Olympus 40X 0.95 NA air objective. Images were collected and analyzed using the Slidebook Software Version 6.0 with 15-20 image stacks with a 0.1 µm step size through the cells.

(Figure 1.1.4.). In contrast, analysis of astrocyte fractions indicates the expression of 5 CLU immunoreactive bands in the cytosolic fraction (CLU_70 kDa, CLU_60 kDa, CLU_49 kDa, CLU_45 kDa, and CLU_39 kDa), 3 CLU immunoreactive bands in the crude mitochondrial

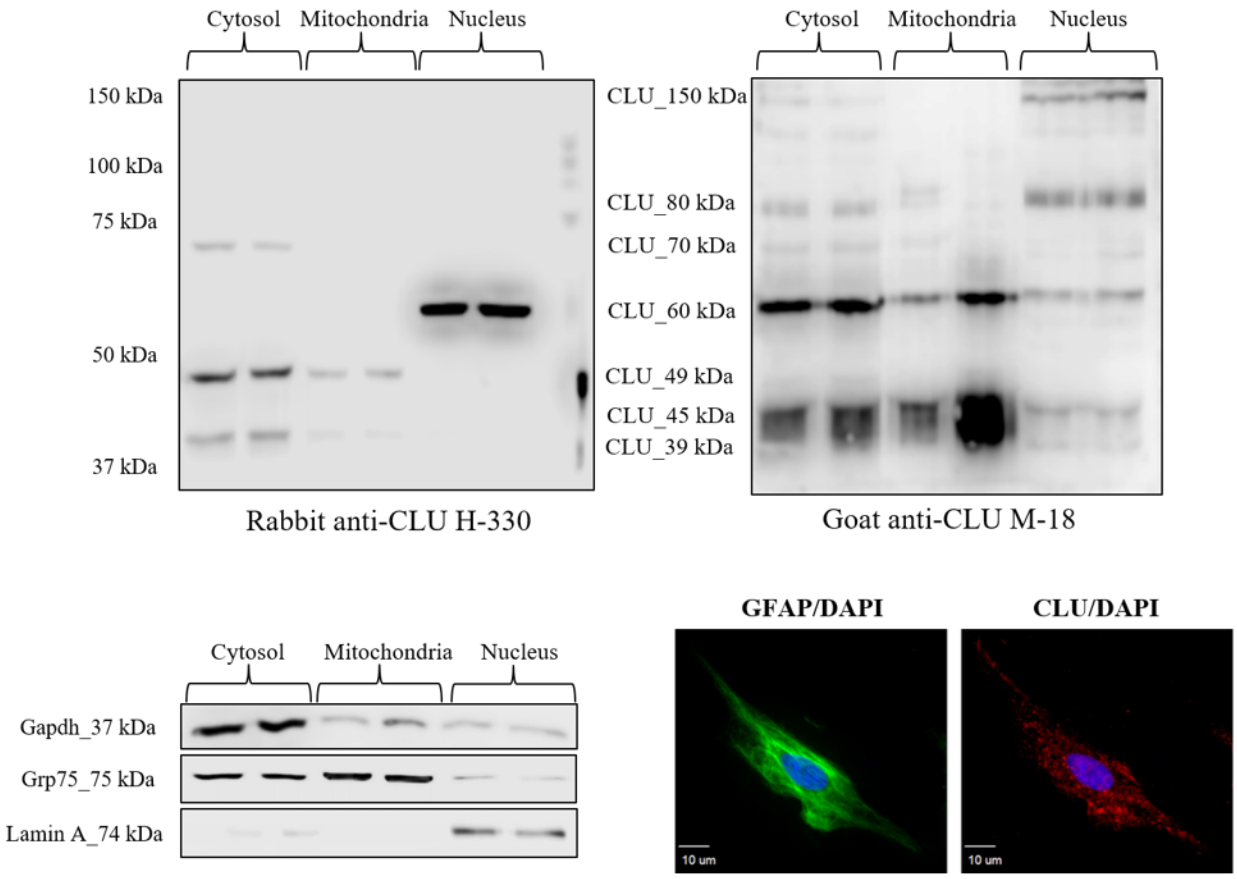

Figure 1.1.5. Characterization of Astrocytic CLU Protein Isoforms. Primary astrocytes were isolated from E18 embryonic rat pups as indicated. **(A)** At DIV 14 astrocytes were subjected to a subcellular fractionation to isolate the cytosolic, crude mitochondrial, and nuclear fractions. 30 µg of each fraction was analyzed for CLU protein expression using 2 CLU antibodies: rabbit anti-CLU H-330 (1:1000, right panel) and goat anti-CLU M-18 (1:1000, left panel) **(B)** Fraction purity was analyzed using three fraction-specific markers (Gapdh (1:8000, 1 hr RT, cytosol), Grp75 (1:8000, 1 hr RT, mitochondria), and Lamin A (1:4000, 1 hr RT, nucleus). **(C)** Isolation of primary neurons was confirmed by double labeling DIV 14 primary astrocytes with the astrocytic marker GFAP (1:500, green) and CLU H-330 (1:500, red) overnight at 4 °C followed by goat-anti-rat IgG Alexa Flour 568 (1:1000) and goat-anti-rabbit FITC (1:1000) for 1 hr at RT protected from light. Confocal images were acquired using a customized Olympus IX81/spinning disk confocal inverted microscope equipped with an Olympus 60X NA 1.42 oil objective. Images were collected and analyzed using the Slidebook Software Version 6.0 with 15-20 image stacks with a 0.1 µm step size through the cells.

fraction (CLU_60 kDa, CLU_45 kDa, and CLU_39 kDa) and 3 CLU immunoreactive bands in the nuclear fraction (CLU_150 kDa, CLU_80 kDa, and CLU_60 kDa) of primary astrocytes (Figure 1.1.5.). Collectively, the CLU immunoreactive bands detected in the astrocytic and neuronal fractions encompass all CLU immunoreactive bands identified in the previously performed cortical

tissue fractionation. These data also reveal similarities and differences between the protein expression profiles. For instance, astrocytes do not appear to express the CLU_53 kDa or the CLU_68 kDa CLU immunoreactive bands while neurons do not appear to express CLU_70 kDa, CLU_45 kDa, or CLU_39 kDa CLU immunoreactive bands. Moreover, while all CLU immunoreactive bands are detected, the subcellular localization appears to differ between adult cortical tissue and embryonic neurons/astrocytes. For instance, CLU_49 kDa is specifically localized to the organelle fraction of adult cortical tissue whereas in embryonic neurons and astrocytes the CLU_49 kDa band appears to be exclusively localized to the cytosolic fraction. In addition, the CLU_45 kDa band, which is robustly expressed in adult cortex in the organelle fraction, is expressed at relatively minute levels in astrocytes. Moreover, the CLU_68 kDa and CLU_80 kDa bands, which appear exclusively in the nuclear fraction of adult cortex, are localized to both the nucleus and the crude mitochondrial fraction of embryonic neurons (CLU_68 kDa), and the cytosol and crude mitochondrial fraction of neurons (CLU_80 kDa). These discrepancies may be the result of differing harvest methods/buffers between the two fractionation protocols, however, another plausible explanation may be that CLU protein isoforms are redistributed as needed with aging to differing subcellular compartments.

A comparison of CLU immunoreactivity in the cortical organelle fractions isolated from postnatal day 1 mouse pups (PN1) and 1-month-old mice (30D) supports this idea. The data indicate that both CLU_49 kDa and CLU_45 kDa protein expression is either undetectable or detected at extremely low levels in the organelle fraction of PN1 mice. However, the levels of both CLU protein isoforms are dramatically increased in the organelle fractions of 30D mice suggesting that CLU protein isoform distribution is altered with aging in young mice (Figure 1.1.6).

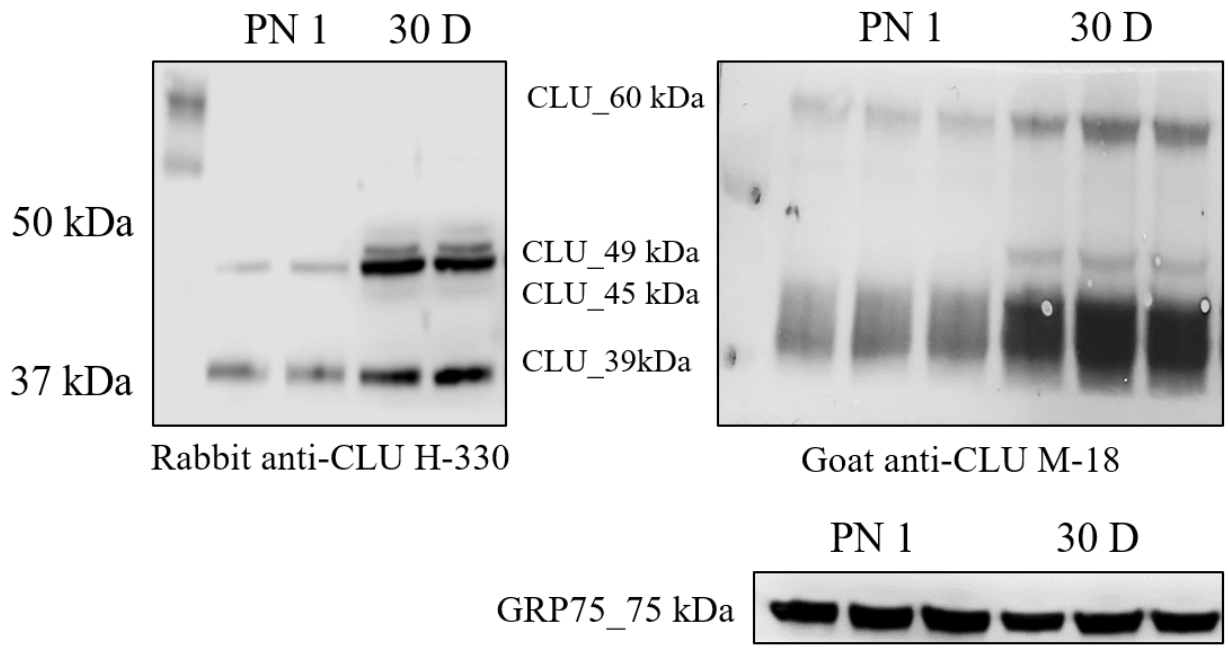

Figure 1.1.6. Comparison of CLU Immunoreactivity in the Organelle Fractions of Postnatal Day 1 and 1-month-old Mice. The organelle fractions were isolated from 30 mg cortical tissue using the Three Buffer Tissue Fractionation as indicated. Fractions were then probed with **(left panel)** rabbit anti-CLU H330 (1:1000) or **(right panel)** goat anti-CLU M-18 (1:1000) overnight at 4°C. Blots were washed and probed with species specific HRP-conjugates secondary antibodies (1:5000) for 1 hr at RT with continual rocking. To ensure equal loading, blots were stripped and re-probed with the Grp75 (mitochondria, 1:8000, 1 hr RT).

1.2. Characterization and Validation of CLU Antibodies using Three Biochemical Approaches

As 10 different CLU immunoreactive bands were detected in rodent cortex using polyclonal antibodies, it is extremely necessary to ensure that the previously observed immunoreactive bands are not the result of antibody artifact. Therefore, the antibodies utilized in the studies presented herein were validated using 3 independent biochemical methods: WT vs. CLU-KO mice, CLU-deficient tissue from a WT animal, and siRNA-mediated knockdown of CLU protein isoforms in a brain-derived immortalized cell line.

1.2.1. Biochemical Validation of CLU Antibodies Using CLU-KO Mice.

The CLU-KO mouse model was generated in 2001 by McLaughlin et al. as a model to study autoimmune myocarditis. Initial characterization indicates a phenotypically normal mouse exhibiting normal organ morphology and reproductive capabilities. Characterization of CLU protein expression in heart, liver, and serum indicates the expression of a 70 kDa CLU protein isoform in WT animals that is deficient in CLU-KO animals demonstrating the successful generation of the mutant animal. In order to demonstrate antibody specificity, cortical tissues were isolated from 6-month-old female WT and CLU-KO mice and probed for CLU protein expression using the 3 previously utilized CLU antibodies. WT cortical tissues express all previously observed CLU immunoreactive bands, however, an examination of CLU-KO cortical tissue indicates that

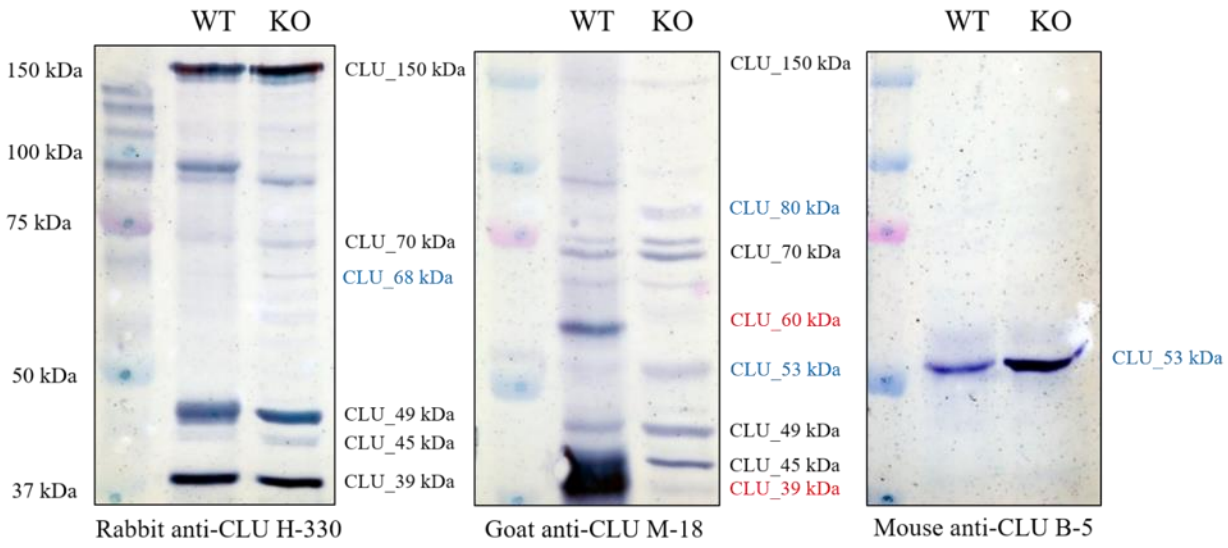

Figure 1.2.1.1. Validation of CLU Antibody Specificity Using CLU-KO Mice. 30 mg cortical tissue isolated from WT and CLU-KO (KO) mice was analyzed via immunoblotting and probed with rabbit anti-CLU H330 (1:1000, left panel), goat anti-CLU M-18 (1:1000, middle panel), or mouse anti-CLU B-5 (1:1000, right panel) overnight at 4°C. Blots were washed and probed with species specific HRP-conjugates secondary antibodies (1:5000) for 1 hr at RT with continual rocking. Following acquisition, the blot was stained with TMB to confirm molecular weights.

only 2 bands are absent in the CLU-KO brain when compared to WT brain: CLU_60 kDa and CLU_39 kDa (Figure 1.2.1.1., middle panel, red lettering).

Furthermore, while not quantifiable in this study, the expression level of 4 CLU immunoreactive bands appears in increase in CLU-KO cortical tissue (Figure 1.2.1.1., blue lettering). While this data does indicate the specificity of both the CLU_39 kDa and CLU_60 kDa band, it also generates several questions regarding the validity of the "CLU-KO" mouse model, which is repeatedly described as an animal that is devoid of CLU mRNA and protein expression. Given the possibility of multiple CLU mRNAs being generated during transcription and the genomic location of the cassette used to generate CLU-deficient (Exon 2 and part of Exon 1) animals by McLaughlin and colleagues, these data suggest that (a) CLU-KO mice are deficient in only 1 CLU mRNA isoform, (b) the deficient mRNA isoform translates to CLU_39 kDa, CLU_60 kDa (our data), and CLU_70 kDa (previous literature), (c) at least 1 alternative CLU mRNA does exist and is transcribed beginning in Exon 3 and (d) the remaining CLU immunoreactive bands may be translated from alternative CLU mRNAs.

To confirm the presence of alternative CLU mRNAs in CLU-KO mice, two primer sets were generated to amplify specific exons and thus represent different CLU mRNA transcripts. The mCLU primer set amplifies Exon 2-containing mRNA and thus represents the mature/secreted CLU protein isoform known to be translated from mRNA Isoform 2. The tCLU primer set amplifies Exon 3 – Exon 4 and, as the sequence of CLU is identical from Exons 3-9, recognizes all CLU mRNAs (Figure 1.2.1.2., Upper Panel). RNA was then isolated from cortical tissues harvested from age-matched female WT and CLU-KO mice and rt-qPCR was used to amplify Exon 2-containing (mCLU) and Exon 3-4-containing (tCLU) CLU mRNAs as well as β-actin mRNA (loading control). The data indicate robust levels of both Exon 2-containing (blue line)

mRNA and Exon 3-4-containing (purple line) mRNA in WT brain tissue. As expected Exon 2-containing mRNA was not present in the CLU-KO animal model, however, rt-qPCR does amplify

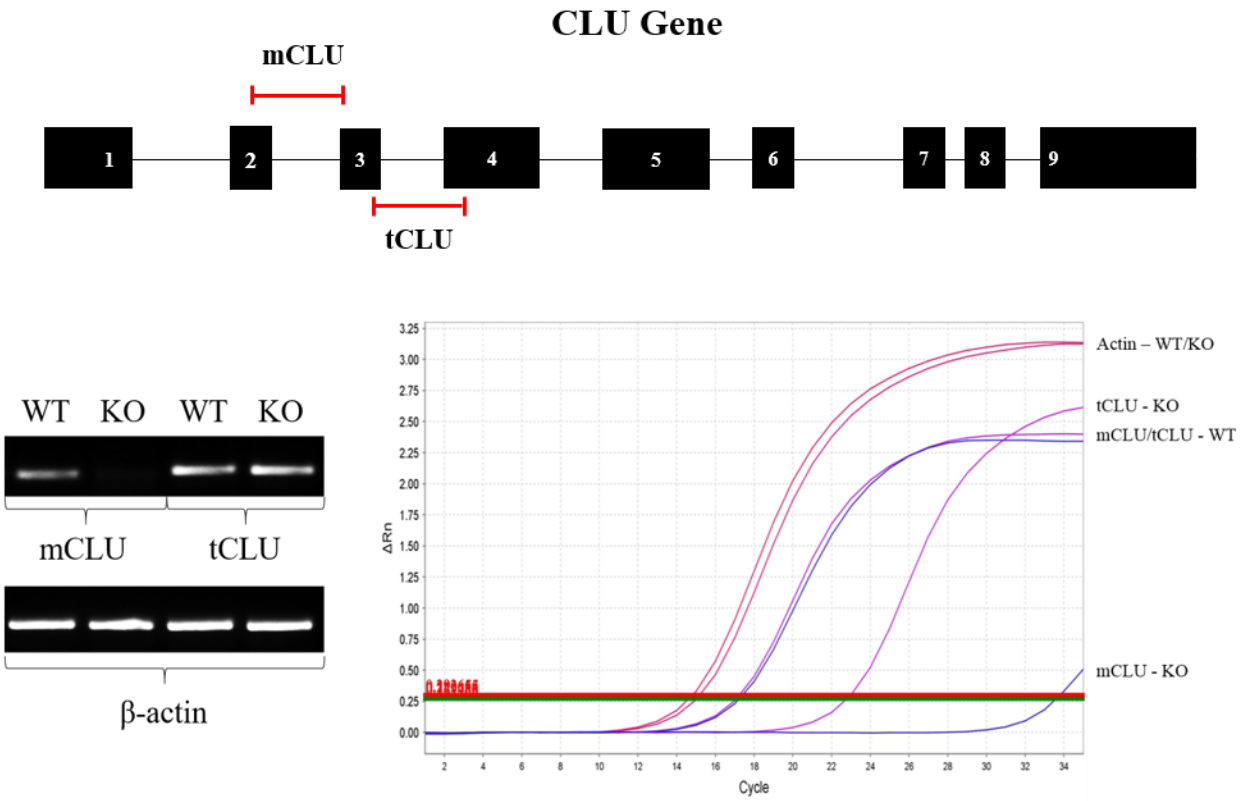

Figure 1.2.1.2. Characterization of CLU mRNA Isoforms in CLU-KO Mice. (A) To analyze CLU mRNA, two primer sets were generated to specifically amplify Exon 2-containing mRNA (mCLU) and Exon 3-4-containing mRNA (tCLU). **(B, right panel)** Total RNA was isolated from 30-50 mg cortical tissue isolated from WT and CLU-KO (KO) mice. 1.5 µg RNA was reverse transcribed and 75 ng cDNA was analyzed for Exon 2- and Exon 3-4 containing mRNA (Exon 2 (mCLU): blue lines, Exon 3 (tCLU); purple lines). To confirm equal loading, β-actin mRNA was amplified using both WT and KO cDNA (red lines) **(B, left panel)** Following amplification, amplimers were run on a 2% agarose gel as indicated.

Exon 3-4-containing mRNA in CLU-KO cortex indicating that CLU-KO mice do express CLU mRNA (Figure 1.2.1.2. Lower Panel). Collectively, this information indicates that the previously advertised CLU-KO mouse model is in fact an mRNA Isoform 2-deficient, or mCLU-deficient, mouse model.

To confirm these findings, a colony of WT, Heterozygous, and CLU-KO mice were generated (genotype confirmed, see methods section) and cortical tissues harvested from each genotype were

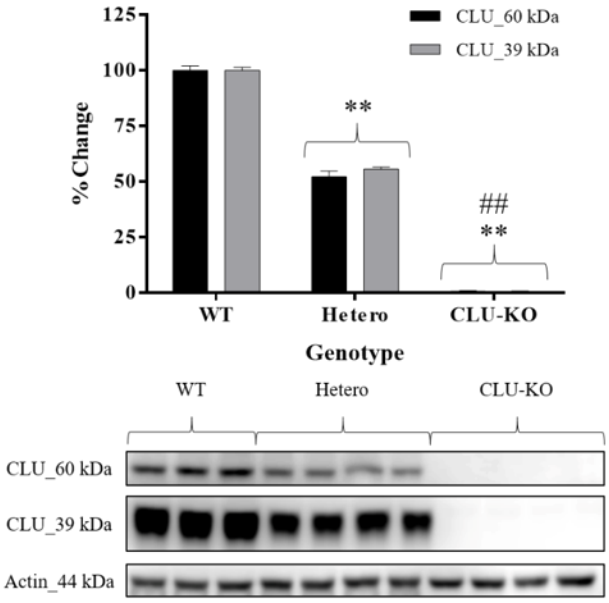

Figure 1.2.1.3. Validation of mCLU-KO in CLU-KO Mice. 30 µg cortical tissue lysate isolated from WT, heterozygous (Hetero) and CLU-KO mice was analyzed via immunoblotting and probed with a mCLU-specific antibody: goat anti-CLU C-18 (1:1000) overnight at 4°C. Blots were washed and probed with species specific HRP-conjugates secondary antibodies (1:5000) for 1 hr at RT with continual rocking. Data were analyzed using One Way Analysis of Variance (AVOVA) with Tukey's Post-hoc Analysis. Data are represented as the mean ± standard error. ** $p<0.01$ when compared to WT animals, ## $p<0.01$ when compared to Hetero animals (n=3-4 animals/genotype)

analyzed for CLU protein expression using an antibody that specifically detects mCLU protein expression. As expected heterozygous animals expressed 50% less CLU_39 kDa and CLU_60 kDa than WT controls while CLU-KO animals expressed no CLU_39 kDa or CLU_60 kDa. These data confirm that the CLU-KO mouse model is deficient in only mCLU and will therefore be referred to as mCLU-KO mouse model throughout the remainder of the dissertation.

1.2.2. Biochemical Validation of CLU Antibodies Using CLU-deficient Tissue.

As the mCLU-KO mouse model provides information regarding only those isoforms derived from Exon 2-containing mRNA, further efforts were made to validate the specificity of CLU antibodies. A review of the literature indicates that adult mouse pancreas should be devoid of any CLU mRNA or protein expression (Min et al., 1998). Therefore, cortical and pancreatic tissues were harvested

from a 9-month-old female mouse and analyzed for CLU immunoreactivity using the rabbit anti-CLU H-330 antibody. To confirm the presence of protein in both lanes, the blot was stripped and re-probed for Gapdh immunoreactivity. In addition, following acquisition, blots were stained with TMB to confirm molecular weight. As expected, WT brain tissue expressed the previously observed CLU immunoreactive bands: CLU_150 kDa, CLU_49 kDa, CLU_39 kDa, and CLU_36 kDa. However, examination of pancreatic tissues indicates a complete lack of CLU immunoreactive bands

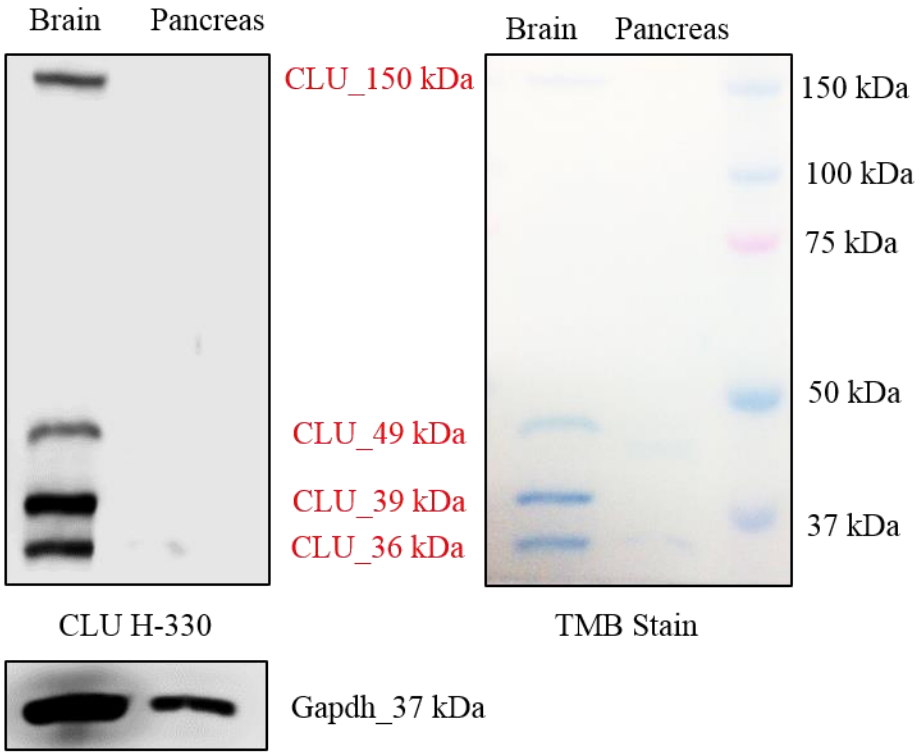

Figure 1.2.2.1. Validation of CLU Antibody Specificity Using CLU-deficient Tissue. 30 mg cortical and pancreatic tissues were isolated from a 9-month-old female WT mouse and homogenized as indicated. Equal concentrations of total protein lysate were analyzed via immunoblotting and probed with rabbit anti-CLU H-330 (1:1000) overnight at 4°C. Blots were washed and probed with species specific HRP-conjugates secondary antibodies (1:5000) for 1 hr at RT with continual rocking. To ensure presence of protein, each sample was also probed with mouse anti-Gapdh (1:5000, 2 hr RT). Following acquisition, blots were stained with TMB to confirm molecular weights. Bands specifically identified by CLU H-330 are indicated in red lettering.

indicating that these 4 CLU immunoreactive bands are indeed CLU protein isoforms (Figure 1.2.2.1.).

1.2.3. siRNA-mediated Knockdown of CLU Protein Isoforms in Mouse Neuroblastoma Cells.

As data from the previous 2 sections indicate the specificity of CLU_150 kDa, CLU_60 kDa, CLU_49 kDa, CLU_39 kDa, and CLU_36 kDa, and data from the initial mouse model

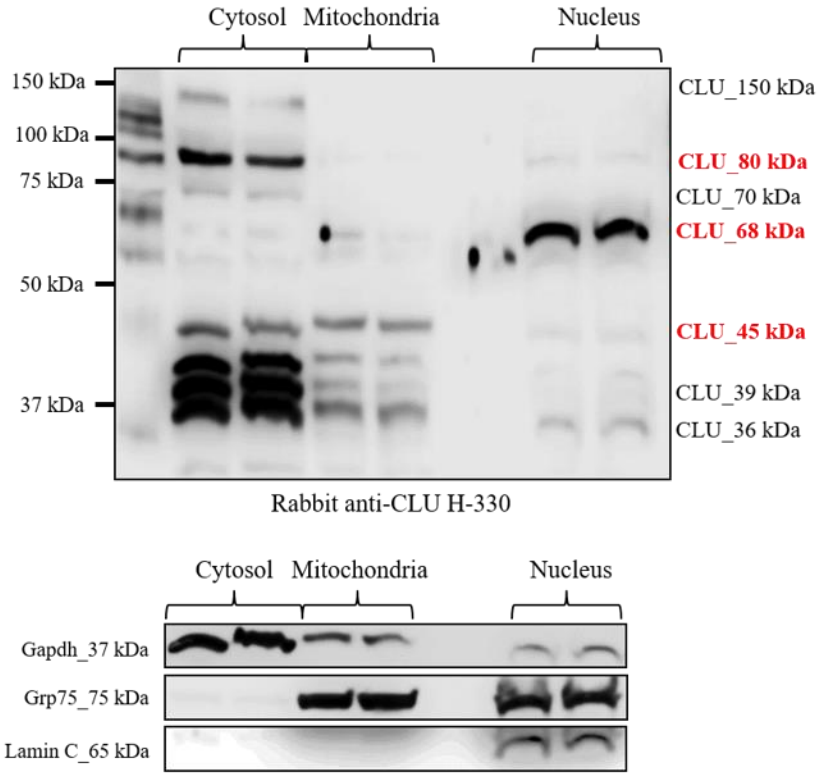

Figure 1.2.3.1. Characterization of CLU Protein Isoforms in Mouse Neuroblastoma Cells. Mouse neuroblastoma cells (Neuro-2a) were cultured and subjected to a subcellular fractionation to isolate the cytosolic, crude mitochondrial, and nuclear fractions. 30 µg of each fraction was analyzed for CLU protein expression using rabbit anti-CLU H-330 (1:1000). Fraction purity was analyzed using three fraction-specific markers (Gapdh (1:8000, 1 hr RT, cytosol), Grp75 (1:8000, 1 hr RT, mitochondria), and Lamin A (1:4000, 1 hr RT, nucleus).

characterization indicate the specificity of CLU_70 kDa, siRNA-mediated knockdown was utilized to confirm the specificity of the remaining identified CLU immunoreactive bands. However, before siRNA studies could be initiated, it was necessary to identify a brain-derived cell line with a CLU protein expression pattern that mimicked that of adult brain. Several cell lines were cultured, fractioned, and analyzed for CLU protein expression (HT22, SH-SY5Y, and Neuro-2a) and the mouse neuroblastoma cell line (Neuro-2a) was selected based on the protein expression pattern. Briefly, analysis of neuro-2a cell fractions indicate the expression of 7 CLU immunoreactive bands including the CLU immunoreactive bands of interest: CLU_80 kDa,

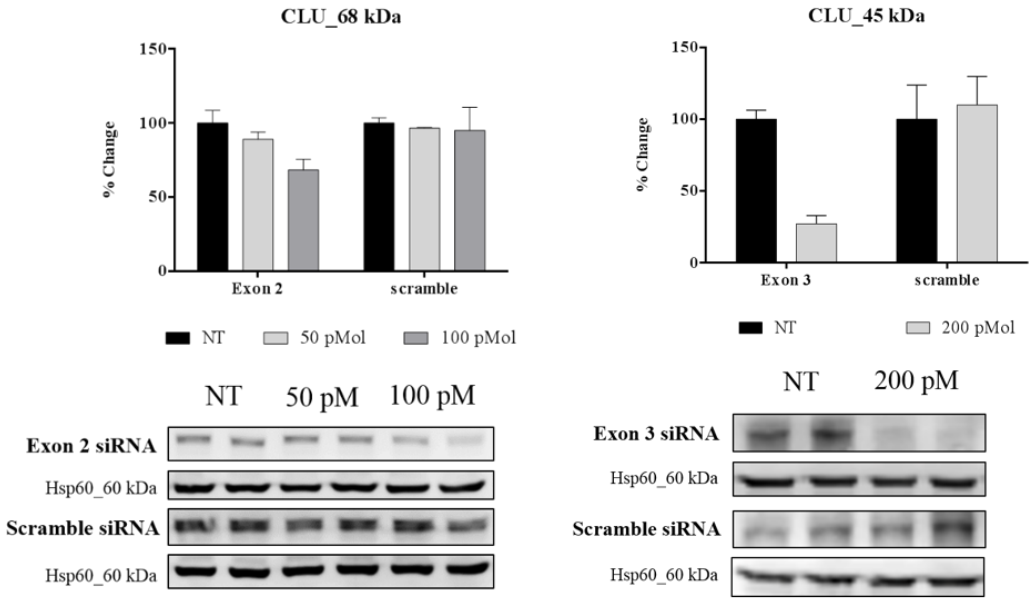

Figure 1.2.3.2. Knockdown of CLU_68 kDa and CLU_45 kDa by Exon 2- and Exon 3-targeting CLU siRNA. Mouse neuroblastoma cells (Neuro-2a) were transfected with increasing concentrations of Exon 2- or Exon 3-targeting siRNA or non-specific scramble for 18 hrs followed by 48-72 hrs incubation. Whole cell lysates were analyzed for CLU protein expression using rabbit anti-CLU H-330 (1:1000) and goat-anti CLU M-18. To ensure consistent loading, blots were stripped and re-probed for Hsp60 immunoreactivity. (n=2)

CLU_68 kDa, and CLU_45 kDa (Figure 1.2.3.1., red lettering). Following the identification of a suitable cell line, increasing concentrations of Exon 2- and Exon 3-targeting siRNA were transfected for 18 hours followed by 48 hrs incubation and whole cell extracts were analyzed for

CLU immunoreactivity. Gapdh-targeting siRNA was used as a positive control for transfection and a non-specific scramble siRNA was utilized as a negative control. Both positive and negative controls were transfected for the same amount of time at the same concentrations as the Exon 2- and 3-targeting siRNA. Analysis of Gapdh expression indicates that transfection of siRNA was efficient at low concentrations (25-50 pMol). Transfection of Exon 2-targeting siRNA resulted in an approximate 30% decrease in CLU_68 kDa expression with no observable decrease in CLU_68 kDa expression in cells transfected with equal concentrations of scramble siRNA (Figure 1.2.3.2.). In addition, transfection of Exon 3-targeting siRNA resulted in an approximate 60-65% decrease in CLU_45 kDa expression (Figure 1.2.3.2., right panel). These data indicate that CLU_68 kDa and CLU_45 kDa are both specific CLU protein isoforms. Taken together, the analysis of adult cortical tissues, embryonic neurons and embryonic astrocytes as well as the antibody validation data indicate that CLU is expressed in rodent brain as 10 different protein isoforms derived from at least 2 CLU mRNAs beginning at Exon 2 and Exon 3, respectively.

1.3. N-linked Glycosylation of at least 2 Individual CLU Precursor Proteins is Responsible for the Generation of Several Higher Molecular Weight Protein Isoforms

Previous data from Harmony and colleagues indicate that CLU protein isoforms are modified by N-linked glycosylation. Specifically, a 70 kDa CLU isoform was found to be modified by sialic acid-containing complex glycans while a 58 kDa CLU protein isoform was found to be modified by high mannose glycans (Burkey et al., 1991). Our protein analysis has identified numerous higher molecular weight CLU protein isoforms that are translated from at least 2 CLU mRNAs Moreover, calculation of relative molecular weights using the ExPasy MW Calculator indicates that a CLU mRNAs containing Exons 2-9 and Exons 3-9 would resolve at approximately 49.4 kDa and 45.8 kDa. Therefore, we hypothesized that the higher molecular weight CLU protein isoforms

(CLU_150 kDa, CLU_80 kDa, CLU_70 kDa, CLU_68 kDa, CLU_60 kDa, and CLU_53 kDa) are glycosylated intermediates of the CLU_49 kDa pre-protein while CLU_45 kDa would remain un-glycosylated.

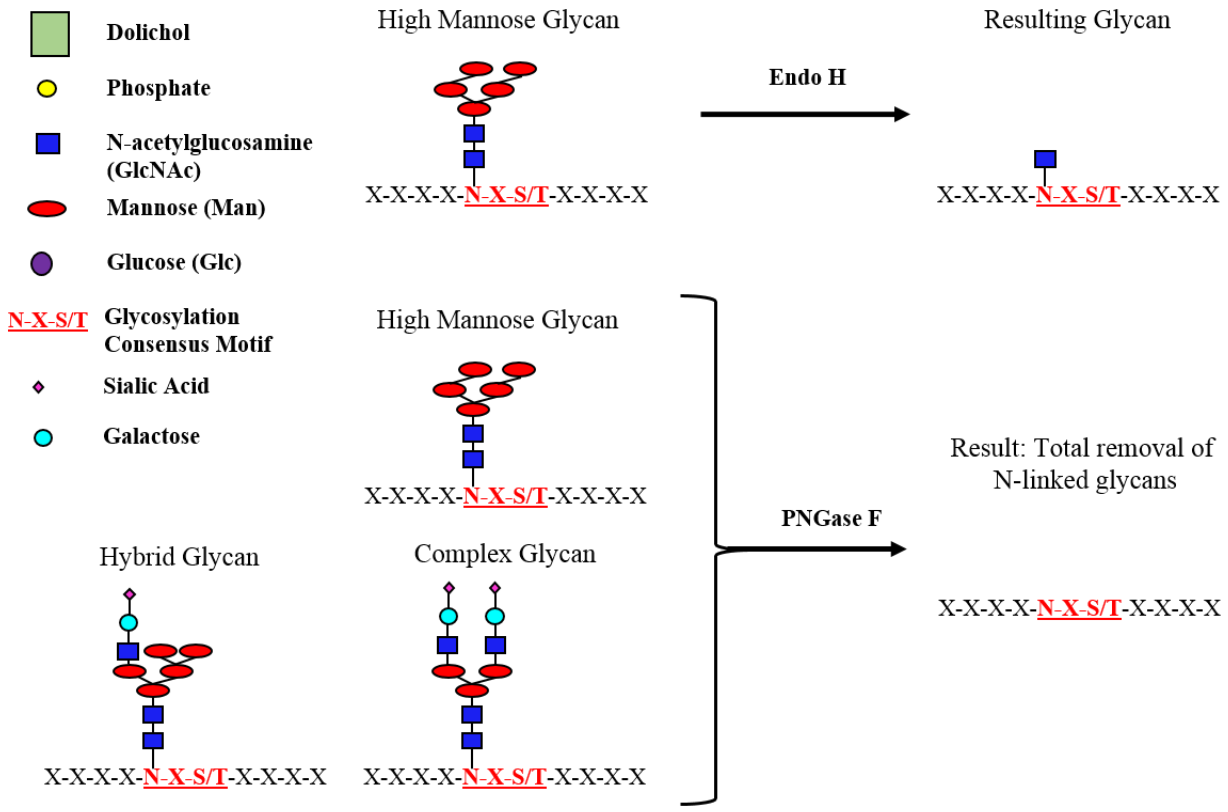

Schematic 11. Mechanism of N-linked Glycan Cleavage by Endo H and PNGase F. N-linked glycosylation occurs on the nitrogen containing side chain of an asparagine molecule within a specific consensus motif. (Upper Panel) Endo H treatment results in the specific cleavage of high mannose type N-linked oligosaccharides. Endo H cleaves glycans by targeting the bond between the two GlcNAC residues that comprise the base of the core N-linked glycan (also known as the chitobiose core). (Lower Panel) PNGase F non-specifically cleaves the bond between the targeted N residue and the proximal GlcNAC resulting in the complete removal of all types of N-linked glycans.

In order to test this hypothesis, fractions isolated from cortical tissues, primary neurons, and primary astrocytes were enzymatically digested with 2 different endoglycosidases that non-specifically cleave all N-linked glycans (PNGase F) or specifically cleave high mannose glycans (Endo H). The mechanism of enzymatic deglycosylation by these two enzymes is represented in

Schematic 11. Prior to initiation of experimental reactions, the activity of both PNGase F and Endo H was confirmed using an in vitro deglycosylation reaction with RNase B as a substrate. As expected, RNase B, which is modified by 1 high mannose glycan, is reduced in size by approximately 4 kDa in the presence of both endoglycosidases demonstrating that both enzymes are active (Figure 1.3.1). Deglycosylation reactions were performed using the exact experimental paradigm used for deglycosylation of RNase B and all control samples were subjected to the same reaction conditions as the experimental groups including denaturing and incubation. Controls and deglycosylated samples were reduced and analyzed for CLU immunoreactivity using CLU H-330 and CLU M-18.

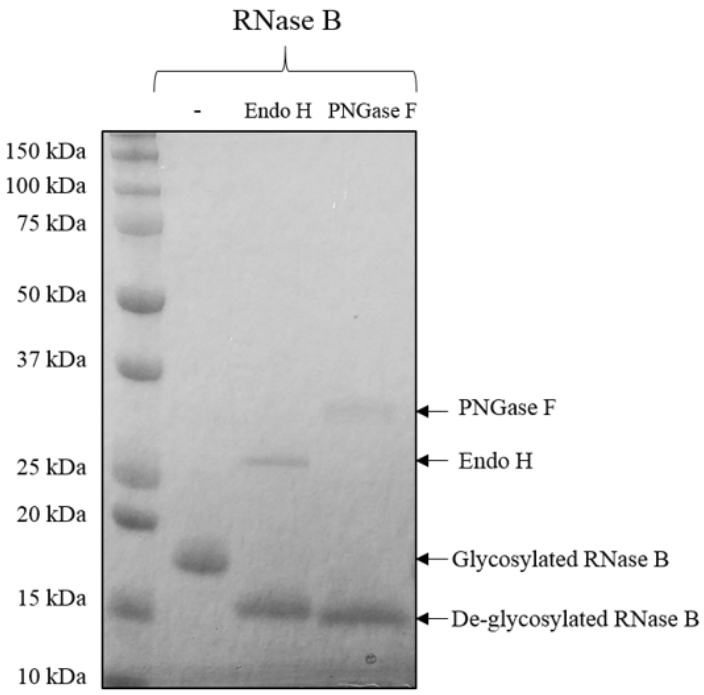

Figure 1.3.1. *In vitro* Validation of Endoglycosidase Activity. To confirm endoglycosidase activity, RNase B, which is modified by 1 high mannose glycan, was deglycosylated *in vitro* by both PNGase F and Endo H. RNase B was denatured for 10 min at 100 °C followed by incubation with 500 units of PNGase F or Endo H for 1 hr at 37 °C. Reactions were then boiled in reducing sample buffer, resolved via SDS-PAGE and stained with coomassie blue. Deglycosylation of RNase B should result in a 4 kDa reduction in size.

Immunoblot analysis of PNGase F and Endo H treated lysates with CLU M-18 indicates the reduction of CLU_60 kDa to CLU_49 kDa in cortical tissue, neurons and astrocytes indicating that CLU_60 kDa is modified by high mannose glycans (Figure 1.3.3, all panels). In addition,

CLU_39 kDa is reduced in size to CLU_25 kDa by PNGase F, but not Endo H, indicating that CLU_39 kDa is modified by either complex or hybrid glycans (Figure 1.3.2). These data are consistent with previous reports which demonstrate that the deglycosylation of the of un-dimerized mCLU subunits results in the generation a de-glycosylated 25 kDa CLU immunoreactive band. Therefore, these data combined with the absence of CLU_39 kDa in

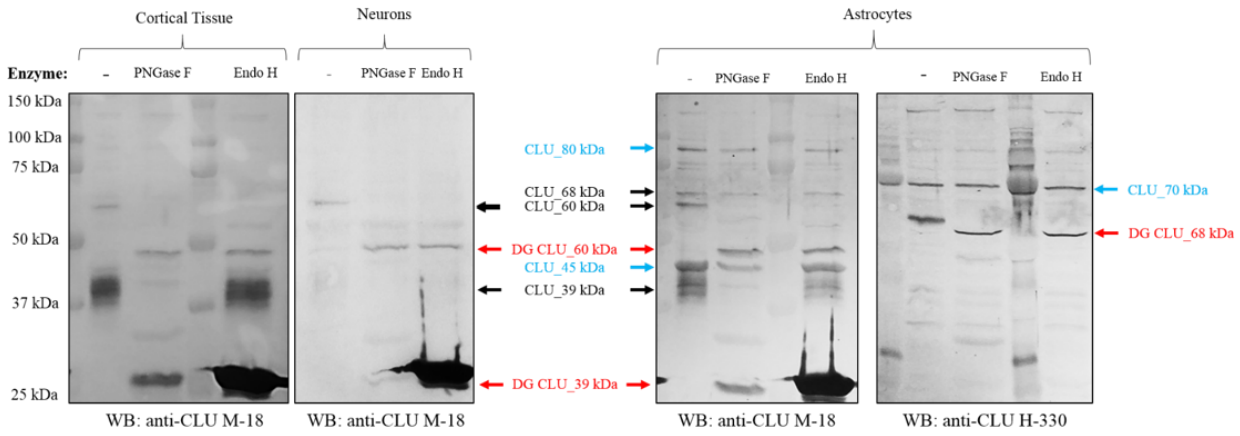

Figure 1.3.2. Analysis of Deglycosylated Cortical, Neuronal, and Astrocytic CLU Protein Isoforms. 15 µg cortical, neuronal, or astrocytic lysate were denatured for 10 min at 100 °C followed by incubation with 500 units of PNGase F or 1,000 units Endo H for 1 hr at 37 °C. Reactions were then boiled in reducing sample buffer for 5 min at 95 °C, resolved via SDS-PAGE and probed for CLU immunoreactivity using goat anti-CLU M-18 (1:1000) or rabbit anti-CLU H-330 at 4 °C overnight with continual rocking. Blots were washed and incubated for 1 hr at RT with species-specific HRP-conjugated secondary antibodies. Following acquisition, blots were stained with TMB to confirm molecular weights. Glycosylated CLU protein isoforms are indicated in black lettering while de-glycosylated protein isoforms are indicated in red lettering. Those CLU protein isoforms unaffected by endoglycosidases are indicated in blue lettering. Cross-reactivity of the Endo H enzyme with the rabbit-anti-goat secondary antibody occurs at 25 kDa and is indicated by a heavy black blotch in the Endo H treated groups.

mCLU-KO mice indicate that CLU_39 kDa, and by extension CLU_36 kDa, represent the un-dimerized glycosylated alpha and beta subunits of the mCLU isoform. Moreover, as CLU_60 kDa was also deficient in mCLU-KO mice and CLU_60 is de-glycosylated to CLU_49 kDa, these data suggest that CLU_49 kDa and CLU_60 kDa represent the un-glycosylated pre-protein and a high mannose glycosylated intermediate of the mCLU protein isoform. In addition, a side-by-side comparison of neurons, and astrocytes indicates that, unlike astrocytes, primary neurons do not

express CLU_39 kDa suggesting that primary neurons do not express the secreted mCLU isoform (Figure 1.3.2, middle and right panels). These data are consistent with early reports suggesting that the predominant amount secreted mCLU in the brain is derived from astrocytes. However, as primary neurons do express both CLU_49 kDa and CLU_60 kDa it appears that CLU protein isoforms generated from Exon 2-containing mRNA may possess intracellular functions.

In addition to observing deglycosylation of CLU_60 kDa and CLU_39 kDa, the data demonstrate that 3 CLU protein isoforms observed in astrocytes remained unaffected by either endoglycosidase: CLU_45 kDa, CLU_70 kDa, and CLU_80 kDa (Figure 1.3.3, right panel). These data both support and refute our initial hypothesis. Based on calculated molecular weights, it was anticipated that the CLU_45 kDa band would be unaffected by endoglycosidases. Thus it is highly probable that the CLU_45 kDa isoform is indeed translated from a CLU mRNA isoform containing Exons 3-9 and thus lacks the ER targeting sequence located in Exon 2. However, the inability to deglycosylate the CLU_80 kDa protein isoform by either endoglycosidase is puzzling as validation of CLU antibodies reveals that the CLU_80 kDa isoform is not the result of antibody artifact. Moreover, the inability to deglycosylate the CLU_70 kDa band conflicts with previous reports that show a direct effect on a 70 kDa CLU protein isoform by both PNGase F and Neuraminidase (cleaves terminal sialic acids on complex glycans) (Burkey et al., 1991). Two possible reasons for a lack of deglycosylation in specific CLU immunoreactive bands may be used to explain these findings: (1) the protein lysate used was not fully denatured in the 10 min step prior to enzyme addition thus allowing steric hindrance to inhibit or slow the removal of glycans and (2) alternative post-translational modifications are responsible for generating CLU immunoreactive higher molecular weight isoforms that are unresponsive to N-linked endoglycosidases. As the CLU amino acid sequence contains no O-linked glycosylation consensus motifs, the most likely candidates for

this large shift in MW would be the addition of SUMO or ubiquitin motifs. In support of this notion, reports have indicated that CLU is targeted by ubiquitin in the cytosol. Moreover, an examination of the CLU amino acid sequence reveals 5 possible SUMO consensus motifs (SUMOplot™ Analysis Program), 1 of which lies 3 amino acids away from an N-linked glycosylation consensus motif. However, despite these findings, more research will be needed to definitively identify alternative PTMs on CLU protein isoforms.

In addition to these data, treatment of an astrocytic lysate results in the generation of the CLU_53 kDa CLU protein isoform: an isoform not previously observed in our astrocyte fractionation (Figure 1.1.5). This band, which is detected by the H-330 antibody, appears to correspond to a decrease in the presence of the CLU_68 kDa band, which is detected by the M-18 antibody, following treatment with endoglycosidases. These data along with the fact that CLU_53 kDa, CLU_68 kDa and CLU_80 kDa appear to increase in mCLU-KO brain (Figure 1.2.1.1.) suggests that the CLU_53 kDa band may represent an alternative CLU pre-protein translated from a third CLU mRNA transcript which is glycosylated to form CLU_68 kDa and/or CLU_80 kDa. Collectively, these data indicate that some, but not all, higher molecular weight CLU protein isoforms represent glycosylated CLU protein isoforms with CLU_60 kDa representing a high mannose glycan and CLU_36-39 kDa representing the mCLU subunits modified by complex glycans. Furthermore, these data suggest that 3 CLU pre-proteins, which are unaffected by reducing conditions or endoglycosidase treatment, exist in rodent brain: CLU_49 kDa (Exons 2-9), CLU_45 kDa (Exons 3-9), and CLU_53 kDa (mRNA isoform unknown).

1.4. Acute Neurotoxicity Results in a Rapid and Significant Alteration in Intracellular Neuronal CLU Protein Expression

Having generated a solid understanding of the expression and localization of brain, neuronal, and astrocytic CLU protein isoforms in physiological conditions, the next investigated the impact of cellular stress on CLU protein isoform expression and localization? Several publications have indicated that CLU mRNA and/or extracellular mCLU protein expression is up-regulated in response to cellular stress (Han et al., 2001; Schreiber et al., 1993) (N. Kim, Han, et al., 2012). However, at this time, it is unclear how cellular stress or cytotoxic insult impacts individual brain CLU protein isoforms, especially intracellular CLU protein isoforms. As neurons are extremely prone to cytotoxic insult and appear to express an abundance of intracellular CLU protein isoforms, neurons were used as a model to investigate this question. Moreover, as neurons express high levels of the N-methyl-D-aspartate (NMDA) receptor and are thus especially prone to excitotoxicity, supra-physiological glutamate exposure was utilized as a model of acute toxicity. Primary neurons were isolated and cultured for 7 days at which time neurons were exposed to 100 µM glutamate for 5 min as indicated. Following glutamate exposure, neurons were incubated for indicated time points and harvested via subcellular fractionation. Our previous analysis of neuronal fractions indicates that neurons do not express robust CLU protein immunoreactivity in the crude mitochondrial fraction, therefore, while all fractions were analyzed for CLU immunoreactivity, only the nuclear and cytosolic fractions are presented here. To confirm neurotoxic insult, lactate dehydrogenase levels were measured in the culture medium prior to subcellular fractionation (Figure 1.4.1., Lower right panel). The data indicate a rapid and significant alteration in the levels of several neuronal CLU protein isoforms. Specifically, the CLU_49 kDa protein isoform is significantly increased in the cytosol with increasing levels of toxicity (Figure 1.4.1.). This increase appears to be specific to the CLU_49 kDa isoform as analysis of fractions with CLU B5 indicates no change in the CLU_53 kDa isoform in either fraction. In contrast, CLU_80 kDa is

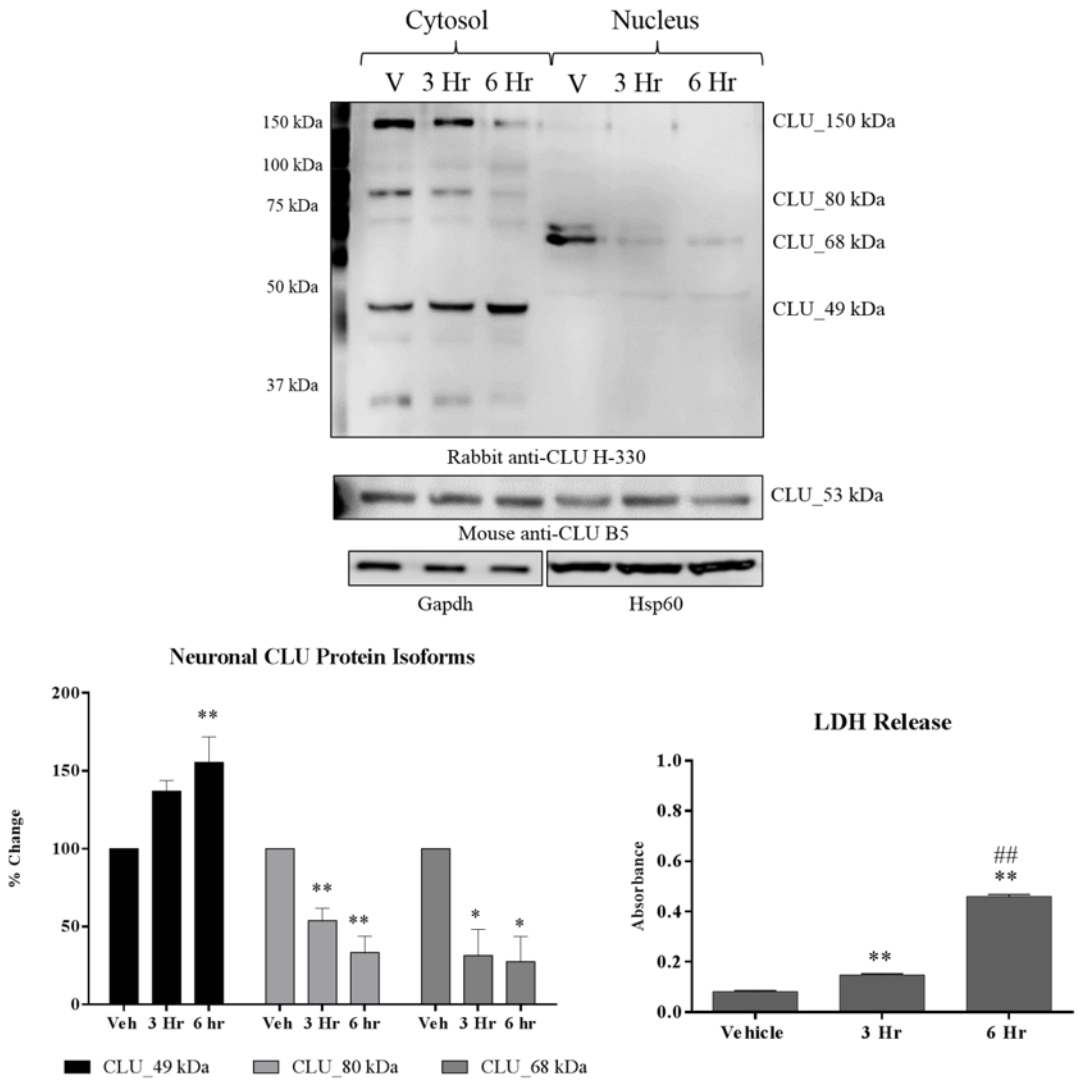

Figure 1.4.1. Analysis of CLU Protein Isoform Distribution Following Acute Excitotoxic Challenge. DIV 7 primary neurons were treated with 100 µM glutamate for 5 min in $CaCl_2$ containing HEPES buffered salt solution. Following glutamate exposure, neurons were incubated for 3 and 6 hrs in Neuronal Maintenance Medium. Prior to harvest, toxicity was confirmed by measuring the release of LDH in the culture medium. Cells were harvested via subcellular fractionation and the cytosolic and nuclear fractions were probed for CLU immunoreactivity using rabbit anti-CLU H-330 (1:1000) or mouse anti-CLU B-5 (1:750) overnight at 4°C. Blots were washed and incubated with species specific HRP-conjugated secondary antibodies for 1 hr at RT prior to acquisition. To confirm equal protein loading in the cytosolic and nuclear fractions, blots were stripped and reprobed with Gapdh (1:5000, 1 hr RT) and Hsp60 (1:6000, 2 hr RT). Changes in protein expression were analyzed from 4 independent experiments are represented here at the mean ± SEM. Data was analyzed using One-way Analysis of Variance (ANOVA) with Tukey's post-hoc analysis. * $p<0.05$, ** $p<0.01$ when compared to Vehicle-treated group.

significantly decreased in the cytosolic fraction with increasing levels of toxicity. In addition, we observe a toxicity-dependent decrease in the cytosolic CLU_150 kDa band, though this isoform was not quantified in this study. Similar to cytosolic CLU_80 kDa, analysis of the nuclear fraction indicates a significant decrease in the levels of CLU_68 kDa with increased toxicity (Figure 1.4.1.). The increase in CLU_49 kDa is consistent with previous reports indicating an increase in CLU mRNA (Rozovsky et al., 1994) and at least one CLU protein isoform (Messmer-Joudrier, Sagot, Mattenberger, James, & Kato, 1996) following glutamate exposure. Though it is unclear which protein isoform was up-regulated in this previous study, it appears that the upregulation of both CLU mRNA (previous work) and CLU_49 kDa (our work) represents the upregulation of the Exon 2-containing mRNA and the resulting protein isoforms following excitotoxicity. As mCLU is known to be rapidly induced following cellular stress, these data are in line with the currently available literature. However, as we have previously observed a lack of the mCLU subunits (CLU_39 kDa and CLU_36 kDa) in primary neurons, it appears that the up-regulation of CLU_49 kDa following glutamate exposure does not serve the purpose of generating additional secreted extracellular CLU. Rather it appears that up-regulation of CLU_49 kDa following neurotoxic challenge serves an intracellular purpose, though that purpose is currently unknown.

The toxicity-dependent disappearance of several CLU protein isoforms following glutamate challenge also provides interesting insight into intracellular CLU protein isoform distribution following stress. We originally postulated that the decrease in CLU_80 kDa expression resulted from the increased secretion of CLU_80 kDa into the culture medium. However, analysis of the culture medium does not indicate the secretion of an 80 kDa band (data not shown) suggesting that increased secretion is not the reason for significantly decreased CLU_80 kDa expression. We next postulated that the inverse relationship between CLU_80 kDa (67% decrease at 6 hrs) and CLU_49

kDa (55% increase at 6 hrs) expression was due to a toxicity-induced reversal or inhibition of N-linked glycosylation. However, our previous deglycosylation studies indicate that CLU_80 kDa is unaffected by endoglycosidase treatment in both neurons (Figure 1.3.3.) and astrocytes (Figure 1.3.2.). Furthermore, the significant decrease in CLU_68 kDa expression (73% decrease at 6 hrs) cannot be attributed to reversal of deglycosylation as CLU_68 kDa was not found to be de-glycosylated to CLU_49 kDa in our previous studies. A third possibility does arise to explain the decrease in CLU protein isoforms with cellular stress. Previous reports have indicated that, in some instances, cellular stress results in the cytosolic localization of certain CLU protein isoforms followed by proteasomal targeting and degradation. As the CLU protein isoforms in question are not being secreted or deglycosylated and cytosolic CLU protein isoforms have been shown to be targeted by ubiquitin via several proposed E3 ligases (Nizard et al., 2007; Fang et al., 2012) we hypothesize that the decline in CLU_80 kDa and CLU_68 kDa protein expression following toxicity is the result in ubiquitin-mediated proteasomal degradation of intracellular CLU protein isoforms, though more work is required to prove this hypothesis.

1.5. Interim Discussion and Working Hypothesis

In this chapter, we have demonstrated that rodent brain expresses 10 different CLU protein isoforms translated from at least 2 CLU mRNAs. These CLU protein isoforms are localized to defined subcellular compartments in both adult tissues as well as embryonic neurons and astrocytes and respond differently to acute neurotoxicity. Furthermore, we find that the distribution of some CLU protein isoforms is altered by aging in young mice. Collectively, the widespread distribution of CLU protein isoforms in brain tissue, astrocytes, and neurons suggests that CLU protein isoforms regulate some aspect of brain homeostasis. Moreover, the observation of age-mediated CLU protein isoform translocation suggests that certain CLU protein isoforms are more crucial in

the developed adult brain. In addition, we observe two key differences in the CLU expression profile between brain cell types. First, fractionation and deglycosylation studies indicate that CLU_39 kDa, which is known to be one of the 2 un-dimerized mCLU subunits, is expressed in embryonic astrocytes, but not neurons. These data suggest that astrocytes are capable of generating and secreting mCLU, whereas neurons are not. This observation is consistent with the previously held notion that astrocytes are primarily responsible for the secretion of extracellular CLU in the brain (Cordero-Llana et al., 2011; Zwain et al., 1994). Secondly, while neurons do not express the mCLU subunits, it does appear that neurons express intracellular CLU protein isoforms derived

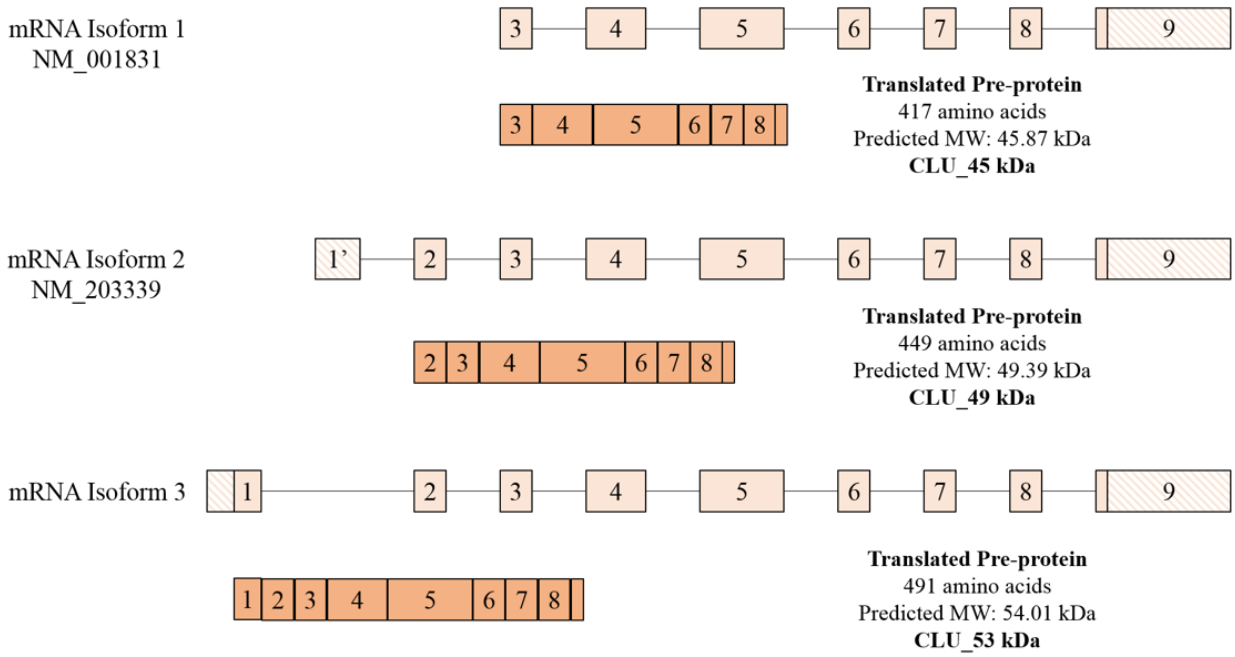

Schematic 12. Hypothesized CLU mRNA Isoforms and Translated Pre-Proteins. Based on protein isoform expression patterns, mRNA studies, and protein deglycosylation data, we hypothesize that at least three CLU mRNAs are generated from the CLU gene. **(Upper Panel)** A truncated mRNA transcript initiated at the ATG in Exon 3. Translation of this mRNA isoform would result in a 417 amino acid polypeptide with a predicted MW of 45.87 kDa. Proteins translated from the mRNA would be unaltered by glycosylation due to the lack of Exon 2 but would retain the NLS. **(Middle Panel)** The 2nd mRNA transcript is initiated at Exon 2 and translates to a 449 amino acid polypeptide with a predicted MW of 49.39 kDa. Proteins translated from this mRNA would be targeted to the ER for glycosylation and would retain a NLS. **(Lower Panel)**. An alternative mRNA variant initiated at the start site in Exon 1 and containing all 9 exons. Transcription of this mRNA would result in the production of a 491 amino acid polypeptide with a predicted MW of 54.01 kDa. Proteins translated from this mRNA would contain the ER targeting sequence translated from Exon 2 as well as the nuclear localization sequence (NLS) found in Exon 3. mRNA Exons with solid coloring indicate translated regions while portions of mRNA with striped fill indicate non-translated regions.

from the same CLU pre-protein as the mCLU subunits (CLU_49 kDa). These data suggest that while secreted mCLU is not generated in neurons, an intracellular form of mCLU derived from Exon 2-containing mRNA may be generated.

Based on the data presented in this chapter, we hypothesize that the myriad of observed higher molecular weight CLU protein isoforms are generated via PTM and/or proteolytic processing of three CLU pre-proteins. These pre-proteins are translated from 3 individual CLU mRNA isoforms (Schematic 12.) and translate to the CLU_53 kDa, CLU_49 kDa, and CLU_45 kDa protein isoforms. Transcription of CLU mRNA Isoform 1b would be initiated at the ATG in Exon 3 and would generate an mRNA isoform containing exons 3-9. The translated pre-protein from this proposed mRNA isoform would be 417 amino acids long with a predicted MW of 45 kDa and would retain the NLS in exon 3 but lack the ER targeting sequence in exon 2. Based on our fractionation and glycosylation studies, we hypothesize that CLU mRNA Isoform 1b is transcribed in the nucleus, translated on cytosolic ribosomes to the CLU_45 kDa isoform and is then imported into the mitochondria through an unknown import mechanism (Schematic 13). The localization of CLU_45 kDa to the mitochondria has been confirmed in this dissertation and will be discussed in detail in Chapter 2.

Transcription of CLU mRNA Isoform 2 would be initiated at the ATG in Exon 2 and would generate an mRNA isoform containing exons 2-9. The translated pre-protein from this proposed mRNA isoform would be 449 amino acids long with a predicted MW of 49 kDa and would retain the NLS in Exon 3 and the ER targeting sequence in Exon 2. We propose that, similar to CLU mRNA isoform 1a and 1b, CLU mRNA Isoform 2 is transcribed in the nucleus and translated on cytosolic ribosomes for form a 449 amino acid long pre-protein (CLU_49 kDa). CLU_49 kDa is the targeted to the ER/Golgi pathway where it is glycosylated into several protein variants

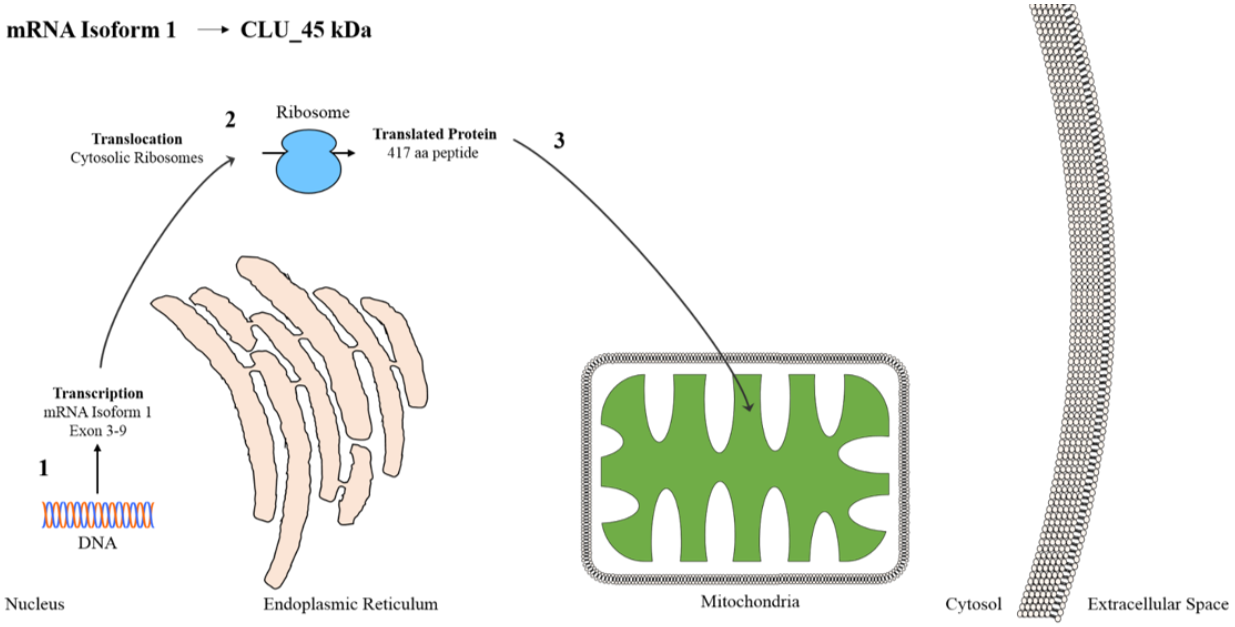

Schematic 13. Transcription, Translation, and Post-translational Modification of a Mitochondrial CLU Protein Isoform. (1) CLU mRNA Isoform 1b is transcribed from the CLU gene in the nucleus **(2)** mRNA Isoform 1b is translocated to the cytosol where it is translated on cytosolic ribosomes to generate a 417 amino acid long polypeptide (CLU_45 kDa) **(3)** CLU_45 kDa is then targeted to the mitochondria.

including CLU_60 kDa (high mannose glycan), CLU_70 kDa (complex glycan, data not from this study), and CLU_39 kDa (complex glycan). Following glycosylation of CLU_49 kDa in astrocytes CLU_39 kDa and CLU_36 kDa are heterodimerized and secreted into the extracellular space. In neurons, CLU_60 kDa and CLU_70 kDa are translocated to the cytosolic fraction to regulate internal neuronal homeostasis (Schematic 14)

Transcription of CLU mRNA Isoform 1 is initiated at the ATG in Exon 1 and would generate an mRNA isoform containing all 9 exons. The translated pre-protein from this proposed mRNA isoform would be approximately 491 amino acids long with a predicted MW of 54 kDa and would possess both the ER targeting sequence in Exon 2 and the NLS in Exon 3. Based on protein isoform localizations, we hypothesize that mRNA isoform 1a is transcribed in the nucleus, translated on

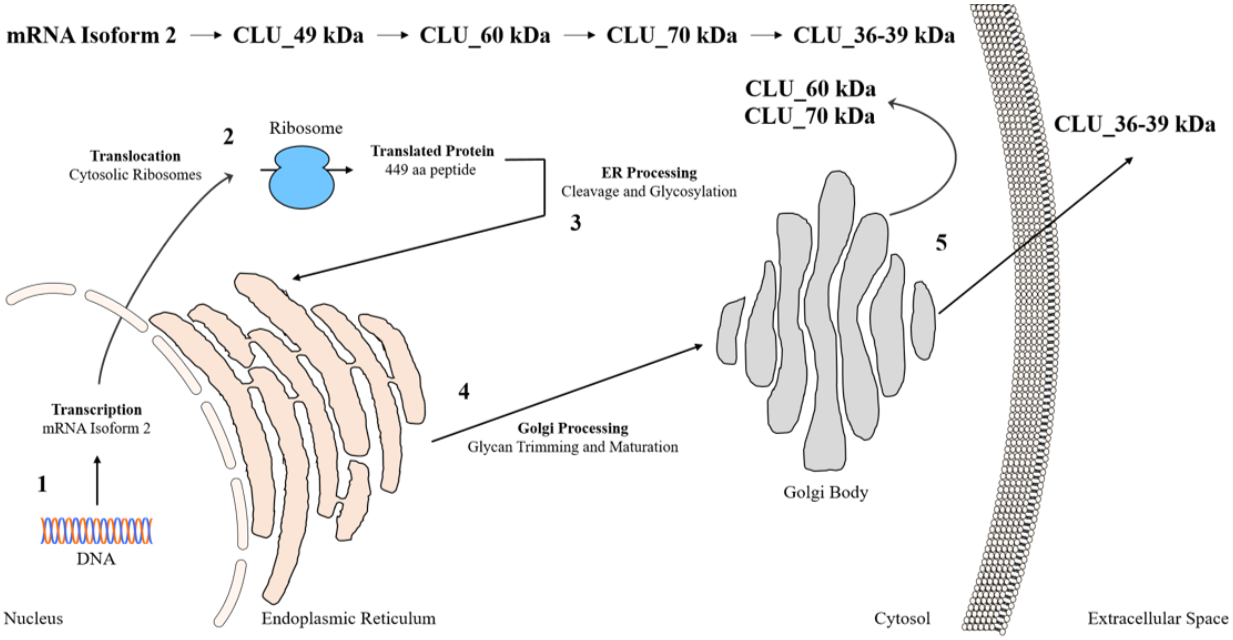

Schematic 14. Transcription, Translation, and Post-translational Modification of Intra- and Extracellular mCLU (1) CLU mRNA Isoform 2 is transcribed from the CLU gene in the nucleus **(2)** mRNA Isoform 2 is translocated to the cytosol where it is translated on cytosolic ribosomes to generate a 449 amino acid long polypeptide (CLU_49 kDa) **(3)** CLU_49 kDa is transported to the ER where it undergoes preliminary glycosylation **(4)** immature glycosylated CLU_49 kDa is transported to the Golgi Body where the attached glycans are trimmed and processed to form CLU_60 kDa, CLU_70 kDa, and CLU_36-39 kDa, and **(5) In astrocytes:** the two mCLU subunits that are now modified by sialic acid containing complex glycans are then heterodimerized and secreted into the extracellular space. **In neurons:** CLU_60 kDa and CLU_70 kDa are translocated to the cytosol and act as undimerized intracellular mCLU protein isoforms.

cytosolic ribosomes to form CLU_53 kDa and glycosylated in the ER/Golgi pathway to form the CLU_68 kDa isoform which is then translocated to the nuclear compartment (Figure 1.5.2.). The generation of a third CLU mRNA isoform is supported by recently generated data indicating the presence of Exon 1-containing mRNA in WT rodent brain. Moreover, CLU_68 kDa is observed in the ER-containing crude mitochondrial and nuclear fractions of primary neurons and the exclusive localization of CLU_68 kDa to the nucleus of adult cortex. Moreover, when examining CLU protein expression in mCLU-KO mice, one observation was a similar increase in the expression of both CLU_53 kDa and CLU_68 kDa in KO animals suggesting that not only that

certain CLU transcripts may be upregulated in the absence of mCLU, but also that CLU_53 kDa and CLU_68 kDa may be inter-related. In addition, CLU_53 kDa remains unaltered by endoglycosidase treatment and the addition of reducing agents during immunoblot analysis thus indicating that this protein isoform is not a heterodimer or a glycosylated intermediate.

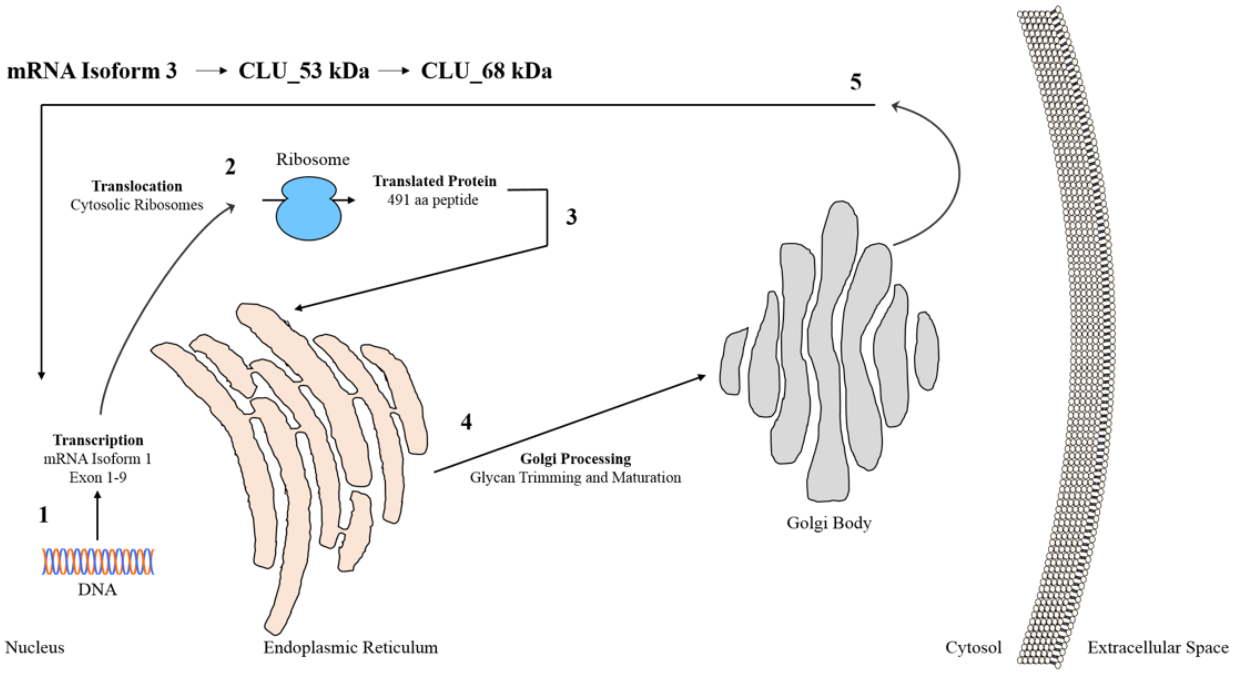

Schematic 15. Transcription, Translation, and Post-translational Modification of a Nuclear CLU Protein Isoform. (1) CLU mRNA Isoform 1a is transcribed from the CLU gene in the nucleus **(2)** mRNA Isoform 1a is translocated to the cytosol where it is translated on cytosolic ribosomes to generate a 491 amino acid long polypeptide (CLU_53 kDa) **(3)** CLU_53 kDa is transported to the ER where it undergoes preliminary glycosylation **(4)** immature glycosylated CLU_68 kDa is transported to the Golgi Body where the attached glycans are trimmed and processed, and **(5)** CLU_68 kDa is targeted to the nucleus

Chapter 2. CLU in Brain Mitochondria

2.1. Identification of a Mitochondria-Localized CLU Protein Isoform

Preliminary analyses of brain CLU immunoreactivity in cortical neurons indicated diffuse punctate CLU staining that appears to overlap with Mitotracker staining in the soma and dendrites of primary neurons (Figure 2.1.1.). As multiple CLU protein isoforms were found to be localized to the mitochondria and ER-containing organelle fraction of adult cortical tissue, embryonic neurons and embryonic astrocytes (Chapter 1, Section 1), and at least one CLU protein isoform is not targeted to the ER, the question of a brain mitochondria-localized CLU protein isoform arises. To answer this question, pure mitochondria were isolated from 5-7-month-old female cortical tissues

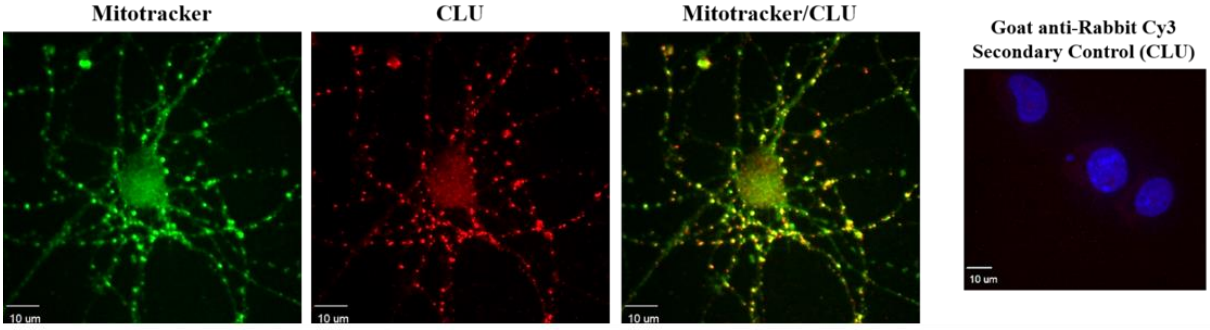

Figure 2.1.1. CLU Immunoreactivity is Associated with Mitotracker Staining in Primary Cortical Neurons. DIV 9 primary cortical neurons were stained with 250 nM Mitotracker Deep Red (Neurons) for 25 min as indicated. Cells were washed, fixed, permeabilized and blocked as indicated and probed for CLU immunoreactivity using rabbit anti-CLU H-330 (1:500) overnight at 4°C with continual rocking. The following day, cells were washed and probed with goat-anti-rabbit Cy3 (Neurons, 1:1000) for 1 hr at RT with continual rocking protected from light. Samples were mounted using Vectashield Hardset Mounting Medium with Dapi and allowed to set overnight before imaging. In addition, control samples were also generated using PBST without the addition of primary antibody. All incubation times were consistent between control and experimental groups. Confocal images were acquired using a customized Olympus IX81/spinning disk confocal inverted microscope equipped with an Olympus 40X 0.95 NA air objective. Images were collected and analyzed using the Slidebook Software Version 6.0 with 15-20 image stacks with a 0.1 µm step size through the cells.

and analyzed via immunoblotting with 2 CLU antibodies. To verify the purity of mitochondrial samples, blots were also probed for cytosolic and ER contamination using Gapdh, calnexin, and calreticulin antibodies.

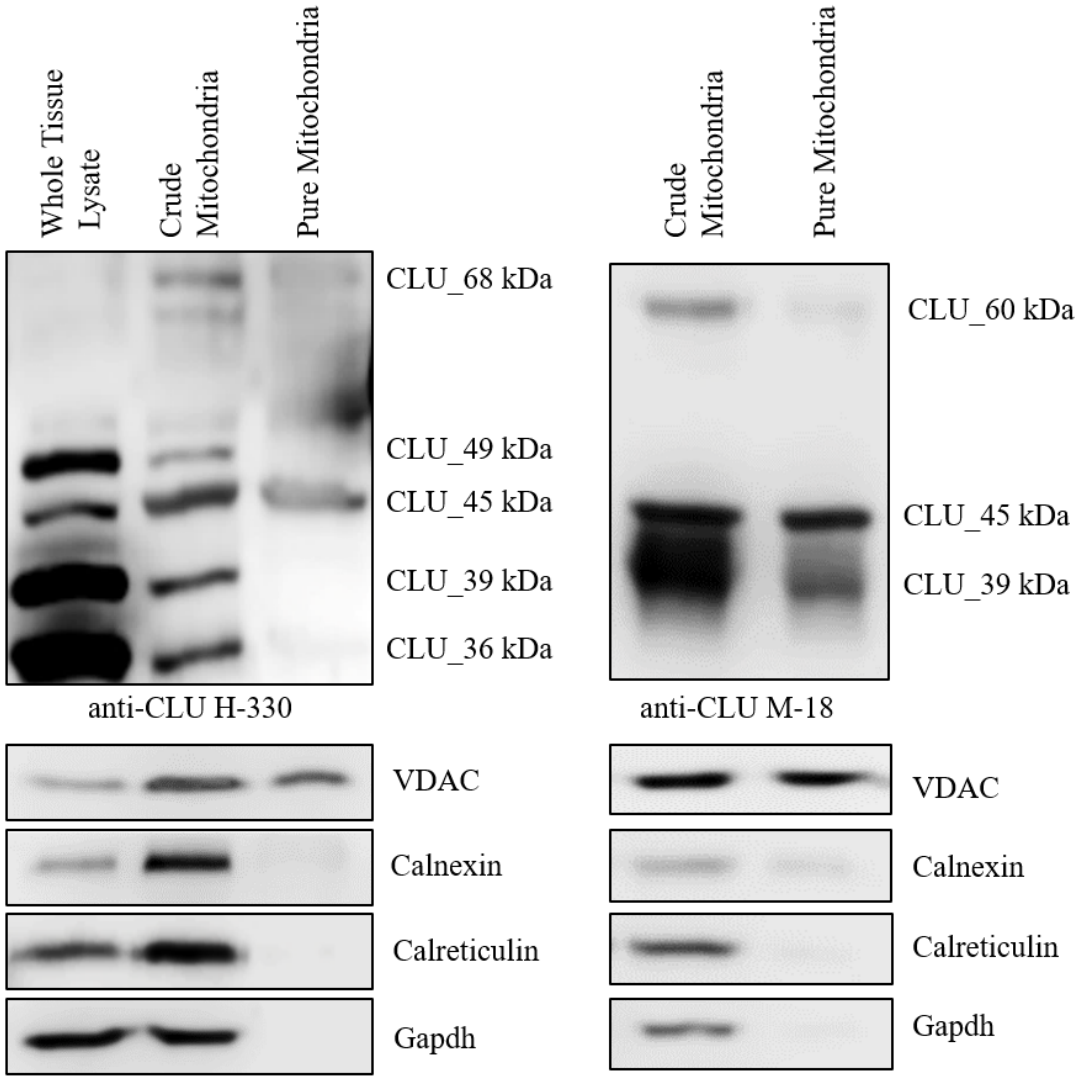

Figure 2.1.2. Identification of a Mitochondrial CLU Protein Isoform. Pure mitochondria were isolated from freshly dissected cortical tissues harvested from female 5-7-month-old WT mice using a discontinuous percoll gradient as indicated. Equal concentrations of whole tissue lysate, crude mitochondria, and pure mitochondria were analyzed via reducing SDS-PAGE and probed for CLU immunoreactivity using either rabbit anti-CLU H-330 (1:1000, left panel) or goat anti-CLU M-18 (right panel) at 4 °C overnight with continual rocking. Blots were washed and incubated for 1 hr at RT with species-specific HRP-conjugated secondary antibodies (1:5000). Following acquisition, blots were stained with TMB to confirm molecular weights. Biochemical characterization of isolated fractions was performed using a panel of organelle-specific antibodies: VDAC (mitochondria, 1:2000 4 hr RT), Calnexin and Calreticulin (Endoplasmic reticulum, 1:8000, 1 hr RT), and Gapdh (cytosol, 1::8000, 2 hr at RT). Pure mitochondria is defined as a mitochondrial sample that is free of ER and cytosolic contamination. (N=3 independent isolations)

As expected, the whole tissue lysate expressed all previously observed CLU protein isoforms (CLU_49 kDa, CLU_45 kDa, and CLU_36-39 kDa) while the crude mitochondrial sample

expressed (CLU_68 kDa, CLU_60 kDa, CLU_49 kDa, CLU_45 kDa, and CLU_36-39 kDa). However, analysis of pure mitochondria, which is characterized as a mitochondrial sample free of ER and cytosolic contamination, indicates the expression of only 1 CLU protein isoform in all sets of samples analyzed: CLU_45 kDa. These data indicate that CLU_45 kDa is localized to brain mitochondria. As we hypothesized that the CLU_45 kDa band is translated from Exon 3-9 containing mRNA into a pre-protein that remains unaffected by glycosylation (Chapter 1), crude and pure mitochondria were treated with the previously utilized endoglycosidases to determine whether the MW of the newly identified mitochondrial CLU isoform would be impacted by deglycosylation. Consistent with our previous observations the CLU_60 kDa band is

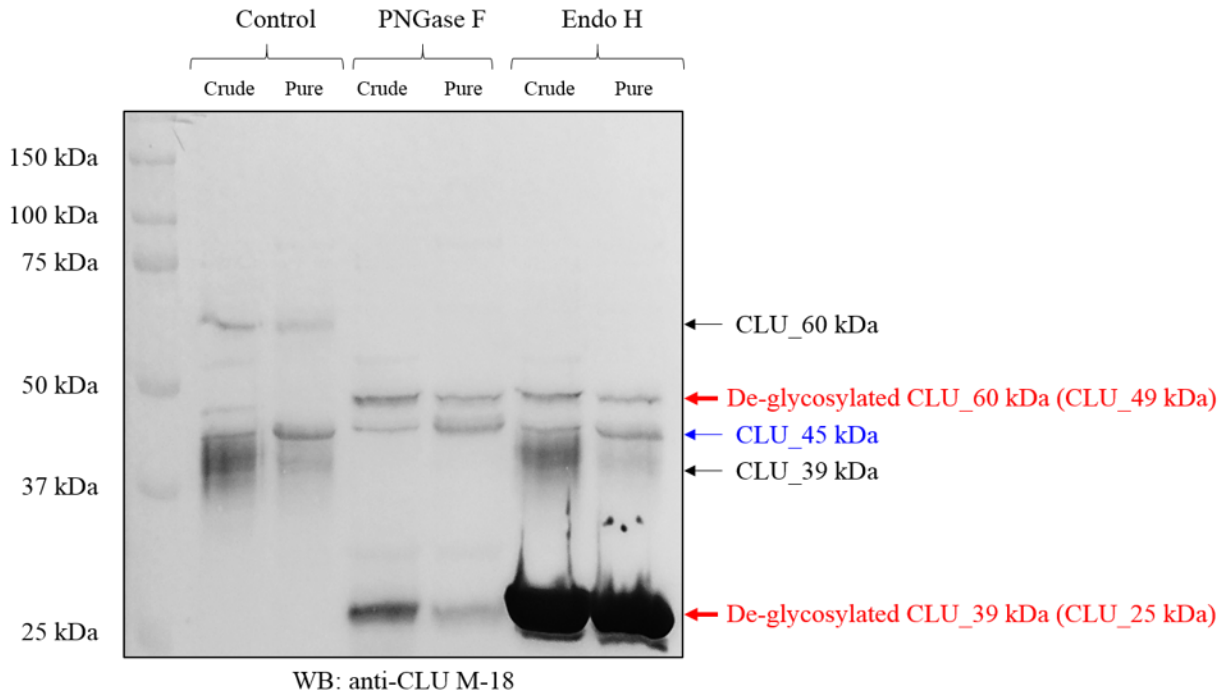

Figure 2.1.3. CLU_45 kDa is not Impacted by Endoglycosidase Treatment. Crude and pure mitochondria were isolated as previously described and subjected to endoglycosidase treatment using Endo H and PNGase F as previously described. Mitochondrial lysates were then analyzed for CLU immunoreactivity using goat anti-CLU M-18 (1:1000) overnight at 4°C. The following morning, blots were incubated in species-specific HRP-conjugated secondary antibody for 1 hr at RT (1:5000). Following acquisition, blots were stained with TMB to confirm the MW of identified bands.

deglycosylated by both PNGase F and Endo H to form the CLU_49 kDa band while the CLU_39 kDa band is deglycosylated into the CLU_25 kDa band. Moreover, in support of our hypothesis, the CLU_45 kDa band, which is expressed more robustly in the pure mitochondrial sample remains unaffected by endoglycosidase treatment (Figure 2.1.3.). These data support our proposed hypothesis for the generation and mitochondrial targeting of the non-glycosylated CLU protein isoform.

To further investigate the localization of CLU_45 kDa to brain mitochondria, pure mitochondria were isolated as previously described and subjected to a Digitonin Mitochondria Sub-fractionation. This technique, which results in the opening of the intermembrane space and the matrix in a successive manner, allows for the identification of submitochondrial localization by matching the expression changes of a protein of interest (i.e. CLU_45 kDa) with that of fraction-specific mitochondrial markers: VDAC (outer mitochondrial membrane), Cytochrome C (intermembrane space), CoxIV (inner mitochondrial membrane), and Grp75 (matrix). The data indicate prominent CLU_45 kDa immunoreactivity in the control group with an approximate 32% decrease in CLU_45 kDa expression occurring between the control-treated group and the 0.1%-treated group. CLU_45 kDa immunoreactivity decreases slightly between the 0.1%- and 0.2%-treated groups (~8% decrease) followed by a sharp decline in the 0.3%-treated group that results in the loss of 94% of mitochondrial CLU_45 kDa expression. This expression profile change does not match that of VDAC which shows the largest change in expression between the 0.1%- and 0.2%-treated groups (80% - 32%) with relatively little change occurring between the 0.2%- and 0.3%-treated groups (32% - 28%). In addition, CLU_45 kDa expression changes do not match the expression changes of Cytochrome C, which are fairly linear in nature (100% - 45% - 27% - 11%). These data

indicate that nCLU is not localized to the outer mitochondrial membrane or the intermembrane space.

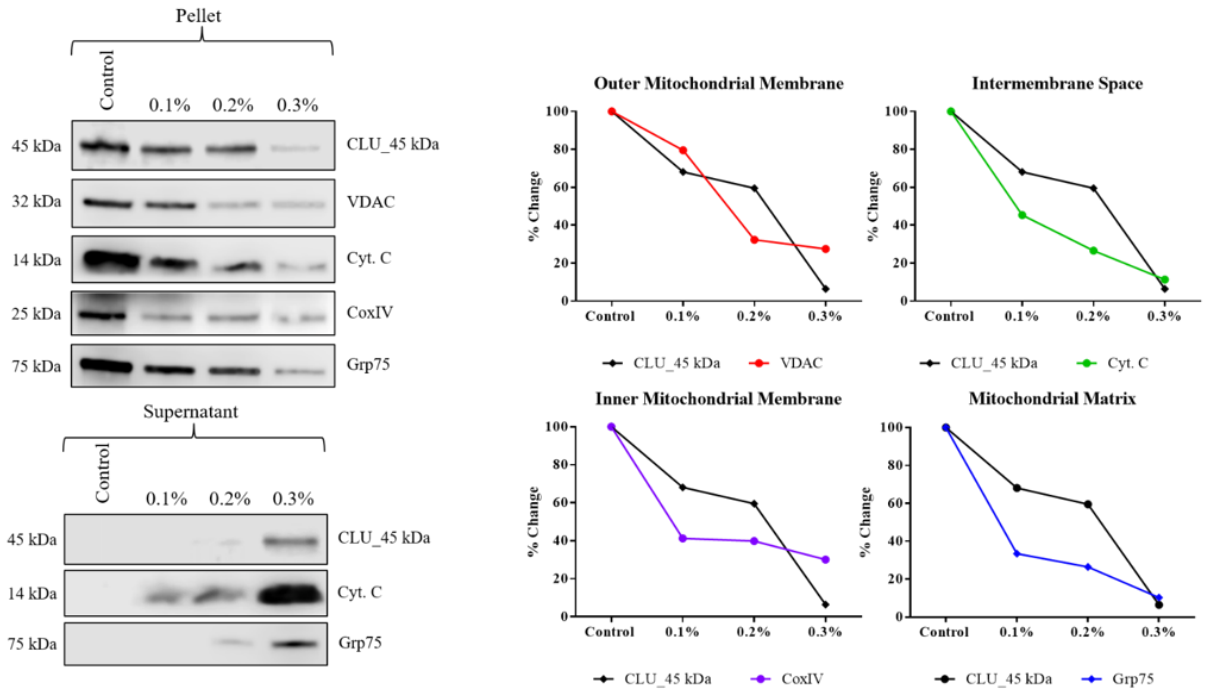

Figure 2.1.4. Identification of the Sub-mitochondrial Localization of CLU_45 kDa. Pure mitochondria were isolated as previously described and subjected to a digitonin mitochondria sub-fractionation as indicated. Briefly, equal volumes and concentrations of pure mitochondria were aliquoted into 4 tubes and incubated with increasing concentrations of digitonin for 5 min on ice. Samples were subjected to ultracentrifugation to separate the remaining mitochondrial pellet (retained proteins) and the mitochondrial supernatant (released proteins) and both sets of samples were analyzed for CLU immunoreactivity using rabbit anti-CLU H-330 (1:1000) at 4 °C overnight with continual rocking. Blots were washed and incubated for 1 hr at RT with secondary antibodies (1:5000). Following acquisition, the membrane was stripped and re-probed for mitochondrial fraction specific markers: VDAC (outer mitochondrial membrane, 1:2000, 4 hrs RT), Cytochrome C (intermembrane space, 1:1000, 4 hrs RT), Cox IV (inner mitochondrial membrane, 1:2000, overnight 4°C), and Grp75 (mitochondrial matrix, 1:8000, 1 hr RT). % change was calculated for each protein examined by setting the control (no digitonin) group to 100% (n=2 independent experiments).

Upon examination of CoxIV immunoreactivity we observe a certain degree of similarity between CLU_45 kDa and CoxIV expression changes with increasing concentrations of Digitonin. Specifically, both CLU_45 kDa and CoxIV decline sharply between the control group and the 0.1%-treated group (32% and 58%) with relatively little change occurring between the 0.1%- and

0.2%-treated groups (8% and 1% change). However, unlike CLU_45 kDa expression, which decreases by 54% between the 0.2%- and 0.3%-treated groups, 0.3% Digitonin treatment results in only a 10% decrease in CoxIV immunoreactivity when compared to the 0.2%-treated group suggesting that CLU_45 kDa is localized to the mitoplast but not specifically to the inner mitochondrial membrane. Similar to that of CoxIV, Grp75 immunoreactivity decreases sharply between the control and 0.1%-treated group (67% decline) with only a slight decrease occurring between the 0.1%- and 0.2%-treated groups (7% decline). However, unlike CoxIV expression, 0.3% Digitonin treatment results in a much steeper decline in Grp75 expression resulting in an expression pattern that is nearly identical to that of CLU_45 kDa. These data indicate that CLU_45 kDa is localized to the matrix of rodent brain mitochondria. To confirm the similar release patterns of CLU_45 kDa and Grp75, the supernatant fraction was examined via immunoblot analysis. As indicated in Figure 2.1.4. (Lower Panel), no CLU_45 kDa or Grp75 immunoreactivity is detected in either the control or the 0.1% Digitonin-treated groups with only minute protein immunoreactivity in the 0.2%-treated group. However, 0.3% Digitonin treatment, which results in the major loss of retained Grp75 and CLU_45 kDa (Figure 2.1.4. Upper Panel), results in a similar increase in protein immunoreactivity in the supernatant (Figure 2.1.4. Lower Panel) further suggesting that CLU_45 kDa is released from the mitochondrial matrix in a manner that is similar to that of soluble matrix proteins. Collectively, these data indicate that the CLU_45 kDa protein isoform is localized to the mitochondrial matrix of rodent brain mitochondria. To our knowledge this is the first report to indicate the localization of an intracellular CLU protein isoform to brain mitochondria. However, despite the novelty of this finding, the localization of a CLU protein isoform to brain mitochondria generates several important questions that are currently unanswered. First and foremost, as CLU_45 kDa does not contain a canonical mitochondrial targeting sequence,

it is unclear how this protein isoform is imported into the mitochondrial matrix. Second, as we are the first to identify mitochondrial CLU localization, the purpose of mitochondrial CLU (i.e. the function of CLU_45 kDa in the mitochondria) it is currently unclear. As the bulk of matrix proteins are dedicated to either the generation of ATP or the synthesis of mitochondrial encoded genes, it is possible that CLU in some way modulates mitochondrial energy production or regulates some aspect of central dogma in the mitochondrial matrix; however more research is needed to confirm this hypothesis.

2.2. Identification of CLU Mitochondrial Interacting Partners

2.2.1. Co-immunoprecipitation of Overexpressed Human CLU in Neuro-2a Cells

As both the import mechanism and function of mitochondrial CLU are currently unknown, we next examined possible functions of CLU_45 kDa within the mitochondrial matrix by identifying

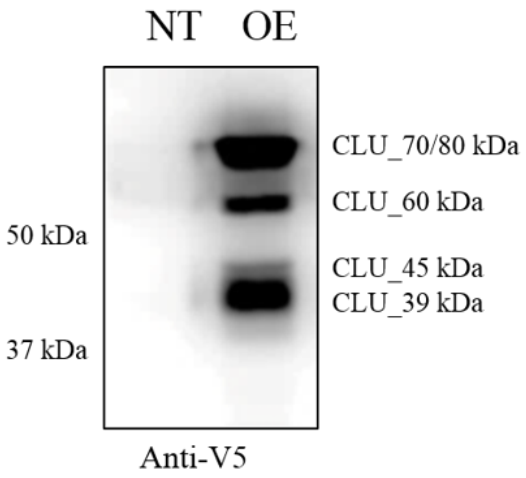

Figure 2.2.1.1. Confirmation of pLX304-hCLU-v5 Overexpression in Neuro-2a Cells. 2 µg pLX304-hCLU-v5 was transfected into Neuro-2a cells for 18 hrs as indicated. Following transfection, cells were allowed to incubate for 96 hrs and harvested via Whole Cell Protein Extraction. Lysates were analyzed via immunoblotting using rabbit anti-v5 (1:5000) for 3 hr at RT with continual rocking. Blots were washed and incubated for 1 hr at RT with species-specific secondary antibodies (1:5000).

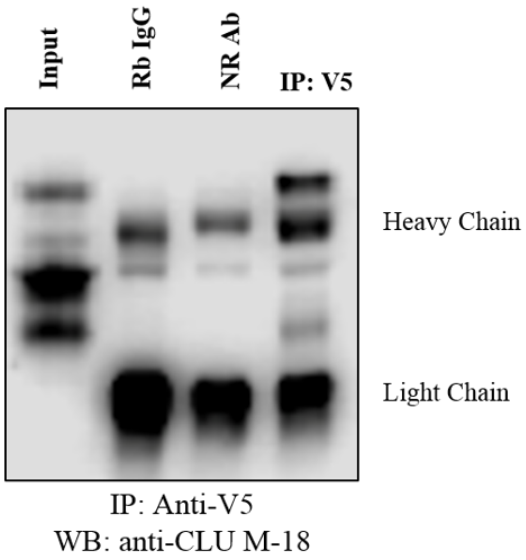

Figure 2.2.1.2. Confirmation of CLU Immunoprecipitation using the v5 Epitope Tag. pLX304-hCLU-v5 was transfected into Neuro-2a and incubated for 96 hrs. Cells were harvested in non-reducing native conditions and 1 mg cell lysate was pre-cleared for 1 hr at 4 °C using Protein G Dynabeads. Precleared samples were separated into 3 tubes and immunoprecipitated overnight with 4 µg nonspecific rabbit IgG (Rb IgG), an unrelated rabbit antibody (NR Ab), or rabbit anti-v5 (IP: V5). The following morning, antibody-antigen complexes were pulled from solution using 30 µL protein G beads for 2 hr at 4 °C. Beads were washed 5 times with 1 mL Co-IP Buffer and eluted in reducing sample buffer by heating at 95 °C for min. 10% total input and 5 µL from each eluted sample was analyzed for CLU immunoreactivity using goat-anti CLU M-18 (1:1000) overnight at 4 °C. Blots were washed and incubated for 1 hr at RT with species-specific secondary antibodies (1:5000).

CLU_45 kDa protein interacting partners. Full length human clusterin cDNA fused to a C-terminal V5 epitope tag (pLX304-hCLU-v5) was transfected into Neuro-2a cells and allowed to replicate

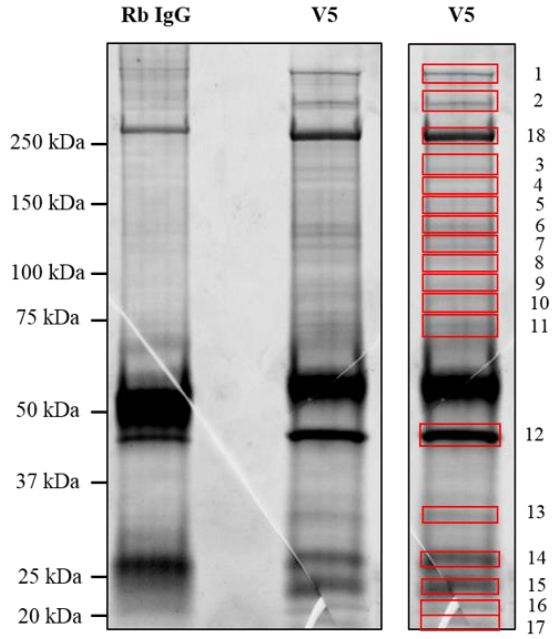

Figure 2.2.1.3. Representation of SYPRO Ruby Stained Co-IP Samples. pLX304-hCLU-v5 was transfected into Neuro-2a and incubated for 96 hrs. Cells were harvested and Co-IP was performed on crude mitochondrial samples as previously indicated. The eluates remaining following confirmation of CLU IP (Figure 2.2.2.) were resolved via SDS-PAGE and the resulting gel was fixed and stained using SYPRO Ruby Stain. The following day, the blot was washed and visualized using UV light. Bands specific to the IP lane (V5, red boxes) were excised and processed for protein identification using mass spectrometry.

for 96 hrs prior to harvest. Following incubation, cells were harvested via whole cell protein extraction and overexpression of the hCLU construct was confirmed via immunoblotting with an antibody raised to the v5 epitope tag (Figure 2.2.1.1.). Following confirmation of overexpressed hCLU, the transfection was repeated on a larger scale and following incubation, crude mitochondria were isolated and resuspended in native, non-reducing buffer that does not disrupt protein-protein interactions. CLU and its interacting partners were then co-immunoprecipitated using rabbit-anti-V5 (IP) with control immunoprecipitations being performed under the same experimental parameters using non-specific rabbit IgG (IgG). Samples were eluted in reducing denaturing conditions and 10% of the eluted sample was analyzed for CLU immunoreactivity to confirm successful immunoprecipitation of overexpressed hCLU (Figure 2.2.1.2.). The remaining portion of the eluate was then resolved in via SDS-PAGE and the resulting gel was stained with SYPRO Ruby and visualized using UV light (Figure 2.2.1.3.). Bands that were

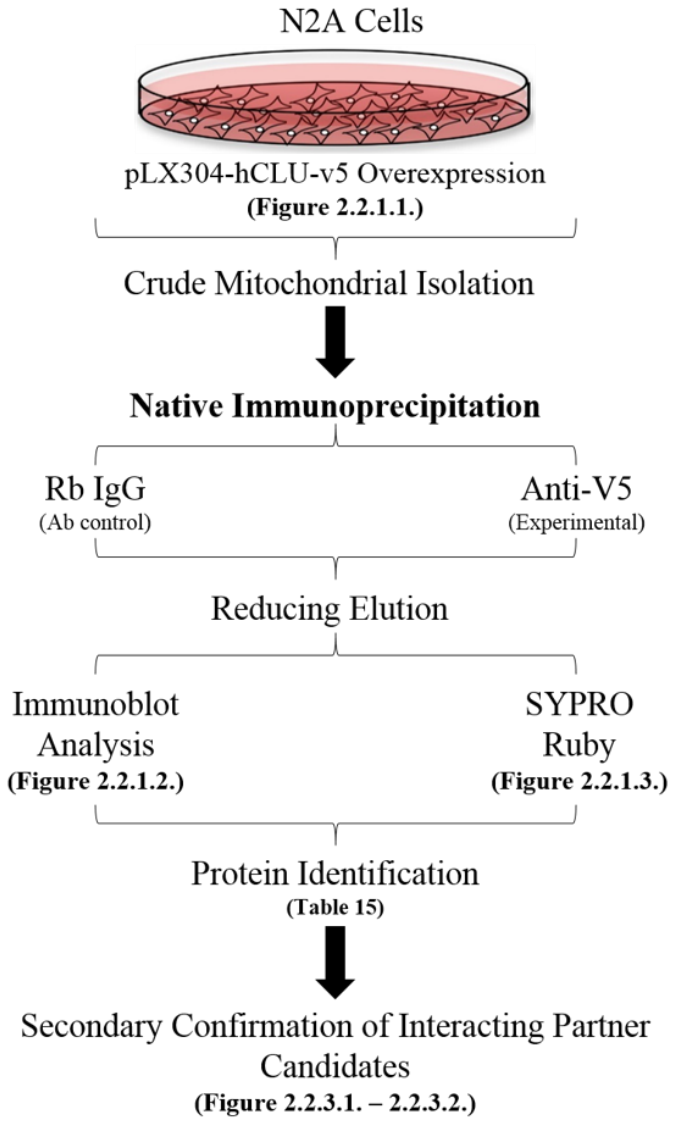

Schematic 16. An Overview of the Experimental Plan used to Identify CLU Mitochondrial Interacting Partners.

specific to the experimental IP lane (18 in total, red boxes) were excised, digested, and sent for protein identification using Multi-dimensional Protein Identification Technology (MUD-Pit). A representation of the entire mitochondrial Co-IP is included in Figure Schematic 16.

Of the 18 samples that were submitted, >100 mitochondrial proteins were identified as possible CLU interacting partners within the following parameters: (a) minimum of 2 unique peptides, (b) a minimum of 2% coverage, (c) a molecular weight corresponding to molecular weight of excised band, and (d) a protein FDR confidence level above medium (5%). A full list of identified proteins with corresponding UniPROT ID numbers, % coverage, and number of unique peptides identified is included in Table 15.

Identified Mitochondrial Proteins

UniProt	Description	% Cov	# Peptides
P38647	Stress-70 protein, mitochondrial [OS=Mus musculus]	41	26
Q91VR2	ATP synthase subunit gamma, mitochondrial [OS=Mus musculus]	33	10
Q99LC5	Electron transfer flavoprotein subunit alpha, mitochondrial [OS=Mus musculus]	32	8
P58059	28S ribosomal protein S21, mitochondrial [OS=Mus musculus]	31	2
Q9CRB9	MICOS complex subunit MIC19 [OS=Mus musculus]	27	9
Q9Z2I8	Succinate--CoA ligase [GDP-forming] subunit beta, mitochondrial [OS=Mus musculus]	27	7
Q60932	voltage-dependent anion-selective channel protein 1 [OS=Mus musculus]	27	6
Q922W5	Pyrroline-5-carboxylate reductase 1, mitochondrial [OS=Mus musculus]	26	5
Q9DCX2	ATP synthase subunit d, mitochondrial [OS=Mus musculus]	25	5
Q60930	Voltage-dependent anion-selective channel protein 2 [OS=Mus musculus]	25	6
Q9DB15	39S ribosomal protein L12, mitochondrial [OS=Mus musculus]	24	2
Q8QZT1	Acetyl-CoA acetyltransferase, mitochondrial [OS=Mus musculus]	24	6
Q9DB20	ATP synthase subunit O, mitochondrial [OS=Mus musculus]	24	4
Q9DCC8	Mitochondrial import receptor subunit TOM20 homolog [OS=Mus musculus]	23	2
Q925I1	ATPase family AAA domain-containing protein 3 [OS=Mus musculus]	22	9

Q9WTQ8	Mitochondrial import inner membrane translocase subunit tim23 [OS=Mus musculus]	22	3
Q9D1I6	39S ribosomal protein L14, mitochondrial [OS=Mus musculus]	19	2
Q99L13	3-hydroxyisobutyrate dehydrogenase, mitochondrial [OS=Mus musculus]	19	4
Q8BK72	28S ribosomal protein S27, mitochondrial [OS=Mus musculus]	18	8
Q8CD10	calcium uptake protein 2, mitochondrial [OS=Mus musculus]	18	6
Q9CQN7	39S ribosomal protein L41, mitochondrial [OS=Mus musculus]	17	2
Q8BFR5	elongation factor Tu, mitochondrial [OS=Mus musculus]	17	5
Q8R03	Peptidyl-tRNA hydrolase ICT1, mitochondrial [OS=Mus musculus]	17	3
Q8VEM8	Phosphate carrier protein, mitochondrial [OS=Mus musculus]	17	5
P35486	Pyruvate dehydrogenase E1 component subunit alpha, somatic form, mitochondrial	17	5
Q9Z2I9	Succinate--CoA ligase [ADP-forming] subunit beta, mitochondrial [OS=Mus musculus]	17	5
Q8VE22	28S ribosomal protein S23, mitochondrial [OS=Mus musculus]	16	2
Q8JZS9	39S ribosomal protein L48, mitochondrial [OS=Mus musculus]	16	3
Q8BH59	Calcium-binding mitochondrial carrier protein Aralar1 [OS=Mus musculus]	16	9
P48758	Carbonyl reductase [NADPH] 1 [OS=Mus musculus]	16	2
Q9CQN1	heat shock protein 75 kDa, mitochondrial [OS=Mus musculus]	16	8
O35857	Mitochondrial import inner membrane translocase subunit TIM44 [OS=Mus musculus]	16	6
Q9CQF0	39S ribosomal protein L11, mitochondrial [OS=Mus musculus]	15	2
Q8R4U6	DNA topoisomerase I, mitochondrial [OS=Mus musculus]	15	7
Q99M87	DnaJ homolog subfamily A member 3, mitochondrial [OS=Mus musculus]	15	5
P54071	Isocitrate dehydrogenase [NADP], mitochondrial [OS=Mus musculus]	15	5
Q91VN4	MICOS complex subunit mic25 [OS=Mus musculus]	15	4
Q9CZW5	Mitochondrial import receptor subunit TOM70 [OS=Mus musculus]	15	5
Q9D773	39S ribosomal protein L2, mitochondrial [OS=Mus musculus]	14	2
Q9DB77	Cytochrome b-c1 complex subunit 2, mitochondrial [OS=Mus musculus]	14	5
Q99MR8	Methylcrotonoyl-CoA carboxylase subunit alpha, mitochondrial [OS=Mus musculus]	14	6
Q9DC70	NADH dehydrogenase [ubiquinone] iron-sulfur protein 7, mitochondrial [OS=Mus musculus]	14	3
Q9D338	39S ribosomal protein L19, mitochondrial [OS=Mus musculus]	13	2
Q9CQ06	39S ribosomal protein L24, mitochondrial [OS=Mus musculus]	13	2
O08756	3-hydroxyacyl-CoA dehydrogenase type-2 [OS=Mus musculus]	13	2
Q8BH95	Enoyl-CoA hydratase, mitochondrial [OS=Mus musculus]	13	3

P16858	glyceraldehyde-3-phosphate dehydrogenase [OS=Mus musculus]	13	3
Q91VD9	NADH-ubiquinone oxidoreductase 75 kDa subunit, mitochondrial [OS=Mus musculus]	13	7
Q8K2B3	Succinate dehydrogenase [ubiquinone] flavoprotein subunit, mitochondrial [OS=Mus musculus]	13	6
Q8CIW5	Twinkle protein, mitochondrial [OS=Mus musculus]	13	5
Q924T2	28S ribosomal protein S2, mitochondrial [OS=Mus musculus]	12	2
Q80X85	28S ribosomal protein S7, mitochondrial [OS=Mus musculus]	12	2
Q8K2Y7	39S ribosomal protein L47, mitochondrial [OS=Mus musculus]	12	3
Q03265	ATP synthase subunit alpha, mitochondrial [OS=Mus musculus]	12	5
Q3UMR5	Calcium uniporter protein, mitochondrial [OS=Mus musculus]	12	3
Q8CGK3	Lon protease homolog, mitochondrial [OS=Mus musculus]	12	8
Q9D6J6	NADH dehydrogenase [ubiquinone] flavoprotein 2, mitochondrial [OS=Mus musculus]	12	2
P40630	Transcription factor A, mitochondrial [OS=Mus musculus]	12	2
Q8BMS1	Trifunctional enzyme subunit alpha, mitochondrial [OS=Mus musculus]	12	7
Q60931	Voltage-dependent anion-selective channel protein 3 [OS=Mus musculus]	12	3
Q9DC71	28S ribosomal protein S15, mitochondrial [OS=Mus musculus]	11	3
Q9CQQ7	ATP synthase F(0) complex subunit B1, mitochondrial [OS=Mus musculus]	11	3
Q9D3D9	ATP synthase subunit delta, mitochondrial [OS=Mus musculus]	11	2
Q9D0M3	Cytochrome c1, heme protein, mitochondrial [OS=Mus musculus]	11	2
Q8BGX2	Mitochondrial import inner membrane translocase subunit Tim29 [OS=Mus musculus]	11	2
Q9CPR5	39S ribosomal protein L15, mitochondrial [OS=Mus musculus]	10	2
P56480	ATP synthase subunit beta, mitochondrial [OS=Mus musculus]	10	3
O35658	Complement component 1 Q subcomponent-binding protein, mitochondrial [OS=Mus musculus]	10	2
Q8CAQ8	MICOS complex subunit Mic60 [OS=Mus musculus]	10	6
Q3V3R1	Monofunctional C1-tetrahydrofolate synthase, mitochondrial [OS=Mus musculus]	10	8
Q9DCN2	NADH-cytochrome b5 reductase 3 [OS=Mus musculus]	10	3
Q9D1B9	39S ribosomal protein L28, mitochondrial [OS=Mus musculus]	9	2
Q9CZU6	citrate synthase, mitochondrial [OS=Mus musculus]	9	3
Q91WD5	NADH dehydrogenase [ubiquinone] iron-sulfur protein 2, mitochondrial [OS=Mus musculus]	9	3
Q8BH04	Phosphoenolpyruvate carboxykinase [GTP], mitochondrial [OS=Mus musculus]	9	4
Q9D051	Pyruvate dehydrogenase E1 component subunit beta, mitochondrial [OS=Mus musculus]	9	2
Q921S7	39S ribosomal protein L37, mitochondrial [OS=Mus musculus]	8	2

Q6PB66	Leucine-rich PPR motif-containing protein, mitochondrial [OS=Mus musculus]	8	12
Q8CGK3	Lon protease homolog, mitochondrial [OS=Mus musculus]	8	6
Q78IK4	MICOS complex subunit MIC27 [OS=Mus musculus]	8	2
Q8K009	Mitochondrial 10-formyltetrahydrofolate dehydrogenase [OS=Mus musculus]	8	5
Q9WUM5	Succinate--CoA ligase [ADP/GDP-forming] subunit alpha, mitochondrial [OS=Mus musculus]	8	2
Q80XN0	D-beta-hydroxybutyrate dehydrogenase, mitochondrial [OS=Mus musculus]	7	2
Q9D6M3	Mitochondrial glutamate carrier 1 [OS=Mus musculus]	7	2
Q99KI0	Aconitate hydratase, mitochondrial [OS=Mus musculus]	6	3
Q9ESW4	Acylglycerol kinase, mitochondrial [OS=Mus musculus]	6	2
Q9Z0X1	Apoptosis-inducing factor 1, mitochondrial [OS=Mus musculus]	6	3
P45952	medium-chain specific acyl-CoA dehydrogenase, mitochondrial [OS=Mus musculus]	6	2
Q62167	ATP-dependent RNA helicase DDX3X [OS=Mus musculus]	5	3
D3Z7P3	Glutaminase kidney isoform, mitochondrial [OS=Mus musculus]	5	2
Q8K411	Presequence protease, mitochondrial [OS=Mus musculus]	5	5
Q9JHS4	ATP-dependent Clp protease ATP-binding subunit clpX-like, mitochondrial [OS=Mus musculus]	4	2
Q8BMF4	Dihydrolipoyllysine-residue acetyltransferase component of pyruvate dehydrogenase complex	4	2
Q60597	Isoform 3 of 2-oxoglutarate dehydrogenase, mitochondrial [OS=Mus musculus]	4	3
O08715	Isoform 4 of A-kinase anchor protein 1, mitochondrial [OS=Mus musculus]	4	2
Q91ZA3	Propionyl-CoA carboxylase alpha chain, mitochondrial [OS=Mus musculus]	4	2
Q91V92	ATP-citrate synthase [OS=Mus musculus]	3	3
P52825	Carnitine O-palmitoyltransferase 2, mitochondrial [OS=Mus musculus]	3	2
Q8BKF1	DNA-directed RNA polymerase, mitochondrial [OS=Mus musculus]	3	2
Q61941	NAD(P) transhydrogenase, mitochondrial [OS=Mus musculus]	3	3
Q05920	pyruvate carboxylase, mitochondrial [OS=Mus musculus]	2	2

Table 15. A Complete List of Proteins Identified Following Co-immunoprecipitation of Overexpressed Human CLU. Proteins are listed with accompanying UniPROT identification numbers as well as the total percent coverage and number of unique peptides identified for each protein. List is organized by percent coverage (highest at top) and is divided into two groups: >10% coverage (yellow) and <10% coverage (blue).

2.2.2. Bioinformatic Analysis of Identified Proteins.

In order to identify possible enriched mitochondrial processes/pathways in the list of possible interacting proteins, bioinformatics analysis was performed using the STRING Pathway Analysis Software. STRING is a database containing experimental and curated protein-protein interaction data from over 9 million proteins derived from 2000+ organisms (Szklarczyk et al., 2015). Parameters for generation of the protein interaction network were restricted to include only those interactions verified by direct experimental evidence or textmining. The minimum required interaction score was set to medium confidence and proteins that were not connected to the protein interaction network were removed from the group. The resulting protein interaction network indicates the enrichment (over 10 proteins) of 4 mitochondrial processes (Figure 2.2.2.1): **(1) TCA Cycle** (red circles): Cs (Q9CZU6), Aco2 (Q99KI0), Idh2 (P54071), Pdha1 (P35486), Pck2 (Q8BH04), Pdhb (Q9D051), Dlat (Q8BMF4), Sdha (Q8K2B3), Suclg1 (Q9WUM5), Sucla2 (Q9Z2I9), Suclg2 (Q9Z2I8), Acly (Q91V92), Pcx (Q05920), and Ogdh (Q60597) **(2) Oxidative Phosphorylation** (green circles): Atp5f1 (Q9CQQ7), Atp5a1 (Q03265), Atp5b (P56480), Atp5h (Q9DCX2), Atp5d (Q9D3D9), Atp5c1 (Q91VR2), Atp5o (Q9DB20), Ndufv2 (Q9D6J6), Ndufs2 (Q91WD5), Ndufs7 (Q9DC70), Ndufs1 (Q91VD9), Uqcrc2 (Q9DB77) and Cyc1 (Q9D0M3) **(3) Mitochondrial Transport** (blue circles): Chchd3 (Q9CRB9), Chchd6 (Q91VN4), Apool (Q78IK4), Immt (Q8CAQ8), Timm 44 (O35857), Tomm20 (Q9DCC8), Tomm70a (Q9CZW5), Tim23 (Q9WTQ8), Vdac1 (Q60932), Vdac 2 (Q60930), and Vdac 3 (Q60931) and **(4) Mitochondrial Ribosomes** (purple circles): Mrps15 (Q9DC71), Mrps2 (Q924T2), Mrps21 (P58059), Mrps23 (Q8VE22), Mrps27 (Q8BK72), Mrps7 (Q80X85), Mrpl11 (Q9CQF0), Mrpl12 (Q9DB15), Mrpl14 (Q9D1I6), Mrpl15 (Q9CPR5), Mrpl19 (Q9D338), Mrpl2 (Q9D773), Mrpl24 (Q9CQ06), Mrpl28 (Q9D1B9), Mrpl37 (Q921S7), Mrpl41 (Q9CQN7), Mrpl47 (Q8K2Y7), and

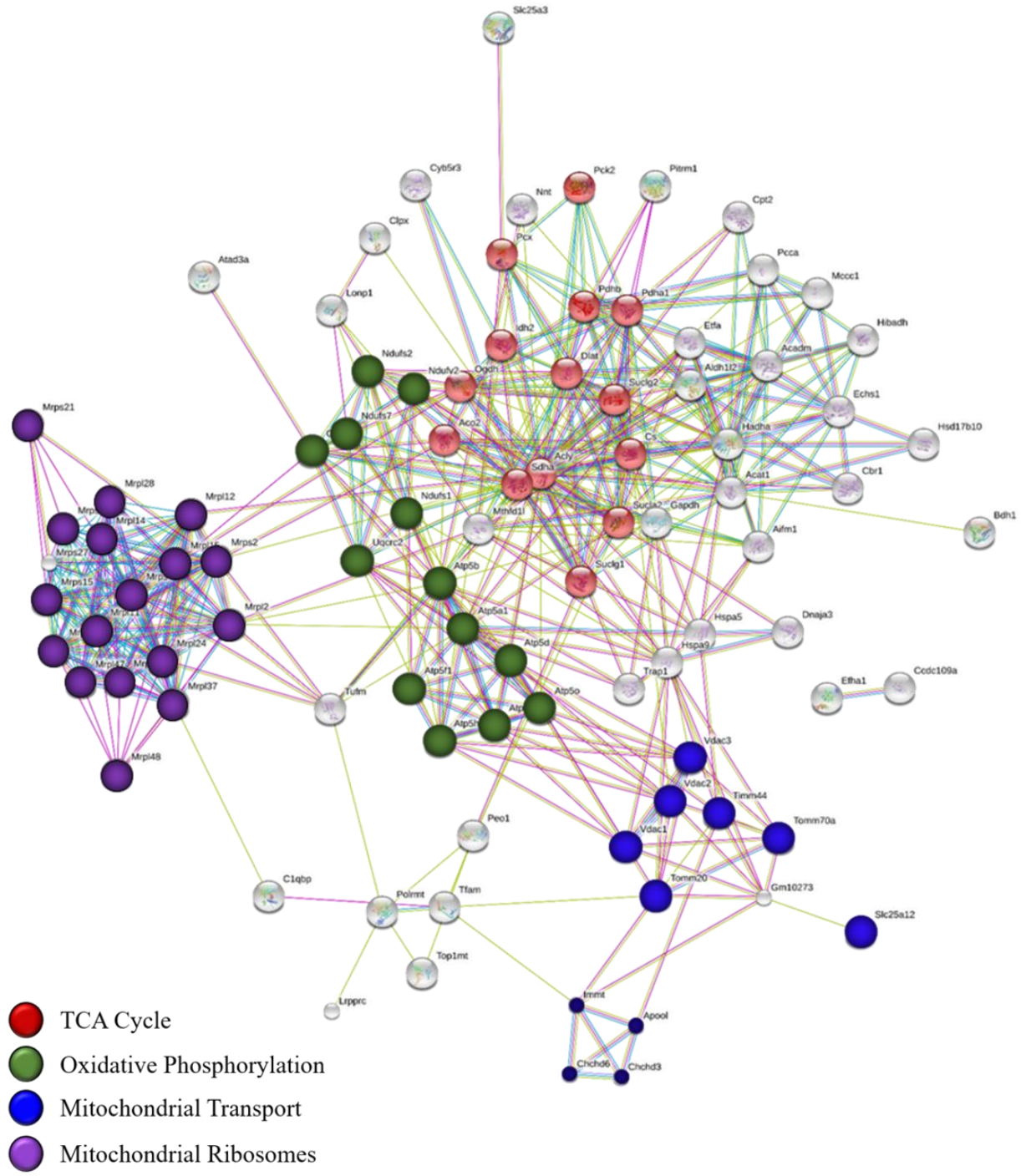

Figure 2.2.2.1. Protein Interaction Network of Identified Mitochondrial Proteins. 103 identified mitochondrial proteins were analyzed for known protein-protein interactions using STRING Pathway Analysis. A protein interaction network was generated using medium confidence for protein interactions and clusters of proteins involved in specific mitochondrial processes were identified and highlighted as indicated.

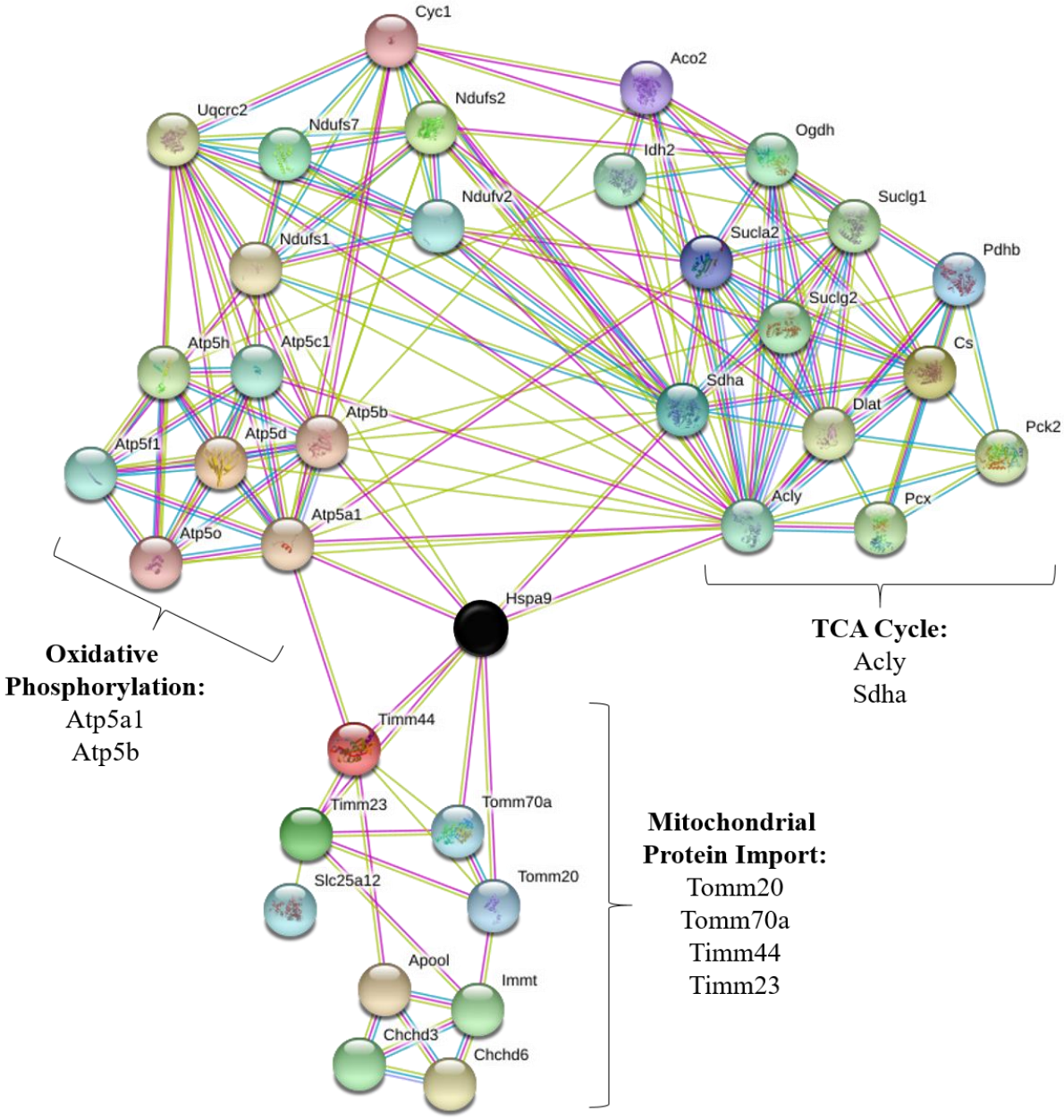

Figure 2.2.2.2. Hspa9 is a Central Interacting Protein that Connects Mitochondrial Import and Energy Production Pathways. Analysis of pathway enriched mitochondrial proteins using STRING Pathway Analysis. A protein interaction network was generated using medium confidence for protein interactions and clusters of proteins involved in specific mitochondrial processes were identified and highlighted as indicated. Bioinformatics indicates that Hspa9 (Grp75, black dot) connects all three pathways and is thus a candidate for a direct CLU_45 kDa protein interacting partner.

Mrpl48 (Q8JZS9). These data indicate that mitochondrial CLU, in some way, interacts with energy metabolism and gene expression pathways in the mitochondrial matrix. In addition, the interaction of mitochondrial CLU with components of the Tom and Tim complexes may provide insight into

the unknown matrix-targeted import pathway of CLU_45 kDa. However, as it is not feasible for CLU_45 kDa to independently interact with over 100 mitochondrial proteins, enriched mitochondrial protein groups were individually analyzed to determine possible proteins that could mediate the interaction between CLU_45 kDa and the identified mitochondrial pathways. These analyses reveal that the mitochondrial chaperone protein Hspa9 (Grp75), one of the most abundantly identified proteins (46% coverage, 26 unique peptides), may be a central mediator of multiple CLU protein interactions. Specifically, Grp75 (Figure 2.2.2.2., black circle) interacts with key mediators of Mitochondrial Transport (Tomm20, Tomm70a, Timm44, Timm23), components of mitochondrial ATP synthase (Atp5a1 and Atp5b), and TCA cycle-associated proteins Acly and Sdha (Figure 2.2.2.2.). These data suggest that CLU_45 kDa may interact with mitochondrial energy metabolism pathways via direct interaction with the mitochondrial matrix protein, Grp75 and thus provide rationale for further investigation of a CLU_45 kDa-Grp75 protein interaction in rodent brain.

In addition to Grp75, several components of the MICOS complex, a complex of proteins that regulate the stability of the cristae and, in coordination with the SAM complex, form the mitochondrial intermembrane space bridging (MIB) complex, were also identified. Specifically, MICOS 19 (27% coverage, 9 unique peptides) and MICOS 60 (10 coverage, 6 unique peptides), which have been identified as the “most important subunits of the MIB complex” were identified. Analysis of protein-protein interactions indicates that Immt (MICOS 60) interacts with components of mitochondrial protein import machinery (Tomm20 and Timm23) as well as two subunits of the mitochondrial ATP synthase (Atp5c1 and Atp5a1) and thus highlights MICOS 60 (Immt) as a possible direct CLU_45 kDa protein interacting partner (Figure 2.2.2.3.).

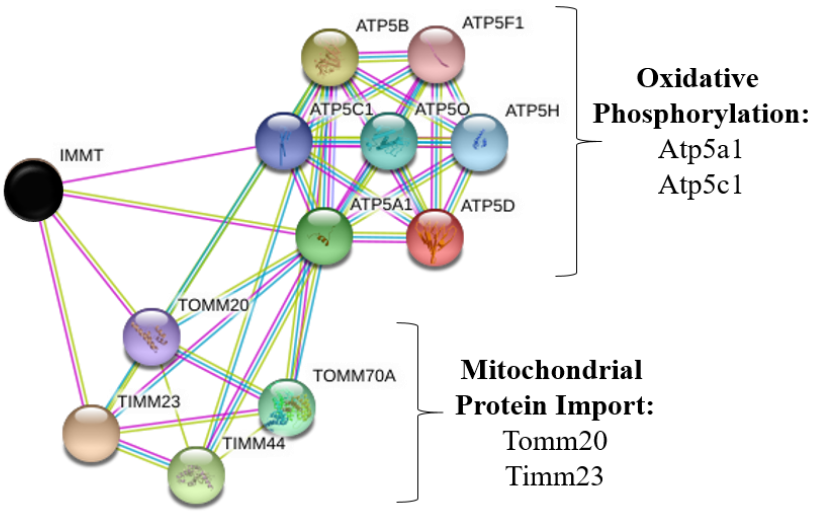

Figure 2.2.2.3. Immt Connects Mitochondrial Import and Energy Production Pathways. Analysis of pathway enriched mitochondrial proteins using STRING Pathway Analysis. A protein interaction network was generated using medium confidence for protein interactions and clusters of proteins involved in specific mitochondrial processes were identified and highlighted as indicated. Bioinformatics indicates that Immt (MICOS 60, black dot) interacts with both mitochondrial import proteins and components of the mitochondrial ATP Synthase

2.2.3. Secondary Confirmation of Selected Interacting Partners

It is well-established that overexpression of proteins *in vitro* may result in artificial protein-protein interactions. Therefore, to ensure the identified proteins are in fact CLU interacting partners, secondary confirmation was performed on select proteins using crude brain mitochondria isolated from adult mice under physiological conditions. Based on bioinformatics analysis, Grp75 and MICOS 60 were selected for secondary confirmation. Crude brain mitochondria were isolated and subjected to co-immunoprecipitation using antibodies against MICOS 60, and Grp75, and CLU followed by immunoblot analysis for CLU or Grp75. The data indicate an interaction between CLU_45 kDa and MICOS 60 *in vivo* (Figure 2.2.3.1.). Interestingly, an interaction between CLU_39 kDa and MICOS 60 was also detected suggesting that both mitochondrial and mature CLU interact with the MICOS complex. In contrast, immunoprecipitation with a Grp75 antibody reveals no interaction between CLU_45 kDa and Grp75 (data not shown). The lack of *in vivo* interaction between CLU_45 kDa and Grp75 was confirmed by performing the reverse co-immunoprecipitation using goat anti-CLU M-18 (Figure 2.2.3.3.). As expected, Grp75 immunoreactivity was not detected when CLU was immunoprecipitated from crude brain

Figure 2.2.3.1. MICOS 60 Interacts with CLU Protein Isoforms *in vivo*. Crude mitochondria were isolated from freshly harvested cortical tissues using differential centrifugation. Lysates were precleared for 1 hr and 500 µg crude mitochondrial lysate was incubated with 2 µg rabbit anti-Immt or non-specific rabbit IgG (IgG) for 4 hrs at 4°C with continual rotation. Antibody-antigen complexes were pulled from solution using 30 µL pre-washed Protein G dynabeads for 1 hr at 4 °C Beads were washed 5 times with cold Co-IP Buffer and samples were eluted using reducing denaturing conditions. 30 µL eluate was resolved via SDS-PAGE and immunoblots were probed for CLU immunoreactivity using goat anti-CLU M-18 (1:1000) overnight at 4°C. Blots were washed and probed for 1 hr using species specific HRP-conjugated secondary antibodies (1:5000). Following acquisition, blots were stained with TMB to confirm molecular weights of identified CLU-immunoreactive bands.

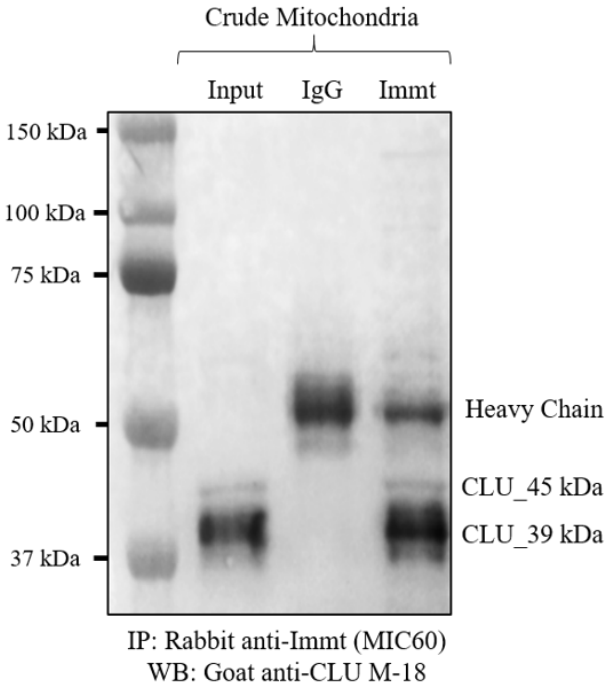

mitochondria. However, co-immunoprecipitation with MICOS 60 does result in the detection of Grp75 immunoreactivity indicating that Grp75, while not interacting with CLU_45 kDa, does interact with the MICOS complex in rodent brain (Figure 2.2.3.2.). While were unable to detect an interaction between CLU_45 kDa and Grp75 *in vivo,* the fact that MICOS 60 interacts with both Grp75 and CLU_45 kDa under physiological conditions solidifies MICOS 60 as a novel mitochondrial CLU interacting partner and indicates that the proteins identified as possible CLU interacting partners are likely not due to the generation of false positives.

In addition to confirming an interaction between CLU_45 kDa and MICOS 60, we also chose to confirm the possible interaction between mitochondrial CLU and key components of the mitochondrial protein import machinery. As the CLU amino acid sequence contains no canonical mitochondria targeting pre-sequence, Tomm70, rather than Tomm20, was selected for secondary

confirmation of protein interaction *in vivo*. Co-immunoprecipitation was performed using Tomm70 or MICOS 60 (positive control for CLU_45 kDa interaction) and eluates were probed

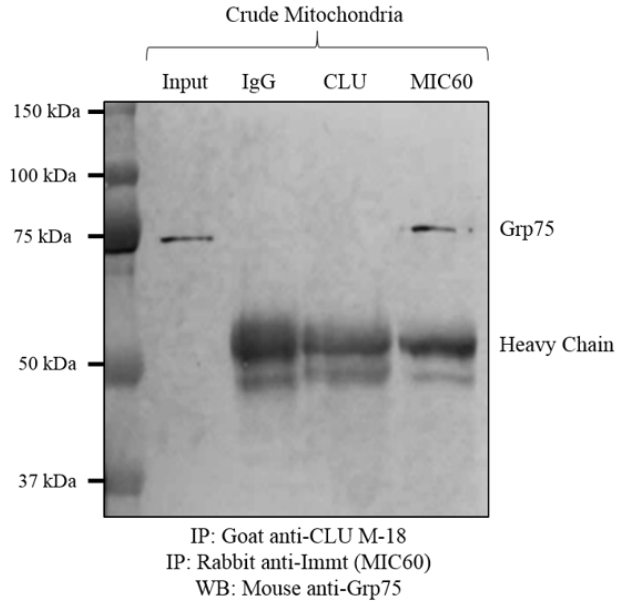

Figure 2.2.3.2. MICOS 60, but not CLU Interacts with Grp75 *in vivo*. Crude mitochondria were isolated from freshly harvested cortical tissues using differential centrifugation. Lysates were precleared for 1 hr and 500 µg crude mitochondrial lysate was incubated with 2 µg mouse anti-Grp75 (Left panel) or 2 µg rabbit anti-Immt or goat anti-CLU (right panel) as well as the corresponding species-specific immunoglobulin (IgG) for 2 hrs at 4°C with continual rotation. Antibody-antigen complexes were pulled from solution using 30 µL pre-washed Protein G dynabeads for 1 hr at 4 °C Beads were washed 5 times with cold Co-IP Buffer and samples were eluted using reducing denaturing conditions. 30 µL eluate was resolved via SDS-PAGE and immunoblots were probed for CLU immunoreactivity using rabbit anti-CLU H-330 (1:1000) overnight at 4°C (left panel) or mouse anti-Grp75 (1:5000) for 2 hr at RT (right panel). Blots were washed and probed for 1 hr using species specific HRP-conjugated secondary antibodies (1:5000). Following acquisition, blots were stained with TMB to confirm molecular weights of identified CLU-immunoreactive bands.

for CLU immunoreactivity. The data indicate similar CLU immunoreactivity profiles between samples immunoprecipitated with MICOS 60 and Tomm70 indicating that CLU_45 kDa interacts with Tomm70 in rodent brain mitochondria (Figure 2.2.3.3.)

2.3. Assessment of Mitochondrial Respiratory Function in mCLU-deficient Mice

As CLU_45 kDa was found to be localized in the mitochondrial matrix and bioinformatics analyses indicate an interaction between CLU and proteins involved in ATP Synthesis and Oxidative Phosphorylation, we next examined the impact of CLU deficiency on brain

Figure 2.2.3.3. Tomm70 Interacts with CLU Protein Isoforms *in vivo*. Crude mitochondria were isolated from freshly harvested cortical tissues using differential centrifugation. Lysates were precleared for 1 hr and 500 µg crude mitochondrial lysate was incubated with 2 µg rabbit anti-Tom70 or 2 µg rabbit anti-Immt as well as the corresponding species-specific immunoglobulin (IgG) for 4 hrs at 4°C with continual rotation. Antibody-antigen complexes were pulled from solution using 30 µL pre-washed Protein G dynabeads for 1 hr at 4 °C Beads were washed 5 times with cold Co-IP Buffer and samples were eluted using reducing denaturing conditions. 30 µL eluate was resolved via SDS-PAGE and immunoblots were probed for CLU immunoreactivity using goat anti-CLU M-18 (1:1000) overnight at 4°C. Blots were washed and probed for 1 hr using species specific HRP-conjugated secondary antibodies (1:5000). Following acquisition, blots were stained with TMB to confirm molecular weights of identified CLU-immunoreactive bands.

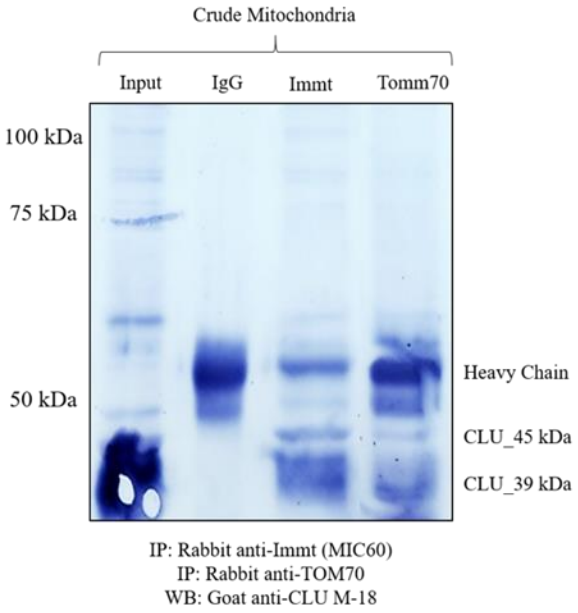

mitochondrial respiration using High Resolution Respirometry (OROBOROS Oxygraph 2K). As a model of CLU_45 kDa deficiency is not currently available and Exon 2-containing mRNA is most predominant in brain tissue, the previously characterized mCLU-KO mouse model was utilized in these experiments. Crude intact mitochondria were isolated from age/sex-matched WT and mCLU-KO mice by differential centrifugation. Protein concentration was determined and 300 µg crude mitochondria was analyzed for mitochondrial respiration. As this study is the first to examine mitochondrial respirometry capacity in mCLU-KO mice, the overall process of oxidative phosphorylation rather than the activity of individual respiratory complexes was analyzed. Baseline respiration was established following the injection of mitochondria and pre-determined concentrations of substrates/compounds/inhibitors were added in the following order at the indicated concentrations (Table 12): pyruvate (Pyr, Complex I), malate (Mal, Complex I), succinate (Succ, Complex II), ADP (Complex V), Oligomycin (Oligo, ATP synthase inhibitor), FCCP (Uncoupler), Rotenone (Rot, Complex I inhibitor), and Antimycin A (AA, Complex III inhibitor). The data indicate an overall decrease in oxidative phosphorylation in 6-month-old

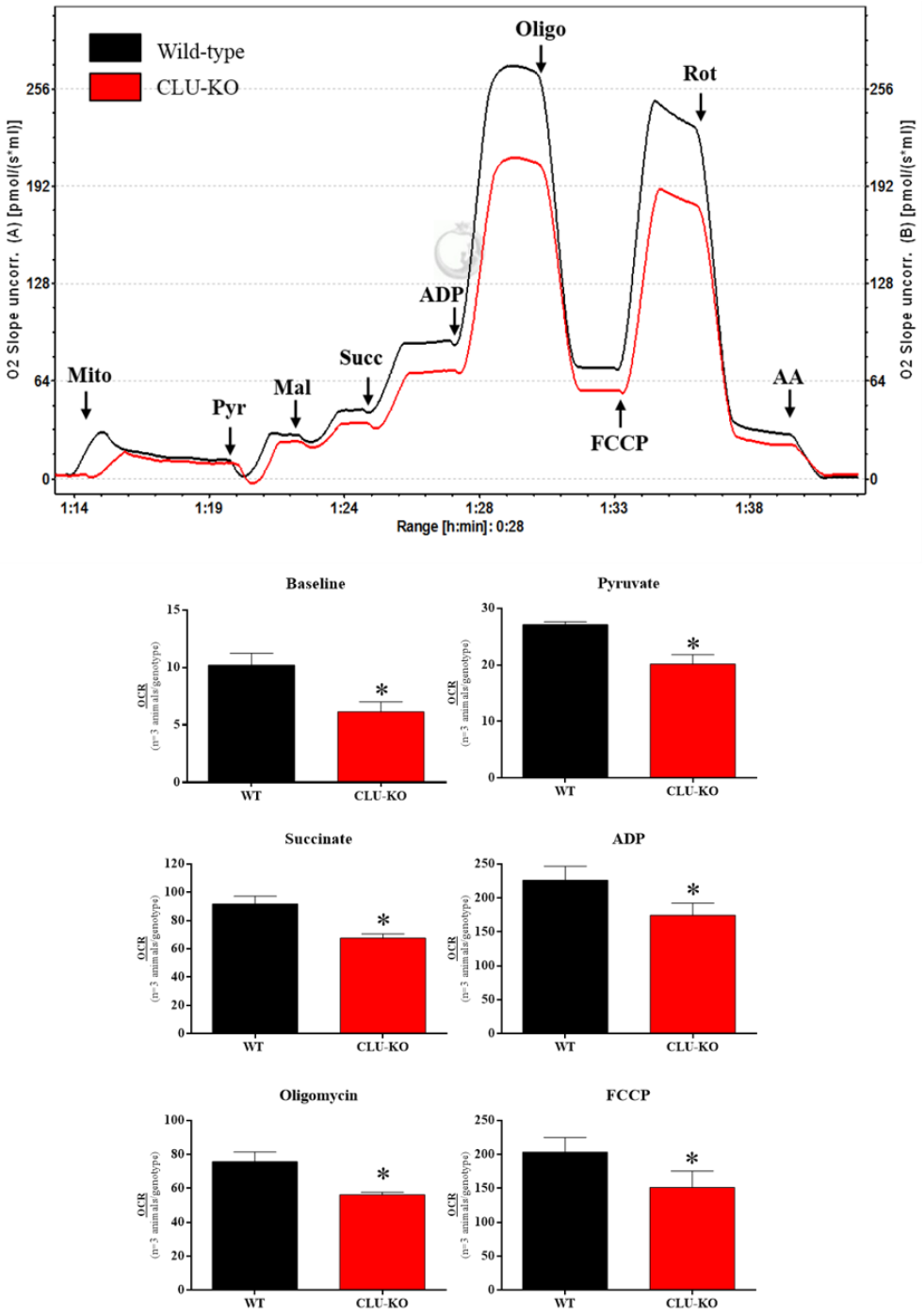

Figure 2.3.1. Assessment of Brain Mitochondrial Respiratory Capacity in Female 6-month-old mCLU-KO Mice. Brain mitochondrial respiration was analyzed using high resolution respirometry (OROBOROS, Oxygraph 2K) in 6-month-old female WT (black) and mCLU-KO (red) mice (n=3-4 animals/group). 300 µg crude brain mitochondria from 1 WT and 1 mCLU-KO mouse were analyzed simultaneously using 10 mM Pyruvate (Pyr), 2 mM Malate (Mal), 5 mM Succinate (Succ), 2 mM ADP, 2µM Oligomycin (Oligo), 125 nM FCCP, 2 µM Rotenone (Rot), and 2 µM Antimycin A. Compounds were injected simultaneously into each chamber and incubated for approximately 1-2 min to allow for the generation of stable signal. Following the completion of each run, the average OCR was generated by selecting 10-20 data point following the injection of each compound. Individual mean comparisons were made using the average OCR following each injection from 3-4 animals. Data were analyzed using a non-parametric student's T-test: * $p<0.05$ when compared to WT animals.

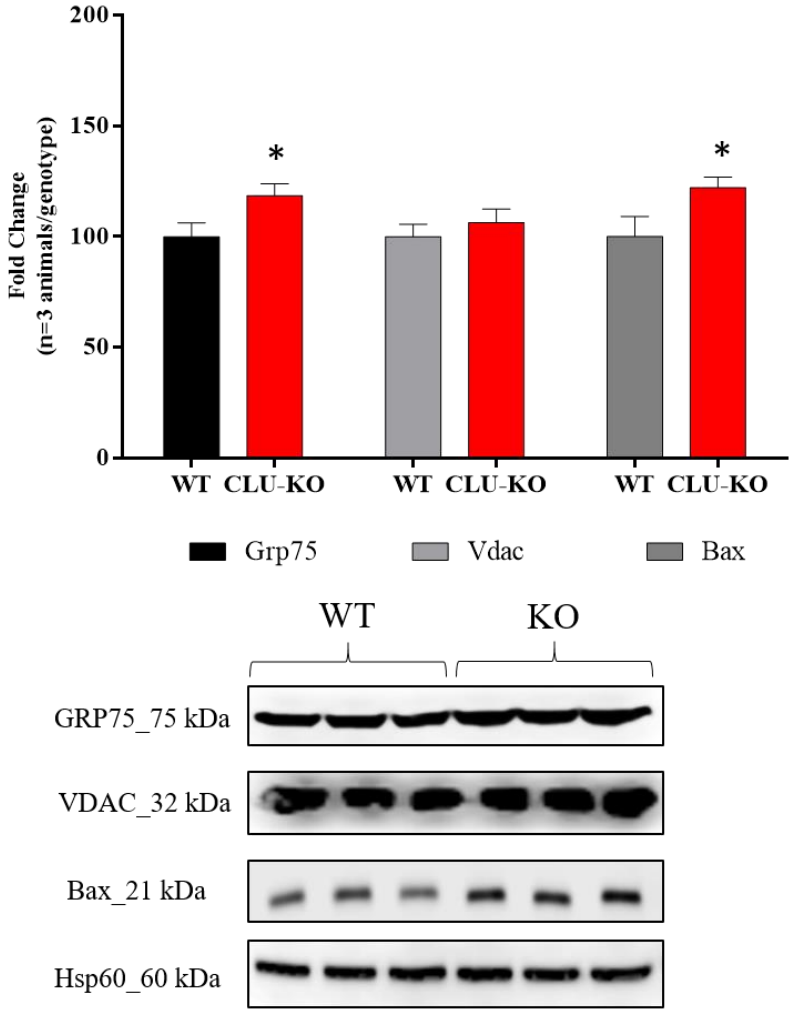

Figure 2.3.2. Assessment of Mitochondrial Protein Levels in Crude Mitochondria Isolated from WT and mCLU-KO Mice. 30 µg crude mitochondrial lysate was resolved via SDS-PAGE. Immunoblots were probed with mouse anti-Grp75 (1:8000, 2 hr RT), rabbit anti-VDAC (1:2000, overnight 4 °C), rabbit anti-Bax (1:2500 overnight 4°C) or rabbit anti-Hsp60 (1:8000 2 hr RT) followed by incubation for 1 hr at RT with species-specific secondary antibodies (1:5000).

female mCLU-deficient animals when compared to WT controls. Specifically, mCLU-KO mice exhibit significantly decreased baseline respiration (WT = 10.19, mCLU-KO = 6.14, 39.75% decrease), as well as significantly lower average OCR values following administration of the complex I substrate Pyruvate (WT = 27.11, mCLU-KO = 20.15, 25.68% decrease), the complex II substrate Succinate (WT = 91.72, mCLU-KO = 67.64, 26.26% decrease), the complex V substrate ADP (WT = 226.24, mCLU-KO = 174.47, 22.89% decrease), the ATP synthase inhibitor Oligomycin A (WT = 75.71, mCLU-KO = 56.24, 25.72% decrease) and the mitochondrial

uncoupler FCCP (WT = 203.19, mCLU-KO = 151.17, 25.61% decrease). These data indicate significantly reduced respiratory capacity in female brain mitochondria and confirm that brain CLU is, in part, associated with or involved in brain bioenergetics in adult female brain.

While protein concentration was determined just prior to respirometry, it is possible that the observed decrease in OCR between WT and mCLU-KO mice could be attributed to a difference in the total mitochondrial mass within each crude mitochondrial sample. Therefore, the expression levels of mitochondrial proteins were evaluated to confirm equal loading of mitochondria in each chamber. Specifically, VDAC and GRP75 protein expression levels were examined in aliquots of the same samples used for high resolution respirometry. In addition, as mCLU deficiency is known to result in elevated mitochondrial Bax expression (Trougakos et al., 2009; H. Zhang et al., 2005), Bax protein levels were utilized as a positive control. Hsp60 which is present in the mitochondria and known to be unaffected by CLU deficiency (Chaiwatanasirikul & Sala, 2011) was utilized as a loading control in this experiment. Despite an approximate 25% decrease in mitochondrial respirometry, the data indicate a significant increase in the expression of both Grp75 and Bax in mCLU-KO mitochondria with no change occurring in the expression of VDAC (Figure 2.3.2.). In addition, the activity of glutamate dehydrogenase, an enzyme that converts glutamate to α-ketoglutarate in the mitochondrial matrix, was not significantly altered between WT and mCLU-KO mitochondrial samples (Figure 2.3.3.) Collectively, these data

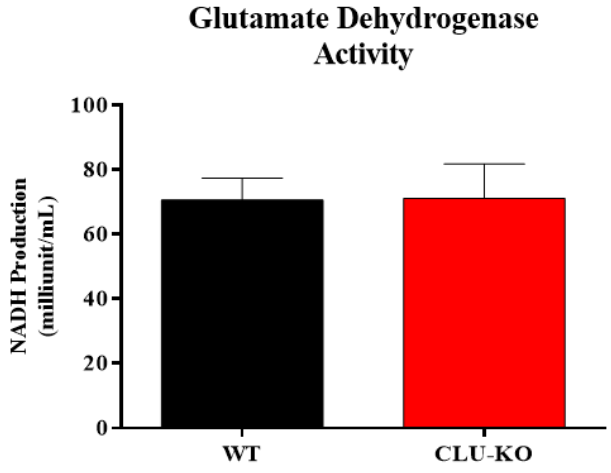

Figure 2.3.3. Assessment of GDH Activity in Crude Mitochondria Isolated from WT and mCLU-KO Mice. 10 µg crude mitochondrial lysate derived from WT and mCLU-KO mice was analyzed for glutamate dehydrogenase activity (NADH Production) as indicated in the corresponding methods section (n=3 animals/genotype)

indicate that the observed decline in brain mitochondrial respiration is in fact due to decreased respiratory capacity and not a decrease in total mitochondrial mass.

2.4. Interim Discussion and Working Hypothesis

In this chapter we have identified a novel mitochondria-localized CLU protein isoform (CLU_45 kDa, Figure 2.1.1) and determined the submitochondrial localization of this isoform to be the mitochondrial matrix (Figure 2.1.2.). In addition, overexpression and co-immunoprecipitation studies indicate that mitochondrial CLU interacts with some aspect of mitochondrial energy metabolism, gene expression, and/or mitochondrial protein import (Section 2.2) and high resolution respirometry confirms that young female mCLU-deficient mice exhibit significantly reduced brain mitochondrial respiration. These data provide insight into two relatively important questions pertaining to CLU in the mitochondria: How is the CLU_45 kDa protein isoform transported into the mitochondria? and What is the function of mitochondria-localized CLU?

2.4.1. CLU in the Mitochondria: A Possible Protein Import Mechanism.

The protein import pathway for matrix-localized proteins has been relatively well characterized in numerous articles. Briefly, proteins synthesized with a mitochondrial targeting sequence or a mitochondrial pre-sequence are recognized by the translocase of outer membrane (TOM) complex, transported through the outer mitochondrial membrane (OMM), recognized by the translocase of inner membrane 23/presequence translocase-associated motor (TIM23/PAM) complex, and transported into the mitochondrial matrix where mitochondrial chaperone proteins assist in the proper folding of matrix-targeted proteins. However, as the amino acid sequence that comprises CLU does not contain a mitochondrial targeting sequence, the mechanism of protein recognition and import has been somewhat elusive until now. Our studies indicate that CLU_45 kDa interacts with a key component of the TOM complex in normal female rodent brain: Tomm70. Moreover, though not yet confirmed in physiological conditions, preliminary Co-IP studies indicate an interaction between CLU and Tomm20, Timm44, and Timm23. As

Tomm20 and Tomm70 have been shown to preferentially target specific structural domains of mitochondrial targeted proteins this presents two possible protein import pathways for mitochondrial

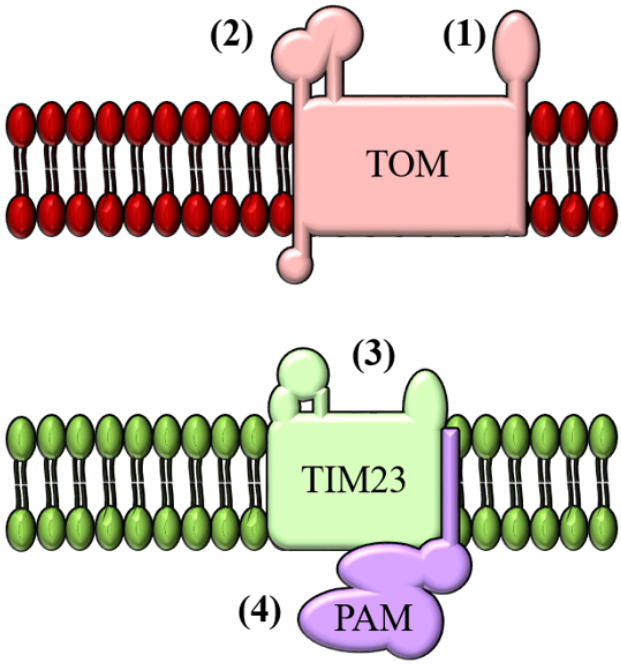

Schematic 17. Representation of Proposed Mechanism of CLU_45 kDa Import. Based on the preliminary and secondary Co-IP data, we hypothesize that Tomm70 recognizes an internal hydrophobic sequence within CLU_45 kDa that signals the import of CLU_45 kDa to the mitochondria **(1)**. Following recognition, CLU_45 kDa is transported through the OMM and passed through the TIM23/PAM complex **(3)**. Once in the matrix, mitochondrial chaperone proteins assist in the proper folding of mitochondrial CLU_45 kDa **(4)**. An alternative mechanism of TOM complex recognition would be Tomm20-mediated recognition of the amphipathic α-helices that comprise approximately 50-60% of the secondary structure of CLU **(2)**.

CLU (Schematic 17). Tomm70 has been shown to preferentially recognize internal hydrophobic import sequences (Wu & Sha, 2006). As CLU is known to contain 2 intrinsically disordered molten globule domains that are exposed to the cytosolic surface and facilitate hydrophobic interactions (Bailey et al., 2001; Dunker et al., 2001), it is possible that Tomm70 recognizes CLU_45 kDa through one or both of these hydrophobic domains. In contrast, Tomm20 has been shown to preferentially recognize positively charged amphipathic α-helices within a protein's secondary structure (Abe et al., 2000; Saitoh et al., 2007). Therefore, a second possible mechanism would be that Tomm20 recognizes one of the 5 α-helices that are predicted to compose 50-60% of the secondary structure of CLU (Bailey et al., 2001; Rohne et al., 2014; Stewart et al., 2007) and, as Tomm20 and Tomm70 are components of the same complex, the Tomm70-CLU_45 kDa interaction detected *in vivo* is, in actuality, a secondary interaction. While not performed in this study, the possibility of a direct interaction between CLU_45 kDa and Tomm20 should be investigated in the near future.

2.4.2. CLU in the Mitochondria: Insights into Protein Function.

In addition to providing insight into the possible import mechanism of mitochondrial CLU, the data presented in this chapter provide insight into a possible function for CLU in the mitochondrial matrix. Co-immunoprecipitation indicates an interaction between CLU and mitochondrial bioenergetics; specifically components of the TCA Cycle and Oxidative Phosphorylation. In addition, high resolution respirometry confirms a functional deficiency in brain mitochondria of mCLU-KO animals. However, one major drawback of these studies is that while a reduction in general mitochondrial respiration is evident, it is not clear if the reduction in respiratory capacity can be attributed to one complex in the respiratory chain or is the result of general mitochondrial decline. Moreover, the mCLU-KO mouse model that was used in this study does not lack the mitochondria-localized CLU isoform indicating that the reduction in mitochondrial energy production is due to a deficiency in mCLU, not mitochondrial CLU. Taken together, these data suggest that both cytosolic mCLU and mitochondria-localized CLU function to protect mitochondrial function through differing mechanisms. First, secondary confirmation of preliminary co-immunoprecipitation data indicates a direct interaction between CLU_45 kDa and at least one key component of the mitochondrial contact site and cristae organizing system, or MICOS, complex: MICOS 60. The MICOS complex is crucial in the formation and maintenance of the cristae on the inner mitochondrial membrane and is thus essential in facilitating oxidative phosphorylation (van der Laan, Horvath, & Pfanner, 2016). Therefore, it is possible that mitochondrial CLU interacts with the MICOS complex to regulate the integrity of the inner mitochondrial membrane. Secondly, mCLU has been shown to sequester cytosolic Bax thereby preventing Bax-induced translocation and apoptosis (Trougakos et al., 2009; H. Zhang et al., 2005). Parallel to these findings, a reduction in cytosolic mCLU has been shown to increase apoptosis by through the release of Bax from the KU70/Bax complex thus resulting in Bax translocation and insertion into the outer mitochondrial membrane (Trougakos et al., 2009). Consistent with previous publications, our data indicate a 22% increase in mitochondrial Bax expression in mice lacking mCLU suggesting that lack of mCLU results in increased Bax translocation and increased mitochondrial

stress. Parallel to these finding, we observe an 18% increase in mitochondrial Grp75 expression in mCLU-KO brain. Previous publications have repeatedly demonstrated that Grp75 overexpression reduces the rate and severity of oxidative stress mediated by glucose deprivation (Y. Liu, Liu, Song, & Zuo, 2005) and H_2O_2 toxicity (E, Liu, Liu, Liu, & Zuo, 2013) and therefore provides some measure of mitochondrial protection. Therefore, it is possible that increased mitochondrial stress triggered by intracellular mCLU deficiency results in a compensatory increase in mitochondrial Grp75. The proposed relationship between mCLU and Grp75 is confirmed by co-immunoprecipitation data indicating a direct interaction between Grp75 and CLU_70 kDa in crude brain mitochondria. While it is unclear how mCLU deficiency results in in vivo alterations in Bax and Grp75 expression, these data do indicate that both mitochondrial CLU (CLU_45 kDa) and cytosolic CLU (CLU_70 kDa and CLU_39 kDa) are associated with aspects of mitochondrial function.

Chapter 3: CLU and Sex Hormones

3.1. The Regulation of mCLU by Estrogens and Androgens in Rodent Brain.

Preliminary data from our lab indicate that CLU mRNA expression is significantly and irreversibly reduced in normally aging female, but not male, rodent brain (Figure 3.1.1.). Specifically, we observed a 47%

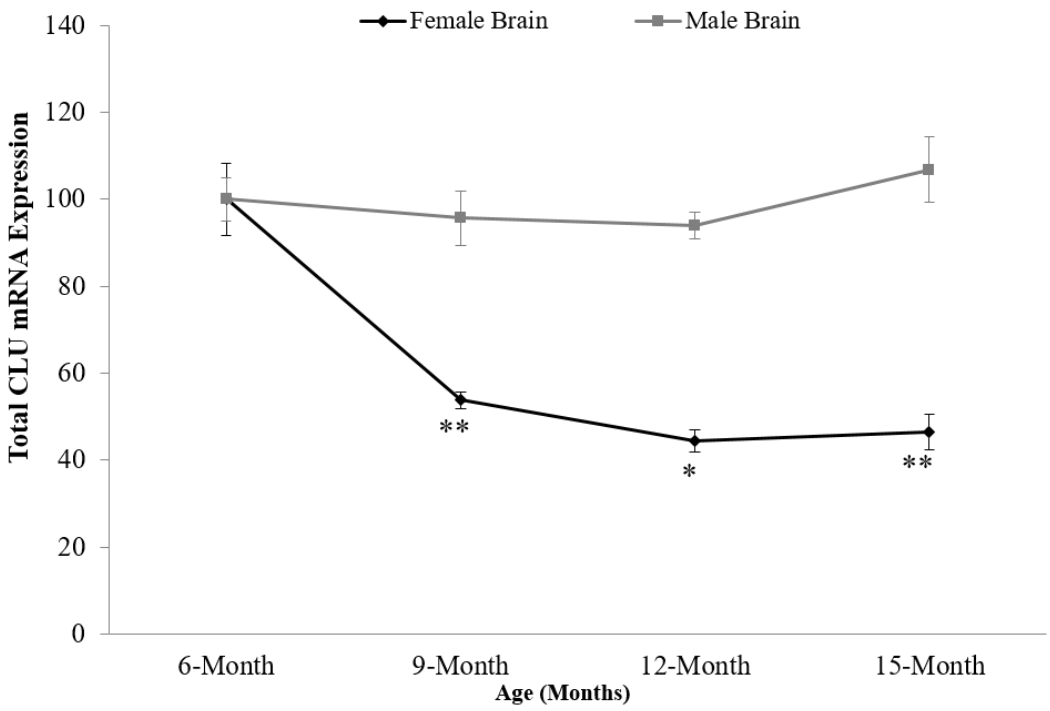

Figure 3.1.1. Analysis of CLU mRNA in Normally Aging Male and Female Mice. CLU mRNA was analyzed in cortical tissue isolated from normally aging male and female mice at ages 6-15 months (n=4 mice/sex/age point). Changes in CLU mRNA were calculated using the ΔΔCt method and analyzed using One-Way ANOVA with Tukey's Post Hoc Analysis. * $p<0.05$, ** $p<0.01$ when compared to 6-month old animals of the same sex.

decrease in CLU mRNA in female brain between the ages of 6 and 9 months whereas CLU mRNA in male brain was altered by only 4%. The observed decrease in CLU mRNA remained consistent from 9 to 12 months (~10% decline) and from 12 to 15 months indicating that CLU mRNA is negatively impacted by early aging in specifically the female brain. One key difference between the aging male and female brain is the alteration in sex hormone patterns with age. For instance, aging negatively impacts male sex hormones in a chronological manner with the average decline in testosterone dropping approximately 2% each year.

In contrast, female sex hormones are known to be significantly and irreversibly depleted during menopausal onset (reproductive aging). Therefore, it is possible that the observed differences in the trajectory of CLU mRNA rodent brain may be due to differences in circulating male and female sex hormones. Therefore, based on this information we hypothesized that CLU protein expression levels are positively regulated by androgens and estrogens in rodent brain.

To test this hypothesis, primary neurons were isolated, cultured for 7 DIV, and treated with increasing concentrations (10 nM – 100 nM) of the female sex hormones 17β-estradiol (E2) and progesterone (P4) or the male sex hormones testosterone and dihydrotestosterone (DHT) for 48 hours. Cells were harvested via whole cell protein extraction and analyzed for CLU immunoreactivity using SDS-PAGE. As this is the first study to explore the possibility of sex-hormone-mediated regulation of a CLU protein isoform in the brain, we chose to focus on the CLU_49 kDa isoform as Exon 2-containing mRNA appears to be predominant in brain tissue. The data indicate a significant increase in the expression of CLU_49 kDa in neurons treated with 100 nM E2 (58% increase), whereas no increase was observed in P4-treated cells (Figure 3.1.2., Upper Panel). While results pertaining to estrogen-mediated regulation of CLU have been mixed, the up-regulation of CLU_49 kDa by E2 treatment is consistent with previous reports which demonstrate an increase in CLU mRNA following E2 treatment in RUCA-1, KLE, and EEC-1 cells (Won, Lee, Yeo, & Park, 2012; Wunsche, Tenniswood, Schneider, & Vollmer, 1998). In contrast, treatment with testosterone and its metabolite DHT resulted in a significant decrease in CLU_49 kDa expression at 10 nM (24-25% decrease) and 100 nM (28% decrease) indicating that androgens, in general, repress mCLU expression in primary neurons (Figure 3.1.2., Lower Panel). While these data do not support our original hypothesis, androgen-mediated suppression of CLU is primary neurons is consistent with previous reports that demonstrate a decrease in CLU mRNA in androgen treated LNCap cells (Waters, Safe, & Gaido, 2001) and an increase in CLU mRNA expression following androgen depletion in human prostate cancer tissue (July et al., 2002). As female brain exhibits the most profound loss of CLU mRNA in our preliminary studies, and E2 was

found to positively regulate CLU_45 kDa protein expression, the remainder of the studies in this chapter will focus on the relationship between CLU_49 kDa and estrogens in the brain.

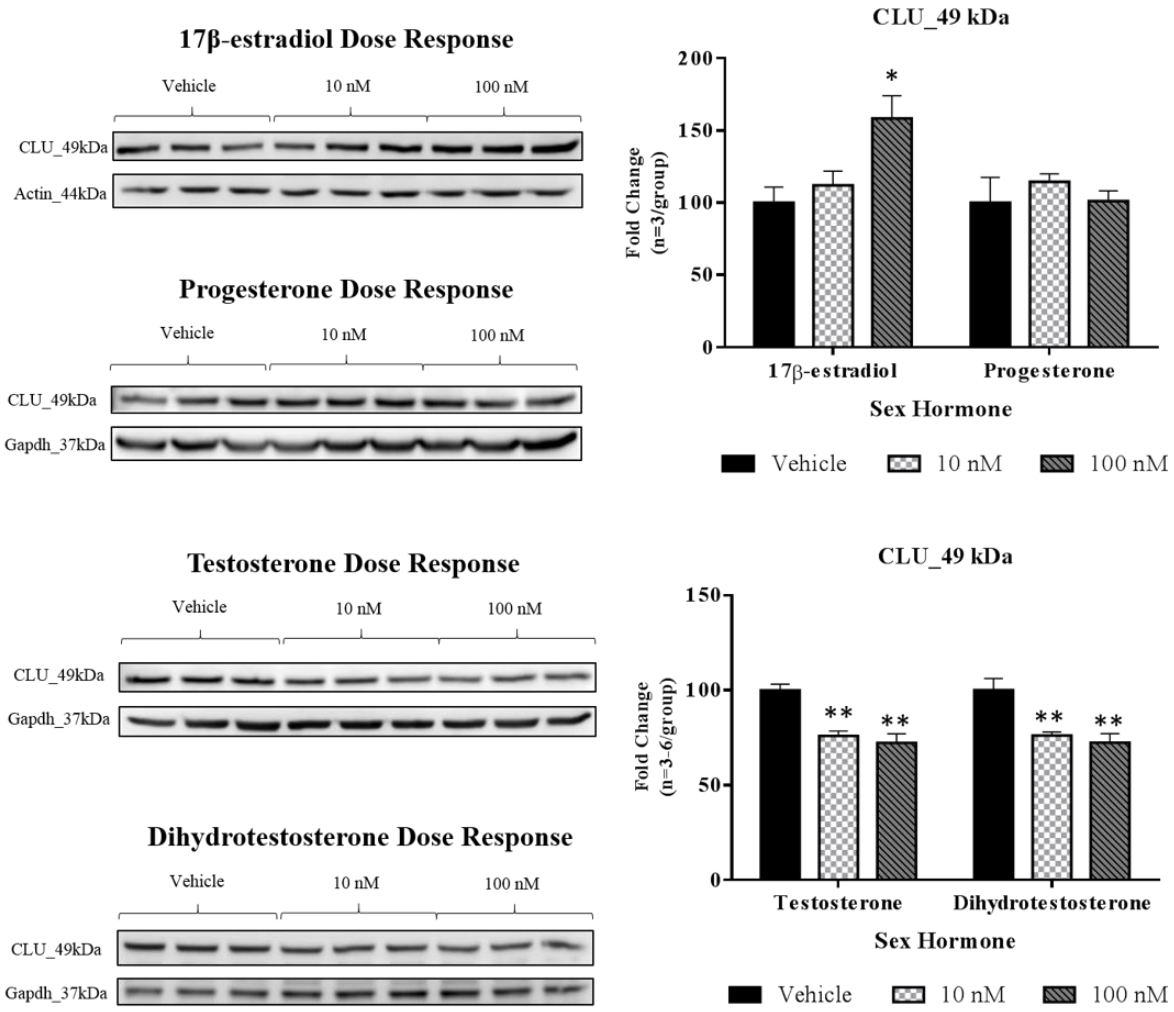

Figure 3.1.2. Regulation of CLU_49 kDa Expression by Estrogen, Progesterone, and Androgens in Primary Neurons. Primary cortical neurons were treated with Vehicle or increasing concentrations of E2 or P4 (upper panel) and Testosterone or DHT (lower panel) as indicated for 48 hrs. Blots were harvested and analyzed for CLU immunoreactivity using rabbit anti-CLU H330 (1:1000) overnight at 4 °C followed by 1 hr incubation with species specific HRP-conjugated secondary antibodies. Densitometry of the CLU_49 kDa band was normalized to the indicated loading control and changes in CLU expression were analyzed using One-Way ANOVA with Holm Sidak's Post Hoc Analysis. * $p<0.05$, ** $p<0.01$ when compared to vehicle-treated group.

3.2. Differential Regulation of mCLU Expression by ERα and ERβ-mediated Signaling.

To determine the mechanism by which estrogens regulate CLU_49 kDa expression, primary neurons were treated with the ER-specific agonists PPT (ERα) or DPN (ERβ) and analyzed for CLU immunoreactivity.

The data indicate a non-significant decrease in CLU_49 kDa expression in PPT-treated cells (13% decrease, p=0.26) while neurons treated with the ERβ agonist DPN exhibited significantly increased CLU_49 kDa expression (28% increase, p=0.0178, Figure 3.2.1.). These data suggest that E2 signaling may

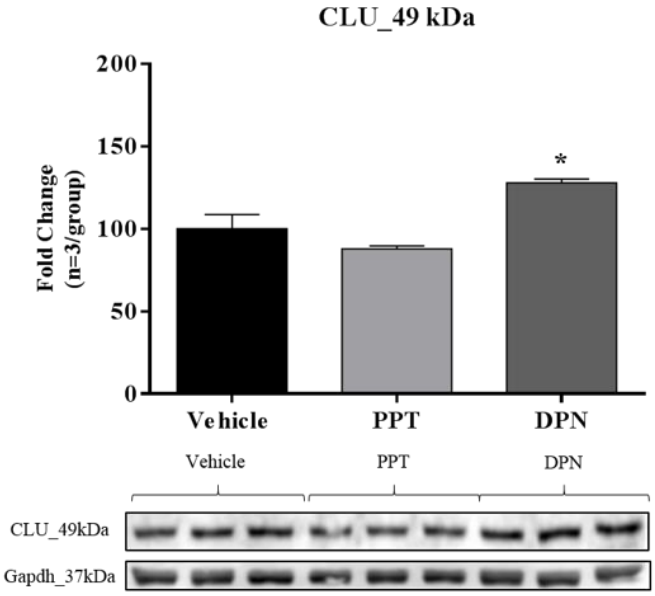

Figure 3.2.1. Differential Regulation of CLU_49 kDa Expression by Estrogen Receptor Agonism in Primary Neurons. Primary cortical neurons were treated with Vehicle, 100 nM PPT (ERα), or 100 nM DPN (ERβ) for 48 hrs. Blots were harvested and analyzed for CLU immunoreactivity using rabbit anti-CLU H330 (1:1000) overnight at 4 °C followed by 1 hr incubation with species specific HRP-conjugated secondary antibodies. Densitometry of the CLU_49 kDa band was normalized to the indicated loading control and changes in CLU expression were analyzed using One-Way ANOVA with Dunnett's Post Hoc Analysis. * $p<0.05$ when compared to vehicle-treated group.

differentially impact mCLU expression through the activation of different ERs with ERα-mediated signaling resulting in negative regulation and ERβ signaling resulting in positive regulation. In addition, as estrogen treatment results in an upregulation of CLU_49 kDa expression, it appears that ERβ-mediated signaling is the predominant regulator of mCLU expression in primary neurons. In support of these data,

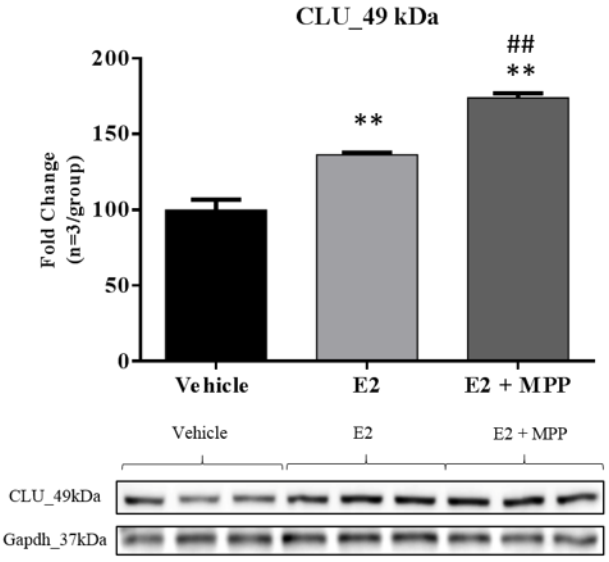

Figure 3.2.2. ERα Inhibition Enhances E2-mediated Upregulation of CLU_49 kDa in Primary Neurons. Primary cortical neurons were treated with Vehicle, and 100 nM E2 ± the ERα inhibitor MPP for 48 hrs. Blots were harvested and analyzed for CLU immunoreactivity using rabbit anti-CLU H330 (1:1000) overnight at 4 °C followed by 1 hr incubation with species specific HRP-conjugated secondary antibodies. Densitometry of the CLU_49 kDa band was normalized to the indicated loading control and changes in CLU expression were analyzed using One-Way ANOVA with Tukey's Post Hoc Analysis. ** $p<0.01$ when compared to vehicle-treated group ## $p<0.01$ when compared to E2-treated group.

pre-treatment of primary neurons with the ERα-specific inhibitor MPP enhances the E2-mediated upregulation of CLU_49 kDa (Figure 3.2.2.) thereby confirming the predominant positive regulation of CLU_49 kDa via ERβ agonism and the proposed negative regulation of CLU_49 kDa via ERα agonism.

To determine if ERβ deficiency impacts CLU_49 kDa *in vivo*, cortical tissues harvested from 10-month-old ERβ-KO rats and WT littermates were analyzed for CLU_49 kDa expression. The data indicate that 10-month-old female ERβ-KO rat cortex expresses significantly lower CLU_49 kDa expression when compared to WT littermates (24% decrease, p=0.0331, Figure 3.2.3.) suggesting that ERβ remains an active and positive regulator of mCLU expression *in vivo*.

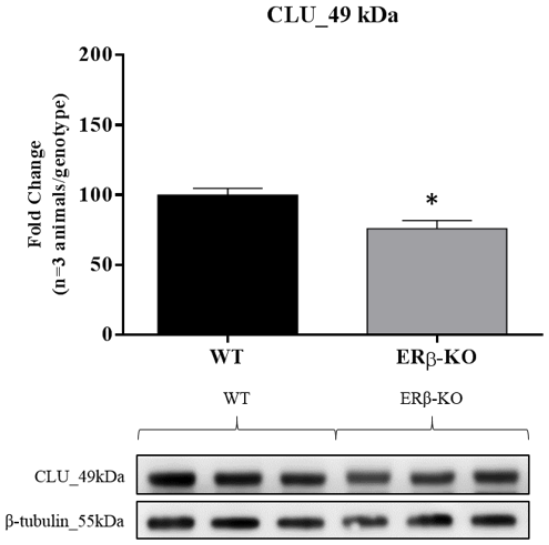

Figure 3.2.3. *In vivo* ERβ Deficiency Negatively Impacts CLU_45 kDa Protein Expression. Cortical tissues isolated from 10-month-old female WT or ERβ-KO rats were harvested and analyzed for CLU immunoreactivity using rabbit anti-CLU H330 (1:1000) overnight at 4 °C followed by 1 hr incubation with species specific HRP-conjugated secondary antibodies. Densitometry of the CLU_49 kDa band was normalized to the indicated loading control and changes in CLU expression were analyzed using Student's T-test. * $p<0.05$ when compared to WT animals (n=3 animals/genotype)

The data presented thus far demonstrate that ERβ positively and significantly up-regulates CLU_49 kDa protein expression in primary neurons. However, at this time, no known estrogen response element has been identified within the CLU promoter. Therefore, *in silico* promoter analysis was performed on the human and rodent CLU promoters using Genomatix MatInspector Software. *In silico* promoter analysis indicates the presence of 2 ESR1 (ERα) binding sites and 1 ESR2 (ERβ) binding sites within the promoter

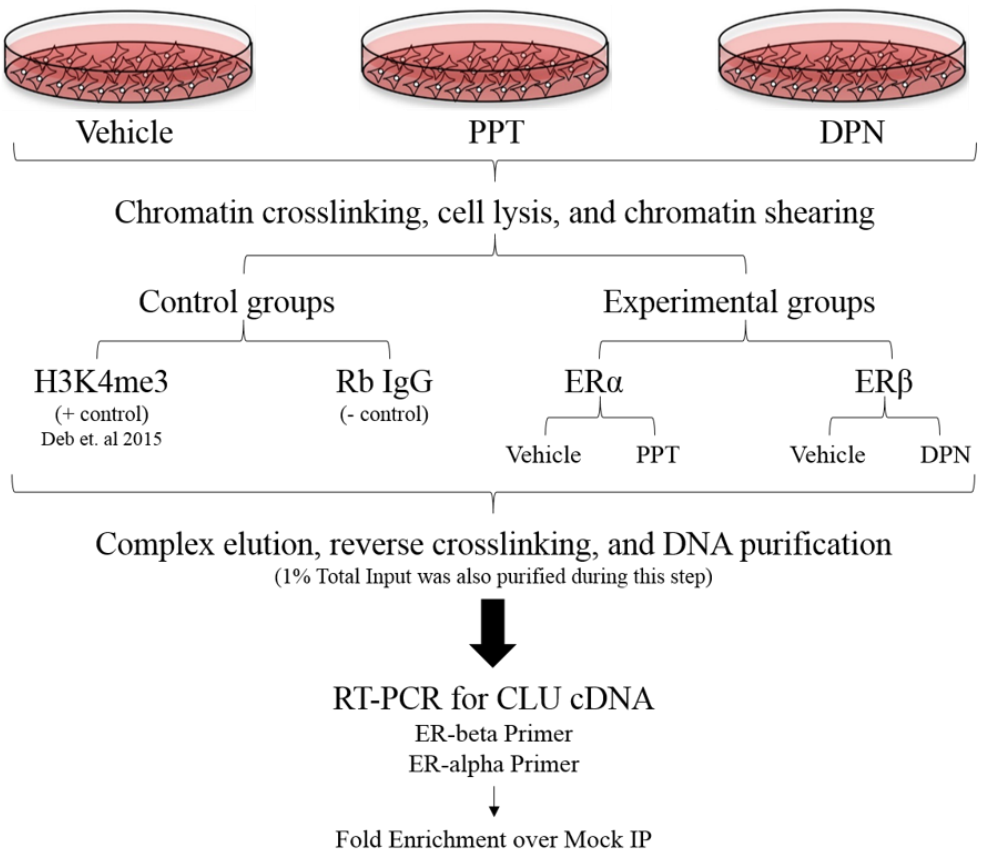

Schematic 18. A Representation of the Experimental Procedure Used to Examine ER-CLU DNA Interactions in SH-SY5Y Cells. SH-SY5y cells were treated with Vehicle, 100 nM PPT or 100 nM DPN for 48 hrs. Cells were crosslinked in formaldehyde, lysed, and chromatin was sheared using sonication to yield chromatin with an average length of 200 bp. Lysates were cleared and equal amounts were subjected to immunoprecipitation with 30 µL protein G dynabeads with 4 µg of the indicated antibodies: rabbit anti-H3K4me3 (positive control), non-specific rabbit IgG (- control/Mock), rabbit anti-estrogen receptor alpha (experimental) or rabbit anti-estrogen receptor beta (experimental). Immunoprecipitated complexes were washed and eluted as indicated in the methods section and the crosslinking process was reversed. cDNA was purified and rt-qPCR was performed using 1 µL of sample/PCR reaction. Fold enrichment over the mock IP was calculated as indicated in the corresponding methods section.

of human and murine CLU suggesting that estrogens regulate CLU_49 kDa expression via direct transcriptional regulation (Table 13). To determine if the CLU promoter does contain an unidentified ERE, ER-CLU DNA interactions were examined in treated and un-treated and SH-SY5Y cells. The SH-SY5Y cell line was chosen as a model based on the following 3 criteria: (1) SH-SY5Y is a human cell line thus rendering the findings in this study applicable to human mCLU, (2) intracellular mCLU is detected in SH-SY5Y cell lysates, and (3) both ERα and ERβ are expressed in this cell line. SH-SY5Y cells were treated for 48 hrs with ER-specific agonists and chromatin immunoprecipitation was performed as indicated in the

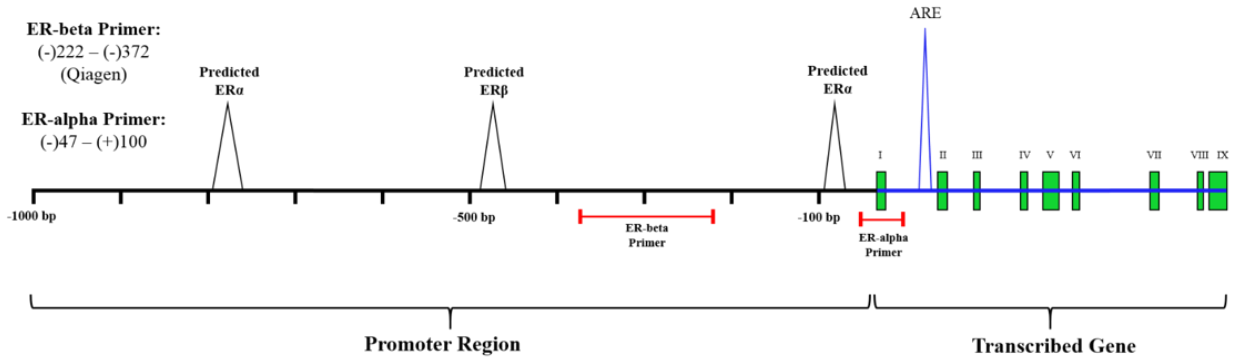

Schematic 19. A Representation of the Predicted CLU EREs and Corresponding Primer Amplification Sites on the Human CLU Promoter. Genomatix MatInspector Software indicates the presence of a proximal and distal ER-alpha ERE (~100 and 800 bp upstream from Exon 1) and 1 ER-beta ERE (~500 bp upstream from Exon 1). Primers used in this study were purchased from Qiagen (ER-beta primer) or generated using IDT (ER-alpha primer) and amplify regions near or directly adjacent to the proposed ERE.

corresponding methods section and/or Schematic 18. Treated and untreated cell lysates were immunoprecipitated using antibodies against ERα or ERβ along with the indicated positive and negative controls and purified cDNA was used for rt-QPCR. To amplify regions adjacent to predicted EREs, two

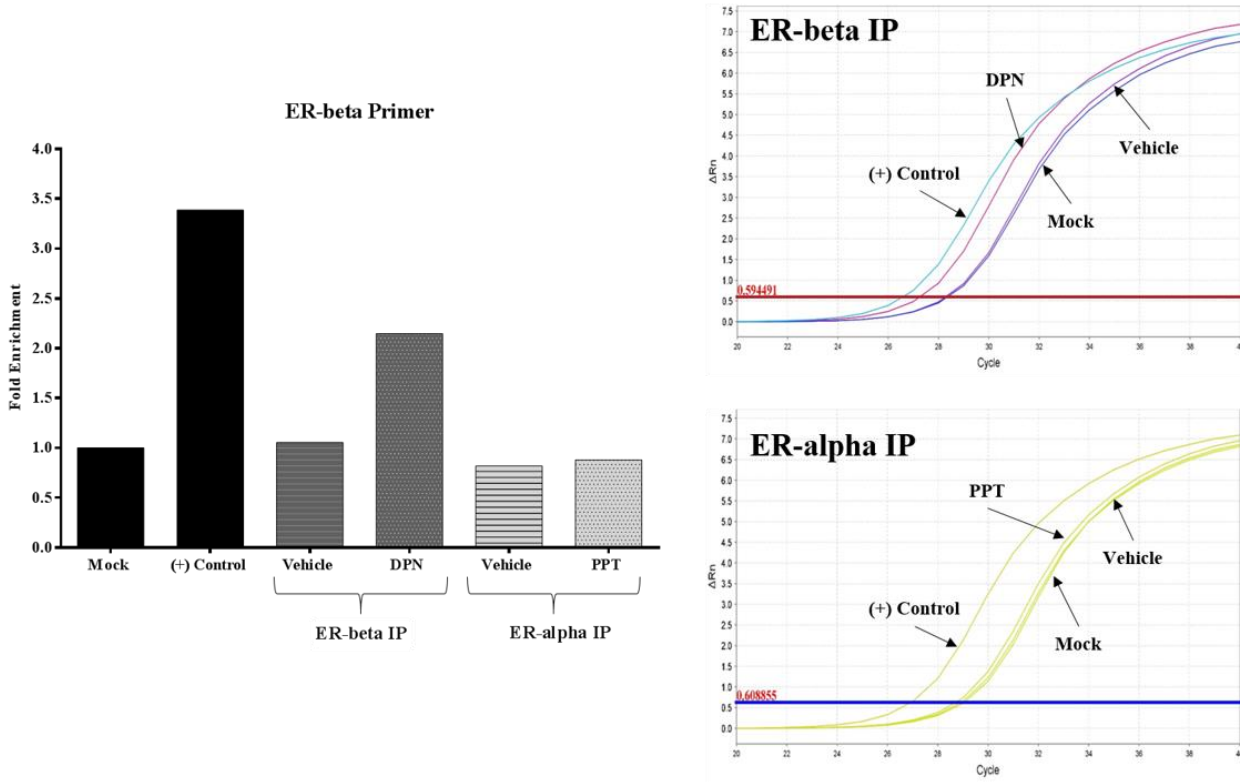

Figure 3.2.4. Ligand Mediated Interaction Between ERβ and the Human CLU Promoter. Chromatin immunoprecipitation was performed as indicated followed by rt-qPCR analysis using the ER-beta primer (right panels) and calculation of fold enrichment (left panel) over the – control (Mock IP)

primer sets were utilized: ER-alpha primer and ER-beta primer. For specific information on the location of EREs within the CLU promoter and the area to which generated ER-specific primers bind, see Schematic 19. For specific primer sequences, see the corresponding methods section. Rt-qPCR of immunoprecipitated DNA indicates an increased interaction between CLU and ERβ in cells treated with DPN (2.1 fold enrichment). As expected amplification with the ERβ primer did not result in an increase in the fold enrichment in either sample immunoprecipitated with ERα (Figure 3.2.4.). Interestingly, amplification of immunoprecipitated DNA with the ER-alpha primer set resulted in an increase in fold enrichment in both ligand-treated groups with DPN-treated cells exhibiting a higher fold enrichment than PPT-treated cells: DPN = 2.47 fold enrichment, PPT = 1.47 fold enrichment (Figure 3.2.5.) Collectively, these data indicate that estrogen receptors regulate mCLU protein expression via direct interaction with one or more EREs in the CLU promoter.

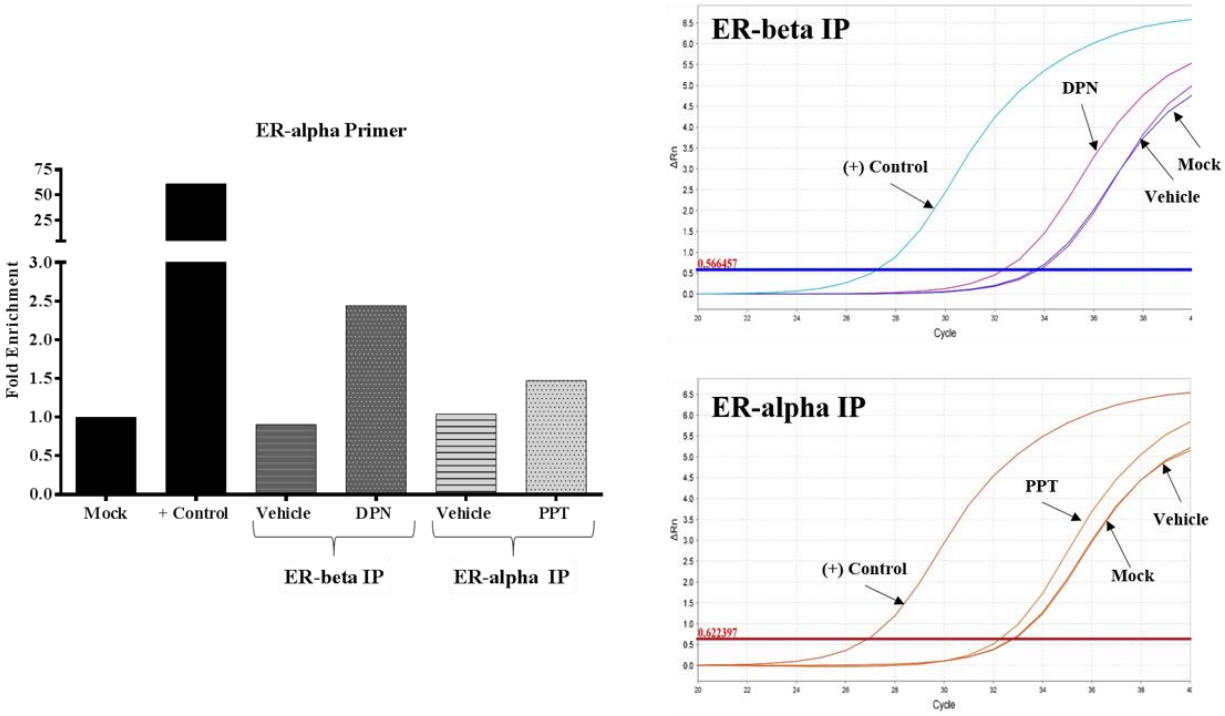

Figure 3.2.5. Ligand Mediated Interaction Between ERβ and ERα and the Human CLU Promoter. Chromatin immunoprecipitation was performed as indicated followed by rt-qPCR analysis using the ER-alpha primer (right panels) and calculation of fold enrichment (left panel) over the – control (Mock IP)

3.3. Interim Discussion and Working Hypothesis

In this chapter we have demonstrated both estrogen- and androgen-mediated regulation of CLU_49 kDa in primary cortical neurons (Figure 3.1.2.). The observed estrogenic signaling resulted in a significant upregulation of CLU_49 kDa protein expression that was mediated through ERβ activation (Figure 3.2.1). Furthermore, inhibition of ERα in the presence of E2 resulted in a significant increase over the E2-treated cells (Figure 3.2.2.) suggesting that ERα-mediated signaling negatively impacts mCLU expression in primary neurons. In addition, i*n vivo* deletion of ERβ results in significantly reduced CLU_49 kDa expression (Figure 3.2.3.) further suggesting that E2 signaling mediated through ERα negatively impacts CLU_49 kDa expression. These data are particularly interesting as the differential regulation of mCLU expression by ERα and ERβ provides some explanation for the discrepancies pertaining to estrogen-mediated regulation of CLU in certain cancer cell lines. For instance, as previously stated, the upregulation of CLU following E2 treatment in our studies is consistent with findings in three cancer cell lines (Won et al., 2012; Wunsche et al., 1998). In contrast, the down-regulation of CLU by ERα-mediated signaling is consistent with reports indicating a repression of CLU mRNA following E2 treatment in ovariectomized rats and mouse uterine tissue (Heikaus, Winterhager, Traub, & Grummer, 2002; Waters et al., 2001) and reports indicating and up-regulation of CLU expression following estrogen depletion in MCF-7 cells (So, Sinnemann, Huntsman, Fazli, & Gleave, 2005). As ERs are not uniformly expressed throughout the body or in immortalized cell lines [Reviewed in (Zhao, Woody, & Chhibber, 2015)], the differing results in the previously mentioned studies are likely due to the differing levels or specific estrogen receptors within the cell types tested. In support of this notion, an examination of tissue-specific ER expression using the Human Protein Atlas Database (www.proteinatlas.org) indicates the prominent expression of ERα, but not ERβ in the uterus and endometrium. Therefore, administration of E2 to these tissues would likely result in the suppression of CLU expression through ERα agonism. While the ratio of ER expression pertaining to all immortalized cell lines is not currently established, the differential regulation of CLU_49 kDa expression sheds light on the importance of taking into consideration the endogenous ER levels in individual cell and

tissue types. In addition, our data demonstrate that E2-mediated regulation occurs via direct transcriptional regulation of CLU through one or more EREs in the CLU promoter. While these data are the first to provide evidence for the presence of EREs in the CLU promoter, one weakness of this study is that, while a ligand-mediated interaction clearly occurs between ERs and CLU DNA, the exact location and number of the ERE(s) is still unknown. The average length of the sheared chromatin in this study was 200-250 bp. Moreover, while the ER-beta primer was centered on bp -297, the size of the generated amplimer indicates a range of ±75 bp from position -297 meaning that, while we have an idea of the approximate location of the ER-beta ERE we cannot ascertain its exact location. Moreover, enrichment of the ERβ-CLU interaction was observed using both sets of CLU primers (ER-alpha and ER-beta). As the predicted ERβ binding site is several hundred bp upstream from area amplified by the ER-alpha primer set, the enrichment of the ERβ-CLU interaction was unexpected in this set of experiments. Three possibilities exist to explain this observation: (1) the sheared chromatin containing the predicted ERE is long enough that it directly overlaps with the region of CLU DNA being amplified by the ER-beta primer, (2) there is an alternative CLU ERE that was not recognized during the *in silico* prediction, or (3) the predicted ER-alpha binding site at ~100 bp allows for the interaction between both ERs and CLU DNA. While more research is needed to establish the exact location(s) of EREs in the CLU promoter, these data confirm the direct estrogenic regulation of CLU in human neuroblastoma cells.

The data in this chapter also indicate that CLU expression which is regulated by E2 in both embryonic and adult brain is negatively affected by aging specifically in young female mice (Figure 3.1.1.). As female mice tend to enter the human equivalent of perimenopause (a period of time prior to menopause characterized by irregularities in the hormonal cycle) by 8-9 months of age (Finch, Felicio, Mobbs, & Nelson, 1984), these data indicate that reproductive aging negatively impacts brain CLU gene expression in female mice. While more work is needed to definitively prove the concepts postulated in this chapter, it is clear that CLU gene and protein expression is regulated in a sex-dependent manner. Moreover, as chronological aging is also known to negatively impact CLU expression

Discussion and Future Directions

CLU is currently the third most significant genetic risk factor for the development of LOAD with multiple clinical studies demonstrating the association between the rs11136000 C SNP and the development of LOAD pathology. In addition, clinical investigations have indicated that the CLU AD risk allele is associated with reduced circulating CLU, faster cognitive decline (Thambisetty et al., 2013), and alterations in synaptic connectivity (Erk et al., 2011) and brain structure (Thambisetty et al., 2012; Ruossotte et al., 2014). However, despite clinical findings, the mechanism(s) by which reduced CLU levels confer increased LOAD risk are not yet described. In addition, while CLU has been heavily studied in metastatic cancer, an extensive gap exists in the literature pertaining to the physiological distribution, expression, and function(s) of CLU protein isoforms in the brain. Moreover, the tendency to refer to CLU as a single protein or mRNA isoforms has resulted in the generation of conflicting reports pertaining to protein and gene expression profiles as well as protein function. Therefore, before the therapeutic potential of CLU in the brain can be ascertained, it is vital that these key deficiencies are addressed on a neurophysiological level. To address the identified deficiencies, we have conducted an in-depth examination of brain CLU protein isoform expression, distribution, and glycosylation status under physiological conditions. The data generated from these studies fill a significant gap in the understanding of CLU in a healthy non-stressed brain and provide key foundational information for future studies pertaining to alterations in CLU protein isoform expression and distribution in various neuropathological conditions. The following sections will include a brief summary of our overall findings and a discussion of our major findings in the context of the currently available literature. In addition, based upon the data presented in this dissertation, we propose an overall working hypothesis that presents a possible mechanism whereby reduced CLU may confer increased LOAD risk. Finally, we present several future directions to directly test the proposed hypothesis as well as two additional future directions that should be considered in the field of brain-based CLU research.

Summary of Overall Findings. The data generated in Chapter 1 demonstrate that CLU exists in the brain as multiple CLU protein isoforms translated from at least 3 potential CLU mRNA transcripts. The 3 translated pre-proteins proposed in this dissertation (CLU_45 kDa, CLU_49 kDa, and CLU_53 kDa) are differentially modified by N-linked glycosylation (complex glycan vs. high-mannose glycan vs. non-glycosylated) with the resulting modified and unmodified protein isoforms exhibiting distinct cellular localizations in both adult brain tissue and embryonic brain cell types. Moreover, we find that the cellular localization of multiple CLU protein isoforms is altered by aging and acute toxicity demonstrating the dynamic nature of CLU protein isoforms within the brain. These data contribute significantly to the resolution of 3 key controversies that currently exist in the literature: (1) the source of brain CLU, (2) the presence of a "nuclear" CLU protein isoform, and (3) the disregarded importance of those CLU protein isoforms that are referred to as "minor" or "intracellular" in previous publications.

The data from Chapter 2 identify, for the first time, a mitochondria-localized CLU protein isoform: CLU_45 kDa. This protein isoform is unaffected by endoglycosidase treatment and corresponds to the predicted MW of a pre-protein translated from an mRNA isoform containing Exons 3-9. Furthermore, the CLU_45 kDa protein isoforms, which is localized to the mitochondrial matrix, physically interacts with components of the MICOS and TOM complexes under physiological conditions suggesting not only a possible protein import pathway but also a possible function for this newly identified mitochondrial isoform. In addition, we find that mCLU, in general, is associated with mitochondrial bioenergetics as a deficiency in mature secreted CLU results in significantly reduced brain mitochondrial respiratory capacity. These data provide solid rationale for novel investigations into the relationship between CLU_45 kDa and the regulation of mitochondrial stability and the relationship between non-mitochondrial CLU and brain bioenergetics.

The data from Chapter 3, which investigated the possible estrogenic regulation of CLU protein isoforms in the brain, show for the first time that estrogen significantly and positively regulates CLU_49 kDa

expression via ERβ-mediated signaling. In addition, the data suggest that ERα-mediated signaling exerts a negative impact on CLU_49 kDa expression. Moreover, we show that the ligand-mediated regulation of CLU_49 kDa by ER signaling occurs via direct DNA-protein interaction between the CLU promoter and ER proteins. These data indicate that estrogens exert an overall positive effect on the mCLU pre-protein in the brain. Additionally, while both ERs were shown to regulate CLU, albeit in opposing manners, the fact that E2 treatment resulted in a significant up-regulation of CLU_49 kDa suggests that ERβ-mediated signaling is the predominant estrogenic regulatory pathway for CLU in cortical tissues. Collectively, the data presented in this chapter provide rationale for the further investigation between CLU protein expression and reproductive aging.

Discussion of Major Findings.

The Relationship Between Astrocyte-Derived and Neuron-Generated mCLU. As previously discussed, the presence of CLU in the brain has been largely attributed to the generation and secretion of CLU from astrocytes in manner that is similar to ApoE (DeMattos et al., 2001; Zwain et al., 1994). In contrast, reports have also indicated the expression of CLU within astrocyte-free cultures of primary neurons suggesting that neurons are capable of generating *de* novo CLU (O'Bryan, Cheema, Bartlett, Murphy, & Pearse, 1993; Pasinetti et al., 1994). Our data suggest that both neurons and astrocytes are capable of generating CLU protein however, analysis of the expression and glycosylation status of CLU protein isoforms in both primary neurons and astrocytes demonstrates that astrocytes, but not neurons, express the mCLU subunits (CLU_39 kDa and CLU_36 kDa). As it is established that the two mCLU subunits represent the glycosylated, non-dimerized subunits of secreted mCLU (Burkey et al., 1991; Burkey, Stuart, & Harmony, 1992; de Silva, Stuart, et al., 1990), these data suggest that astrocytes are responsible for generating and secreting mCLU into the extracellular space. This notion is consistent with previous reports indicating that astrocyte-derived secreted mCLU functions to regulate aspects of neuronal development in the extracellular space (Cordero-Llana et al., 2011). Astrocytes are known to provide neuroprotection via regulation of

several key physiological processes including, but not limited to, clearance of extracellular glutamate (Jensen, Fahlke, Bjorn-Yoshimoto, & Bunch, 2015), regulation of pH and ion homeostasis (Barres, 1991; Orkand, Nicholls, & Kuffler, 1966) (Belanger & Magistretti, 2009), contribution of energy substrates (Mosienko, Teschemacher, & Kasparov, 2015; Teschemacher, Gourine, & Kasparov, 2015), protection from oxidative stress (Belanger & Magistretti, 2009), regulation of the BBB (Alvarez, Katayama, & Prat, 2013; Haseloff, Blasig, Bauer, & Bauer, 2005), regulation of the synapse (Guillamon-Vivancos, Gomez-Pinedo, & Matias-Guiu, 2015), and secretion of neurotrophic factors (B. Liu, Teschemacher, & Kasparov, 2017). Moreover, extracellular mCLU, which is known clear extracellular debris and protect from oxidative stress (H. O. Jun et al., 2011; Trougakos, 2013; Viard et al., 1999), has been implicated in neuronal process formation, elongation, and plasticity in primary spinal cord cell cultures (Cordero-Llana et al., 2011) and neurite outgrowth in PC12 cells (Kang et al., 2005). Therefore, it is highly plausible that astrocyte-derived extracellular mCLU confers some level of neuroprotection via reduction of oxidative stress, clearance of cellular debris, and positive regulation of synaptic function and/or formation.

While primary neurons do not appear to express the secreted mCLU subunits, our analysis does indicate the expression of both CLU_49 kDa and CLU_60 kDa in cultures of primary neurons; two protein isoforms that represent the mCLU pre-protein and a high mannose-modified mCLU intermediate. Therefore, these data suggest that primary neurons are capable of generating mCLU protein isoforms that remain non-secreted (i.e. intracellular mature CLU). While the exact function of the intracellular mCLU protein isoforms is yet to be determined, it is clear that these intracellular isoforms do play some role in the response to neurotoxic stimuli. Our data demonstrate a rapid and significant decrease in cytosolic CLU_80 kDa and nuclear CLU_68 kDa protein expression in primary neurons following acute excitotoxic insult. In contrast, we see a rapid and significant increase in the expression of cytosolic CLU_49 kDa, but not CLU_53 kDa expression. As NMDA receptor-mediated excitotoxicity is known to increase the heat shock response (Rordorf, Koroshetz, & Bonventre, 1991) and CLU gene expression is known to be transcriptionally regulated via one or more HSEs (Loison et al., 2006), the observed up-regulation in CLU_49 kDa protein

isoform could be the result of a general increase in the transcription of Exon 2-9 containing mRNA mediated by increased heat shock protein signaling. However, this HSP-mediated up-regulation does not correspond with the observations associated with either CLU_80 kDa or CLU_68 kDa following administration of supraphysiological glutamate. Our data indicate a relatively rapid and significant decrease in protein expression cannot be attributed to a reversal of N-linked glycosylation or increased secretion of a mCLU protein isoform. Therefore, alternative mechanisms of toxicity-induced protein degradation must be considered. Two such mechanisms could be the proteasomal and/or lysosomal breakdown of toxin-bound intracellular CLU proteins following neurotoxic insult. It has been previously demonstrated that inhibition of proteasomal and lysosomal function results in the accumulation of multiple intracellular CLU protein isoforms (Balantinou, Trougakos, Chondrogianni, Margaritis, & Gonos, 2009) indicating that intracellular CLU protein isoforms are degraded by one or more cellular breakdown processes. As the targeting and degradation of intracellular proteins by the ubiquitin-proteasome pathway occurs in rapidly (Cooper, 2000) and CLU is a known target of ubiquitin (Xue et al., 2012), it is feasible to hypothesize that the rapid disappearance of intracellular CLU_80 kDa and/or CLU_68 kDa protein isoforms is due to the poly-ubiquitination and subsequent proteasomal degradation of the aforementioned CLU protein isoforms following excitotoxic challenge. Moreover, a recent report indicates that at least 1 intracellular neuronal CLU protein isoform is degraded by the lysosome via interaction with sortilin following the administration of $A\beta_{1\text{-}42}$ (Y. Wang, Qin, & Paudel, 2017). Therefore, it is also feasible that the observed changes in protein expression are the result of lysosomal degradation. However, as no aspects of proteolytic breakdown were investigated in the studies presented in this dissertation, more research is needed to explain the alterations in CLU protein expression following excitotoxic challenge. Whatever the mechanism, our data suggest a mechanism whereby intracellular and extracellular mCLU protein isoforms confer neuroprotection with astrocytes contributing the extracellular mCLU and neurons contributing the intracellular mCLU.

Nuclear and Intracellular CLU Protein Isoforms. While it is generally agreed that at least 1 Exon 2-deficient CLU protein isoform is generated, the importance of this and other alternative CLU protein isoforms has been diminished in the currently available literature. It is suggested that this Exon 2-deficient CLU protein isoform represents the nuclear pro-apoptotic CLU protein that is commonly associated with increased cancer cell death (Debure et al., 2003; Dia & Mejia, 2010; Leskov et al., 2003), however, results pertaining to this protein are controversial at best. Our data demonstrate that there is indeed a nuclear CLU protein isoform as well as several other intracellular CLU protein isoforms that can be defined by distinct targeted subcellular localizations (cytosolic, mitochondrial, nuclear, etc…) and modifications (high mannose glycan, complex glycan, non-glycosylated). While the confirmed existence of a nucleus-targeted CLU protein isoform parallels previous reports, the exact isoform targeted to the nucleus has been misinterpreted in previous studies. These investigations suggest that "nuclear CLU" is derived from the Exon 3-9 mRNA isoform which translates a non-glycosylated protein that shuttles between the cytosol and nucleus (Leskov et al., 2003; Reddy et al., 1996). However, our data indicate that the nucleus-targeted CLU protein isoform is a high mannose glycan (CLU_68 kDa) derived from the CLU_53 kDa pre-protein which we hypothesize to be translated from a CLU mRNA containing Exons 1-9. These discrepancies are likely due to the fact that the numerous possible CLU mRNA transcripts and the corresponding translated proteins are yet to be fully characterized. Prior to this investigation, the widely accepted view was that all CLU protein isoforms were translated from 2 CLU mRNA transcripts: Exon 2-9 and Exon 3-9 (Reddy et al., 1996). However, as canonical translational start sites exist in Exons 1, 2, and 3, and studies in immortalized cell lines indicate the inducible expression of several intracellular CLU immunoreactive proteins between 45-53 kDa (Nizard et al., 2007), it is highly plausible that 3 or more CLU coding mRNA transcripts are produced from the CLU gene. In addition, previous studies pertaining to the function of "nuclear CLU" indicate that this alternative protein isoform is solely pro-apoptotic in nature (Dia & Mejia, 2010; N. Kim, Han, et al., 2012; N. Kim, Yoo, et al., 2012; Leskov et al., 2003; Yang et al., 2000). However, our data indicate that these alternative intracellular CLU protein isoforms, which are nearly ubiquitous in the brain and are expressed under physiological conditions, may function to regulate certain aspects of cellular

homeostasis in the subcellular compartments to which they are targeted. In addition, our examination of CLU protein immunoreactivity in mCLU-KO mice suggests that the alternative CLU pre-proteins are up-regulated in the absence of mCLU. While it is possible that the observed up-regulation of alternative CLU protein isoforms results in cellular stress or increased apoptosis, another explanation of this up-regulation can be hypothesized. It is possible that in the absence of mCLU, the expression of intracellular CLU protein isoforms may be increased to compensate for the reduction in mCLU-mediated cyto-protection. This is a particularly intriguing observation as the notion of increased alternative CLU mRNAs could be translated to the clinical setting. Clinical investigations have indicated an increase in one or more CLU mRNA transcripts in patients who carry the rs11136000 and/or the rs9331888 CLU SNPs (Szymanski, Wang, Bassett, & Avramopoulos, 2011). Interestingly, the transcripts shown to be up-regulated in carriers of the rs11136000 SNP have either been removed from the NCBI database (NCBI Accession #CR617497) or are indicated to be a non-coding RNA (NCBI Accession #NM_203339). Therefore, it is possible that possession of the CLU AD risk genotype may result in the up-regulation of one or more CLU mRNA transcript which results in a significantly altered CLU protein expression profile. While this notion requires further testing, these data underscore the importance of (a) identifying all CLU mRNA transcripts in the healthy brain, (b) determining the translated proteins of each identified mRNA, and (c) examining the function(s) of individual CLU protein isoforms with particular emphasis on separating information pertaining to intracellular CLU protein isoforms and the secreted extracellular mCLU.

Mitochondrial CLU: A Novel Avenue of CLU Research. The mitochondrial cascade hypothesis of AD postulates that an individual's genetic makeup determines their baseline mitochondrial function which is differentially impacted though time by inherited and/or environmental factors to regulate the chronology of AD. (Swerdlow & Khan, 2004). Since the proposal of this hypothesis, several studies have demonstrated significant alterations in mitochondrial function in mouse models and human cell lines containing genetic mutations which result in a predisposition for the development of LOAD pathology. For instance, analysis

of whole brain mitochondria in 3-month-old female WT and 3xTg-AD (a triple-transgenic AD mouse model that exhibits age-related amyloid accumulation) mice indicates a significant increase in lipid peroxidation and oxidative stress in 3xTg-AD mice prior to the onset of AD pathology (Yao et al., 2009). Furthermore, embryonic neurons cultured from the same mouse model indicate significantly lower baseline OCR and maximal respiratory capacity in hippocampal neurons cultured from 3xTg-AD mice (Yao et al., 2009). Parallel to these findings, human AD cytoplasmic hybrid (cybrid) cells (a cell line that contains mitochondrial DNA from either AD or control platelets) exhibit increased oxidative stress, decreased mitochondrial membrane potential, and reduced ATP levels in the absence of amyloid pathology (Cardoso, Santana, Swerdlow, & Oliveira, 2004). Our data, which demonstrate functional abnormalities in oxidative phosphorylation in 6-month-old female mCLU-KO mice, indicate that brain mitochondrial bioenergetics are negatively impacted by the genetic depletion of CLU at a young age; a finding that further supports the relationship between genetic predisposition and mitochondrial dysfunction. However, it is important to note that the newly identified mitochondrial CLU protein isoform (CLU_45 kDa) is still present in the mCLU-KO mouse model utilized in our mitochondrial respirometry studies. Therefore, these data indicate that the observed alterations in mitochondrial respiration are due to the lack of mCLU: a protein isoform that is not localized to pure mitochondria. While increased bioenergetic stress mediated by mCLU deficiency presents another possible mechanism whereby reduced CLU may confer increased LOAD risk, these data give rise to the important question of how a non-mitochondrial protein may negatively impact mitochondrial energy production; a process that occurs on the inner mitochondrial membrane. As discussed in Chapter 2, it is possible that the lack of mCLU results in increased mitochondrial Bax translocation and thus results in increased activation of intrinsic apoptotic pathways. However, while increased mitochondrial Bax expression was observed in cortical mitochondrial isolated from mCLU-KO mice no aspects of apoptosis were investigated in this study and thus more research is needed to confirm this hypothesis. It is also possible that mCLU-KO mice are more prone to mitochondria-generated oxidative stress due to the lack of mCLU, which is known to protect from oxidative stress in several cell lines and animals models. A significant increase in the expression of Grp75, another mitochondrial protein that regulates oxidative stress

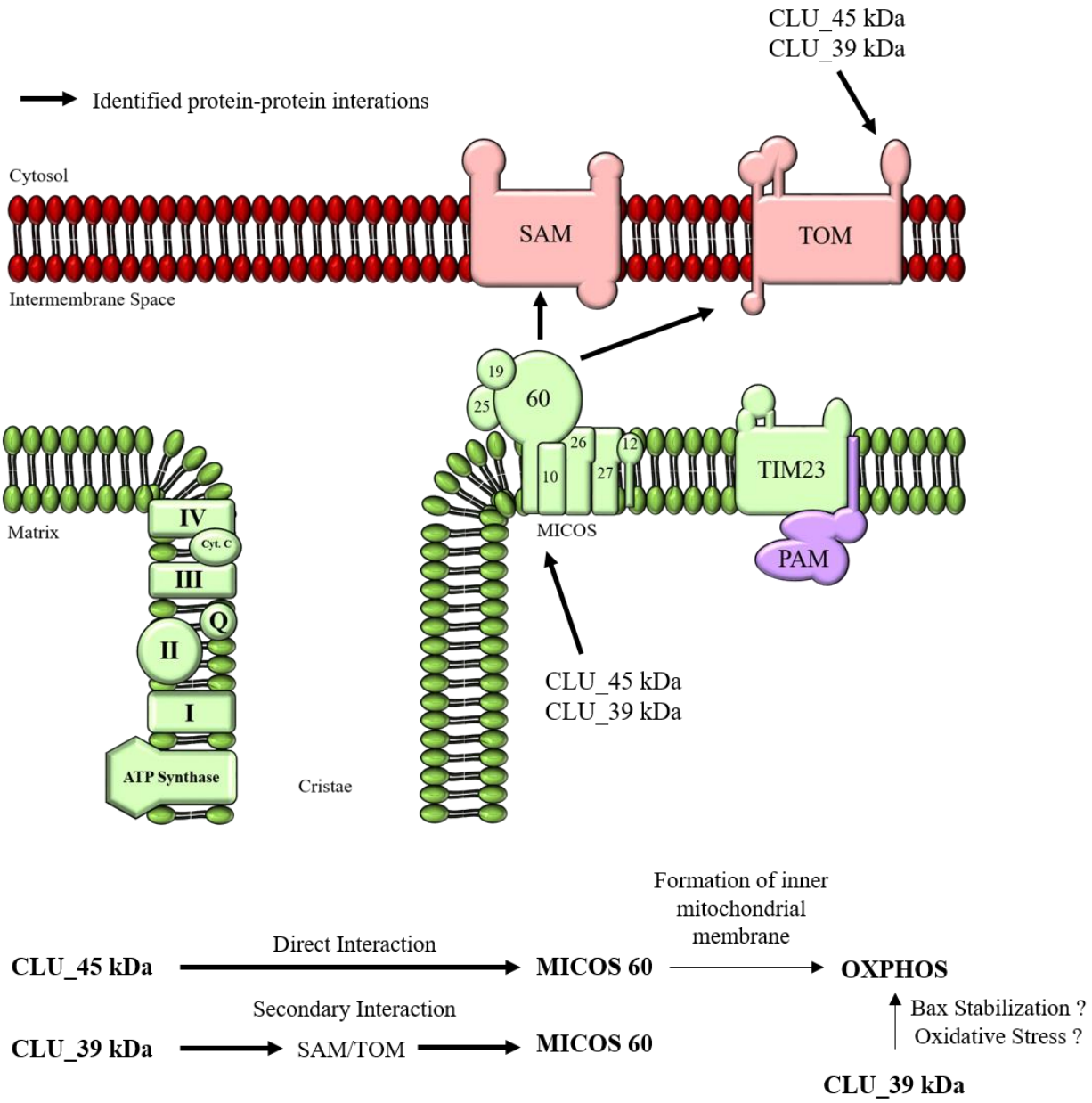

Schematic 20. Proposed Mechanism to Explain the Relationship between Brain Mitochondria and both Mitochondrial and Non-Mitochondrial CLU Protein Isoforms. Our data indicate that both mitochondrial and non-mitochondrial CLU are associated with mitochondrial function. As discussed in Chapter 2, we hypothesize that CLU_45 kDa is imported into the mitochondrial matrix through the TOM70/TIM23/PAM pathway. We hypothesize that CLU_45 kDa assists in the regulation of the stability and structure of the inner mitochondrial membrane via its interaction with the MICOS complex. In reference to non-mitochondrial CLU (CLU_39 kDa), we hypothesize that the observed interaction between CLU_39 kDa and MICOS 60 in brain mitochondria is mediated through the interaction between CLU_39 kDa and a MICOS 60 interacting partner localized to the outer mitochondrial membrane, such as the TOM or SAM complex. Moreover, we hypothesize that CLU_39 is associated with the mitochondria and functions to reduce mitochondria-generated oxidative stress and/or Bax stabilization in the cytosol. Collectively, both CLU protein isoforms function to optimize oxidative phosphorylation via regulation of inner mitochondrial membrane stability and structure, reduction in oxidative stress, and inhibition of Bax-mediated apoptosis.

(E et al., 2013; Y. Liu et al., 2005), supports the idea of increased oxidative stress in young female mCLU-KO mice, however, as ROS levels were not examined in this study, this mechanism is yet to be tested.

In addition to demonstrating the localization of a mitochondrial CLU protein isoform and reduced brain mitochondrial respiration in mCLU-KO mice, our co-immunoprecipitation studies demonstrate a physical interaction between components of the TOM and MICOS complexes and both mitochondrial and mature CLU (CLU_45 kDa and CLU_39 kDa) under physiological conditions. While an interaction between mitochondrial proteins and the CLU_45 kDa protein isoform was expected, the interaction between CLU_39 kDa and mitochondrial proteins was not. The question again becomes, how a non-mitochondrial CLU protein isoform interacts with a protein complex that is specifically localized to the inner mitochondrial membrane. One possibility is that the lysis and immunoprecipitation buffer used in these experiments, which does not disrupt protein-protein interactions, results in the interaction between CLU_39 kDa and MICOS 60 via its interaction with another mitochondrial protein on the outer mitochondrial membrane (i.e. a secondary interaction). As both the SAM complex and the TOM complex have been shown to physically interact with the MICOS complex (Ding et al., 2015; von der Malsburg et al., 2011) and our data indicate an interaction between CLU_39 kDa and TOM70 (Schematic 20, black arrows) it is possible that CLU_39 kDa interacts with MICOS 60 through its interaction with the TOM complex (Schematic 20), though this hypothesis requires further testing. In addition, the list of possible CLU protein interacting partners and the protein interacting partners that were confirmed in physiological conditions present several potential functions for CLU within the mitochondria. One such function would be the regulation of mitochondrial gene expression through the interaction with mitochondrial ribosomes. Mitochondrial ribosomes, which are anchored to the matrix side of the inner mitochondrial membrane (Greber & Ban, 2016), are essential in the generation of mitochondrial proteins encoded by mitochondrial DNA. As over 20 mitochondrial ribosomes were identified in our preliminary studies, the confirmation of

a direct interaction between CLU_45 kDa and mitochondrial translation machinery represents a novel and insightful avenue of research into mitochondrial CLU function. Another possible function for mitochondrial CLU is the regulation of IMM formation through an interaction with the MICOS complex. The MICOS complex, which is integral to mitochondrial energy production, is crucial in the formation of the IMM and thus regulates OXPHOS via formation and stabilization of cristae (van der Laan et al., 2016). As both our preliminary and secondary analysis indicate a physical interaction between CLU_45 kDa and MICOS 60 it is therefore possible that mitochondrial CLU regulates some aspect of IMM stability. Collectively, we hypothesize that mCLU and mitochondrial CLU regulate different aspects of brain mitochondrial function with mCLU impacting some aspect of mitochondrial respiration and mitochondrial CLU regulating inner mitochondrial membrane stability. While several aspects of the relationship between CLU and mitochondria are yet to be examined, one key obstacle will be the inability to selectively silence the expression or inhibit the localization of the CLU_45 kDa protein. However, as brain bioenergetics are integrally linked to the pathology of LOAD, it is essential that the relationship between CLU and mitochondrial function be evaluated in the future.

Brain CLU and Estrogen: a Novel Regulatory Mechanism. An emerging topic in the study of AD is the impact of sex on the development and progression of LOAD. As previously discussed, the female population is more susceptible to developing LOAD and the risk conferred by some genetic factors, such as APOE, is greater in females (Altmann et al., 2014). While the AD risk conferred by the CLU risk variant has not been indicated to be sex-dependent, our data indicate that CLU gene expression is significantly and irreversibly altered during a time that corresponds to the onset of irregular cycling in normally aging female mice. Furthermore, normally aging male mice exhibited no decrease in CLU gene expression indicating that reproductive aging may be integrally involved in the regulation of CLU in the brain. As chronological aging is also known to negatively impact CLU protein isoform expression, these data lead us to wonder whether the chronological loss of CLU protein expression is exacerbated by loss of estrogenic signaling in

the female brain during menopausal onset. This exacerbation could contribute to the female vulnerability that is associated with LOAD development. However, one inconsistency does arise. Previous studies and our own data indicate that androgens significantly repress CLU protein expression in the brain and reproductive tissues (Cochrane, Wang, Muramaki, Gleave, & Nelson, 2007; July et al., 2002). Therefore, if decreased CLU expression results in increased vulnerability to AD, one would expect males to exhibit increased CLU-mediated AD risk until the onset of andropause when the CLU gene would be free of androgen-mediated repression. While the mechanisms underlying differing trajectories in CLU expression are not yet understood, these data underscore the importance of including sex as a variable in the study of risk factors that mediate the development of LOAD.

The CLU-KO Animal Model: Not a Total Knockout. Several studies in recent years have utilized the CLU-KO mouse model to demonstrate the involvement of CLU in a myriad of pathological conditions including, but not limited to, diabetes (Byun et al., 2014; Zeng, Lu, Lee, & Friedman, 2015), cardiovascular disease (Shirasawa et al., 2009), ischemia (Imhof et al., 2006), Creutzfeldt-Jakob Disease (Sasaki, Doh-ura, Ironside, Mabbott, & Iwaki, 2006), cancer (Chayka et al., 2009), kidney disease or injury (Ghiggeri et al., 2002; Jung et al., 2012; Zhou et al., 2010), and atherosclerosis (Hamada et al., 2011; Seo et al., 2013). In addition, this mouse model has been used to implicate CLU in developmental processes (Jiao et al., 2011; J. H. Kim, Kim, Yu, Min, & Kim, 2007) as well as the regulation of inflammation (Hong et al., 2016; Savkovic et al., 2007) and oxidative stress (Mishima et al., 2012). However, few studies have included an in-house validation of the CLU-KO mouse model. Those studies which have verified the absence of CLU protein in the animals used in their studies examine only the mature secreted form of CLU represented as CLU_60 kDa and/or CLU_39 kDa; a finding that is consistent with our own data. However, further characterization of the CLU-KO mouse model on both the protein and gene level indicate that this mouse model, which is indicated to be completely devoid of CLU protein and mRNA, contains at least 1 CLU mRNA and several CLU protein isoforms. A review of the publication which described the generation of

the CLU-KO mouse model indicates that the mutant cassette used to create the CLU-KO animal blocks transcription starting in Exon 2 (McLaughlin et al., 2000). Therefore, the remaining mRNA transcripts must be initiated at Exon 3 or possibly in Exon 1. However, our protein data do not match the expected outcome of this mouse model. For instance, while our data indicate the expected deficiency in CLU_60 kDa and CLU_39 kDa, the mCLU pre-protein (CLU_49 kDa) is still expressed in mCLU-KO mice. Therefore, these data suggest that, while the mCLU pre-protein is still translated, the glycosylation and maturation of mCLU is inhibited in this mouse model. This discovery is potentially problematic as it changes our entire interpretation of the studies that have identified potential protein functions, properties, and/or regulatory pathways pertaining to CLU. Instead of identifying basic molecular properties of CLU in general, researchers have instead been identifying physiological functions pertaining to only the mature secreted CLU protein isoform meaning that we know even less about protein isoforms that are translated from alternative mRNA transcripts. While the generation of a total CLU knockout mouse model is proposed in the future directions, the accidental knockout of only mCLU does provide a tool that could be unknowingly used to study the combined effects of aging, sex, and mCLU deficiency on neurocognitive decline from both a biochemical and behavioural standpoint. While these animals have been extensively utilized in the past and are phenotypically and reproductively normal, no published study, to date, has performed a behavioural characterization of this mouse model. Moreover, as our mitochondrial data clearly indicate differences between WT and mCLU-KO animals at a young age, it would be extremely interesting to perform a long-term behavioural and biochemical study using normally aging male and female WT and mCLU-KO mice. This study should include a sex-dependent examination of neurocognitive behaviour and mitochondrial function at 3, 6, 10, and 15 months of age. Data derived from this study would provide a plethora of insight pertaining to the understanding of the interaction between sex, brain bioenergetics, aging, and mCLU deficiency.

Working Hypothesis and Future Directions. Based on the data presented in this dissertation, we hypothesize that possession of CLU AD risk SNPs result in significantly lower levels of astrocyte-derived extracellular and neuron-generated intracellular CLU in young adult brain rendering neurons more vulnerable to extracellular insult and/or neurotoxic damage. In addition, reduced intracellular CLU results in increased bioenergetic stress in young adult brain which is exacerbated by the loss of estrogen and estrogen-mediated CLU regulation associated with reproductive aging. Collectively, an increase in the level of mitochondrial stress and a decrease in the amount of secreted, intracellular, and mitochondrial CLU significantly contributes to neurodegenerative decline in the preclinical phase of LOAD in female brain (Schematic 21). While this hypothesis seems quite complex, a breakdown of the overall hypothesis into 4 individual working hypotheses will allow for the successful testing of the aforementioned mechanism. The following 4 sections will discuss the short- and long-term future directions that will significantly contribute to our understanding of CLU in AD development and directly test our working hypothesis.

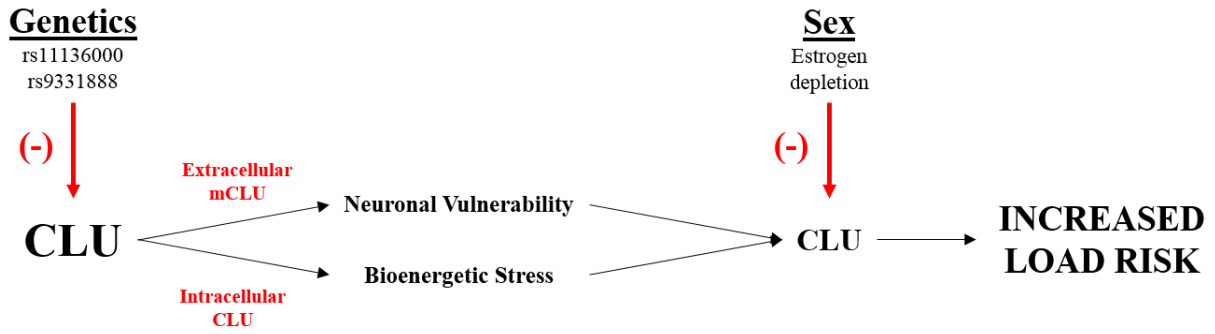

Schematic 21. Proposed Overall Working Hypothesis. Based on the data presented in this dissertation we hypothesize that possession of a CLU AD risk SNP results in significantly reduced astrocyte-derived extracellular and neuron-generated young adult brain rendering neurons more vulnerable to extracellular insult and/or neurotoxic damage. In addition, reduced intracellular CLU results in increased bioenergetic stress in young adult brain which is exacerbated by the loss of estrogen and estrogen-mediated CLU regulation associated with reproductive aging. Collectively, an increase in the level of mitochondrial stress and a decrease in the amount of secreted, intracellular, and mitochondrial CLU significantly contributes to neurodegenerative decline in the preclinical phase of LOAD in female brain

Working Hypothesis Part I: Possession of a CLU AD risk SNP results in an altered CLU mRNA and/or protein expression profile. While studies have indicated alterations in the expression of plasma CLU in carriers of the CLU AD risk allele, the impact of CLU AD SNP possession on individual mRNA transcript levels and protein isoform expression have not been characterized. However, as altered

expression of at least 1 CLU mRNA transcript has been observed in carriers of two identified CLU AD-related SNPs, it is possible that possession of CLU SNP results in significant alterations at the messenger or protein level. As the single mutation of one nucleotide with in an intron is technically improbable at this time, we will focus on the creation of a cDNA overexpression construct that contains the risk-conferring rs9331888 SNP (G allele), which is located in Exon 1 of CLU mRNA (chromosomal location 27611345). It has been demonstrated that 1 copy of the G allele results in a significant reduction in CLU mRNA and protein levels (Xing et al., 2012), therefore our experiment will aim to generate a cDNA construct that possesses the CG genotype at the aforementioned chromosomal location. Full length human CLU cDNA derived from the pLX304-hCLU-v5 cDNA overexpression construct will be sequence analyzed to determine the existing genotype at the appropriate location (CC, CG, or GG). Primer sets will then be generated to create the CC-containing cDNA construct (if genotype is CG or GG) or the CG-containing cDNA construct (if genotype is CC) and site directed mutagenesis will be performed with generated primers. Mutations will be confirmed via DNA sequencing and overexpression constructs will be transfected into one or more human cells lines. Total RNAs and protein will be isolated and alterations in protein and/or mRNA levels will be detected via rt-qPCR or SDS-PAGE. The data generated from these studies will directly demonstrate the impact of at least 1 CLU AD-associated SNP on human CLU protein and mRNA levels.

Working Hypothesis Part II: Reduced astrocyte-derived extracellular CLU renders neurons more vulnerable to extracellular insult/neurotoxic damage. While the discovery that the previously described total CLU-KO mouse was in fact a mCLU-KO animal was unexpected, the knockout of only mCLU does actually prove beneficial in testing the first part of our hypothesis. We propose the generation of an astrocyte-neuron co-culture using postnatal day 1 WT and mCLU-KO mouse pups. These co-cultures will be exposed to acute (Supraphysiological glutamate) or chronic (neurotoxic Aβ) neurodegenerative stimuli

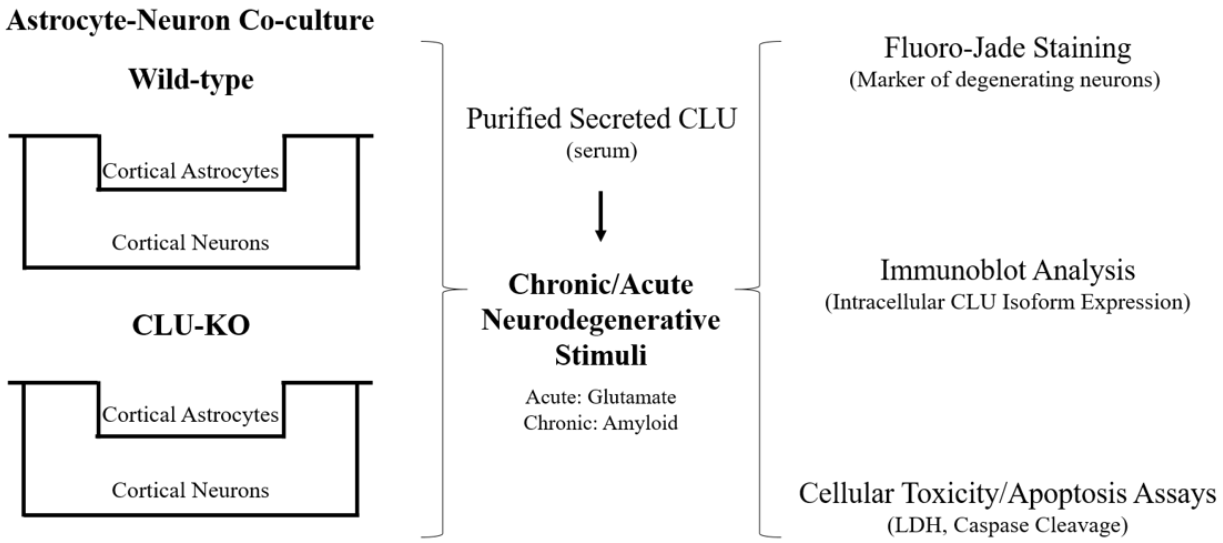

Schematic 22. Proposed Experimental Plan to Investigate Working Hypothesis Part II. Astrocyte-neuron co-cultures will be isolated from WT and mCLU-KO mouse pups and treated with acute or chronic neurodegenerative stimuli in the presence of absence of exogenously added purified secreted CLU. Neurotoxicity and neurodegeneration will then be assessed with the indicated assays and CLU protein expression will be evaluated via immunoblotting.

for pre-determined amounts of time and neurons will be assessed for neuronal toxicity and degeneration using the LDH Assay and Fluoro-Jade Staining. Fluoro-Jade staining was selected based on the preferred staining of both degenerating neurons and reactive microglia: both of which should be visible in this experiment. Moreover, Fluoro-Jade Staining has been shown to be an effective tool for staining both acutely and chronically degenerating neurons. In addition to assessing neurotoxicity and neurodegeneration, CLU levels will be assessed in the culture medium at each time point to ensure the loss in mCLU secretion in mCLU-KO co-cultures and the increase in mCLU secretion from WT co-cultures (positive control). Moreover, neurons and astrocytes will be subjected to subcellular fractionation and analyzed for CLU immunoreactivity to examine the impact of acute and chronic toxicity on intracellular CLU protein isoforms across both co-culture models (Schematic 21). Following the completion of these preliminary experiments and the establishment of a consistent response, this experiment can be repeated with the addition of exogenously purified secreted mCLU. The data generated from these experiments are expected to answer two very important questions: (1) Does genetic deficiency in the mCLU isoform result in exacerbated

neuronal damage under acute/chronic neurotoxic conditions? and (2) Can the addition of purified mCLU attenuate the exacerbated neuronal degeneration?

Working Hypothesis Part III: Reduced intracellular CLU results in increased bioenergetic stress and reduced mitochondrial stability in young adult brain. Our previous data indicate that mCLU-KO mice exhibit significantly reduced brain mitochondrial respiration. However, as this mouse model is known to be deficient in only a portion of CLU protein, the next part of our working hypothesis will examine the impact of intracellular CLU deficiency on brain bioenergetics. We propose a two-step evaluation using an *in vitro* and *in vivo* system. For the first part of our proposed experimental plan, primary cultures of neurons or astrocytes will be isolated from E18 rat pups and grown to maturity as described in this dissertation. Lentiviral vectors targeting Exon 1, Exon 2, or Exon 3 of CLU will be used to silence specific CLU protein isoforms in each model followed by the confirmation of CLU knockdown. As we propose that mitochondrial CLU (CLU_45 kDa) plays some role in the regulation of the stability of the inner mitochondrial membrane in coordination with the MICOS complex, mitochondrial stability will be initially examined using TMRM staining. In addition, mitochondrial respiration will be examined using high-resolution respirometry coupled with safranin dye to further assess the mitochondrial membrane potential. In addition, changes in CLU protein expression will be assessed using immunoblot analysis in both culture models.

Pending the positive outcome of the *in vitro* experimentation, we will proceed with the *in vivo* portion of our experimental plan. Exon 3-targeting lentivirus will be injected into WT and mCLU-KO female mice. While there are several types of viral delivery vectors, lentivirus was selected based previous publications indicating that recombinant lentiviral vectors are applicable for stable, long-term gene delivery to neurons *in vivo* (Osten, Dittgen, & Licznerski, 2006). Moreover, preliminary rt-qPCR studies aimed at characterizing CLU mRNA transcripts in mCLU-KO mice indicate that the majority of Exon 1 is not

transcribed, therefore, only Exon 3-targeting lentivirus will be utilized in our *in vivo* experimentation. Following the delivery of lentivirus, crude mitochondria will be isolated and analyzed for mitochondrial respirometry using the protocol established in this dissertation. As stated in the previous section,

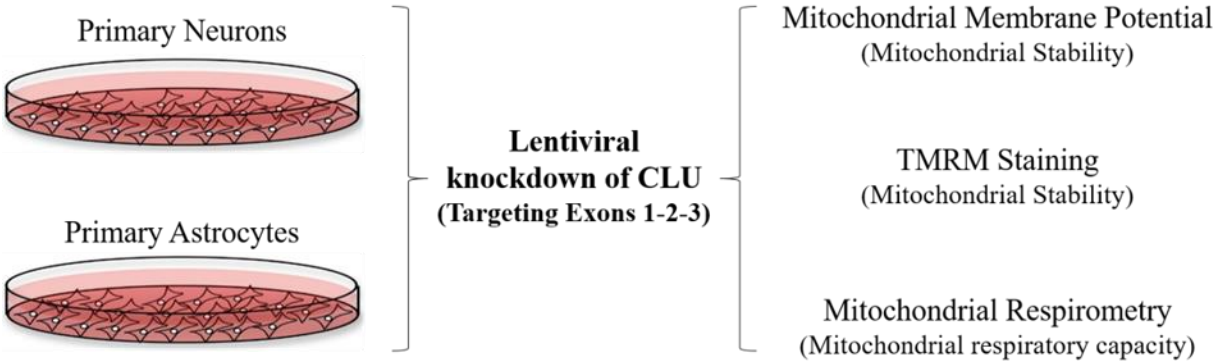

Schematic 23. Proposed Experimental Plan to Investigate Working Hypothesis Part III. (Top, *in vitro*) Primary astrocytes and neruons will be subjected to lentivirus mediated silencing of CLU as indicated. Isoform knockdown will be confirmed and mitochondrial stability and respiratory capacity will be analyzed as indicated. **(Bottom, *in vivo*)** Female WT and mCLU-KO mice will be injected with Exon 3-targeting CLU siRNA. Protein knockdown will be confirmed via immunoblotting and mitochondrial respiration and stability will be assessed.

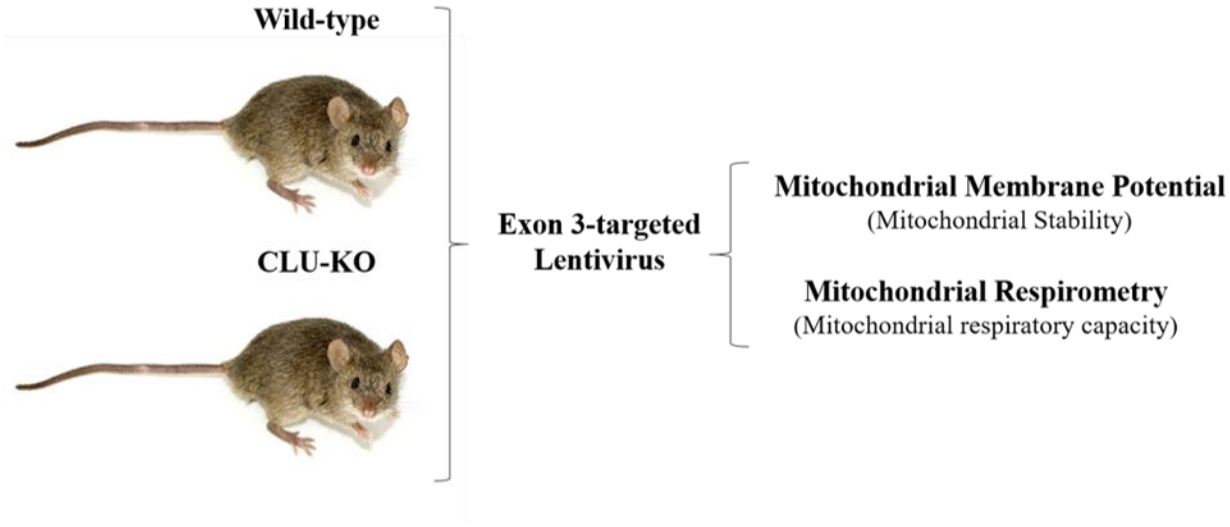

respirometry will be performed in conjunction with the assessment of mitochondrial membrane potential using Safranin in a protocol similar to that of Chowdhury and colleagues (Chowdhury, Djordjevic, Albensi, & Fernyhough, 2015). Similar to that of our previous experimentation, changes in CLU protein isoform expression will be evaluated/confirmed via immunoblot analysis. The data generated from these studies is expected to answer 4 key questions pertaining to the relationship between brain CLU and mitochondrial

bioenergetics: (1) Does knockdown of intracellular CLU in general impact respiratory capacity or mitochondrial stability in primary astrocytes and/or neurons? (2) Which brain cell type is more significantly bioenergetically impacted by CLU deficiency? (3) Does deficiency in intracellular CLU exacerbate the respiratory deficiencies previously observed in mCLU-KO mice? and (4) Does CLU deficiency negatively impact mitochondrial stability?

Working Hypothesis Part IV: Loss of estrogen signaling exacerbates bioenergetic stress mediated by mCLU deficiency. Data presented in this dissertation indicate that CLU_49 kDa is significantly regulated by estrogen signaling in the brain. While we have yet to examine whether estrogen signaling regulates CLU_45 kDa and/or CLU_53 kDa, these data demonstrate that all CLU protein isoforms derived from the CLU_49 kDa band are regulated by estrogen signaling in one way or another. Indeed, though not presented in this dissertation, we did observe significant alterations in the expression of CLU_80 kDa following E2 treatment in primary cortical neurons. Moreover, based on the location of the predicted EREs in the CLU promoter (upstream of Exon 1), it is feasible to suspect that estrogenic signaling may regulate the expression of all three predicted CLU pre-proteins and likewise, loss of estrogen signaling may negatively affect the expression of all three pre-proteins and the resultant higher molecular weight CLU protein isoforms. Therefore, the possible estrogenic regulation of both CLU_53 kDa and CLU_45 kDa will be examined in primary cortical neurons using the protocols established in this dissertation. Following the completion of preliminary studies, we will determine whether estrogen depletion exacerbates the previously observed bioenergetic stress in mCLU-KO mice, using an *in vivo* experiment designed to directly assess the interaction between sex, CLU, and brain metabolism. Briefly, 3-month-old female WT and mCLU-KO mice will be subjected to a sham surgery or ovariectomized (OVX) to create 4 different experimental groups: WT – Sham = Total control, WT – OVX = Control for estrogen loss, CLU-KO – Sham = Control for CLU deficiency, and CLU-KO – OVX – Experimental Group. Crude mitochondria will be isolated from cortical tissues and mitochondrial respiration will be evaluated using high-resolution respirometry as

previously described. In addition, CLU pre-protein expression levels will also be examined in each group to determine the impact of estrogen deficiency on the expression of CLU_45 kDa and CLU_53 kDa. The data generated from these studies is expected to answer the following 2 questions: (1) Are all CLU pre-proteins positively regulated by estrogenic signaling in cortical neurons? (2) Are the observed mCLU-KO-dependent deficiencies in brain mitochondrial respiration exacerbated by loss of estrogen signaling in young female brain?

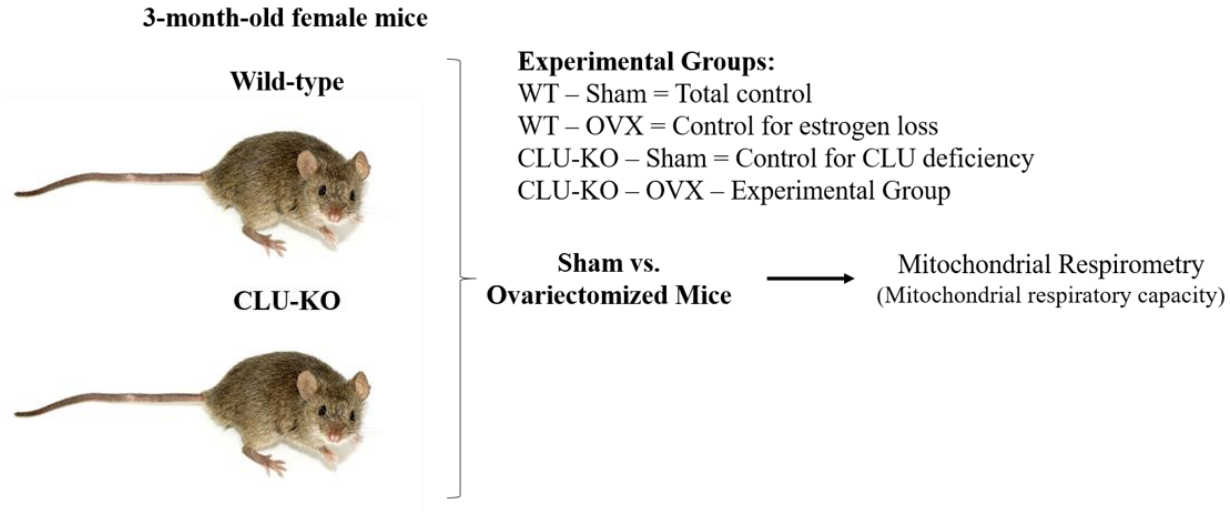

Schematic 24. Proposed Experimental Plan to Investigate Working Hypothesis Part IV. Female WT and mCLU-KO mice will be subjected to either Sham surgery or ovariectomized to create the indicated 4 groups. Mitochondrial respirometry, membrane potential and mitochondrial oxidative stress will then be measured in each group and CLU protein expression will be analyzed.

The Generation of a Total CLU-KO Mouse Model. As previously discussed, the assumed commercially available CLU-KO mouse model is not in fact a total CLU-KO. Therefore, we propose the generation of a truly CLU-deficient animal model via targeted deletion of Exons 1-3. Targeted disruption or deletion of Exons 1-3 would eliminate the transcription of any CLU mRNA isoform generating a total CLU knockout animal. A total knockout mouse model, which could be used in conjunction with WT and mCLU-KO animals, would be an invaluable tool for investigating the impact of not only total CLU deficiency, but also the impact of mitochondrial CLU deficiency on brain function.

The Compensatory Relationship Between CLU and APOE. It is particularly interesting that 2 of the top 5 genetic risk factors associated with the development of LOAD are members of the apolipoprotein family: APOE and CLU. Therefore, another avenue of research to be considered in the AD field is the possibility of intersecting or overlapping risk pathways mediated by similar genetic risk factors. Studies have shown that APOE and CLU share a number of important physiological characteristics. For instance, they are among the few proteins associated with brain lipoproteins (Elliott, Weickert, & Garner, 2010; Koch et al., 2001). They interact with a shared set of cell-surface receptors (Kounnas et al., 1995) and both APOE and CLU promote neurite outgrowth (Kang et al., 2005; Nathan et al., 1994). Moreover, elimination of either protein in an AD mouse model results in increased accumulation of Aβ (DeMattos et al., 2004). Furthermore, presence of the C-allele of the CLU AD-risk SNP has been shown to exacerbate the APOE ε4-mediated decrease in brain activity during executive attention tasks in young healthy dementia-free adults (Green et al., 2014). In addition, the genetic variance that results in increased AD risk from both genes is also associated with compromised or reduced protein expression and/or binding capabilities. Our preliminary data indicate that APOE protein expression levels are significantly increased in 6-month-old female mCLU-KO mice. However, mCLU expression levels are significantly reduced in 6-month-old female human APOE ε4 gene targeted-replacement mice when compared to APOE ε3 mice indicating that reduced CLU expression may contribute to APOE ε4-mediated AD risk. Collectively, these studies indicate that APOE and CLU could share common risk pathways that contribute to the development of LOAD. Delineation of such pathways will potentially provide valuable insights for an increased understanding of the etiology of LOAD and ultimately help to devise therapeutic strategies to prevent or reduce the risk of developing the disease during the preclinical stage of AD.

References

Abe, Y., Shodai, T., Muto, T., Mihara, K., Torii, H., Nishikawa, S., . . . Kohda, D. (2000). Structural basis of presequence recognition by the mitochondrial protein import receptor Tom20. *Cell, 100*(5), 551-560.

Aging, N. I. o. (2015). Alzheimer's Disease. 1-8.

Akiyama, H., Barger, S., Barnum, S., Bradt, B., Bauer, J., Cole, G. M., . . . Wyss-Coray, T. (2000). Inflammation and Alzheimer's disease. *Neurobiol Aging, 21*(3), 383-421.

Altmann, A., Tian, L., Henderson, V. W., Greicius, M. D., & Alzheimer's Disease Neuroimaging Initiative, I. (2014). Sex modifies the APOE-related risk of developing Alzheimer disease. *Ann Neurol, 75*(4), 563-573. doi: 10.1002/ana.24135

Alvarez, J. I., Katayama, T., & Prat, A. (2013). Glial influence on the blood brain barrier. *Glia, 61*(12), 1939-1958. doi: 10.1002/glia.22575

Alzheimer's, A. (2015). 2015 Alzheimer's disease facts and figures. *Alzheimers Dement, 11*(3), 332-384.

Amy S. Yokoyama, J. C. R. a. V. M. (2017). DNA methylation alterations in Alzheimer's Disease. *Environmental Epigenetics, 3*(2), 1-11. doi: 10.1093/eep/dvx008

Baghirova, S., Hughes, B. G., Hendzel, M. J., & Schulz, R. (2015). Sequential fractionation and isolation of subcellular proteins from tissue or cultured cells. *MethodsX, 2*, 440-445. doi: 10.1016/j.mex.2015.11.001

Bailey, R. W., Dunker, A. K., Brown, C. J., Garner, E. C., & Griswold, M. D. (2001). Clusterin, a binding protein with a molten globule-like region. *Biochemistry, 40*(39), 11828-11840.

Balantinou, E., Trougakos, I. P., Chondrogianni, N., Margaritis, L. H., & Gonos, E. S. (2009). Transcriptional and posttranslational regulation of clusterin by the two main cellular proteolytic pathways. *Free Radic Biol Med, 46*(9), 1267-1274.

Barres, B. A. (1991). Glial ion channels. *Curr Opin Neurobiol, 1*(3), 354-359.

Bartl, M. M., Luckenbach, T., Bergner, O., Ullrich, O., & Koch-Brandt, C. (2001). Multiple receptors mediate apoJ-dependent clearance of cellular debris into nonprofessional phagocytes. *Exp Cell Res, 271*(1), 130-141. doi: 10.1006/excr.2001.5358

Beer, T. M., Hotte, S. J., Saad, F., Alekseev, B., Matveev, V., Flechon, A., . . . Fizazi, K. (2017). Custirsen (OGX-011) combined with cabazitaxel and prednisone versus cabazitaxel and prednisone alone in patients with metastatic castration-resistant prostate cancer previously treated with docetaxel (AFFINITY): a randomised, open-label, international, phase 3 trial. *Lancet Oncol*. doi: 10.1016/S1470-2045(17)30605-8

Belanger, M., & Magistretti, P. J. (2009). The role of astroglia in neuroprotection. *Dialogues Clin Neurosci, 11*(3), 281-295.

Bell, R. D., Sagare, A. P., Friedman, A. E., Bedi, G. S., Holtzman, D. M., Deane, R., & Zlokovic, B. V. (2007). Transport pathways for clearance of human Alzheimer's amyloid beta-peptide and apolipoproteins E and J in the mouse central nervous system. *J Cereb Blood Flow Metab, 27*(5), 909-918. doi: 10.1038/sj.jcbfm.9600419

Bertram, L., McQueen, M. B., Mullin, K., Blacker, D., & Tanzi, R. E. (2007). Systematic meta-analyses of Alzheimer disease genetic association studies: the AlzGene database. *Nat Genet, 39*(1), 17-23. doi: 10.1038/ng1934

Blacker, D., Haines, J. L., Rodes, L., Terwedow, H., Go, R. C., Harrell, L. E., . . . Tanzi, R. (1997). ApoE-4 and age at onset of Alzheimer's disease: the NIMH genetics initiative. *Neurology, 48*(1), 139-147.

Bradley-Whitman, M. A., & Lovell, M. A. (2013). Epigenetic changes in the progression of Alzheimer's disease. *Mech Ageing Dev, 134*(10), 486-495. doi: 10.1016/j.mad.2013.08.005

Braskie, M. N., Jahanshad, N., Stein, J. L., Barysheva, M., McMahon, K. L., de Zubicaray, G. I., . . . Thompson, P. M. (2011). Common Alzheimer's disease risk variant within the CLU gene affects white matter microstructure in young adults. *J Neurosci, 31*(18), 6764-6770. doi: 10.1523/JNEUROSCI.5794-10.2011

Burkey, B. F., deSilva, H. V., & Harmony, J. A. (1991). Intracellular processing of apolipoprotein J precursor to the mature heterodimer. *J Lipid Res, 32*(6), 1039-1048.
Burkey, B. F., Stuart, W. D., & Harmony, J. A. (1992). Hepatic apolipoprotein J is secreted as a lipoprotein. *J Lipid Res, 33*(10), 1517-1526.
Byun, K., Gil, S. Y., Namkoong, C., Youn, B. S., Huang, H., Shin, M. S., . . . Kim, M. S. (2014). Clusterin/ApoJ enhances central leptin signaling through Lrp2-mediated endocytosis. *EMBO Rep, 15*(7), 801-808. doi: 10.15252/embr.201338317
Cao, X., Yeo, G., Muotri, A. R., Kuwabara, T., & Gage, F. H. (2006). Noncoding RNAs in the mammalian central nervous system. *Annu Rev Neurosci, 29*, 77-103. doi: 10.1146/annurev.neuro.29.051605.112839
Cardoso, S. M., Santana, I., Swerdlow, R. H., & Oliveira, C. R. (2004). Mitochondria dysfunction of Alzheimer's disease cybrids enhances Abeta toxicity. *J Neurochem, 89*(6), 1417-1426. doi: 10.1111/j.1471-4159.2004.02438.x
Cartharius, K., Frech, K., Grote, K., Klocke, B., Haltmeier, M., Klingenhoff, A., . . . Werner, T. (2005). MatInspector and beyond: promoter analysis based on transcription factor binding sites. *Bioinformatics, 21*(13), 2933-2942. doi: 10.1093/bioinformatics/bti473
Cascella, R., Conti, S., Tatini, F., Evangelisti, E., Scartabelli, T., Casamenti, F., . . . Cecchi, C. (2013). Extracellular chaperones prevent Abeta42-induced toxicity in rat brains. *Biochim Biophys Acta, 1832*(8), 1217-1226. doi: 10.1016/j.bbadis.2013.04.012
Cervellera, M., Raschella, G., Santilli, G., Tanno, B., Ventura, A., Mancini, C., . . . Sala, A. (2000). Direct transactivation of the anti-apoptotic gene apolipoprotein J (clusterin) by B-MYB. *J Biol Chem, 275*(28), 21055-21060. doi: 10.1074/jbc.M002055200
Chaiwatanasirikul, K. A., & Sala, A. (2011). The tumour-suppressive function of CLU is explained by its localisation and interaction with HSP60. *Cell Death Dis, 2*, e219. doi: 10.1038/cddis.2011.99
Chapman, R. M., Mapstone, M., Gardner, M. N., Sandoval, T. C., McCrary, J. W., Guillily, M. D., . . . DeGrush, E. (2011). Women have farther to fall: gender differences between normal elderly and Alzheimer's disease in verbal memory engender better detection of Alzheimer's disease in women. *J Int Neuropsychol Soc, 17*(4), 654-662. doi: 10.1017/S1355617711000452
Chayka, O., Corvetta, D., Dews, M., Caccamo, A. E., Piotrowska, I., Santilli, G., . . . Sala, A. (2009). Clusterin, a haploinsufficient tumor suppressor gene in neuroblastomas. *J Natl Cancer Inst, 101*(9), 663-677. doi: 10.1093/jnci/djp063
Chen, L. H., Kao, P. Y., Fan, Y. H., Ho, D. T., Chan, C. S., Yik, P. Y., . . . Song, Y. Q. (2012). Polymorphisms of CR1, CLU and PICALM confer susceptibility of Alzheimer's disease in a southern Chinese population. *Neurobiol Aging, 33*(1), 210 e211-217. doi: 10.1016/j.neurobiolaging.2011.09.016
Chi, K. N., Eisenhauer, E., Fazli, L., Jones, E. C., Goldenberg, S. L., Powers, J., . . . Gleave, M. E. (2005). A phase I pharmacokinetic and pharmacodynamic study of OGX-011, a 2'-methoxyethyl antisense oligonucleotide to clusterin, in patients with localized prostate cancer. *J Natl Cancer Inst, 97*(17), 1287-1296. doi: 10.1093/jnci/dji252
Chi, K. N., Higano, C. S., Blumenstein, B. A., Reeves, J. A., Feyerabend, S., Gravis, G., . . . Investigators, S. (2015). Phase III SYNERGY trial: Docetaxel +/- custirsen and overall survival in patients (pts) with metastatic castration-resistant prostate cancer (mCRPC) and poor prognosis. *Journal of Clinical Oncology, 33*(15).
Chi, K. N., Hotte, S. J., Yu, E. Y., Tu, D., Eigl, B. J., Tannock, I., . . . Eisenhauer, E. A. (2010). Randomized phase II study of docetaxel and prednisone with or without OGX-011 in patients with metastatic castration-resistant prostate cancer. *J Clin Oncol, 28*(27), 4247-4254. doi: 10.1200/JCO.2009.26.8771
Chi, K. N., Siu, L. L., Hirte, H., Hotte, S. J., Knox, J., Kollmansberger, C., . . . Eisenhauer, E. (2008). A phase I study of OGX-011, a 2'-methoxyethyl phosphorothioate antisense to clusterin, in combination with docetaxel in patients with advanced cancer. *Clin Cancer Res, 14*(3), 833-839. doi: 10.1158/1078-0432.CCR-07-1310

Chia, S., Dent, S., Ellard, S., Ellis, P. M., Vandenberg, T., Gelmon, K., . . . Eisenhauer, E. A. (2009). Phase II trial of OGX-011 in combination with docetaxel in metastatic breast cancer. *Clin Cancer Res, 15*(2), 708-713. doi: 10.1158/1078-0432.CCR-08-1159

Choi, N. H., Mazda, T., & Tomita, M. (1989). A serum protein SP40,40 modulates the formation of membrane attack complex of complement on erythrocytes. *Mol Immunol, 26*(9), 835-840.

Choi, N. H., Nakano, Y., Tobe, T., Mazda, T., & Tomita, M. (1990). Incorporation of SP-40,40 into the soluble membrane attack complex (SMAC, SC5b-9) of complement. *Int Immunol, 2*(5), 413-417.

Chouliaras, L., Mastroeni, D., Delvaux, E., Grover, A., Kenis, G., Hof, P. R., . . . van den Hove, D. L. (2013). Consistent decrease in global DNA methylation and hydroxymethylation in the hippocampus of Alzheimer's disease patients. *Neurobiol Aging, 34*(9), 2091-2099. doi: 10.1016/j.neurobiolaging.2013.02.021

Chowdhury, S. R., Djordjevic, J., Albensi, B. C., & Fernyhough, P. (2015). Simultaneous evaluation of substrate-dependent oxygen consumption rates and mitochondrial membrane potential by TMRM and safranin in cortical mitochondria. *Biosci Rep, 36*(1), e00286. doi: 10.1042/BSR20150244

Cochrane, D. R., Wang, Z., Muramaki, M., Gleave, M. E., & Nelson, C. C. (2007). Differential regulation of clusterin and its isoforms by androgens in prostate cells. *J Biol Chem, 282*(4), 2278-2287. doi: 10.1074/jbc.M608162200

Connor, J. R., Kumar, S., Sathe, G., Mooney, J., O'Brien, S. P., Mui, P., . . . Lark, M. W. (2001). Clusterin expression in adult human normal and osteoarthritic articular cartilage. *Osteoarthritis Cartilage, 9*(8), 727-737. doi: 10.1053/joca.2001.0475

Cooper, G. a. S. M. (2000). Protein Degradation *The Cell: A Molecular Approach* (2nd Edition ed.): Sinauer Associates.

Coppieters, N., Dieriks, B. V., Lill, C., Faull, R. L., Curtis, M. A., & Dragunow, M. (2014). Global changes in DNA methylation and hydroxymethylation in Alzheimer's disease human brain. *Neurobiol Aging, 35*(6), 1334-1344. doi: 10.1016/j.neurobiolaging.2013.11.031

Corder, E. H., Saunders, A. M., Risch, N. J., Strittmatter, W. J., Schmechel, D. E., Gaskell, P. C., Jr., . . . et al. (1994). Protective effect of apolipoprotein E type 2 allele for late onset Alzheimer disease. *Nat Genet, 7*(2), 180-184. doi: 10.1038/ng0694-180

Corder, E. H., Saunders, A. M., Strittmatter, W. J., Schmechel, D. E., Gaskell, P. C., Small, G. W., . . . Pericak-Vance, M. A. (1993). Gene dose of apolipoprotein E type 4 allele and the risk of Alzheimer's disease in late onset families. *Science, 261*(5123), 921-923.

Cordero-Llana, O., Scott, S. A., Maslen, S. L., Anderson, J. M., Boyle, J., Chowhdury, R. R., . . . Caldwell, M. A. (2011). Clusterin secreted by astrocytes enhances neuronal differentiation from human neural precursor cells. *Cell Death Differ, 18*(5), 907-913. doi: 10.1038/cdd.2010.169

Corneveaux, J. J., Myers, A. J., Allen, A. N., Pruzin, J. J., Ramirez, M., Engel, A., . . . Huentelman, M. J. (2010). Association of CR1, CLU and PICALM with Alzheimer's disease in a cohort of clinically characterized and neuropathologically verified individuals. *Hum Mol Genet, 19*(16), 3295-3301. doi: 10.1093/hmg/ddq221

Dabbs, R. A., & Wilson, M. R. (2014). Expression and purification of chaperone-active recombinant clusterin. *PLoS One, 9*(1), e86989. doi: 10.1371/journal.pone.0086989

de Silva, H. V., Harmony, J. A., Stuart, W. D., Gil, C. M., & Robbins, J. (1990). Apolipoprotein J: structure and tissue distribution. *Biochemistry, 29*(22), 5380-5389.

de Silva, H. V., Stuart, W. D., Park, Y. B., Mao, S. J., Gil, C. M., Wetterau, J. R., . . . Harmony, J. A. (1990). Purification and characterization of apolipoprotein J. *J Biol Chem, 265*(24), 14292-14297.

Debure, L., Vayssiere, J. L., Rincheval, V., Loison, F., Le Drean, Y., & Michel, D. (2003). Intracellular clusterin causes juxtanuclear aggregate formation and mitochondrial alteration. *J Cell Sci, 116*(Pt 15), 3109-3121. doi: 10.1242/jcs.00619

DeMattos, R. B., Brendza, R. P., Heuser, J. E., Kierson, M., Cirrito, J. R., Fryer, J., . . . Holtzman, D. M. (2001). Purification and characterization of astrocyte-secreted apolipoprotein E and J-containing lipoproteins from wild-type and human apoE transgenic mice. *Neurochem Int, 39*(5-6), 415-425.

DeMattos, R. B., Cirrito, J. R., Parsadanian, M., May, P. C., O'Dell, M. A., Taylor, J. W., . . . Holtzman,

D. M. (2004). ApoE and clusterin cooperatively suppress Abeta levels and deposition: evidence that ApoE regulates extracellular Abeta metabolism in vivo. *Neuron, 41*(2), 193-202.
DeMattos, R. B., O'Dell M, A., Parsadanian, M., Taylor, J. W., Harmony, J. A., Bales, K. R., . . . Holtzman, D. M. (2002). Clusterin promotes amyloid plaque formation and is critical for neuritic toxicity in a mouse model of Alzheimer's disease. *Proc Natl Acad Sci U S A, 99*(16), 10843-10848. doi: 10.1073/pnas.162228299
Dia, V. P., & Mejia, E. G. (2010). Lunasin promotes apoptosis in human colon cancer cells by mitochondrial pathway activation and induction of nuclear clusterin expression. *Cancer Lett, 295*(1), 44-53. doi: 10.1016/j.canlet.2010.02.010
Dietzsch, E., Murphy, B. F., Kirszbaum, L., Walker, I. D., & Garson, O. M. (1992). Regional localization of the gene for clusterin (SP-40,40; gene symbol CLI) to human chromosome 8p12-->p21. *Cytogenet Cell Genet, 61*(3), 178-179.
Ding, C., Wu, Z., Huang, L., Wang, Y., Xue, J., Chen, S., . . . Chen, S. (2015). Mitofilin and CHCHD6 physically interact with Sam50 to sustain cristae structure. *Sci Rep, 5*, 16064. doi: 10.1038/srep16064
Drzezga, A., Grimmer, T., Henriksen, G., Muhlau, M., Perneczky, R., Miederer, I., . . . Kurz, A. (2009). Effect of APOE genotype on amyloid plaque load and gray matter volume in Alzheimer disease. *Neurology, 72*(17), 1487-1494. doi: 10.1212/WNL.0b013e3181a2e8d0
Drzezga, A., Riemenschneider, M., Strassner, B., Grimmer, T., Peller, M., Knoll, A., . . . Kurz, A. (2005). Cerebral glucose metabolism in patients with AD and different APOE genotypes. *Neurology, 64*(1), 102-107. doi: 10.1212/01.WNL.0000148478.39691.D3
Dukic, L., Simundic, A. M., Martinic-Popovic, I., Kackov, S., Diamandis, A., Begcevic, I., & Diamandis, E. P. (2016). The role of human kallikrein 6, clusterin and adiponectin as potential blood biomarkers of dementia. *Clin Biochem, 49*(3), 213-218. doi: 10.1016/j.clinbiochem.2015.10.014
Dunker, A. K., Lawson, J. D., Brown, C. J., Williams, R. M., Romero, P., Oh, J. S., . . . Obradovic, Z. (2001). Intrinsically disordered protein. *J Mol Graph Model, 19*(1), 26-59.
E, Q., Liu, X., Liu, Y., Liu, W., & Zuo, J. (2013). Over-expression of GRP75 inhibits liver injury induced by oxidative damage. *Acta Biochim Biophys Sin (Shanghai), 45*(2), 129-134. doi: 10.1093/abbs/gms098
Elliott, D. A., Weickert, C. S., & Garner, B. (2010). Apolipoproteins in the brain: implications for neurological and psychiatric disorders. *Clin Lipidol, 51*(4), 555-573. doi: 10.2217/CLP.10.37
Erk, S., Meyer-Lindenberg, A., Opitz von Boberfeld, C., Esslinger, C., Schnell, K., Kirsch, P., . . . Walter, H. (2011). Hippocampal function in healthy carriers of the CLU Alzheimer's disease risk variant. *J Neurosci, 31*(49), 18180-18184. doi: 10.1523/JNEUROSCI.4960-11.2011
Essabbani, A., Margottin-Goguet, F., & Chiocchia, G. (2010). Identification of clusterin domain involved in NF-kappaB pathway regulation. *J Biol Chem, 285*(7), 4273-4277. doi: 10.1074/jbc.C109.057133
Esteller, M. (2011). Non-coding RNAs in human disease. *Nat Rev Genet, 12*(12), 861-874. doi: 10.1038/nrg3074
Farrer, L. A., Cupples, L. A., Haines, J. L., Hyman, B., Kukull, W. A., Mayeux, R., . . . van Duijn, C. M. (1997). Effects of age, sex, and ethnicity on the association between apolipoprotein E genotype and Alzheimer disease. A meta-analysis. APOE and Alzheimer Disease Meta Analysis Consortium. *JAMA, 278*(16), 1349-1356.
Ferrari, R., Moreno, J. H., Minhajuddin, A. T., O'Bryant, S. E., Reisch, J. S., Barber, R. C., & Momeni, P. (2012). Implication of common and disease specific variants in CLU, CR1, and PICALM. *Neurobiol Aging, 33*(8), 1846 e1847-1818. doi: 10.1016/j.neurobiolaging.2012.01.110
Finch, C. E., Felicio, L. S., Mobbs, C. V., & Nelson, J. F. (1984). Ovarian and steroidal influences on neuroendocrine aging processes in female rodents. *Endocr Rev, 5*(4), 467-497. doi: 10.1210/edrv-5-4-467
Fleisher, A., Grundman, M., Jack, C. R., Jr., Petersen, R. C., Taylor, C., Kim, H. T., . . . Alzheimer's Disease Cooperative, S. (2005). Sex, apolipoprotein E epsilon 4 status, and hippocampal volume

in mild cognitive impairment. *Arch Neurol, 62*(6), 953-957. doi: 10.1001/archneur.62.6.953
Fritz, I. B., Burdzy, K., Setchell, B., & Blaschuk, O. (1983). Ram rete testis fluid contains a protein (clusterin) which influences cell-cell interactions in vitro. *Biol Reprod, 28*(5), 1173-1188.
Fu, Y., Lai, Y., Wang, Q., Liu, X., He, W., Zhang, H., . . . Yang, G. (2013). Overexpression of clusterin promotes angiogenesis via the vascular endothelial growth factor in primary ovarian cancer. *Mol Med Rep, 7*(6), 1726-1732. doi: 10.3892/mmr.2013.1436
Gao, S., Hendrie, H. C., Hall, K. S., & Hui, S. (1998). The relationships between age, sex, and the incidence of dementia and Alzheimer disease: a meta-analysis. *Arch Gen Psychiatry, 55*(9), 809-815.
Ghiggeri, G. M., Bruschi, M., Candiano, G., Rastaldi, M. P., Scolari, F., Passerini, P., . . . Ponticelli, C. (2002). Depletion of clusterin in renal diseases causing nephrotic syndrome. *Kidney Int, 62*(6), 2184-2194. doi: 10.1046/j.1523-1755.2002.00664.x
Ghiso, J., Matsubara, E., Koudinov, A., Choi-Miura, N. H., Tomita, M., Wisniewski, T., & Frangione, B. (1993). The cerebrospinal-fluid soluble form of Alzheimer's amyloid beta is complexed to SP-40,40 (apolipoprotein J), an inhibitor of the complement membrane-attack complex. *Biochem J, 293 (Pt 1)*, 27-30.
Ghosh, P., Hale, E. A., & Lakshman, M. R. (2001). Plasma sialic-acid index of apolipoprotein J (SIJ): a new alcohol intake marker. *Alcohol, 25*(3), 173-179.
Golenkina, S. A., Gol'tsov, A., Kuznetsova, I. L., Grigorenko, A. P., Andreeva, T. V., Reshetov, D. A., . . . Rogaev, E. I. (2010). [Analysis of clusterin gene (CLU/APOJ) polymorphism in Alzheimer's disease patients and in normal cohorts from Russian populations]. *Mol Biol (Mosk), 44*(4), 620-626.
Greber, B. J., & Ban, N. (2016). Structure and Function of the Mitochondrial Ribosome. *Annu Rev Biochem, 85*, 103-132. doi: 10.1146/annurev-biochem-060815-014343
Green, A. E., Gray, J. R., Deyoung, C. G., Mhyre, T. R., Padilla, R., Dibattista, A. M., & William Rebeck, G. (2014). A combined effect of two Alzheimer's risk genes on medial temporal activity during executive attention in young adults. *Neuropsychologia, 56*, 1-8. doi: 10.1016/j.neuropsychologia.2013.12.020
Guillamon-Vivancos, T., Gomez-Pinedo, U., & Matias-Guiu, J. (2015). Astrocytes in neurodegenerative diseases (I): function and molecular description. *Neurologia, 30*(2), 119-129. doi: 10.1016/j.nrl.2012.12.007
Gutacker, C., Klock, G., Diel, P., & Koch-Brandt, C. (1999). Nerve growth factor and epidermal growth factor stimulate clusterin gene expression in PC12 cells. *Biochem J, 339 (Pt 3)*, 759-766.
Hamada, N., Miyata, M., Eto, H., Ikeda, Y., Shirasawa, T., Akasaki, Y., . . . Tei, C. (2011). Loss of clusterin limits atherosclerosis in apolipoprotein E-deficient mice via reduced expression of Egr-1 and TNF-alpha. *J Atheroscler Thromb, 18*(3), 209-216.
Han, B. H., DeMattos, R. B., Dugan, L. L., Kim-Han, J. S., Brendza, R. P., Fryer, J. D., . . . Holtzman, D. M. (2001). Clusterin contributes to caspase-3-independent brain injury following neonatal hypoxia-ischemia. *Nat Med, 7*(3), 338-343. doi: 10.1038/85487
Harold, D., Abraham, R., Hollingworth, P., Sims, R., Gerrish, A., Hamshere, M. L., . . . Williams, J. (2009). Genome-wide association study identifies variants at CLU and PICALM associated with Alzheimer's disease. *Nat Genet, 41*(10), 1088-1093. doi: 10.1038/ng.440
Haseloff, R. F., Blasig, I. E., Bauer, H. C., & Bauer, H. (2005). In search of the astrocytic factor(s) modulating blood-brain barrier functions in brain capillary endothelial cells in vitro. *Cell Mol Neurobiol, 25*(1), 25-39.
Hassan, M. K., Watari, H., Han, Y., Mitamura, T., Hosaka, M., Wang, L., . . . Sakuragi, N. (2011). Clusterin is a potential molecular predictor for ovarian cancer patient's survival: targeting clusterin improves response to paclitaxel. *J Exp Clin Cancer Res, 30*, 113. doi: 10.1186/1756-9966-30-113
He, L. R., Liu, M. Z., Li, B. K., Rao, H. L., Liao, Y. J., Zhang, L. J., . . . Xie, D. (2009). Clusterin as a predictor for chemoradiotherapy sensitivity and patient survival in esophageal squamous cell

carcinoma. *Cancer Sci, 100*(12), 2354-2360. doi: 10.1111/j.1349-7006.2009.01349.x
Heikaus, S., Winterhager, E., Traub, O., & Grummer, R. (2002). Responsiveness of endometrial genes Connexin26, Connexin43, C3 and clusterin to primary estrogen, selective estrogen receptor modulators, phyto- and xenoestrogens. *J Mol Endocrinol, 29*(2), 239-249.
Higano, C. S. (2013). Potential use of custirsen to treat prostate cancer. *Onco Targets Ther, 6*, 785-797. doi: 10.2147/OTT.S33077
Hoeller, C., Pratscher, B., Thallinger, C., Winter, D., Fink, D., Kovacic, B., . . . Jansen, B. (2005). Clusterin regulates drug-resistance in melanoma cells. *J Invest Dermatol, 124*(6), 1300-1307. doi: 10.1111/j.0022-202X.2005.23720.x
Hof, P. R., & Morrison, J. H. (1990). Quantitative analysis of a vulnerable subset of pyramidal neurons in Alzheimer's disease: II. Primary and secondary visual cortex. *J Comp Neurol, 301*(1), 55-64. doi: 10.1002/cne.903010106
Hong, G. H., Kwon, H. S., Moon, K. A., Park, S. Y., Park, S., Lee, K. Y., . . . Cho, Y. S. (2016). Clusterin Modulates Allergic Airway Inflammation by Attenuating CCL20-Mediated Dendritic Cell Recruitment. *J Immunol, 196*(5), 2021-2030. doi: 10.4049/jimmunol.1500747
Hsu, Y. T., Wolter, K. G., & Youle, R. J. (1997). Cytosol-to-membrane redistribution of Bax and Bcl-X(L) during apoptosis. *Proc Natl Acad Sci U S A, 94*(8), 3668-3672.
Imhof, A., Charnay, Y., Vallet, P. G., Aronow, B., Kovari, E., French, L. E., . . . Giannakopoulos, P. (2006). Sustained astrocytic clusterin expression improves remodeling after brain ischemia. *Neurobiol Dis, 22*(2), 274-283. doi: 10.1016/j.nbd.2005.11.009
Irvine, K., Laws, K. R., Gale, T. M., & Kondel, T. K. (2012). Greater cognitive deterioration in women than men with Alzheimer's disease: a meta analysis. *J Clin Exp Neuropsychol, 34*(9), 989-998. doi: 10.1080/13803395.2012.712676
Jenne, D. E., & Tschopp, J. (1989). Molecular structure and functional characterization of a human complement cytolysis inhibitor found in blood and seminal plasma: identity to sulfated glycoprotein 2, a constituent of rat testis fluid. *Proc Natl Acad Sci U S A, 86*(18), 7123-7127.
Jensen, A. A., Fahlke, C., Bjorn-Yoshimoto, W. E., & Bunch, L. (2015). Excitatory amino acid transporters: recent insights into molecular mechanisms, novel modes of modulation and new therapeutic possibilities. *Curr Opin Pharmacol, 20*, 116-123. doi: 10.1016/j.coph.2014.10.008
Jiao, S., Dai, W., Lu, L., Liu, Y., Zhou, J., Li, Y., . . . Duan, C. (2011). The conserved clusterin gene is expressed in the developing choroid plexus under the regulation of notch but not IGF signaling in zebrafish. *Endocrinology, 152*(5), 1860-1871. doi: 10.1210/en.2010-1183
Jin, G., & Howe, P. H. (1997). Regulation of clusterin gene expression by transforming growth factor beta. *J Biol Chem, 272*(42), 26620-26626.
Jin, G., & Howe, P. H. (1999). Transforming growth factor beta regulates clusterin gene expression via modulation of transcription factor c-Fos. *Eur J Biochem, 263*(2), 534-542.
Jongbloed, W., van Dijk, K. D., Mulder, S. D., van de Berg, W. D., Blankenstein, M. A., van der Flier, W., & Veerhuis, R. (2015). Clusterin Levels in Plasma Predict Cognitive Decline and Progression to Alzheimer's Disease. *J Alzheimers Dis, 46*(4), 1103-1110. doi: 10.3233/JAD-150036
July, L. V., Akbari, M., Zellweger, T., Jones, E. C., Goldenberg, S. L., & Gleave, M. E. (2002). Clusterin expression is significantly enhanced in prostate cancer cells following androgen withdrawal therapy. *Prostate, 50*(3), 179-188.
Jun, G., Naj, A. C., Beecham, G. W., Wang, L. S., Buros, J., Gallins, P. J., . . . Schellenberg, G. D. (2010). Meta-analysis confirms CR1, CLU, and PICALM as alzheimer disease risk loci and reveals interactions with APOE genotypes. *Arch Neurol, 67*(12), 1473-1484. doi: 10.1001/archneurol.2010.201
Jun, H. O., Kim, D. H., Lee, S. W., Lee, H. S., Seo, J. H., Kim, J. H., . . . Kim, K. W. (2011). Clusterin protects H9c2 cardiomyocytes from oxidative stress-induced apoptosis via Akt/GSK-3beta signaling pathway. *Exp Mol Med, 43*(1), 53-61. doi: 10.3858/emm.2011.43.1.006
Jung, G. S., Kim, M. K., Jung, Y. A., Kim, H. S., Park, I. S., Min, B. H., . . . Lee, I. K. (2012). Clusterin attenuates the development of renal fibrosis. *J Am Soc Nephrol, 23*(1), 73-85. doi:

10.1681/ASN.2011010048
Kamboh, M. I., Minster, R. L., Demirci, F. Y., Ganguli, M., Dekosky, S. T., Lopez, O. L., & Barmada, M. M. (2012). Association of CLU and PICALM variants with Alzheimer's disease. *Neurobiol Aging, 33*(3), 518-521. doi: 10.1016/j.neurobiolaging.2010.04.015
Kang, S. W., Shin, Y. J., Shim, Y. J., Jeong, S. Y., Park, I. S., & Min, B. H. (2005). Clusterin interacts with SCLIP (SCG10-like protein) and promotes neurite outgrowth of PC12 cells. *Exp Cell Res, 309*(2), 305-315. doi: 10.1016/j.yexcr.2005.06.012
Kapron, J. T., Hilliard, G. M., Lakins, J. N., Tenniswood, M. P., West, K. A., Carr, S. A., & Crabb, J. W. (1997). Identification and characterization of glycosylation sites in human serum clusterin. *Protein Sci, 6*(10), 2120-2133. doi: 10.1002/pro.5560061007
Killick, R., Ribe, E. M., Al-Shawi, R., Malik, B., Hooper, C., Fernandes, C., . . . Lovestone, S. (2014). Clusterin regulates beta-amyloid toxicity via Dickkopf-1-driven induction of the wnt-PCP-JNK pathway. *Mol Psychiatry, 19*(1), 88-98. doi: 10.1038/mp.2012.163
Kim, J. H., Kim, J. H., Yu, Y. S., Min, B. H., & Kim, K. W. (2007). The role of clusterin in retinal development and free radical damage. *Br J Ophthalmol, 91*(11), 1541-1546. doi: 10.1136/bjo.2007.115220
Kim, N., Han, J. Y., Roh, G. S., Kim, H. J., Kang, S. S., Cho, G. J., . . . Choi, W. S. (2012). Nuclear clusterin is associated with neuronal apoptosis in the developing rat brain upon ethanol exposure. *Alcohol Clin Exp Res, 36*(1), 72-82. doi: 10.1111/j.1530-0277.2011.01588.x
Kim, N., Yoo, J. C., Han, J. Y., Hwang, E. M., Kim, Y. S., Jeong, E. Y., . . . Choi, W. S. (2012). Human nuclear clusterin mediates apoptosis by interacting with Bcl-XL through C-terminal coiled coil domain. *J Cell Physiol, 227*(3), 1157-1167. doi: 10.1002/jcp.22836
Kimura, K., Asami, K., & Yamamoto, M. (1997). Effect of heat shock treatment on the production of variant testosterone-repressed prostate message-2 (TRPM-2) mRNA in culture cells. *Cell Biochem Funct, 15*(4), 251-257. doi: 10.1002/(SICI)1099-0844(199712)15:4<251::AID-CBF748>3.0.CO;2-3
Kirszbaum, L., Bozas, S. E., & Walker, I. D. (1992). SP-40,40, a protein involved in the control of the complement pathway, possesses a unique array of disulphide bridges. *FEBS Lett, 297*(1-2), 70-76.
Klimkowicz-Mrowiec, A., Sado, M., Dziubek, A., Dziedzic, T., Pera, J., Szczudlik, A., & Slowik, A. (2013). Lack of association of CR1, PICALM and CLU gene polymorphisms with Alzheimer disease in a Polish population. *Neurol Neurochir Pol, 47*(2), 157-160.
Koch, S., Donarski, N., Goetze, K., Kreckel, M., Stuerenburg, H. J., Buhmann, C., & Beisiegel, U. (2001). Characterization of four lipoprotein classes in human cerebrospinal fluid. *J Lipid Res, 42*(7), 1143-1151.
Koltai, T. (2014). Clusterin: a key player in cancer chemoresistance and its inhibition. *Onco Targets Ther, 7*, 447-456. doi: 10.2147/OTT.S58622
Komatsu, M., Shibata, N., Kuerban, B., Ohnuma, T., Baba, H., & Arai, H. (2011). Genetic association between clusterin polymorphisms and Alzheimer's disease in a Japanese population. *Psychogeriatrics, 11*(1), 14-18. doi: 10.1111/j.1479-8301.2010.00346.x
Kounnas, M. Z., Loukinova, E. B., Stefansson, S., Harmony, J. A., Brewer, B. H., Strickland, D. K., & Argraves, W. S. (1995). Identification of glycoprotein 330 as an endocytic receptor for apolipoprotein J/clusterin. *J Biol Chem, 270*(22), 13070-13075.
Kumita, J. R., Poon, S., Caddy, G. L., Hagan, C. L., Dumoulin, M., Yerbury, J. J., . . . Dobson, C. M. (2007). The extracellular chaperone clusterin potently inhibits human lysozyme amyloid formation by interacting with prefibrillar species. *J Mol Biol, 369*(1), 157-167. doi: 10.1016/j.jmb.2007.02.095
L, I. J., Dekker, L. J., Koudstaal, P. J., Hofman, A., Sillevis Smitt, P. A., Breteler, M. M., & Luider, T. M. (2011). Serum clusterin levels are not increased in presymptomatic Alzheimer's disease. *J Proteome Res, 10*(4), 2006-2010. doi: 10.1021/pr101221h
Lakins, J. N., Poon, S., Easterbrook-Smith, S. B., Carver, J. A., Tenniswood, M. P., & Wilson, M. R.

(2002). Evidence that clusterin has discrete chaperone and ligand binding sites. *Biochemistry, 41*(1), 282-291.
Lambert, J. C., Heath, S., Even, G., Campion, D., Sleegers, K., Hiltunen, M., . . . Amouyel, P. (2009). Genome-wide association study identifies variants at CLU and CR1 associated with Alzheimer's disease. *Nat Genet, 41*(10), 1094-1099. doi: 10.1038/ng.439
Lancaster, T. M., Baird, A., Wolf, C., Jackson, M. C., Johnston, S. J., Donev, R., . . . Linden, D. E. (2011). Neural hyperactivation in carriers of the Alzheimer's risk variant on the clusterin gene. *Eur Neuropsychopharmacol, 21*(12), 880-884. doi: 10.1016/j.euroneuro.2011.02.001
Lancaster, T. M., Brindley, L. M., Tansey, K. E., Sims, R. C., Mantripragada, K., Owen, M. J., . . . Linden, D. E. (2015). Alzheimer's disease risk variant in CLU is associated with neural inefficiency in healthy individuals. *Alzheimers Dement, 11*(10), 1144-1152. doi: 10.1016/j.jalz.2014.10.012
Langbaum, J. B., Chen, K., Lee, W., Reschke, C., Bandy, D., Fleisher, A. S., . . . Alzheimer's Disease Neuroimaging, I. (2009). Categorical and correlational analyses of baseline fluorodeoxyglucose positron emission tomography images from the Alzheimer's Disease Neuroimaging Initiative (ADNI). *Neuroimage, 45*(4), 1107-1116. doi: 10.1016/j.neuroimage.2008.12.072
Laskin, J. J., Nicholas, G., Lee, C., Gitlitz, B., Vincent, M., Cormier, Y., . . . Hao, D. (2012). Phase I/II trial of custirsen (OGX-011), an inhibitor of clusterin, in combination with a gemcitabine and platinum regimen in patients with previously untreated advanced non-small cell lung cancer. *J Thorac Oncol, 7*(3), 579-586. doi: 10.1097/JTO.0b013e31823f459c
Lau, S. H., Sham, J. S., Xie, D., Tzang, C. H., Tang, D., Ma, N., . . . Guan, X. Y. (2006). Clusterin plays an important role in hepatocellular carcinoma metastasis. *Oncogene, 25*(8), 1242-1250. doi: 10.1038/sj.onc.1209141
Law, G. L., & Griswold, M. D. (1994). Activity and form of sulfated glycoprotein 2 (clusterin) from cultured Sertoli cells, testis, and epididymis of the rat. *Biol Reprod, 50*(3), 669-679.
Lee, C. H., Jin, R. J., Kwak, C., Jeong, H., Park, M. S., Lee, N. K., & Lee, S. E. (2002). Suppression of clusterin expression enhanced cisplatin-induced cytotoxicity on renal cell carcinoma cells. *Urology, 60*(3), 516-520.
Lee, J. H., Cheng, R., Barral, S., Reitz, C., Medrano, M., Lantigua, R., . . . Mayeux, R. (2011). Identification of novel loci for Alzheimer disease and replication of CLU, PICALM, and BIN1 in Caribbean Hispanic individuals. *Arch Neurol, 68*(3), 320-328. doi: 10.1001/archneurol.2010.292
Leeb, C., Eresheim, C., & Nimpf, J. (2014). Clusterin is a ligand for apolipoprotein E receptor 2 (ApoER2) and very low density lipoprotein receptor (VLDLR) and signals via the Reelin-signaling pathway. *J Biol Chem, 289*(7), 4161-4172. doi: 10.1074/jbc.M113.529271
Lemansky, P., Brix, K., & Herzog, V. (1999). Subcellular distribution, secretion, and posttranslational modifications of clusterin in thyrocytes. *Exp Cell Res, 251*(1), 147-155. doi: 10.1006/excr.1999.4555
Leskov, K. S., Klokov, D. Y., Li, J., Kinsella, T. J., & Boothman, D. A. (2003). Synthesis and functional analyses of nuclear clusterin, a cell death protein. *J Biol Chem, 278*(13), 11590-11600. doi: 10.1074/jbc.M209233200
Li, J., Jia, L., Zhao, P., Jiang, Y., Zhong, S., & Chen, D. (2012). Stable knockdown of clusterin by vectorbased RNA interference in a human breast cancer cell line inhibits tumour cell invasion and metastasis. *J Int Med Res, 40*(2), 545-555. doi: 10.1177/147323001204000216
Lidstrom, A. M., Bogdanovic, N., Hesse, C., Volkman, I., Davidsson, P., & Blennow, K. (1998). Clusterin (apolipoprotein J) protein levels are increased in hippocampus and in frontal cortex in Alzheimer's disease. *Exp Neurol, 154*(2), 511-521. doi: 10.1006/exnr.1998.6892
Lin, Y. L., Chen, S. Y., Lai, L. C., Chen, J. H., Yang, S. Y., Huang, Y. L., . . . Chen, Y. C. (2012). Genetic polymorphisms of clusterin gene are associated with a decreased risk of Alzheimer's disease. *Eur J Epidemiol*. doi: 10.1007/s10654-012-9650-5
Liu, B., Han, M. T., Zhang, J., Lu, P., Li, J., Song, N., . . . Zhang, W. (2013). Downregulation of clusterin expression in human testicular seminoma. *Cell Physiol Biochem, 32*(4), 1117-1123. doi:

10.1159/000354511
Liu, B., Teschemacher, A. G., & Kasparov, S. (2017). Neuroprotective potential of astroglia. *J Neurosci Res, 95*(11), 2126-2139. doi: 10.1002/jnr.24140
Liu, C. C., Kanekiyo, T., Xu, H., & Bu, G. (2013). Apolipoprotein E and Alzheimer disease: risk, mechanisms and therapy. *Nat Rev Neurol, 9*(2), 106-118. doi: 10.1038/nrneurol.2012.263
Liu, Y., Liu, W., Song, X. D., & Zuo, J. (2005). Effect of GRP75/mthsp70/PBP74/mortalin overexpression on intracellular ATP level, mitochondrial membrane potential and ROS accumulation following glucose deprivation in PC12 cells. *Mol Cell Biochem, 268*(1-2), 45-51.
Loison, F., Debure, L., Nizard, P., le Goff, P., Michel, D., & le Drean, Y. (2006). Up-regulation of the clusterin gene after proteotoxic stress: implication of HSF1-HSF2 heterocomplexes. *Biochem J, 395*(1), 223-231. doi: 10.1042/BJ20051190
Londou, A., Mikrou, A., & Zarkadis, I. K. (2008). Cloning and characterization of two clusterin isoforms in rainbow trout. *Mol Immunol, 45*(2), 470-478. doi: 10.1016/j.molimm.2007.05.027
Lu, S. J., Li, H. L., Sun, Y. M., Liu, Z. J., Yang, P., & Wu, Z. Y. (2014). Clusterin variants are not associated with southern Chinese patients with Alzheimer's disease. *Neurobiol Aging, 35*(11), 2656 e2659-2611. doi: 10.1016/j.neurobiolaging.2014.05.015
Lynch, J. R., Tang, W., Wang, H., Vitek, M. P., Bennett, E. R., Sullivan, P. M., . . . Laskowitz, D. T. (2003). APOE genotype and an ApoE-mimetic peptide modify the systemic and central nervous system inflammatory response. *J Biol Chem, 278*(49), 48529-48533. doi: 10.1074/jbc.M306923200
Ma, J. F., Liu, L. H., Zhang, Y., Wang, Y., Deng, Y. L., Huang, Y., . . . Chen, S. D. (2011). Association study of clusterin polymorphism rs11136000 with late onset Alzheimer's disease in Chinese Han population. *Am J Alzheimers Dis Other Demen, 26*(8), 627-630. doi: 10.1177/1533317511432735
Masoodi, T. A., Al Shammari, S. A., Al-Muammar, M. N., Alhamdan, A. A., & Talluri, V. R. (2013). Exploration of deleterious single nucleotide polymorphisms in late-onset Alzheimer disease susceptibility genes. *Gene, 512*(2), 429-437. doi: 10.1016/j.gene.2012.08.026
Mastroeni, D., Grover, A., Delvaux, E., Whiteside, C., Coleman, P. D., & Rogers, J. (2010). Epigenetic changes in Alzheimer's disease: decrements in DNA methylation. *Neurobiol Aging, 31*(12), 2025-2037. doi: 10.1016/j.neurobiolaging.2008.12.005
Mastroeni, D., McKee, A., Grover, A., Rogers, J., & Coleman, P. D. (2009). Epigenetic differences in cortical neurons from a pair of monozygotic twins discordant for Alzheimer's disease. *PLoS One, 4*(8), e6617. doi: 10.1371/journal.pone.0006617
Matsubara, E., Soto, C., Governale, S., Frangione, B., & Ghiso, J. (1996). Apolipoprotein J and Alzheimer's amyloid beta solubility. *Biochem J, 316 (Pt 2)*, 671-679.
May, P. C., Lampert-Etchells, M., Johnson, S. A., Poirier, J., Masters, J. N., & Finch, C. E. (1990). Dynamics of gene expression for a hippocampal glycoprotein elevated in Alzheimer's disease and in response to experimental lesions in rat. *Neuron, 5*(6), 831-839.
McBride, R. (2012). Pharma counts just 3 Alzheimer's drug wins in 13 years (101 losses!) [Press release]
McGeer, P. L., Klegeris, A., Walker, D. G., Yasuhara, O., & McGeer, E. G. (1994). Pathological proteins in senile plaques. *Tohoku J Exp Med, 174*(3), 269-277.
McLaughlin, L., Zhu, G., Mistry, M., Ley-Ebert, C., Stuart, W. D., Florio, C. J., . . . Aronow, B. J. (2000). Apolipoprotein J/clusterin limits the severity of murine autoimmune myocarditis. *J Clin Invest, 106*(9), 1105-1113. doi: 10.1172/JCI9037
Messmer-Joudrier, S., Sagot, Y., Mattenberger, L., James, R. W., & Kato, A. C. (1996). Injury-induced synthesis and release of apolipoprotein E and clusterin from rat neural cells. *Eur J Neurosci, 8*(12), 2652-2661.
Michel, D., Chabot, J. G., Moyse, E., Danik, M., & Quirion, R. (1992). Possible functions of a new genetic marker in central nervous system: the sulfated glycoprotein-2 (SGP-2). *Synapse, 11*(2), 105-111. doi: 10.1002/syn.890110203
Michel, D., Chatelain, G., North, S., & Brun, G. (1997). Stress-induced transcription of the clusterin/apoJ gene. *Biochem J, 328 (Pt 1)*, 45-50.

Min, B. H., Jeong, S. Y., Kang, S. W., Crabo, B. G., Foster, D. N., Chun, B. G., . . . Park, I. S. (1998). Transient expression of clusterin (sulfated glycoprotein-2) during development of rat pancreas. *J Endocrinol, 158*(1), 43-52.

Mishima, K., Inoue, H., Nishiyama, T., Mabuchi, Y., Amano, Y., Ide, F., . . . Saito, I. (2012). Transplantation of side population cells restores the function of damaged exocrine glands through clusterin. *Stem Cells, 30*(9), 1925-1937. doi: 10.1002/stem.1173

Miyake, H., Chi, K. N., & Gleave, M. E. (2000). Antisense TRPM-2 oligodeoxynucleotides chemosensitize human androgen-independent PC-3 prostate cancer cells both in vitro and in vivo. *Clin Cancer Res, 6*(5), 1655-1663.

Miyake, H., Gleave, M., Kamidono, S., & Hara, I. (2002). Overexpression of clusterin in transitional cell carcinoma of the bladder is related to disease progression and recurrence. *Urology, 59*(1), 150-154.

Miyake, H., Gleave, M. E., Arakawa, S., Kamidono, S., & Hara, I. (2002). Introducing the clusterin gene into human renal cell carcinoma cells enhances their metastatic potential. *J Urol, 167*(5), 2203-2208.

Mosienko, V., Teschemacher, A. G., & Kasparov, S. (2015). Is L-lactate a novel signaling molecule in the brain? *J Cereb Blood Flow Metab, 35*(7), 1069-1075. doi: 10.1038/jcbfm.2015.77

Mukaetova-Ladinska, E. B., Abdel-All, Z., Andrade, J., Alves da Silva, J., O'Brien, J. T., & Kalaria, R. N. (2015). Plasma and platelet clusterin ratio is altered in Alzheimer's disease patients with distinct neuropsychiatric symptoms: findings from a pilot study. *Int J Geriatr Psychiatry, 30*(4), 368-375. doi: 10.1002/gps.4145

Mukaetova-Ladinska, E. B., Abdel-All, Z., Dodds, S., Andrade, J., Alves da Silva, J., Kalaria, R. N., & O'Brien, J. T. (2012). Platelet immunoglobulin and amyloid precursor protein as potential peripheral biomarkers for Alzheimer's disease: findings from a pilot study. *Age Ageing, 41*(3), 408-412. doi: 10.1093/ageing/afr171

Murphy, B. F., Kirszbaum, L., Walker, I. D., & d'Apice, A. J. (1988). SP-40,40, a newly identified normal human serum protein found in the SC5b-9 complex of complement and in the immune deposits in glomerulonephritis. *J Clin Invest, 81*(6), 1858-1864. doi: 10.1172/JCI113531

Nair, J. R., & McGuire, J. J. (2005). Submitochondrial localization of the mitochondrial isoform of folylpolyglutamate synthetase in CCRF-CEM human T-lymphoblastic leukemia cells. *Biochim Biophys Acta, 1746*(1), 38-44. doi: 10.1016/j.bbamcr.2005.08.004

Nathan, B. P., Bellosta, S., Sanan, D. A., Weisgraber, K. H., Mahley, R. W., & Pitas, R. E. (1994). Differential effects of apolipoproteins E3 and E4 on neuronal growth in vitro. *Science, 264*(5160), 850-852.

Niu, Z., Li, X., Hu, B., Li, R., Wang, L., Wu, L., & Wang, X. (2012). Small interfering RNA targeted to secretory clusterin blocks tumor growth, motility, and invasion in breast cancer. *Acta Biochim Biophys Sin (Shanghai), 44*(12), 991-998. doi: 10.1093/abbs/gms091

Nizard, P., Tetley, S., Le Drean, Y., Watrin, T., Le Goff, P., Wilson, M. R., & Michel, D. (2007). Stress-induced retrotranslocation of clusterin/ApoJ into the cytosol. *Traffic, 8*(5), 554-565. doi: 10.1111/j.1600-0854.2007.00549.x

Nuutinen, T., Suuronen, T., Kyrylenko, S., Huuskonen, J., & Salminen, A. (2005). Induction of clusterin/apoJ expression by histone deacetylase inhibitors in neural cells. *Neurochem Int, 47*(8), 528-538. doi: 10.1016/j.neuint.2005.07.007

O'Bryan, M. K., Cheema, S. S., Bartlett, P. F., Murphy, B. F., & Pearse, M. J. (1993). Clusterin levels increase during neuronal development. *J Neurobiol, 24*(4), 421-432. doi: 10.1002/neu.480240402

Oda, T., Wals, P., Osterburg, H. H., Johnson, S. A., Pasinetti, G. M., Morgan, T. E., . . . et al. (1995). Clusterin (apoJ) alters the aggregation of amyloid beta-peptide (A beta 1-42) and forms slowly sedimenting A beta complexes that cause oxidative stress. *Exp Neurol, 136*(1), 22-31.

Orkand, R. K., Nicholls, J. G., & Kuffler, S. W. (1966). Effect of nerve impulses on the membrane potential of glial cells in the central nervous system of amphibia. *J Neurophysiol, 29*(4), 788-806.

Osten, P., Dittgen, T., & Licznerski, P. (2006). Lentivirus-Based Genetic Manipulations in Neurons In

Vivo. In J. T. Kittler & S. J. Moss (Eds.), *The Dynamic Synapse: Molecular Methods in Ionotropic Receptor Biology*. Boca Raton (FL).
Park, D. C., Yeo, S. G., Wilson, M. R., Yerbury, J. J., Kwong, J., Welch, W. R., . . . Wong, K. K. (2008). Clusterin interacts with Paclitaxel and confer Paclitaxel resistance in ovarian cancer. *Neoplasia, 10*(9), 964-972.
Pasinetti, G. M., Johnson, S. A., Oda, T., Rozovsky, I., & Finch, C. E. (1994). Clusterin (SGP-2): a multifunctional glycoprotein with regional expression in astrocytes and neurons of the adult rat brain. *J Comp Neurol, 339*(3), 387-400. doi: 10.1002/cne.903390307
Payami, H., Montee, K. R., Kaye, J. A., Bird, T. D., Yu, C. E., Wijsman, E. M., & Schellenberg, G. D. (1994). Alzheimer's disease, apolipoprotein E4, and gender. *JAMA, 271*(17), 1316-1317.
Payami, H., Zareparsi, S., Montee, K. R., Sexton, G. J., Kaye, J. A., Bird, T. D., . . . Schellenberg, G. D. (1996). Gender difference in apolipoprotein E-associated risk for familial Alzheimer disease: a possible clue to the higher incidence of Alzheimer disease in women. *Am J Hum Genet, 58*(4), 803-811.
Pedraza, O., Allen, M., Jennette, K., Carrasquillo, M., Crook, J., Serie, D., . . . Ertekin-Taner, N. (2014). Evaluation of memory endophenotypes for association with CLU, CR1, and PICALM variants in black and white subjects. *Alzheimers Dement, 10*(2), 205-213. doi: 10.1016/j.jalz.2013.01.016
Phipps, A. J., Vickers, J. C., Taberlay, P. C., & Woodhouse, A. (2016). Neurofilament-labeled pyramidal neurons and astrocytes are deficient in DNA methylation marks in Alzheimer's disease. *Neurobiol Aging, 45*, 30-42. doi: 10.1016/j.neurobiolaging.2016.05.003
Poon, S., Easterbrook-Smith, S. B., Rybchyn, M. S., Carver, J. A., & Wilson, M. R. (2000). Clusterin is an ATP-independent chaperone with very broad substrate specificity that stabilizes stressed proteins in a folding-competent state. *Biochemistry, 39*(51), 15953-15960.
Poon, S., Rybchyn, M. S., Easterbrook-Smith, S. B., Carver, J. A., Pankhurst, G. J., & Wilson, M. R. (2002). Mildly acidic pH activates the extracellular molecular chaperone clusterin. *J Biol Chem, 277*(42), 39532-39540. doi: 10.1074/jbc.M204855200
Prochnow, H., Gollan, R., Rohne, P., Hassemer, M., Koch-Brandt, C., & Baiersdorfer, M. (2013). Non-secreted clusterin isoforms are translated in rare amounts from distinct human mRNA variants and do not affect Bax-mediated apoptosis or the NF-kappaB signaling pathway. *PLoS One, 8*(9), e75303. doi: 10.1371/journal.pone.0075303
Purrello, M., Bettuzzi, S., Di Pietro, C., Mirabile, E., Di Blasi, M., Rimini, R., . . . Sichel, G. (1991). The gene for SP-40,40, human homolog of rat sulfated glycoprotein 2, rat clusterin, and rat testosterone-repressed prostate message 2, maps to chromosome 8. *Genomics, 10*(1), 151-156.
Rao, J. S., Keleshian, V. L., Klein, S., & Rapoport, S. I. (2012). Epigenetic modifications in frontal cortex from Alzheimer's disease and bipolar disorder patients. *Transl Psychiatry, 2*, e132. doi: 10.1038/tp.2012.55
Reddy, K. B., Jin, G., Karode, M. C., Harmony, J. A., & Howe, P. H. (1996). Transforming growth factor beta (TGF beta)-induced nuclear localization of apolipoprotein J/clusterin in epithelial cells. *Biochemistry, 35*(19), 6157-6163. doi: 10.1021/bi952981b
Redondo, M., Villar, E., Torres-Munoz, J., Tellez, T., Morell, M., & Petito, C. K. (2000). Overexpression of clusterin in human breast carcinoma. *Am J Pathol, 157*(2), 393-399. doi: 10.1016/S0002-9440(10)64552-X
Rohne, P., Prochnow, H., Wolf, S., Renner, B., & Koch-Brandt, C. (2014). The chaperone activity of clusterin is dependent on glycosylation and redox environment. *Cell Physiol Biochem, 34*(5), 1626-1639. doi: 10.1159/000366365
Rordorf, G., Koroshetz, W. J., & Bonventre, J. V. (1991). Heat shock protects cultured neurons from glutamate toxicity. *Neuron, 7*(6), 1043-1051.
Roussotte, F. F., Gutman, B. A., Madsen, S. K., Colby, J. B., Thompson, P. M., & Alzheimer's Disease Neuroimaging, I. (2014). Combined effects of Alzheimer risk variants in the CLU and ApoE genes on ventricular expansion patterns in the elderly. *J Neurosci, 34*(19), 6537-6545. doi: 10.1523/JNEUROSCI.5236-13.2014

Rozovsky, I., Morgan, T. E., Willoughby, D. A., Dugichi-Djordjevich, M. M., Pasinetti, G. M., Johnson, S. A., & Finch, C. E. (1994). Selective expression of clusterin (SGP-2) and complement C1qB and C4 during responses to neurotoxins in vivo and in vitro. *Neuroscience, 62*(3), 741-758.

Rumi, M. A. K., Singh, P., Roby, K. F., Zhao, X., Iqbal, K., Ratri, A., . . . Soares, M. J. (2017). Defining the Role of Estrogen Receptor beta in the Regulation of Female Fertility. *Endocrinology, 158*(7), 2330-2343. doi: 10.1210/en.2016-1916

Saad, F., Hotte, S., North, S., Eigl, B., Chi, K., Czaykowski, P., . . . Canadian Uro-Oncology, G. (2011). Randomized phase II trial of Custirsen (OGX-011) in combination with docetaxel or mitoxantrone as second-line therapy in patients with metastatic castrate-resistant prostate cancer progressing after first-line docetaxel: CUOG trial P-06c. *Clin Cancer Res, 17*(17), 5765-5773. doi: 10.1158/1078-0432.CCR-11-0859

Saitoh, T., Igura, M., Obita, T., Ose, T., Kojima, R., Maenaka, K., . . . Kohda, D. (2007). Tom20 recognizes mitochondrial presequences through dynamic equilibrium among multiple bound states. *EMBO J, 26*(22), 4777-4787. doi: 10.1038/sj.emboj.7601888

Sasaki, K., Doh-ura, K., Ironside, J., Mabbott, N., & Iwaki, T. (2006). Clusterin expression in follicular dendritic cells associated with prion protein accumulation. *J Pathol, 209*(4), 484-491. doi: 10.1002/path.2009

Sattlecker, M., Kiddle, S. J., Newhouse, S., Proitsi, P., Nelson, S., Williams, S., . . . Dobson, R. J. (2014). Alzheimer's disease biomarker discovery using SOMAscan multiplexed protein technology. *Alzheimers Dement, 10*(6), 724-734. doi: 10.1016/j.jalz.2013.09.016

Saunders, A. M., Schmader, K., Breitner, J. C., Benson, M. D., Brown, W. T., Goldfarb, L., . . . et al. (1993). Apolipoprotein E epsilon 4 allele distributions in late-onset Alzheimer's disease and in other amyloid-forming diseases. *Lancet, 342*(8873), 710-711.

Savkovic, V., Gantzer, H., Reiser, U., Selig, L., Gaiser, S., Sack, U., . . . Bodeker, H. (2007). Clusterin is protective in pancreatitis through anti-apoptotic and anti-inflammatory properties. *Biochem Biophys Res Commun, 356*(2), 431-437. doi: 10.1016/j.bbrc.2007.02.148

Schmidt, R., Kienbacher, E., Benke, T., Dal-Bianco, P., Delazer, M., Ladurner, G., . . . Wehringer, C. (2008). [Sex differences in Alzheimer's disease]. *Neuropsychiatr, 22*(1), 1-15.

Schnabel, J. (2013). Why Do All the Large Alzheimer's Drug Trials Fail? [Press release]

Schreiber, S. S., Tocco, G., Najm, I., & Baudry, M. (1993). Seizure activity causes a rapid increase in sulfated glycoprotein-2 messenger RNA in the adult but not the neonatal rat brain. *Neurosci Lett, 153*(1), 17-20.

Schrijvers, E. M., Koudstaal, P. J., Hofman, A., & Breteler, M. M. (2011). Plasma clusterin and the risk of Alzheimer disease. *JAMA, 305*(13), 1322-1326. doi: 10.1001/jama.2011.381

Schurmann, B., Wiese, B., Bickel, H., Weyerer, S., Riedel-Heller, S. G., Pentzek, M., . . . Jessen, F. (2011). Association of the Alzheimer's disease clusterin risk allele with plasma clusterin concentration. *J Alzheimers Dis, 25*(3), 421-424. doi: 10.3233/JAD-2011-110251

Seo, H. Y., Kim, M. K., Jung, Y. A., Jang, B. K., Yoo, E. K., Park, K. G., & Lee, I. K. (2013). Clusterin decreases hepatic SREBP-1c expression and lipid accumulation. *Endocrinology, 154*(5), 1722-1730. doi: 10.1210/en.2012-2009

Seshadri, S., Fitzpatrick, A. L., Ikram, M. A., DeStefano, A. L., Gudnason, V., Boada, M., . . . Consortium, E. (2010). Genome-wide analysis of genetic loci associated with Alzheimer disease. *JAMA, 303*(18), 1832-1840. doi: 10.1001/jama.2010.574

Shi, H., Deng, J. H., Wang, Z., Cao, K. Y., Zhou, L., & Wan, H. (2013). Knockdown of clusterin inhibits the growth and migration of renal carcinoma cells and leads to differential gene expression. *Mol Med Rep, 8*(1), 35-40. doi: 10.3892/mmr.2013.1470

Shirasawa, T., Miyata, M., Eto, H., Hamada, N., Akasaki, Y., Miyauchi, T., . . . Tei, C. (2009). Deficiency of clusterin inhibits neointimal hyperplasia after vascular injury. *J Atheroscler Thromb, 16*(6), 772-781.

Shuai, P., Liu, Y., Lu, W., Liu, Q., Li, T., & Gong, B. (2015). Genetic associations of CLU rs9331888 polymorphism with Alzheimer's disease: A meta-analysis. *Neurosci Lett, 591*, 160-165. doi:

10.1016/j.neulet.2015.02.040
Silajdzic, E., Minthon, L., Bjorkqvist, M., & Hansson, O. (2012). No diagnostic value of plasma clusterin in Alzheimer's disease. *PLoS One, 7*(11), e50237. doi: 10.1371/journal.pone.0050237
So, A., Sinnemann, S., Huntsman, D., Fazli, L., & Gleave, M. (2005). Knockdown of the cytoprotective chaperone, clusterin, chemosensitizes human breast cancer cells both in vitro and in vivo. *Mol Cancer Ther, 4*(12), 1837-1849. doi: 10.1158/1535-7163.MCT-05-0178
Song, F., Poljak, A., Crawford, J., Kochan, N. A., Wen, W., Cameron, B., . . . Sachdev, P. S. (2012). Plasma apolipoprotein levels are associated with cognitive status and decline in a community cohort of older individuals. *PLoS One, 7*(6), e34078. doi: 10.1371/journal.pone.0034078
Stewart, E. M., Aquilina, J. A., Easterbrook-Smith, S. B., Murphy-Durland, D., Jacobsen, C., Moestrup, S., & Wilson, M. R. (2007). Effects of glycosylation on the structure and function of the extracellular chaperone clusterin. *Biochemistry, 46*(5), 1412-1422. doi: 10.1021/bi062082v
Swerdlow, R. H., & Khan, S. M. (2004). A "mitochondrial cascade hypothesis" for sporadic Alzheimer's disease. *Med Hypotheses, 63*(1), 8-20. doi: 10.1016/j.mehy.2003.12.045
Sylvester, S. R., Skinner, M. K., & Griswold, M. D. (1984). A sulfated glycoprotein synthesized by Sertoli cells and by epididymal cells is a component of the sperm membrane. *Biol Reprod, 31*(5), 1087-1101.
Szklarczyk, D., Franceschini, A., Wyder, S., Forslund, K., Heller, D., Huerta-Cepas, J., . . . von Mering, C. (2015). STRING v10: protein-protein interaction networks, integrated over the tree of life. *Nucleic Acids Res, 43*(Database issue), D447-452. doi: 10.1093/nar/gku1003
Szymanski, M., Wang, R., Bassett, S. S., & Avramopoulos, D. (2011). Alzheimer's risk variants in the clusterin gene are associated with alternative splicing. *Transl Psychiatry, 1*. doi: 10.1038/tp.2011.17
Tang, M., Li, J., Liu, B., Song, N., Wang, Z., & Yin, C. (2013). Clusterin expression and human testicular seminoma. *Med Hypotheses, 81*(4), 635-637. doi: 10.1016/j.mehy.2013.07.019
Teschemacher, A. G., Gourine, A. V., & Kasparov, S. (2015). A Role for Astrocytes in Sensing the Brain Microenvironment and Neuro-Metabolic Integration. *Neurochem Res, 40*(12), 2386-2393. doi: 10.1007/s11064-015-1562-9
Thambisetty, M., An, Y., Kinsey, A., Koka, D., Saleem, M., Guntert, A., . . . Resnick, S. M. (2012). Plasma clusterin concentration is associated with longitudinal brain atrophy in mild cognitive impairment. *Neuroimage, 59*(1), 212-217. doi: 10.1016/j.neuroimage.2011.07.056
Thambisetty, M., Beason-Held, L. L., An, Y., Kraut, M., Nalls, M., Hernandez, D. G., . . . Resnick, S. M. (2013). Alzheimer risk variant CLU and brain function during aging. *Biol Psychiatry, 73*(5), 399-405. doi: 10.1016/j.biopsych.2012.05.026
Tobe, T., Minoshima, S., Yamase, S., Choi, N. H., Tomita, M., & Shimizu, N. (1991). Assignment of a human serum glycoprotein SP-40,40 gene (CLI) to chromosome 8. *Cytogenet Cell Genet, 57*(4), 193-195.
Toral-Rios, D., Franco-Bocanegra, D., Rosas-Carrasco, O., Mena-Barranco, F., Carvajal-Garcia, R., Meraz-Rios, M. A., & Campos-Pena, V. (2015). Evaluation of inflammation-related genes polymorphisms in Mexican with Alzheimer's disease: a pilot study. *Front Cell Neurosci, 9*, 148. doi: 10.3389/fncel.2015.00148
Tropschug, M., Nicholson, D. W., Hartl, F. U., Kohler, H., Pfanner, N., Wachter, E., & Neupert, W. (1988). Cyclosporin A-binding protein (cyclophilin) of Neurospora crassa. One gene codes for both the cytosolic and mitochondrial forms. *J Biol Chem, 263*(28), 14433-14440.
Trougakos, I. P. (2013). The molecular chaperone apolipoprotein J/clusterin as a sensor of oxidative stress: implications in therapeutic approaches - a mini-review. *Gerontology, 59*(6), 514-523. doi: 10.1159/000351207
Trougakos, I. P., & Gonos, E. S. (2006). Regulation of clusterin/apolipoprotein J, a functional homologue to the small heat shock proteins, by oxidative stress in ageing and age-related diseases. *Free Radic Res, 40*(12), 1324-1334. doi: 10.1080/10715760600902310
Trougakos, I. P., Lourda, M., Antonelou, M. H., Kletsas, D., Gorgoulis, V. G., Papassideri, I. S., . . .

Gonos, E. S. (2009). Intracellular clusterin inhibits mitochondrial apoptosis by suppressing p53-activating stress signals and stabilizing the cytosolic Ku70-Bax protein complex. *Clin Cancer Res, 15*(1), 48-59. doi: 10.1158/1078-0432.CCR-08-1805

Van Beek, J., Chan, P., Bernaudin, M., Petit, E., MacKenzie, E. T., & Fontaine, M. (2000). Glial responses, clusterin, and complement in permanent focal cerebral ischemia in the mouse. *Glia, 31*(1), 39-50.

van der Laan, M., Horvath, S. E., & Pfanner, N. (2016). Mitochondrial contact site and cristae organizing system. *Curr Opin Cell Biol, 41*, 33-42. doi: 10.1016/j.ceb.2016.03.013

Viard, I., Wehrli, P., Jornot, L., Bullani, R., Vechietti, J. L., Schifferli, J. A., . . . French, L. E. (1999). Clusterin gene expression mediates resistance to apoptotic cell death induced by heat shock and oxidative stress. *J Invest Dermatol, 112*(3), 290-296. doi: 10.1046/j.1523-1747.1999.00531.x

von der Malsburg, K., Muller, J. M., Bohnert, M., Oeljeklaus, S., Kwiatkowska, P., Becker, T., . . . van der Laan, M. (2011). Dual role of mitofilin in mitochondrial membrane organization and protein biogenesis. *Dev Cell, 21*(4), 694-707. doi: 10.1016/j.devcel.2011.08.026

von Mering, C., Jensen, L. J., Snel, B., Hooper, S. D., Krupp, M., Foglierini, M., . . . Bork, P. (2005). STRING: known and predicted protein-protein associations, integrated and transferred across organisms. *Nucleic Acids Res, 33*(Database issue), D433-437. doi: 10.1093/nar/gki005

Wang, X., Luo, L., Dong, D., Yu, Q., & Zhao, K. (2014). Clusterin plays an important role in clear renal cell cancer metastasis. *Urol Int, 92*(1), 95-103. doi: 10.1159/000351923

Wang, Y., Qin, X., & Paudel, H. K. (2017). Amyloid beta peptide promotes lysosomal degradation of clusterin via sortilin in hippocampal primary neurons. *Neurobiol Dis, 103*, 78-88. doi: 10.1016/j.nbd.2017.04.003

Waters, K. M., Safe, S., & Gaido, K. W. (2001). Differential gene expression in response to methoxychlor and estradiol through ERalpha, ERbeta, and AR in reproductive tissues of female mice. *Toxicol Sci, 63*(1), 47-56.

Wehrli, P., Charnay, Y., Vallet, P., Zhu, G., Harmony, J., Aronow, B., . . . Giannakopoulos, P. (2001). Inhibition of post-ischemic brain injury by clusterin overexpression. *Nat Med, 7*(9), 977-979. doi: 10.1038/nm0901-977

Wei, L., Xue, T., Wang, J., Chen, B., Lei, Y., Huang, Y., . . . Xin, X. (2009). Roles of clusterin in progression, chemoresistance and metastasis of human ovarian cancer. *Int J Cancer, 125*(4), 791-806. doi: 10.1002/ijc.24316

Won, Y. S., Lee, S. J., Yeo, S. G., & Park, D. C. (2012). Effects of female sex hormones on clusterin expression and paclitaxel resistance in endometrial cancer cell lines. *Int J Med Sci, 9*(1), 86-92.

Wong, P., Pineault, J., Lakins, J., Taillefer, D., Leger, J., Wang, C., & Tenniswood, M. (1993). Genomic organization and expression of the rat TRPM-2 (clusterin) gene, a gene implicated in apoptosis. *J Biol Chem, 268*(7), 5021-5031.

Wu, Y., & Sha, B. (2006). Crystal structure of yeast mitochondrial outer membrane translocon member Tom70p. *Nat Struct Mol Biol, 13*(7), 589-593. doi: 10.1038/nsmb1106

Wunsche, W., Tenniswood, M. P., Schneider, M. R., & Vollmer, G. (1998). Estrogenic regulation of clusterin mRNA in normal and malignant endometrial tissue. *Int J Cancer, 76*(5), 684-688.

Wyatt, A., Yerbury, J., Poon, S., Dabbs, R., & Wilson, M. (2009). Chapter 6: The chaperone action of Clusterin and its putative role in quality control of extracellular protein folding. *Adv Cancer Res, 104*, 89-114. doi: 10.1016/S0065-230X(09)04006-8

Wyatt, A. R., Yerbury, J. J., & Wilson, M. R. (2009). Structural characterization of clusterin-chaperone client protein complexes. *J Biol Chem, 284*(33), 21920-21927. doi: 10.1074/jbc.M109.033688

Xie, Z., Harris-White, M. E., Wals, P. A., Frautschy, S. A., Finch, C. E., & Morgan, T. E. (2005). Apolipoprotein J (clusterin) activates rodent microglia in vivo and in vitro. *J Neurochem, 93*(4), 1038-1046. doi: 10.1111/j.1471-4159.2005.03065.x

Xing, Y. Y., Yu, J. T., Cui, W. Z., Zhong, X. L., Wu, Z. C., Zhang, Q., & Tan, L. (2012). Blood clusterin levels, rs9331888 polymorphism, and the risk of Alzheimer's disease. *J Alzheimers Dis, 29*(3), 515-519. doi: 10.3233/JAD-2011-111844

Xiu, P., Dong, X. F., Li, X. P., & Li, J. (2015). Clusterin: Review of research progress and looking ahead to direction in hepatocellular carcinoma. *World J Gastroenterol, 21*(27), 8262-8270. doi: 10.3748/wjg.v21.i27.8262

Xue, J., Lv, D. D., Jiao, S., Zhao, W., Li, X., Sun, H., . . . Fang, J. (2012). pVHL mediates K63-linked ubiquitination of nCLU. *PLoS One, 7*(4), e35848. doi: 10.1371/journal.pone.0035848

Yang, C. R., Leskov, K., Hosley-Eberlein, K., Criswell, T., Pink, J. J., Kinsella, T. J., & Boothman, D. A. (2000). Nuclear clusterin/XIP8, an x-ray-induced Ku70-binding protein that signals cell death. *Proc Natl Acad Sci U S A, 97*(11), 5907-5912.

Yang, C. R., Yeh, S., Leskov, K., Odegaard, E., Hsu, H. L., Chang, C., . . . Boothman, D. A. (1999). Isolation of Ku70-binding proteins (KUBs). *Nucleic Acids Res, 27*(10), 2165-2174.

Yao, J., Irwin, R. W., Zhao, L., Nilsen, J., Hamilton, R. T., & Brinton, R. D. (2009). Mitochondrial bioenergetic deficit precedes Alzheimer's pathology in female mouse model of Alzheimer's disease. *Proc Natl Acad Sci U S A, 106*(34), 14670-14675. doi: 10.1073/pnas.0903563106

Yerbury, J. J., Poon, S., Meehan, S., Thompson, B., Kumita, J. R., Dobson, C. M., & Wilson, M. R. (2007). The extracellular chaperone clusterin influences amyloid formation and toxicity by interacting with prefibrillar structures. *FASEB J, 21*(10), 2312-2322. doi: 10.1096/fj.06-7986com

Yu, J. T., Li, L., Zhu, Q. X., Zhang, Q., Zhang, W., Wu, Z. C., . . . Tan, L. (2010). Implication of CLU gene polymorphisms in Chinese patients with Alzheimer's disease. *Clin Chim Acta, 411*(19-20), 1516-1519. doi: 10.1016/j.cca.2010.06.013

Yu, J. T., Ma, X. Y., Wang, Y. L., Sun, L., Tan, L., Hu, N., & Tan, L. (2013). Genetic variation in clusterin gene and Alzheimer's disease risk in Han Chinese. *Neurobiol Aging, 34*(7), 1921 e1917-1923. doi: 10.1016/j.neurobiolaging.2013.01.010

Zeng, W., Lu, Y. H., Lee, J., & Friedman, J. M. (2015). Reanalysis of parabiosis of obesity mutants in the age of leptin. *Proc Natl Acad Sci U S A, 112*(29), E3874-3882. doi: 10.1073/pnas.1510378112

Zhang, D., Sun, B., Zhao, X., Cui, Y., Xu, S., Dong, X., . . . Chi, J. (2012). Secreted CLU is associated with the initiation of triple-negative breast cancer. *Cancer Biol Ther, 13*(5), 321-329. doi: 10.4161/cbt.19072

Zhang, H., Kim, J. K., Edwards, C. A., Xu, Z., Taichman, R., & Wang, C. Y. (2005). Clusterin inhibits apoptosis by interacting with activated Bax. *Nat Cell Biol, 7*(9), 909-915. doi: 10.1038/ncb1291

Zhang, S., Li, X., Ma, G., Jiang, Y., Liao, M., Feng, R., . . . Liu, G. (2015). CLU rs9331888 Polymorphism Contributes to Alzheimer's Disease Susceptibility in Caucasian But Not East Asian Populations. *Mol Neurobiol*. doi: 10.1007/s12035-015-9098-1

Zhao, L., & Brinton, R. D. (2005). Structure-based virtual screening for plant-based ERbeta-selective ligands as potential preventative therapy against age-related neurodegenerative diseases. *J Med Chem, 48*(10), 3463-3466. doi: 10.1021/jm0490538

Zhao, L., Mao, Z., & Brinton, R. D. (2009). A select combination of clinically relevant phytoestrogens enhances estrogen receptor beta-binding selectivity and neuroprotective activities in vitro and in vivo. *Endocrinology, 150*(2), 770-783. doi: 10.1210/en.2008-0715

Zhao, L., Mao, Z., Woody, S. K., & Brinton, R. D. (2016). Sex differences in metabolic aging of the brain: insights into female suceptibility to Alzheimer's disease *Neurobiol Aging*, 1-11. doi: 10.1016/j.neurobiolaging.2016.02.011

Zhao, L., Woody, S. K., & Chhibber, A. (2015). Estrogen receptor beta in Alzheimer's disease: From mechanisms to therapeutics. *Ageing Res Rev*. doi: 10.1016/j.arr.2015.08.001

Zhao, L., Wu, T. W., & Brinton, R. D. (2004). Estrogen receptor subtypes alpha and beta contribute to neuroprotection and increased Bcl-2 expression in primary hippocampal neurons. *Brain Res, 1010*(1-2), 22-34. doi: 10.1016/j.brainres.2004.02.066

Zhao, L., Yao, J., Mao, Z., Chen, S., Wang, Y., & Brinton, R. D. (2011). 17beta-Estradiol regulates insulin-degrading enzyme expression via an ERbeta/PI3-K pathway in hippocampus: relevance to Alzheimer's prevention. *Neurobiol Aging, 32*(11), 1949-1963. doi: 10.1016/j.neurobiolaging.2009.12.010

Zhou, W., Guan, Q., Kwan, C. C., Chen, H., Gleave, M. E., Nguan, C. Y., & Du, C. (2010). Loss of

clusterin expression worsens renal ischemia-reperfusion injury. *Am J Physiol Renal Physiol, 298*(3), F568-578. doi: 10.1152/ajprenal.00399.2009

Zoubeidi, A., Ettinger, S., Beraldi, E., Hadaschik, B., Zardan, A., Klomp, L. W., . . . Gleave, M. E. (2010). Clusterin facilitates COMMD1 and I-kappaB degradation to enhance NF-kappaB activity in prostate cancer cells. *Mol Cancer Res, 8*(1), 119-130. doi: 10.1158/1541-7786.MCR-09-0277

Zwain, I. H., Grima, J., & Cheng, C. Y. (1994). Regulation of clusterin secretion and mRNA expression in astrocytes by cytokines. *Mol Cell Neurosci, 5*(3), 229-237. doi: 10.1006/mcne.1994.1027

Appendices

List of Publications

Research Articles:

Sarah K. Woody, Anindit Chhibber, and Liqin Zhao. Identification and Characterization of Brain CLU Protein Isoforms. (*In progress*)

Sarah K. Woody and Liqin Zhao. Estrogen Receptor beta (ERβ) Regulates Mature CLU in Rodent Brain. (*In Progress*)

Chhibber A, Woody SK, Karim Rumi MA, Soares MJ, Zhao L., *Estrogen receptor β deficiency impairs BDNF-5-HT2A signaling in the hippocampus of female brain: A possible mechanism for menopausal depression.*. Psychoneuroendocrinology. 2017 Aug;82:107-116. doi: 10.1016/j.psyneuen.2017.05.016

Woody, S.K., Zhou, H., Ibrahimi, S., Dong, Y., Zhao, L. *Human Apolipoprotein E ε2 (APOE2) Promotes RegulatoryMechanisms of Bioenergetic and Synaptic Function in Female Brain: A Focus on V-Type H+-ATPase*. J Alzheimers Dis. 2016 Jun 18;53(3):1015-31. doi: 10.3233/JAD-16030

Liqin Zhao, Zisu Mao, **Sarah K. Woody**, Roberta D. Brinton. *Sex Differences in Metabolic Aging of the Brain: Insights into Female Susceptibility to Alzheimer's disease*. Neurobiol Aging. 2016 June; 42:69-79. doi:10.1016/j.neurobiolaging.2016.02.011

Sun, M, Cui, W, **Woody, S. K**, Staudinger, J. *Pregnane x receptor modulates the inflammatory response in primary cultures of hepatocytes.* Drug Metab Dispos**.** 2015 Mar; 43(3): 335-43. doi: 10.1124/dmd.114.062307

Review Articles:

Zhao, L., **Woody, S.K**., Chhibber, A. *Estrogen Receptor β in Alzheimer's disease: From Mechanisms to Therapeutics.* Ageing Res Rev. 2015 Nov; 24(B): 178-90. doi:10.1016/j.arr.2015.08.001

Nuclear-receptor-mediated regulation of drug- and bile-acid-transporter proteins in gut and liver. Staudinger JL, **Woody S**, Sun M, Cui W. Drug Metab Rev. 2013 Feb; 45(1):48-59. doi: 10.3109/03602532.2012.748793.

Book Chapters:

Sarah K. Woody and Liqin Zhao (2016). *Clusterin (APOJ) in Alzheimer's Disease: An Old Molecule with a New Role*, Update on Dementia, Dr. Davide Moretti (Ed.), InTech, DOI: 10.5772/64233. Available from: http://www.intechopen.com/books/update-on-dementia/clusterin-apoj-in-alzheimer-s-disease-an-old-molecule-with-a-new-role

Honors and Awards

Lecturer, 2017
32nd Annual Graduate Honors Symposium, University of Kansas School of Pharmacy
Topic: The impact of neurodegeneration on CLU brain isoform distribution

Pre-doctoral Fellowship in the Pharmaceutical Sciences, 2016-2017
American Foundation for Pharmaceutical Education
Amount: $10,000.00

A.D. Sobel Education Fund Trainee Travel Award, 2016
American Society for Investigative Pathology
Amount: $500.00

Summer Research Fellowship, 2015
University of Kansas
Amount: $5,000.00

Trainee Professional Development Award, 2015
Society for Neuroscience
Amount: $1,500.00

Graduate Scholarly Presentation Travel Award, 2015
University of Kansas
Amount: $500.00

Junior Speaker, 2014
Experimental Biology Meeting, San Diego, CA
Session Title: "Nuclear Receptors as Therapeutic Targets"
Lecture Title: SUMO-Modification of Pregnane X Receptor Alters Protein-Cofactor Interactions

12th Annual K-INBRE Symposium Award of Excellence, 2014
Kansas IDeA Network of Biomedical Research Excellence
Topic: CLU protein isoforms and redistribution in neurodegeneration